Decision support framework for offshore wind farm electrical networks : Robust design and assessment under uncertainties

Swann Gasnier

N° d'ordre : *327*

CENTRALE LILLE

THESE

Présentée en vue
d'obtenir le grade de

DOCTEUR

En

Spécialité : Génie Electrique

Par

Swann GASNIER

DOCTORAT DELIVRE PAR CENTRALE LILLE

Titre de la thèse :
Environnement d'aide à la décision pour les réseaux électriques de raccordement des fermes éoliennes en mer : conception et évaluation robuste sous incertitudes.

Soutenue le 07 novembre 2017 devant le jury d'examen :

Président	*Jean-Paul GAUBERT, Professeur, ENSIP - Université de Poitiers*
Rapporteur	*Xavier ROBOAM, Directeur de Recherches, CNRS, LAPLACE*
Rapporteur	*Mohamed MACHMOUM, Professeur, Université de Nantes, IREENA*
Membre	*Delphine RIU, Professeur, Univ. Grenoble Alpes, CNRS, Grenoble INP*
Membre	*Diana FLOREZ, Enseignante-chercheur, YNCREA HEI*
Co-encadrant	*Serge POULLAIN, HDR, SuperGrid Institute*
Co-encadrant	*Vincent DEBUSSCHERE, Maître de conférences, Univ. Grenoble Alpes, CNRS, Grenoble INP*
Directeur de thèse	*Bruno FRANCOIS, Professeur, Ecole Centrale de Lille, L2EP*

Thèse préparée dans le Laboratoire L2EP

Ecole Doctorale SPI 072 (Lille I, Lille III, Artois, ULCO, UVHC, EC Lille)

PhD thesis title:

Decision support framework for offshore wind farm electrical networks:
Robust design and assessment under uncertainties

ACKNOWLEDGEMENT

Je remercie tout d'abord les non francophones de tolérer la rédaction de ces remerciements en français. Je tiens à remercier chalheureusement tous ceux sans qui ce projet de recherche n'aurait pas pu être ce qu'il est. Ces travaux de thèse ont été menés en partenariat entre le laboratoire L2EP et l'entreprise SuperGrid Institute, avec la participation du laboratoire G2Elab.

Je tiens tout d'abord à remercier Bruno FRANÇOIS, qui a dirigé mes travaux de thèse. Je mesure l'envergure de ce qu'il m'a appris, notamment en communication et valorisation, orale et écrite. J'ai été particulièrement impressioné par ses relectures rapides et édifiantes.

J'adresse également ma gratitude à Vincent DEBUSSCHERE, pour son encadrement scientifique, fait de conseils méthodologiques, mais aussi pour ses encouragements, qui m'ont beaucoup aidé à persévérer.

Je remercie grandement Serge POULLAIN pour son encadrement scientifique et industriel, ainsi que pour la confiance qu'il m'a accordé durant ce projet de thèse. Je remercie également Bruno LUSCAN, directeur du programme 1 de SuperGrid Institute, pour sa confiance ainsi que pour son aide dans l'établissement des objectifs de la thèse. Je suis également reconnaissant envers Hubert DE LA GRANDIERE, directeur de SuperGrid Institute, en tant que représentant de cette entreprise, mais également pour sa proximité : par exemple, pour ses conseils en vue d'améliorer ma soutenance orale.

Je tiens à remercier Mohammed MACHMOUM et Xavier ROBOAM qui m'ont honoré en acceptant d'expertiser mes travaux de recherche. Leurs remarques et questions m'ont permis de percevoir de nouveaux axes d'amélioration de mes travaux de thèse. J'adresse de même ma gratitude à Delphine RIU, Diana FLOREZ et Jean-Paul GAUBERT qui m'ont fait l'honneur de leurs présences lors de ma soutenance, en vue d'évaluer mes travaux.

Je tiens à remercier l'ensemble des membres du L2EP et notamment, les doctorants que j'ai eu la chance de cotoyer lors de mes séjours Lillois : Julian, Guillaume, Silvio, Reda, Gislain et les autres. Je tiens également à remercier tous mes collègues de SuperGrid, qui ont contribué à la très bonne ambiance de travail dont j'ai pu profiter. Je remercie donc, au programme 1, David, Boussaad, Sellé, Raga, Ahmed, Dieynaba, Kosei, William, Janailson, Juan-Carlos, Guilherme, Miguel, Léo, Frédéric, Mathieu, Philippe C, Philippe E, Alberto, Sébastien, Abdelkrim, Seddik et les autres. Je remercie également l'ensemble des personnes de SuperGrid Institute avec lesquels j'ai interragi. En particulier, je remercie grandement Aymeric pour l'aide précieuse qu'il m'a apporté sur les câbles sous-marin. Je remercie également particulièrement le programme 3 et en particulier Piotr, Thomas, Nathan, Mohammed, Juan, José et Sneha.

Je remercie tous mes amis et notamment les lyonnais, qui m'on fait vivre bien d'autres choses en dehors de la thèse et qui ont contribué à rendre ces trois années agréables et enrichissantes. Je remercie donc Anil, Thomas, Mélanie, Maxime, Mimi, Loïc, Anne-Cécile, Clélia, Sophie, George, Gill, Olivier, Thibault, Angélique, Mélodie, Sylvain, Bruno, Vincent et tous les autres.

Je remercie les membres de ma famille, notamment mes parents et mes deux soeurs qui ont tous contribué à me façonner. Je remercie notamment mon père, qui m'a donné le goût de la technique, mon grand père, qui m'a poussé à l'excellence, et ma mère, qui m'a toujours rappelé l'importance des langues vivantes et du français.

Je tiens à remercier une personne très spéciale, Janine, ma fiancée, avec tout l'amour qu'elle m'inspire, pour le soutien et les encouragemets qu'elle m'a apporté ces dernières années ; ainsi que pour m'avoir permis de vivre bien des choses en dehors de mes travaux de thèse, et ainsi, garder un équilibre essentiel.

Par la grâce de Dieu, ces trois années ont donc été, comme l'avaient été les précédentes et comme le seront les suivantes, un merveilleux moyen de grandir, et de simplement, vivre.

CONTENT

TABLE OF ACRONYMS

CAPEX	Capital Expenditure
CMST	Capacitated Minimal Spanning Tree
COP	Conference Of the Parties
COPT	Capacity Outage Probability Table
DAB	Dual Active Bridge
DRU	Diode Rectifier Unit
EEA	European Environment Agency
EENS	Expected Energy Not Supplied
ENTSO-E	European Network of Transmission System Operators for Electricity
HVAC	High Voltage Alternative Current
HVDC	High Voltage Direct Current
IGBT	Insulated Gate Bipolar Transistor
LCC	Line Commutated Converter
LCOE	Levelized Cost Of Energy
LOLE	Loss Of Load Expectation
LVAC	Low Voltage Alternative Current
LVDC	Low voltage Direct Current
MINLP	Mixed Integer Non Linear Programming
MIP	Mixed Integer Programming
MLCMST	Multi-Level Capacitated Minimal Spanning Tree
MMC	Modular Multilevel Converter
MPPT	Maximum Power Point Tracking
MTTF	Mean Time To Failure
MTTR	Mean Time to Repair
MVAC	Medium Voltage Alternative Current
MVDC	Medium Voltage Direct Current
NLCC	Network Life Cycle Cost

NPC	Neutral Point Clamped
OFGEM	British Office of Gas and Electricity Market
OPEX	Operational Expenditure
PCC	Point of Common Coupling
PMSG	Permanent Magnet Synchronous Machine
RMS	Root Mean Square
SAB	Single Active Bridge
STATCOM	Static Compensator
UNFCCC	United Nations Framework Convention on Climate Change
VSC	Voltage Source Converters
WACC	Weighted Average Cost of Capital
XLPE	Cross-linked Polyethylene

GENERAL INTRODUCTION

The installation of offshore wind power is quickly increasing all over the world, contributing to reach the renewable energy targets, particularly in Europe. A significant part of the required assets is the necessary electrical network to collect, transport and inject the electricity to the national grid. Hence, the electrical infrastructure (connecting an offshore wind farm up to the onshore grid coupling point) has a large impact on the cost-effectiveness of offshore wind farm projects, approximately 17% of CAPEX according to the International Renewable Energy Agency [1] (IRENA). The Levelized Cost Of Energy (LCOE) measures this cost and is used to schedule the benefit return of industrials investments and the reduction of costs for the society.

As new offshore wind farm projects are further and further away from shore, the impact of the cost of the connection electrical network on the wind farm project profitability increases as well. Accomplished progresses in high voltage power electronic converters and their control make now efficient electrical conversions and lead to consider possible uses of DC waveforms in electrical networks under different voltage levels according to the transmitted power and economic interests. From an economic perspective, for distances above 100 km, the HVDC transmission technology can be more interesting than the HVAC one. In relation with these two HV technologies, various electrical architectures of networks can be considered. Among others, some of them could include MVDC collection networks.

Such large offshore wind farms represent themselves systems whose design must be optimized and particularly the internal electrical architecture (electrical energy collecting network), the connection to the on-shore electricity network and the behavior within this network in case of various faults. The main challenge then is to propose optimized architectures considering a set of various problems. Among these issues, the cost in terms of both investment (CAPEX) and operation (OPEX) appears to be a major contribution, especially considering the intermittent nature of the wind power production (even in the offshore context). In addition, the issues of the obtained global reliability (through redundancy) and availability of the proposed power system should be taken into account.

In this context, the technical and economical assessment of electrical network architectures is extremely complex. In simpler terms, one can ask, what is the best network architecture? This question raises several scientific challenges and associated problems. Some of them are relative to the modeling and assessment of the network, while the design of the network is a significant challenge.

To answer those questions, research activities have been performed by a partnership between the Laboratory of Electrical Engineering and Power electronic at Lille (L2EP) and the SuperGrid Institute at Villeurbanne, with the participation of the G2ELab from Grenoble Alps University, Grenoble INP. The work is dedicated to the modeling and optimization of architectures for supergrid networks. Objectives are to identify and evaluate relevant power system architectures, to define their functional requirements, inherent to their architectures, and to provide specifications associated with these architecture needs.

For that purpose, this thesis proposes systematic tools for the study and optimization of the architecture of the internal electrical network of an off-shore wind farm as well as the connection system to the on-shore network, considering the complete electrical system, from each elementary wind turbine to the connection point of the on-shore power grid. The proposed method has been developed and implemented through a stepwise approach. The design and sizing methods have been chosen to be generic enough so that they can be scalable and applied to various architectures with various technologies. The synthesis of the complete work into a rigorous framework is now the foundation of a decision based support system tool for investors to select the optimum electrical architecture for their projects.

The work presented in this PhD thesis is structured as follows (refer to Table 1):

- Chapter 1: Topology and definition of the considered network architectures. Review of methodological approaches associated to the modeling and evaluation problems. Description of decision criteria and required framework for the assessment,

- Chapter 2: Models and methods for calculation of wind power production and for load flow calculations. Description of the coupling method of the wind power calculation module, the load flow module and a probabilistic estimation method,

- Chapter 3: Cost models for components of the electrical network and for the wind turbines.

- Chapter 4: Novel methods for the fast and accurate reliability assessment of the electrical connection network,

- Chapter 5: Novel formulation and solving approach for a (near) optimal design of the electrical network,

- Chapter 6: Proposal of a methodology to take into account the uncertainties affecting the economic assessment of electrical network architectures.

Chapter 1 introduces in details the context of offshore wind power. It exposes a review of possible architectures for the electrical connection of offshore wind farms. This makes possible the selection of various architectures with which the methodological developments of this research must be compatible. Also, Chapter 1 proposes a review of the methodological approaches dedicated to the assessment of offshore wind farm networks. It notably raises the need for a near optimal design of an architecture network before any assessment can be done. Finally, Chapter 1 details the criteria, which will be used to compare economic interests and technical performances of various architectures.

Chapter 2 details the models and methods associated to what is called in this manuscript “wind power simulator” and “load flow simulator”. The “wind power simulator” encompasses the wind turbine production model. Calculations are executed over many (20-25) years in order to take into account technical variable operation points and, later asses the operational costs. Load flow simulators integrate detailed static electrical models of components. The later models are either used to determine parameters used in load flow calculations or used within a sequential load flow. The coupling of the load flow simulator and wind power simulator in order to calculate annual expected energies is detailed. Additionally, in

Chapter 2, an analysis of the network steady state power management is proposed and will simplify the design optimization (presented in Chapter 5).

Chapter 3 aims at obtaining cost models for each of the electrical network components and for offshore wind turbines. To achieve this goal, a gathering of cost data sources is done. Then, a method to determine data driven cost models is proposed. Analytical formulations of models are justified by expertise when possible. An identification method is used to take into account scenarios ("optimistic", "mean" "pessimistic").

After a state of the art of existing indexes and methodologies for the reliability assessment of offshore networks, the Chapter 4 proposes two novel methodologies to estimate the annual curtailed energy. Both methods are based on the use of

1) the constrained max flow problem applied to the electrical network

2) the probabilistic transfer theorem, which allows the estimation of the expected curtailed power for a given state of the network availability.

The first method allows a quick calculation of the expected value of the annual curtailed energy along the operating life of the electrical network. The second network is based on Monte Carlo simulations, where the states of the system availability are randomly generated. This last method allows the simulation of the stochastic process associated to the failures and repairs of components. Thus, it allows the determination of an empirical probability distribution of the annual curtailed energy.

With the models and methods from Chapter 2, Chapter 3 and Chapter 4, the assessment of electrical network architectures is possible if an architecture design is known. Assessing or comparing various architectures thus requires the determination of their designs. Accordingly, Chapter 5 proposes a novel formulation of the electrical network design optimization. The formulation is compatible with the various architectures, which are considered in the present research work. The formulation is based on a separation of the general design problem into sub-problems, which are then solved sequentially. The proposed formulation and associated solving methods allow a fast solving of the problem.

Finally, Chapter 6 proposes methods taking into account uncertainties which affect the assessment of network architectures. The first method, applying the Monte Carlo based method of Chapter 4 allows the analysis of uncertainties associated to the annual curtailed energy due to the reliability and its propagation to the economic criteria (LCOE or NLCC). With the second method it is possible to analyze the propagation of model parameter uncertainties to these decision criteria. To do so, a novel application of a result from the probability field is applied. It takes advantage of the fact that the LCOE can be written as a ratio of normal variables. The two methods are applied to an optimized design, obtained in Chapter 5.

Table 1: PhD thesis content

	State of the art	Proposed method	Case study
Chapter 1	Possible network architecture concepts for offshore wind farm connection. Methodological approaches for the assessment of electrical architectures		
Chapter 2	Models and methods for wind power production calculation, power components and load flow calculations	Sequential load flow integrating component models. Energetic quantification based on the probabilistic transfer theorem	
Chapter 3	Existing cost models and data	Least squares method for identification of cost model parameters taking into account uncertainties via scenarios.	
Chapter 4	Indexes for the reliability assessment. Existing simulation and analytical methods for reliability assessment. Reliability data collection	Two quick methods to estimate the annual curtailed energy. One for the expected value, the other to determine the empirical probability distribution	Reliability assessment of a benchmark architecture with few nodes to validate and compare the methods.
Chapter 5	Methodological approaches for optimization of offshore wind farm network architectures.	Formulation and solving method for the problem of optimization for the design of the complete electrical network	Application to the design of three architectures for three different wind farm sites
Chapter 6	Source of uncertainties affecting the cost-effectiveness of offshore networks	Methodology to study the propagation of uncertainties due to reliability and to model uncertainties up to the economic criteria	Analysis of uncertainties to one architecture design obtained in Chapter 5

Chapter 1: CONNECTION OF OFFSHORE WIND FARMS: CONTEXT OF DECISION SUPPORT FOR ELECTRICAL NETWORK ARCHITECTURES

1.1 Introduction

These last years, the cost of onshore wind projects has largely lowered and in the same time, the capacity factor of onshore wind projects has increased. Hence, the large scale development in the wind industry has brought the LCOE to a competitive level compared to that of the fossil fuel plants. However, the target remains a challenge for offshore wind industry.

Chapter 1 presents the economic and technological context of offshore wind farm projects. It introduces the subject of the PhD thesis and presents its objectives.

First, section 1.2 presents the global macro energetic context and opportunities for offshore wind power development. It exposes the factors, which impact the economic competitiveness of this power production means. In particular, it shows that the electrical network architecture connecting an offshore wind farm can impact the profitability of the project. Thus, the following question is raised:

How to assess and compare different architecture concepts and associated technological solutions?

Answering this question is not straightforward. Some important required elements are highlighted by state of the art analyses.

A primary required review is exposed in section 1.3, where a synthesis of architectures is proposed.

The section 1.4 presents the core of the research work, which aims to propose a framework for robust decision making of electrical network architectures. A state of the art regarding the existing studies for the assessment of architectures is exposed in section 1.4.1. In particular, it raises the need for a "fair" comparison of different architectures, as justified in section 1.4.2. The different criteria, which must be quantified in order to provide the required decision support are highlighted in section 1.4.3. The retained aggregating objectives for this work are presented in section 1.4.4.

Finally, the different models and methods, which are required for the quantification of the different decision criteria are presented. The general structure of the decision support framework developed within this work is exposed in section 1.4.5.

1.2 Macro energetic context in the world: opportunities and challenges for offshore wind power

1.2.1 Renewable energy targets, offshore wind context, macro factors

The global warming is now a widespread concern. In 1997, 37 countries signed the Kyoto Protocol, which has implemented the objectives of the UNFCCC (United Nations Framework Convention on Climate Change, 1992). The Kyoto Protocol commits the participants to binding targets for reduction of greenhouse effect gas emissions.

The first commitment period was between 2008 and 2012. Accordingly, the European Union Countries shared an overall target for a 8% reduction in tons of CO_2 equivalent. This self-imposed target was beyond

the 5%, which was given to the 15 European Union members by the Kyoto Protocol [2]. For the second commitment period (2013-2020), the European Union countries have agreed to meet, jointly, a 20% reduction target compared to 1990. To meet these objectives, the UE sets three targets to meet jointly:

- An energy efficiency target to drive the reduction of energy consumption,
- A renewable energy target to drive the increase of energy production from renewable sources,
- A greenhouse gas reduction target, which is the direct application of the Kyoto Protocol and is normally a result of the other two previous ones.

As stated on the European commission website, countries "(they) are on track to do so" [3]**.** The EEA (European Environment Agency) is tracking the progress towards Europe's climate and energy targets and has confirmed it by recent figures given in the report [4].

The story is still ongoing. Each year, the COP (Conference of the Parties) takes place within the UNFCC so to keep on discussing the need for the reduction of greenhouse effect gas emissions and to share the burden. The COP 21 took place in Paris in 2015 and gathered all the countries of the world so to set fair global targets.

As the reduction of gross energy consumption (particularly in the industry) was a key element of the reduction of gas emissions for the first commitment period, the introduction of more renewable power electrical production already played an important role. For the second commitment period and beyond, increasing the proportion of renewable energy in the energetic mix is a cornerstone, at global and European level.

In this context, wind power is a major renewable source. In 2009, the EEA (European Energy Agency) assessed the wind energy potential in Europe with a macroscopic methodology [5]**.** Main conclusions are:

- The technical potential is around 70 000 TWh/year, corresponding to around 15 TW installed (with an arbitrary capacity factor of 50%),
- The potential is reduced if we consider the environmental constraints (around 42 000 TWh/year, corresponding to around 10 TW installed with a capacity factor of 50%).
- The "economically competitive" potential is further reduced. The report estimates it at around 12 000 TWh/year (corresponding to an installed power of 2 780 GW with a 50% capacity factor) in 2020. These figures remain around 5 times higher than the European annual electricity consumption.
- The wind power potential is higher onshore than offshore. The latter remains high though (around 10 000 TWh/year, corresponding to around 2200 GW of installed power, with an assumed 50% capacity factor).

No more recent "official" figures have been found in 2017 on the wind power potential at the European level. Even in case these figures are optimistic, wind power remains a major electricity source to reach the targets for the reduction of emissions.

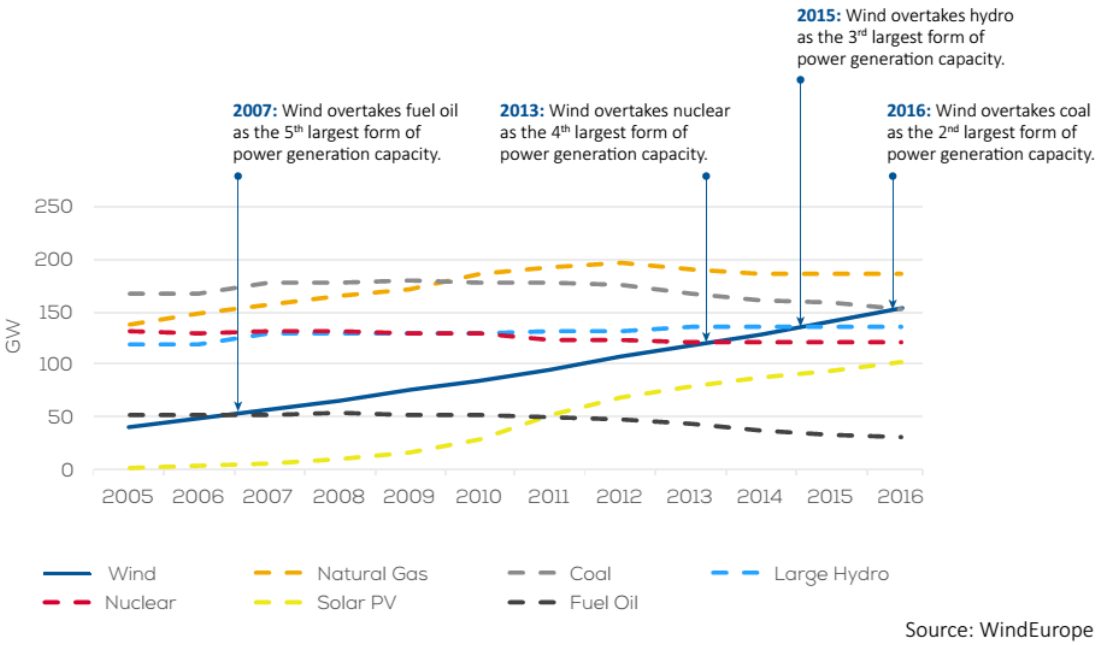

Figure 1-1: Installed power for electricity sources in Europe (2005-2016) [6]

The *Wind Europe* association (ex EWEA) states in its statistical report in 2016 [6] that the total installed capacity for wind power is 154 GW, with 12.5 of gross additional wind capacity in 2016. Wind power also represents the second electricity source in Europe in terms of installed power (see Figure 1-1). These figures are deep below the potential estimated by the EEA in 2009. Though the share of installed offshore power is limited, as shown in the "Wind Europe" report on offshore wind statistics [7], it is the subject of an important growth (see Figure 1-2). It can be explained by the fact that onshore wind power infrastructures are already installed at the most promising locations is Europe. In the same time and with the advantage of higher wind resources and a reduced intermittency, installed offshore wind power generation is rapidly increasing, contributing to reach renewable energy rate targets. ENTSO-E in 2011 considers that it could represent an installed power of 25 GW in 2020 and 83 GW in 2030 [8].

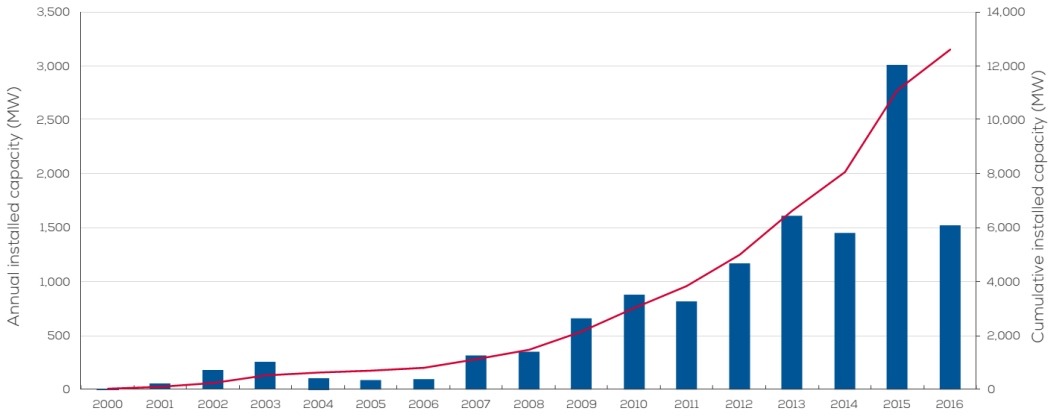

Figure 1-2: Annual and cumulative european offshore wind power installed in 2016 (statistics by Wind Europe [7]).

A very similar situation of offshore wind power important growth happens globally. It is highlighted by IRENA (International Renewable Energy Agency) in its innovation outlook report in 2016 [9]. This is because Europe is a world leader in offshore wind power installations (see Figure 1-3.)

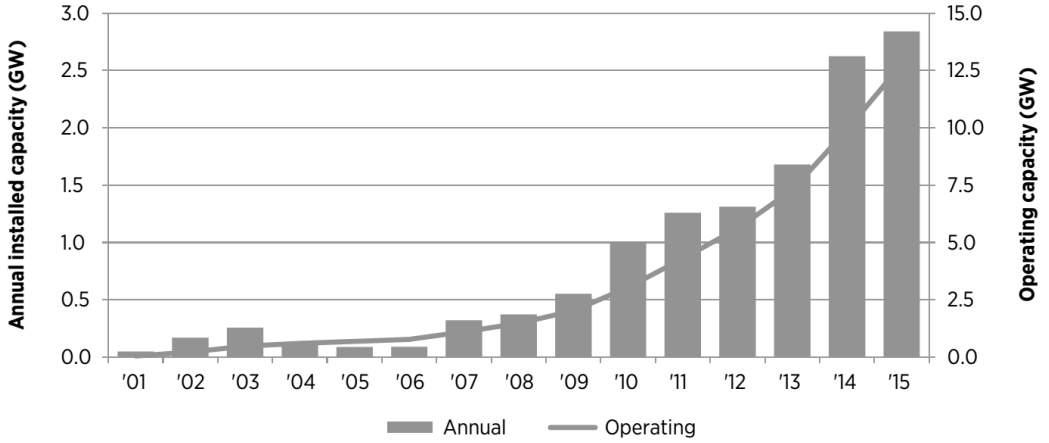

Figure 1-3: Annual and cumulative global offshore wind power installed in 2016 (statistics by IRENA [9]).

1.2.2 Offshore wind cost-effectiveness: role of general innovation and grid connection

As considered by the European Environmental Agency when assessing wind energy potential in Europe [5], the economic competitiveness of wind power is a key consideration to take into account. It is particularly true offshore, where the involved costs are higher a priori. Among other studies and in line with this observation, in Europe, the company DNV GL on behalf of *The Crown Estate* (UK, 2012) [10] and Prognos and Fichtner for *The German Offshore Wind Energy Foundation and partners* (Germany, 2013) [11] undertook studies on the cost reduction of offshore wind energy. The study of Prognos and Fichtner is based on a very similar methodology as the one undertook by DNV GL. The quantitative criterion used for assessing the cost of energy in these studies is the standard LCOE (Levelized Cost of Energy) (see (1-1)). IRENA (international, 2016) also undertook a similar study; quantifying the impact of various innovations for global offshore wind by using the LCOE [9].

$$LCOE = \frac{\sum_{t=1}^{N} \frac{I_t + O_t + F_t}{(1+r)^t}}{\sum_{t=1}^{N} \frac{E_t}{(1+r)^t}} \qquad (1\text{-}1)$$

where:

I_t: is the investment cost at year t

O_t: is the operating cost at year t; it includes at least maintenance

F_t: is the fuel cost of year t (zero for wind power)

E_t: is the produced energy at year t

r: is the discount rate

N: is the exploitation duration in years

The above mentioned studies have highlighted main factors which, can impact the reduction of the LCOE:

- The technological innovations relative to:
    - Support structures of wind turbines reducing I_t of equation (1-1)). For more details on support structures, see the book chapter on the matter [12]. The main technologies are depicted in Figure 1-4. As stated by IRENA [9]; jacket and monopile structures are the most used technologies. Floating structures are also considered today in order to exploit deeper sea sites [13].
    - Wind turbine rotor diameter increases, resulting to a lower specific cost of wind turbines (cost per MW installed).
    - Optimization of aerodynamics (efficiency of the wind turbines converting the kinetic energy into rotating energy) thus increasing E_t in (1-1)).
    - Innovation and optimization relative to the electrical system for the connection of offshore wind turbines up to the onshore grid. This is the core of the present thesis.
- The finance and the supply chain:
    - Weighted Average Cost of Capital (WACC), taking into account the risk of a project and corresponding to the discount rate r is used to compute the LCOE with (1-1),
    - The project planning in relation with finance,
    - The supply chain, in relation with the project planning.
- The wind farm maintenance methods.

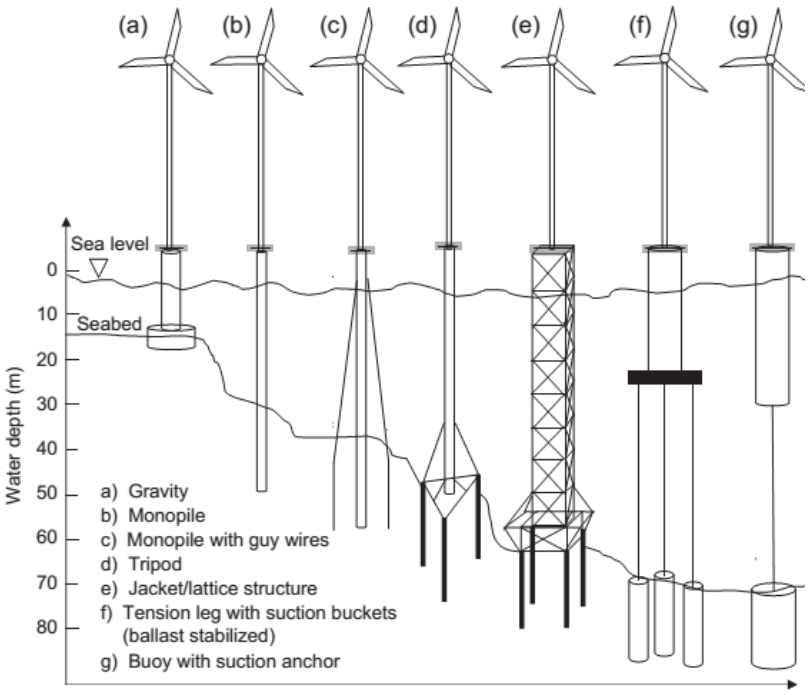

Figure 1-4: Offshore wind turbines support structure options [12].

Some factors impact the LCOE of a given project and are relative to the offshore wind farm site:

- The distance of the offshore wind farm from the shore (from the point of connection to the onshore grid), impacting the maintenance cost and energetic efficiency of the transmission electrical network from the wind farm to the shore.
- The water depth, impacting the cost of the wind turbines foundations and of the offshore substations platform foundations.
- The wind conditions (wind resources, velocity and occurrence), impacting the so called capacity factor [7] and thus, the annual produced energy (E_t).

It must therefore be understood that the reduction of the LCOE is the subject of innovations at different levels and places of the offshore wind industry. One can remember that "little brooks make great rivers". However, when the wind farm is far from the point of electrical connection with the onshore grid, the electrical network architecture accounts for a substantial share of the LCOE.

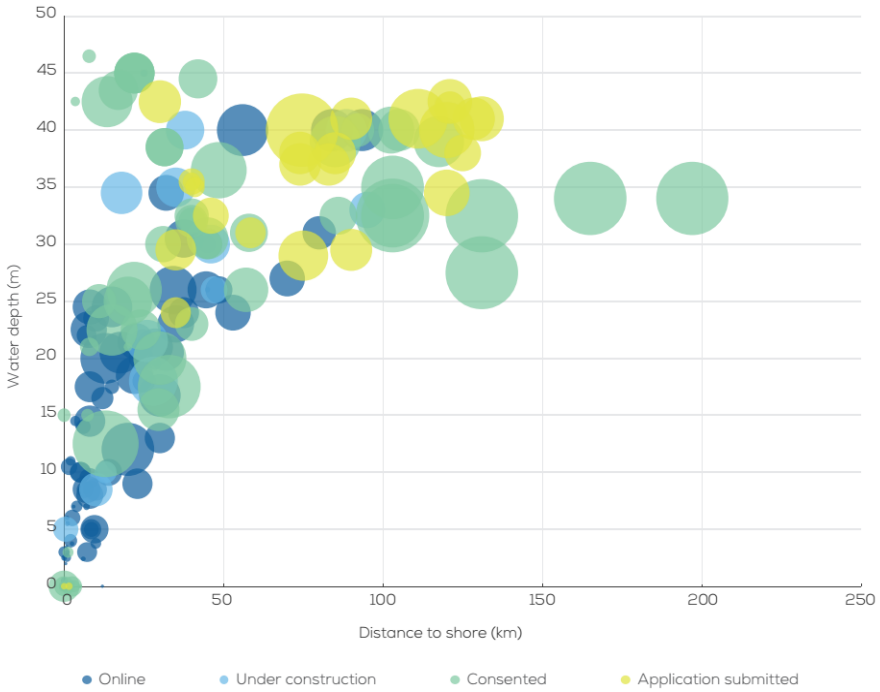

Figure 1-5: Water depth and distance from shore for offshore wind farms in Europe [7].

Moreover, the locations of offshore wind farms in Europe tend to be further from shore, as it can be found from Wind Europe statistics [7] (see Figure 1-5). In the above mentioned studies and in this thesis, the cost of the electrical network for connection up to the shore will be understood as the "shallow cost". It means that the cost of reinforcement of the existing onshore grid is not taken into account.

In 2016, major actors of the offshore wind industry co-signed a statement in June 2016 for offshore wind power cost reduction [14]:

"With the right build out and regulatory framework the industry is confident that it can achieve cost levels below €80/MWh for projects reaching final investment decision in 2025, including the costs of connecting to the grid . "

Already in 2016, some projects have been retained with LCOEs well below what was predicted by the different studies [10], [11] in 2012 and 2013. As an example, a LCOE target set by the study for The Crown

Estate [10] was 100£/MWh. Tis target has been reached on average in UK [15]. Besides, the study from Prognos and Fichtner [11] has concluded in 2013 that in the best case scenario, the LCOE could be of 82€/MWh in 2023. Well ahead of schedule, some projects in Europe were retained with LCOEs at the final decision in the tendering project well below expectations:

- Borssele I and II, Netherlands, cost of 72.7€/MWh [16]. The water depth is very low though, which naturally offers a low cost of wind turbines foundations [17]. The Danish government pays for the transmission and associated risks. The LCOE is therefore closer to 82 €/MWh.
- Krieger Flak, final decision retained for a LCOE of 49 €/MWh [18], excluding the cost of connection to the onshore grid.

The offshore wind industry is increasing its economic competitiveness and the LCOE is rapidly decreasing, even apparently sooner than expected. However, the system connecting the wind farms up to the onshore grid still has a potential for LCOE reduction. Moreover, in its "cost monitoring framework" report [15], the UK's organization "Catapult" points out that the transmission system for connecting the offshore wind farms is a subject of uncertainties.

As a result, within this state of the art work, some questions are asked:

- *What are the best network architectures and associated technologies for transmitting offshore power up to the onshore grid?*
- *How to assess them?*
- *How to optimize them whilst respecting the standard objective of minimizing the LCOE?*
- *For which site conditions?*

1.3 State of the art on electrical network architectures for offshore wind connection

Electrical networks for the connection of offshore wind farms (as depicted in Figure 1-6) must fulfil three functions:

- **Collect** power from the wind turbines. This function is performed by the collection network(s), sometimes referred to as the "inter-array" grid in the literature.
- **Export** the power from the wind farm clusters to the transmission network.
- **Transmit** the power to the onshore grid at the PCC (Point of Common Coupling).

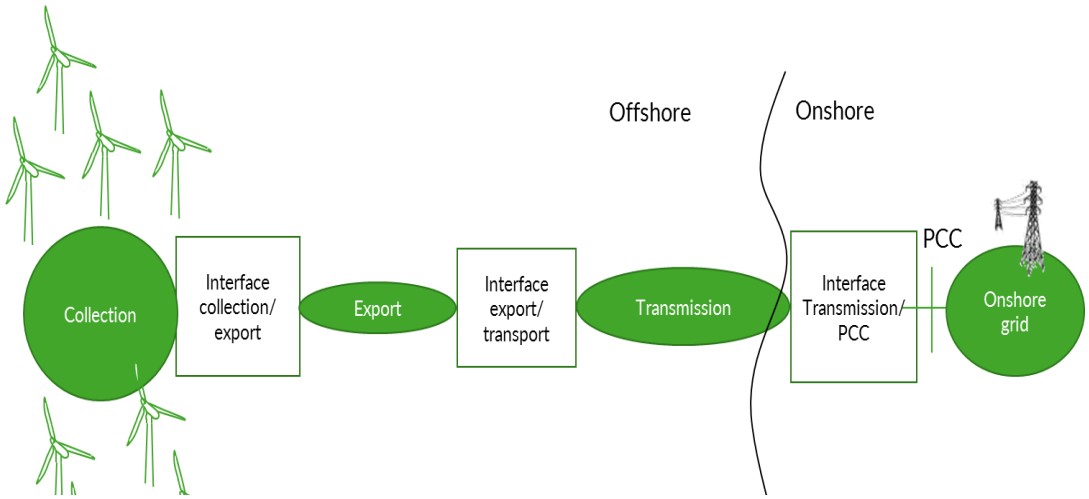

Figure 1-6: Virtual representation of the functions of the electrical network connecting an offshore wind farm.

The above described terminology is in line with the specialized literature on the matter. The distinction between export and transmission functions/grids is taken from De Prada et al. [19]. The distinction mainly aims at differentiating the HVAC (High Voltage Alternative Current) export grid from the HVDC (High Voltage Direct Current) transmission grid.

In practice, for some architectures, detailed in the next section, the export function can be fulfilled by the collection network. Similarly, the transmission function can be fulfilled by the export network.

In the remaining of this PhD thesis, unless stated otherwise, the "electrical network" designates the entire electrical network system, which connects the wind turbines up to the onshore grid.

To describe an architecture of the electrical network, some definitions are proposed:

- **An architecture concept** defines the current form (AC or DC) used for the power transfer and the voltage level (e.g. MVAC[1], HVAC[2], MVDC[3], HVDC[4]) for each electrical network which implements a function (Figure 1-6) (collection, export and transmission). Subsidiary, the architecture concept defines the function of the interfaces. Their primary functions are to adapt the current form when interfacing an AC network with a DC network and to adapt the voltage level. For a given architecture concept, if an interface does not have to fulfill any of these two functions, it means it will be considered that the downstream network (the further from wind turbines) function is fulfilled by the upstream network (e.g. the export function is fulfilled by the collection network as mentioned above).

[1] From 10 kV up to 66 kV

[2] Strictly above 66 kV (e.g. 132 kV, 150 kV, 220 kV)

[3] From ±10 kV up to ±80 kV

[4] Strictly above ±80 kV (e.g. ±150 kV, ±320 kV, ±500 kV)

- **The technological solution** corresponds to the definition of actual technologies that perform network functions and associated interface functions for a given architecture. In other words, the retained technologies for all the components must be defined so to fulfill the defined functions.

In the next sub-sections, a state of the art of some architecture concepts, which have been developed by the industry or found in the literature, is exposed. When they are well defined, some associated technological solutions are detailed. The architecture concepts and associated technological solutions are exposed, starting from the conventional and industrially deployed ones and going to the most innovative ones. An emphasis is put on offshore sites that are far from shore. As seen in 1.2.2, their electrical networks account for an important part in the LCOE. In this case, the uncertainties relative to the reliability, notably due to failures of a submarine cable can also be particularly high.

1.3.1 Variable speed technology for wind turbines

Modern wind turbine generators can be double fed asynchronous generators or permanent magnet synchronous machines (PMSG) [20], in cases technology operating is variable speed. It is necessary so to achieve an optimal conversion of fluid kinetic power into rotating power whatever the wind velocity. This optimal operation of the wind turbine is called MPPT (Maximum Power Point Tracking) [21]. In this work, an emphasis is put on PMSG wind turbines despite their main drawback: the use of rare earth element materials. It seems that there is a consensus in favor of PMSG from a technic and economical point of view, due to their efficiency and robustness [20], [22]. Each generator is connected to a collection electrical network by means of a conversion chain, comprising power electronic converters AC/DC/AC with an intermediary DC bus and a transformer (see Figure 1-7). The converter allows speed and frequency supply of the generator and the transformer adapts the voltage from low voltage to medium voltage.

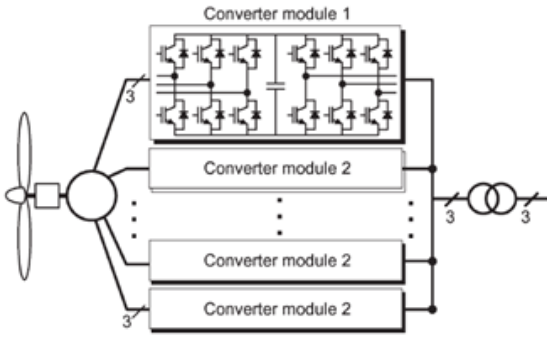

Figure 1-7: Converting chain for classical PMSG generators [20].

As shown in Figure 1-7, the trend up to now, to reach the power levels of wind turbines, is to put several converters in parallel so to keep on with the same mature technologies and with the advantage of possible degraded modes. However, multi-level converters are proposed as a serious alternative. Among multi-level topologies, 3-levels topologies [23] are considered such as the NPC (Neutral Point Clamped), which already exists in the industry (e.g. PCS 6000 from ABB). Whatever the technological solution, there is a requirement to remain connected to the grid in fault conditions. This can require energy dissipating devices (such as "braking resistor chopper") which thus prevent the DC bus voltages from rising above acceptable limits.

1.3.2 MVAC collection and HVAC export and transmission networks

The most conventional architecture concept is based on a MVAC collection at 33 kV or 66 kV for newly developed offshore wind farms [24] (see Figure 1-8), HVAC submarine cables up to 220 kV [25] for export/transmission. These collection and export networks are then interfaced with offshore substation(s) whose primary function is to adapt the voltage by means of classical transformers, thus aggregating the power to be exported. In addition to the transformers, the offshore substation(s) housed on offshore platforms comprise(s) bus bars, switchgears (MVAC and HVAC) and potentially shunt reactors for compensation of charging currents injected by long HVAC cables. Some shunt reactors (as in Figure 1-8) can also be installed onshore for compensation of the reactive power injected by the HVAC cables. Other compensation devices such as STATCOM [26] can also be considered if it is though necessary, notably for stability reasons, preferably onshore. Indeed, this architecture concept raises challenges for the stable operation of the overall network. Wind turbine must be able to operate connected on a network, which is sometimes qualified to be "weak" [27]. The transient stability of the network is not deeply analyzed within this work. However, these aspects remain important drivers in the selection of an architecture concept and associated technological solutions.

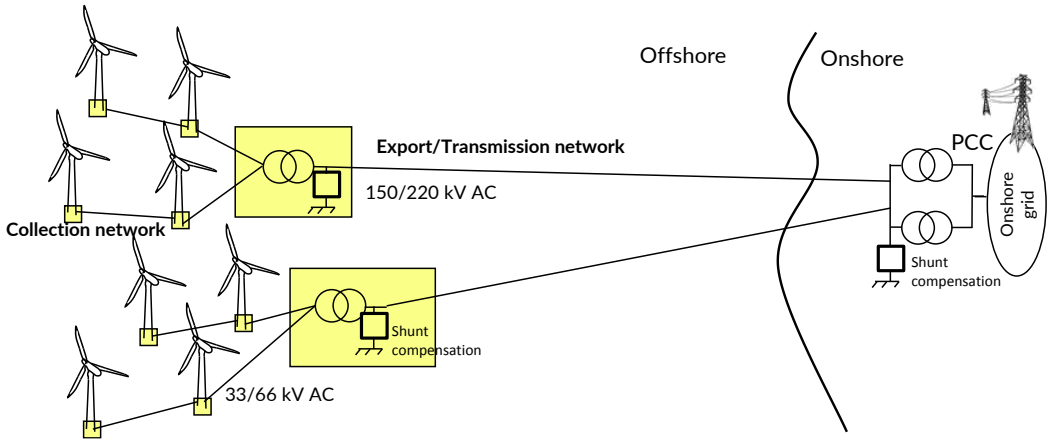

Figure 1-8: Conventional architecture concept (a): with MVAC collection and HVAC export up to the onshore grid

A recent innovation for HVAC export and transmission was proposed by Siemens in 2015 [28] and consists in housing the AC substations on wind turbines support structures rather than on dedicated platforms. The objective is to reduce the cost related to offshore platforms. To the author's knowledge, this innovation collides with acceptances issues related to the security: the wind turbine operators do not want to have high voltage components on their wind turbines where their maintenance technicians may work.

1.3.3 HVDC transmission network

1.3.3.1 Motivation for HVDC transmission

When the distance from the shore and more precisely to the point of connection with the onshore grid is important, the charging current injected along the HVAC cables can become substantial. The compensation of the resulting reacting current at ends of the HVAC cables can improve the operating conditions but the cables still have to be sized for the maximum current flowing though the cables at bottlenecks (the current

along the cable is no constant along the cable due to the charging current which is injected along the cable). For very long distances, the cable ampacity may be entirely "used" by the charging current and the cable cannot transmit active power. Even with distances below this extreme case, the cost-effectiveness of the solution can be affected by the growing cost of HVAC cables and compensation devices (direct cost and impact on offshore platform, plus the losses due to higher currents). In other words, the HVAC export and transmission networks can be uncompetitive in comparison with HVDC transmission networks [29].

The first advantage is that reactive power does not exist in DC. Thus, the current flowing in a DC cable contributes to transmit only (useful) active power. Moreover, skin effects, proximity effects and dielectric power losses can be neglected in DC. Another advantage of DC is that the insulation voltage (peak voltage) of DC cables corresponds to the RMS (Real Mean Square) voltage; while there is a decreased rate of $\sqrt{2}$ in AC. The drawbacks of HVAC are especially growing as the transmission distance increases. As a consequence, power transmission losses and cost of cables are higher in HVAC than in HVDC. The technic and economic analysis, for which the conclusion requires a comprehensive study (including investment costs, power losses and reliability for cables, transformers, HVDC converters and associated platforms) is often said to be in favor of HVDC for distances above 100 km. The precise figures depends on numerous factors including the wind farm peak power, the wind resources and others as stated in the CIGRE technical brochure on HVDC connection of offshore wind farms [30].

1.3.3.2 MMC based HVDC solution for transmission

In case of HVDC transmission network, the interface function between export and transmission networks (or between collection and transmission networks depending on the architecture concept), must be fulfilled so to convert DC currents into AC currents and adapt the voltage. Several technological solutions can be considered:

- Line Commutated Converters (LCC) [31] with thyristors or GTOs (Gate Turn Off).
- Voltage Source Converters (VSC), whose first existing topologies for HVDC were PWM (Pulse Width Modulation) 2-levels topologies [32], are now using Modular Multilevel Converter (MMC) [33].

The implementation of a LCC requires a reactive compensation equipment at the AC side. Additional STATCOM can also be used for dynamic reactive power compensation and power quality enhancement of the voltage [34]. But the MMC, which is free from the main drawbacks of the two-levels VSC (consequences from the 2-levels PWM: high power losses and need for bulky passive filtering of harmonics) is a better solution [30]:

- From a technic and economical point of view, due to a lower footprint than the LCC[5] [35] (which is a major driver offshore, where platforms are very costly).

[5] For a 1GW LCC pole substation, more than 8000 m^2 for the converter itself; to which the compensation devices must be added (see Figure 2.2 of CIGRE TB 492). Less than 5000 m^2 for a 1GW MMC substation (see Figure 2.7 of CIGRE TB 492).

- Technically, the MMC allows to emulate a HVAC voltage offshore so that the wind turbines can, in theory, operate as if connected on a classical AC grid. The onshore inverter MMC also allows better performances at the point of connection with the onshore grid: reactive power can be controlled continuously and independently with the active power [36].

As a matter of fact, the MMC solution is a future technology for electrical connection of offshore wind farms over long distance. For existing projects, including Dolwin beta in Germany [37], there are distinct HVAC export and HVDC transmission networks as depicted in Figure 1-9. There is one export connection for each cluster of wind turbines and associated AC platform as explained in Nowitech didactic document [38]. This architecture concept has the drawback to have several costly offshore platforms (one AC platform per cluster and one platform housing the MMC based converter station).

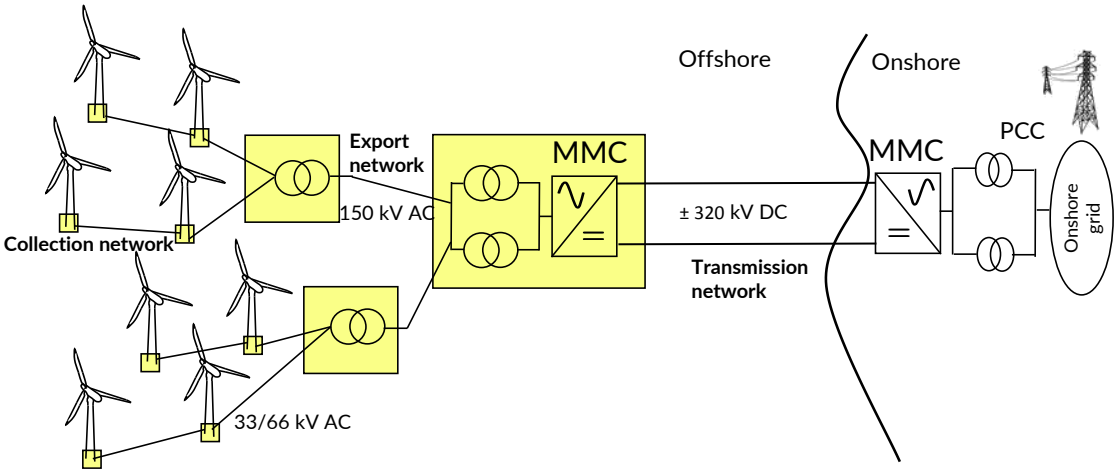

Figure 1-9: Architecture technological solution (b): MVAC collection, HVAC export and MMC based HVDC transmission.

1.3.3.3 MMC based HVDC transmission without AC platforms

One short term innovation can be to introduce a new architecture concept where there is no export networks. Thus, there is no AC platforms and the collection network is directly connected to the HVDC stations. It is realistic thanks to the introduction of 66 kV AC collection cables, which reduce the number of MVAC feeders that would be connected to the HVDC station [39]. Then, the number of HVDC stations can be a decision variable, as depicted in Figure 1-10 where two HVDC stations are represented.

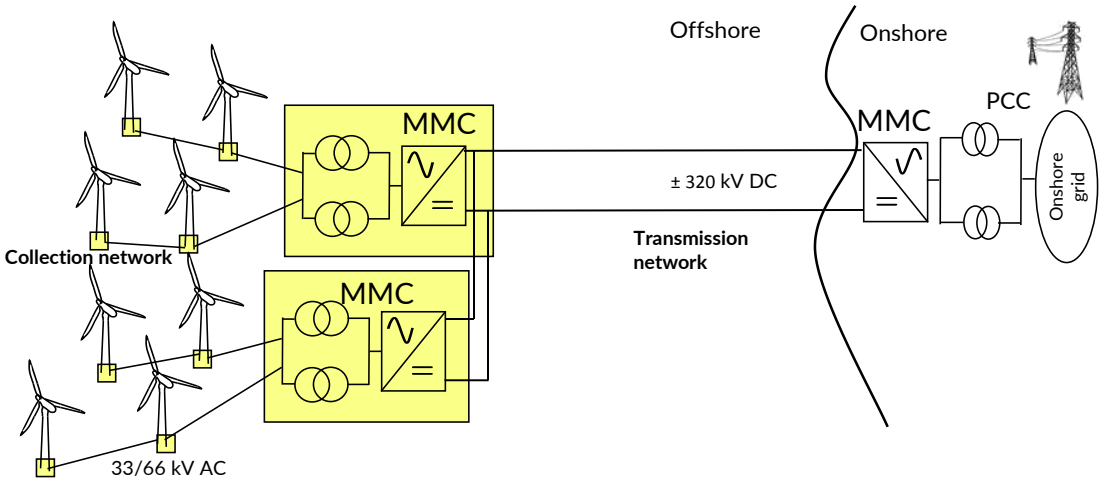

Figure 1-10: Architecture technological solution (c1): MVAC collection network(s) connected to MMC based HVDC transmission station(s).

1.3.3.4 HVDC transmission with modified interface with collection-export network

For long distances from shore, it is industrially shown that MMC based HVDC transmission is technically feasible. However, investment costs associated to the offshore HVDC converter station and to its associated platform are high and there is a motivation to look for cheaper solutions. In the medium term, the collection network will probably remain AC, at 66 kV, which will probably be widespread. The major advantages of MVAC collection are the high technological maturity, notably in regard to protection. Moreover, the wind turbine technologies are currently ready for connection to MVAC networks.

A medium term innovation aiming at reducing the cost of offshore platforms can be to modify the interface between the MVAC collection and the HVDC transmission. In that direction, Bernal-Perez et al. [40] propose a passive diodes rectifier associated to a transformer, which adapts the voltage in the interface between collection and transmission networks (see Figure 1-11). The interface between the HVDC transmission and the AC onshore grid can remain based on the MMC.

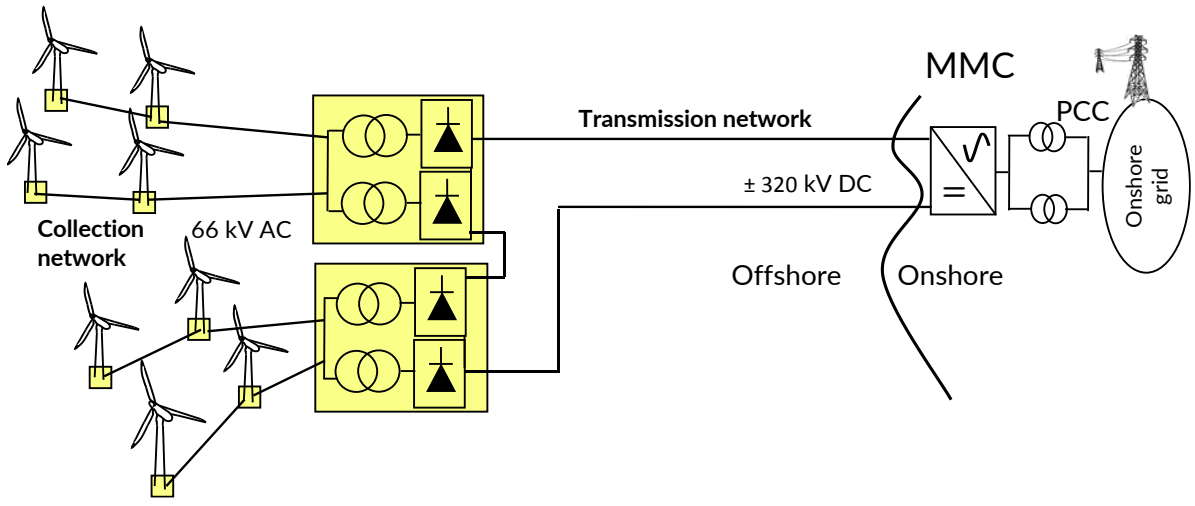

Figure 1-11: Architecture technological solution (c2): MVAC collection network(s) connected to the HVDC transmission network via DRU based converter station(s).

Beyond the cost decrease for HVDC platform(s), Perez et al claim that this solution has less power losses (mainly due to soft commutations at the collection network frequency). Moreover, the technological solution for the diode rectifier and associated transformer could be encompassed in oil filled container DRU (Diode Rectifier Unit), as proposed by Siemens [28] (see Figure 1-12). The robustness of such a solution would be high, with a reduced need for maintenance. The obtained volume, footprint and weight compared to a MMC would be highly reduced and also the investment costs (notably associated to the offshore platform). Siemens claims that a platform housing such as a HVDC converter would be of similar size of an export AC platform of the same power rating.

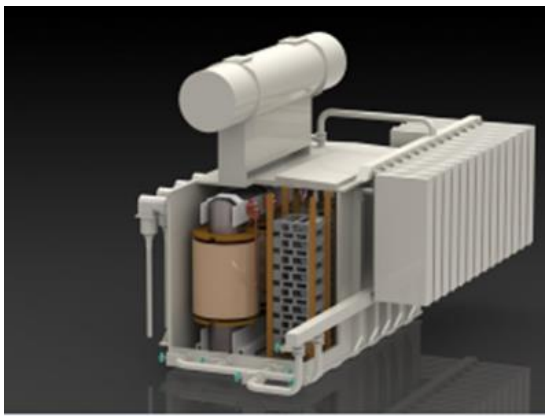

Figure 1-12: Diode rectifier associated to a transformer and encapsulated in a oil filled container (Siemens) [28]

However, the solution still has some challenges to take up. First, the obtained HVDC converter is not reversible in power. Thus, the auxiliaries must be supplied with another system. Siemens proposes to use an additional 66 kV cable from shore, which comes with additional investment costs to take into account. Moreover, the harmonics, which are generated by the DRU and injected to both the MVAC collection network and to the HVDC transmission network, can be a crucial issue. It depends on the number of pulses of the rectifier: Seman et al. [41] conclude without surprise that there are less harmonics with 12 pulses than with 6 pulses. The challenge regarding non-linear interactions and power management of the coupled MVAC and HVDC networks for this architecture technological solution remains.

1.3.3.5 HVDC transmission network and MVDC collection network

Several authors [19], [42] see the use of DC current for the collection grid as natural, in the continuity of what is employed for the HVDC transmission. However, the intrinsic advantages of DC does not make it straightforward to conclude on the cost-effectiveness of a MVDC collection network. This is because it depends on the technological solution employed to fulfill the interfacing functions adapting the voltage between a MVDC collection and the HVDC transmission. Meyer [43] thus refers to such a "DC/DC transformer" as a "key component" for which there are high uncertainties related to its cost, efficiency and reliability.

This being said and by considering the challenges encountered in regard to stability, harmonics and more generally, power management for MVAC collection networks, there are potential opportunities in considering "all-in DC solutions".

Choice of architecture concept with MVDC collection network

De Prada et al. [19] formalize well the different possible architecture concepts employing DC for both the collection and the transmission network:

- One possible architecture concept is to have a unique conversion stage MVDC/HVDC in the interface between the collection network and the transmission network (unique from functional perspective; it could have partial redundancies). This is the same principle as the one considered by Monjean [42].
- A dedicated export network with an intermediary voltage can also be considered. In this case, two interfaces would be required, one DC/DC converter between the collection grid and the export grid and another one between the DC export network and the transmission network. This concept corresponds to the "large DC wind farm" of Lunberg [44].

In the present work, it is considered that the savings in export cable costs and power losses are very unlikely to justify two interfaces, with additional high expenses and power losses. As a result, the architecture concept of Figure 1-13 is considered. A MVDC collection voltage in the range of ±50kV is considered because it corresponds to the insulation level of 66 MVAC cables. The exact magnitude of MVDC voltage remains a decision variable though.

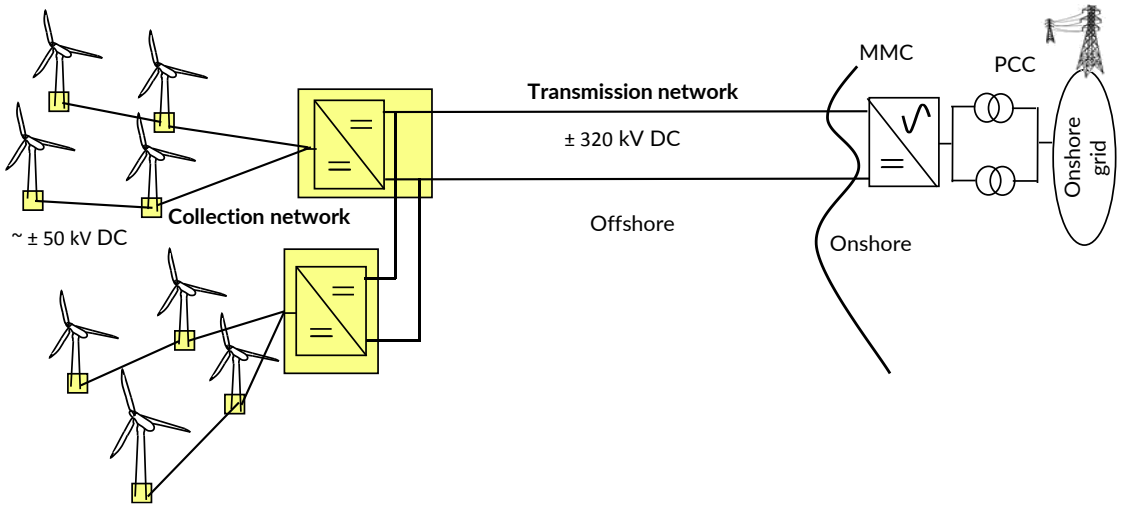

Figure 1-13: Architecture concept (d): MVDC collection and HVDC transmission interfaced by MVDC/HVDC converter station(s).

The number of MVDC/HVDC cluster converter stations is also a major decision variable whose optimum value depends on the technological solution for the MVDC/HVDC conversion (for instance, two in Figure 1-13). Another driver regarding whether going for a MVDC collection is related to the protection. Among others, the subject is tackled by De Prada [19]and Meyer [43], who both consider the cost of MVDC switchgears and its quantitative impact on the cost-effectiveness of a DC collection grid. Monjean [42] proposes an embryonic protection strategy and Ehnberg and Nordlander [45] propose an advanced protection strategy and associated analysis. ABB provides methods for the protection of "converter-based DC distribution systems" within a patent [46].

Potential technological solution for MVDC/HVDC conversion

The required function is to adapt the voltage of the MVDC collection network to the HVDC transmission network. As stated by Barker et al. [47], it is equivalent to the function fulfilled by a conventional AC transformer in AC but it is a novel technology in DC. It explains why the pioneer authors on the matter have considered solutions known for low or medium power, such as boost converters [48]. In practice, such solutions are not feasible for high power and high voltage applications. The technological challenge increases with the voltage elevation ratio. For the sake of synthesis, all the potential technological solutions of the literature are not exposed in the present PhD thesis. It also prevents from giving a delusionary impression of exhaustiveness. However, some key elements are given.

Robinson, Jovcic et al. [49] propose a DC/DC converter topology based on thyristors for power levels and ratio high enough but with a very low efficiency (95%, while, for comparison, the MMC has a 99% efficiency). Numerous authors consider a DC/DC conversion with an intermediary AC link with medium frequency transformer. Max [50] considers several topologies related to this principle: the SAB (Single Active Bridge) and the DAB (Dual Active Bridge). Among other authors, Monjean [42] and Lagier [51] consider the DAB or SAB or associated topologies (resonant or non-resonant). These technologies does not allow to reach the required MVDC and HVDC voltages levels and ratio. Other authors consider topologies inspired from the MMC. This is the case of the front to front MMC [52] or of the M2DC converter [53] which is a kind of multilevel chopper. More recently, Hu et al. propose an alternative multilevel topology [54]. The research on the matter is still ongoing. One objective of the present work is to prepare an agile framework allowing to assess any new technological solution for the MVDC/HVDC converter fulfilling the required function.

Adaptation of wind turbines for the connection to MVDC collection networks

An additional characteristic of architecture concepts employing MVDC collection is that it is disruptive in regard to the technology for the wind turbine power take-off. In other words, the wind turbine must be connected to a DC voltage and output DC current. Pan [55] exposes several principles allowing to do so, as depicted in Figure 1-14. The second principle seems complicated to perform because, according to the authors knowledge, the voltage level output for generators is difficult to increase above 5kV. This order of magnitude is very low for a MVDC collection voltage for wind turbines up to 10 MW [56]. The first principle of Figure 1-14 (“two stages”) is the one which is the most often considered in the literature. It is the case of Monjean [42]. It is preferred in the present work because it is the less disruptive in regard to wind turbines technology as the first conversion stages remain unchanged. However, the framework developed within this work does not depend on it and is agile enough to adapt to other principles such as the last one of Figure 1-14, where Pan et al. consider the use of a MVDC MMC. They claim that a low frequency operation is feasible [57] but the frequency considered for the generators suggests that it is highly disruptive for the generator drive train.

For a more exhaustive review of alternatives for wind turbines with DC output, Robinson et al. [49], and the review from Islam et al. [58] can be considered. For Doubly fed asynchronous machines, there are some

solutions which are proposed and even a patent [59]. Any solution has to fulfill the requirements which are related to the security and to the protection. It is thus very likely that any of the power take-off for DC output wind turbines will comprise a braking resistor.

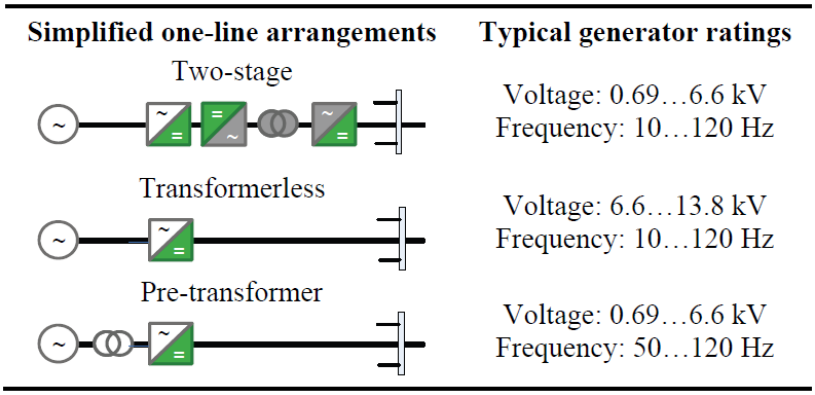

Figure 1-14: Principle for power take-off of DC output wind turbines [55]

1.3.4 MVDC collection and transmission network up to the onshore grid

As it is mentioned in sub-section 1.3.3.5, when considering a MVDC collection network, the design of a transmission network at a voltage different to the MVDC voltage raises the challenge of MVDC to HVDC conversion. As proposed by Lundberg in 2006 [44], considering a MVDC voltage from the wind turbine up to the onshore grid can have an interest for moderate distance from the onshore grid. Lundberg calls the principle "small DC wind farm". Pan et al. [55] also raise the principle as an alternative and calls it "MVDC direct to shore". TNEI [60] also considers this principle.

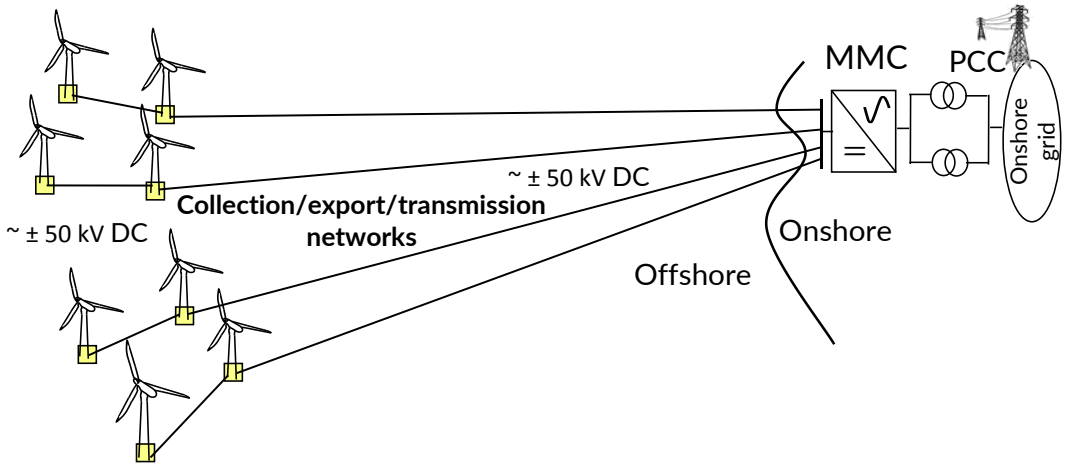

Figure 1-15: Architecture concept (e): MVDC collection network and direct transmission to the shore

In this work, this architecture concept is considered as depicted in Figure 1-15. The onshore, is a MVDC MMC and thus, putting several MMCs in parallels could be possible if the total power to transmit to the onshore grid is too high. An important driver with this concept is that there is no offshore platform if the connections can be done on simple bus-bars housed on wind turbines supports. Moreover, due to the low power losses occurring in DC, a MVDC cable has a substantial ampacity compared to an AC cable of the same

level of insulation. It can therefore transmit a substantial power. Key decision variables for this architecture concept are thus the MVDC voltage level (from around ±40 kV up to ±80 kV), and the number of wind turbines per feeder (which determines the cross section of a MVDC cables fulfilling the transmission function).

The question of wind turbines with DC output remains unchanged in comparison with what is exposed in the previous sub-section. The protection strategy and associated components (such as DC circuit breakers of disconnectors [61]) of such a MVDC grid must be defined. The decision of the MVDC voltage must be done in relation with these considerations, which are more challenging as the MVDC voltage level increases. In the same time, the advantage of increasing the voltage is to reduce the cross sections of MVDC cables and thus their costs. Finally, this is an innovative architecture concept for medium terms with a limited maturity. It must be further investigated as it comes with appealing potential costs savings.

1.3.5 Series based MVDC collection network

The reader can wonder why the series connection of DC output wind turbines (see Figure 1-16) is not considered in the present work. It is indeed considered by several authors [42], [44], [62–64] for the main reason that it theoretically avoids the offshore platform and that series connected wind turbines can directly output an MVDC or HVDC voltage. However, it was considered here that there are too many uncertainties related to this architecture concept. Among others, the main critical points are:

- the voltage balancing between the series connected wind turbines;
- As shown by Monjean [42], the reliability is thought to be low because of series connection of the wind turbines: the loss of one wind turbine or cable of a string results to the loss of the whole string.

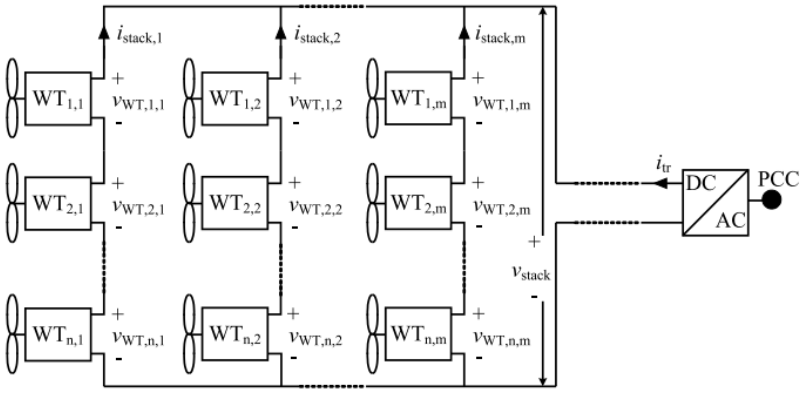

Figure 1-16: DC electrical system with series connected wind turbines. [44]

1.3.6 Synthesis of selected architecture concepts

With this state of the art, there is no claim for exhaustiveness. Indeed, the literature is very rich and still growing, particularly when it comes to the technological solutions (e.g. for DC/DC conversion).

The different architecture concepts presented in the previous sections are depicted within the single line diagrams of Figure 1-17.

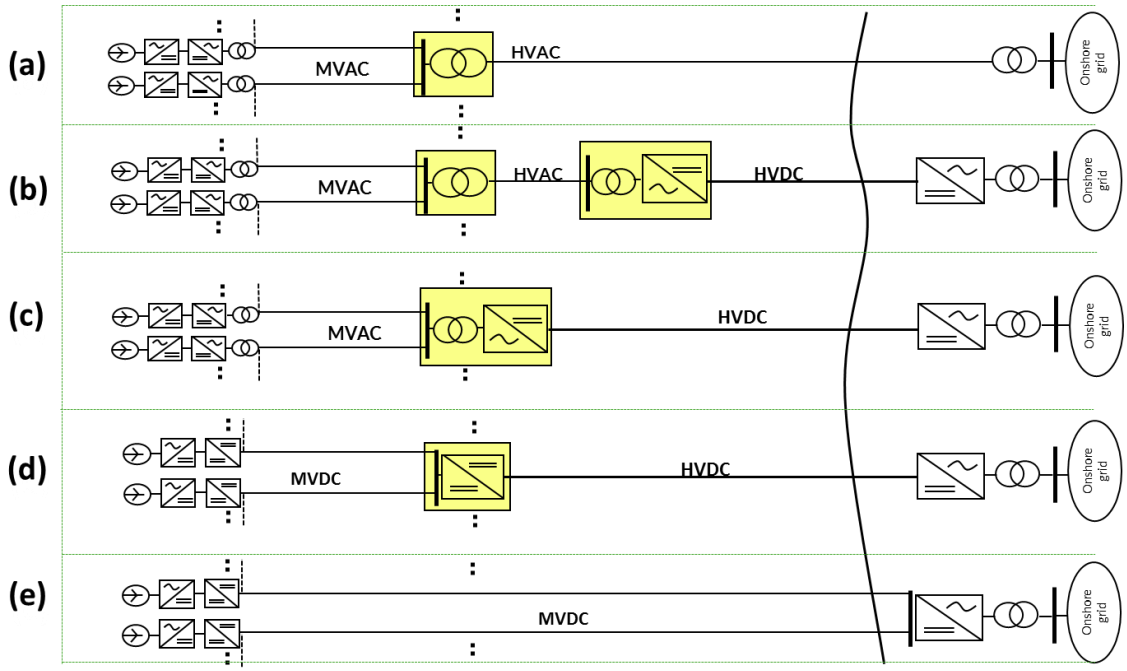

Figure 1-17: single line diagrams for the various architecture concepts considered within this work

The architecture concept (c) corresponds to two different selected technological solutions:

- (c1) MVAC collection and HVDC MMC based transmission network without dedicated export network (case represented for principle (c) in Figure 1-17).
- (c2) MVAC collection and HVDC DRU based transmission.

The assessment framework developed within this work is compatible with all these architecture concepts. It must also be flexible in order to be adapted to different architecture technological solutions.

1.4 Towards a framework for robust decision making of electrical network architectures

Some architecture concepts have been exposed in the previous sections. However, the question remains:

How to assess and compare different architecture concepts and associated technological solutions?

Answering this question is not straightforward. However, some authors tackled the issue and thus, in the next sub-section, a state of the art of the existing studies assessing architectures for the electrical connection of offshore wind farms is exposed.

Then, the need for a "fair" comparison of different architectures is justified. The different criteria which must be quantified in order to provide the required decision support are highlighted. The retained aggregating objective for this work is presented.

Finally, the different models and methods, which are required for the quantification of the different decision criteria are presented. The general structure of the decision support framework developed within this work is exposed.

1.4.1 State of the art on the assessment of architecture and associated technological solutions

There is a clear scientific richness in the literature on the assessment of different architectures for the electrical connection of offshore wind farms. Therefore, it is challenging to faithfully account for the existing contributions on the matter. The main objective of this state of this art is to raise the scientific opportunities for the present PhD thesis so to then bring a humble stone.

Bauer et al. [48] (2000), Lazaridis and Ackermann et al. [65], [66] (2005) and Lundberg [44] (2006) are pioneers in the assessment and comparison of architecture concepts for electrical connection of offshore wind farms.

Bauer et al. [48], [67] developed a framework resulting to an assessment tool "eEFarm" so to compare architecture concepts. A comprehensive framework allowing to assess power losses, energy unavailability, investment costs and wake losses between wind turbines have been developed in the Matlab Simulink environment. Similarly as for Lundberg [44], the chosen technological solutions that were once selected are now questionable (e.g. boost converter for MVDC/HVDC conversion and two-levels VSC for AC/DC HVDC). However, over the years, the work kept on progressing until a very complete framework, which includes a holistic optimization of the wind farm [68]. To the author's knowledge, innovative architecture concepts are not taken into account though, and the reliability is not taken into account.

Lundberg defines and compares architecture concepts in an abstract manner by defining his own architecture concepts ("small AC", "large AC", "AC/DC" and "large DC"). In his work and especially in posterior contributions citing him, the retained technological solutions are not highlighted. It can be misleading because his conclusions are about technological solutions, which are considered for the different architecture concepts. For instance, the assessment that he performs on "large DC" principle is based on a 2-levels VSC HVDC converters, which have a lower efficiency than recent MMC HVDC converters. A "large DC" wind farm based on MMC is therefore more cost-effective.

Stamatiou [69] aims at comparing architecture concepts, with an emphasis to principles with the MVDC collection. In accordance with Meyer [43], who writes that some "key components" (DC/DC converters and DC breakers) drive the conclusion on the cost-effectiveness of MVDC collection, Stamatiou reminds that it depends on the chosen technological solution. The dependency to the models (costs and losses) and associated parameters/data leads him to a sensitivity analysis, unfortunately without a general conclusion. Similarly, De Prada et al. [19] undertake a technical and economic feasibility analysis of the DC collection by comparing it with the AC collection network (HVDC transmission in both cases) ending with a sensitivity analysis, which still does not make it possible to conclude. Bahirat [62] also assesses different architecture concepts including series connection of DC wind turbines, sometimes without basing the quantitative analysis on any technological solution: for instance, he writes "A DC-DC converter with power rating of 350 MW is assumed in this design".

Holtsmark, Bahirat et al. [63] perform a comprehensive comparative analysis of different architecture technological solutions for the electrical system connecting offshore wind turbines to the onshore grid. They

compare the MVAC collection network with HVDC transmission network with two different technological solutions corresponding to the same architecture concepts: series connection of DC output wind turbines and HVDC transmission. Their objective is to highlight the advantage of the matrix converter in place of back to back two-levels converters in wind turbine power take-off. Few details on the design of the overall system or on the assessment models are given. It is therefore not possible to reuse the work beyond the very same context as the studied one.

Ackermann et al. [65] limit the scope of their study to the assessment of technological solutions for the export/transmission network (excluding the collection). They compare with quite accurate models HVAC and HVDC transmission network. However, one can wonder why they retained LCC technology for AC/DC conversion in HVDC transmission case. The reliability of the two alternatives considered is taken into account but the choice of overall decision objective is questionable (ratio between the actual energy transmitted over the energy which is produced by the wind turbines over a year). The overall system including the collection grid is not included in the framework. The conclusions may change because the collection network(s) depend(s) on the actual location of the offshore subsation(s) in the wind farm.

Ali [70] has developed a very complete theoretical framework along with a software tool for the comparative assessment of various electrical network architectures. He takes into account wake effects, investment costs, reliability and power losses. The tool allows to investigate the design of the architecture for different principles and actual technological solutions (MVAC collection and HVAC or MMC based HVDC transmission) and has been presented by Siemens. One limitation is that the design of the network must be defined manually by settings the number of decision variables. In consequence, the time consuming to assess innovative prospective architecture concepts and associated technological solutions is very important.

Gonzalez et al. [71] perform a complete comparison of different architecture concepts for the transmission network by taking into account the losses, the investment costs and the reliability. The studied electrical system is limited to the transmission network.

Nieradzinska and Bell et al. [72] assess different designs of MMC based HVDC transmission network for the connection of the Dogger Bank offshore wind farm. The study does not aim at raising generic conclusions beyond the scope of this project. Elliott and Bell et al [73] undertake a “comparison of AC and HVDC options for the connection of offshore wind”. They include a quantitative technical and economic analysis for mature architecture concepts. They assess the impact of the two options on the stability and fault behaviour of the onshore Britain network on the basis of a case study.

Lakshmanan et al. [74] compare the use of a MVDC collection network with a MVAC collection network associated to a HVDC transmission network. An accurate quantitative comparison is made, on the basis of the investment costs and annual energy losses. The protection challenge is tackled. However, the analysis does not take into account the reliability of the system. The paper, again, cannot give a final conclusion due to the uncertainties in regard to the cost and efficiency of DC/DC converters.

Beyond the above presented state of the art, Rodriguez and Bauer et al. [68] provide a very complete review and analysis of the existing softwares, which exist for the planning and assessment of wind farm projects. OpenWind, WAsP, WindFarmer and WindPRO are examples of such softwares. The emphasis in most of these software is not on the electrical network design and selection.

In most of the above exposed contributions, for a given architecture concept and an associated technological solution, the design of the electrical network is not detailed and it could be sub-optimal. It can happen to distort the conclusion on the comparative assessment of different alternatives.

1.4.2 Opportunities for the assessment of conventional and innovative architecture concepts

In relation with the state of the art regarding studies for the assessment of different architectures, it appears that:

- It is possible to conclude on the cost-effectiveness of a given architecture concept (e.g. AC or DC for collection/export/transmission networks) provided that the technological solution used at the interfaces between those networks is specified (e.g. MMC or DRU for rectifying function from AC to DC between those networks).
- For a given architecture concept and an associated technological solution, the design of the network must be (near) optimal so that the assessment is “fair”. For instance, if the collection grid is sub-optimally designed, the cost of collection cables and associated power losses are high and the conclusions can be biased. These considerations are schematically represented in Figure 1-18. As a result, an optimization formulation, generic in regard to the different architecture concepts, is developed in this work. The formulation detailed in Chapter 5 takes into account the whole system and can be used for pre-planning or planning of actual offshore wind farm projects.
- Due to the bad knowledge, notably regarding investment costs and the reliability of “key components”, some sensitivity analyses can be required. However, if the range of variation of parameters, which are subject to uncertainties is high (e.g. above 50% of variation), it seems disputable to perform a sensitivity analysis, which would not bring much information. Moreover, the use of an adapted assessment objective can help in the understanding of the contribution of the different components in an architecture to the overall cost-effectiveness.

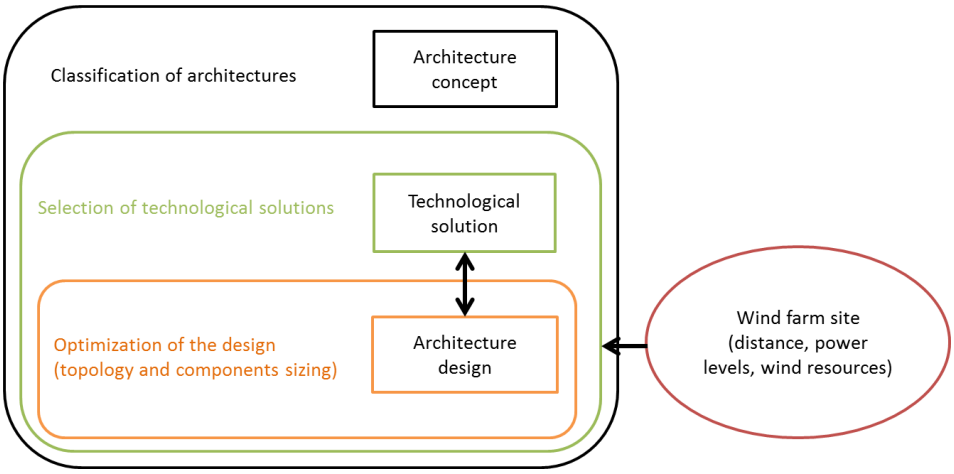

Figure 1-18: Decision support considerations for an architecture concept and associated technological solution.

1.4.3 Quantitative criteria for the decision support regarding the architecture of the electrical network

In accordance with the state of the art exposed in the section 1.4.1, from a quantitative point of view, the different criteria, which must be taken into account in the decision making for the selection and design of the electrical network architecture are:

- The CAPEX (CAPital EXpenditure) of the system;
- The maintenance costs of the system;
- The reliability of the system;
- The power losses dissipated throughout the system.

For the sake of simplicity, a schematic representation of the electrical network system S connecting an offshore wind farm to the onshore grid is depicted in Figure 1-19. It describes cost and energetic indexes that should be taken into account whatever the architecture concept is considered. The system S takes into account the collection, export and transmission networks and associated interfaces when applicable. A given architecture concept with associated technological solution depends on design variables encompassed in the vector variable X *(detailed in the Chapter 5).*

The wind turbines are assumed to be selected a priori, thus, their total CAPEX C_C and their OPEX (Operational Expenditure) Oc_t do not depend on X. However, the maintenance costs Oc_t can potentially vary over the years. A given year is designated by the subscript t. The total annual energy produced by the wind turbines AEP_0 does not depend on X neither: it depends on the wind resources and on the wind turbines power characteristic. This is detailed in Chapter 2. It means that AEP_0 is the hypothetic energy that is produced annually by the wind turbines if the system S is perfectly reliable.

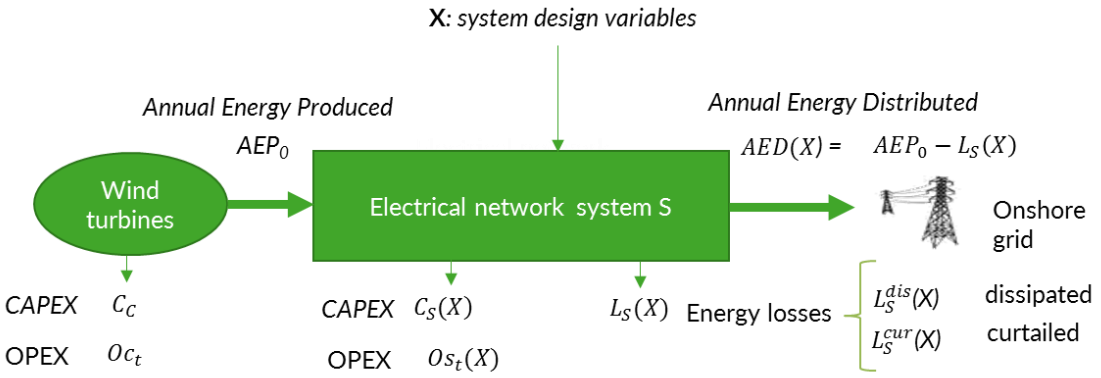

Figure 1-19: Schematic representation of the electrical network system connecting an offshore wind farm to the shore and definition of elementary indexes.

The electrical system S has an investment cost $C_S(X)$ obviously depending on its design X. Each year t, a maintenance cost $Os_t(X)$ is introduced. S also induces annual energy losses $L_S(X)$. The latter is separated into two kinds of energy losses:

- The energy losses, which are dissipated by the power components of the system $L_S^{dis}(X)$;
- The energy losses corresponding to a curtailed energy due to the component unavailability $L_S^{cur}(X)$. It is a measure of the reliability of the system S (which inherits the reliability of its components, depending on its topology).

These two kinds of energy losses are obviously linked to $L_S(X)$ by (1-2).

$$L_S(X) = L_S^{cur}(X) + L_S^{dis}(X) \quad (1\text{-}2)$$

Following a conservation principle, the annual energy, which is distributed/injected to the onshore grid $AED(X)$, is given by the equation (1-3).

$$AED(X) = AEP_0 - L_S(X) \quad (1\text{-}3)$$

An additional index, which is often used as an indicator of a wind farm profitability, is the capacity factor [7], [10], [14]. It is defined as the ratio between the annual energy, which is actually produced, divided by the energy, which would be produced if the wind farm operated at its peak power during the whole year. It is named $CF(X)$. It is a function of X because it depends on the availability of the system, itself depending on its design. $CF(X)$ can be calculated from the above defined indexes by using (1-4), where T_{year} is the duration of one year and P_{peak} is the installed power of the wind farm.

$$CF(X) = \frac{AEP_0 - L_S^{cur}(X)}{P_{peak} \cdot T_{year}} \quad (1\text{-}4)$$

1.4.4 Technical and economic objectives for decision making

To provide a support for decision making, two main approaches can be considered:

- Using a multi-objective approach. Among others, Brisset [75] uses a multi-objective optimization formulation for the design and optimization of power components. A multi-objective dominant

solution is a solution in the neighboring of which it is not possible to improve any of the objectives without degrading one of the others. The set of dominant solutions is called a Pareto front. In the context of offshore wind farms with many objectives corresponding to criteria among those presented in the previous sub-section, Rodriguez and Bauer et al. [68] argue that it allows to leave the decision to the decision maker. They argue that the optimization engineer does not have the expertise to give relative importance to the criteria. A practical example in power systems is to associate a weight (a cost of energy) to energy losses (e.g. L_S^{dis}) so that is can be compared to an investment cost (e.g. $C_S(X)$). A multi-objective analysis or optimization requires substantial computational resources and is mathematically challenging, though some powerful algorithm for solving multi-objective problems have been developed (such as NSGA-II [76]).

- Another approach is to use a unique objective, which aggregates the elementary criteria. Obviously, the choice of such an objective requires an expertise. Several mono-objective candidates for the present problem are considered in the literature and Rodriguez and Bauer et al. [68] provide, again, a very complete state of the art on the matter. Among them, the NPV (Net Present value), and the ROI (Return On Investment) are widespread project oriented objectives [71], [77]. As also highlighted in section 1.2.2, Rodriguez states that the LCOE is an unbiased objective unlike most of the others. However, he states that the LCOE depends on parameters such as financial ones whose values thus affect the decision.

With the criteria defined in the previous sub-section, the LCOE of the whole system including the electrical network can be calculated with equation (1-5).

$$LCOE_{N,r}(X) = \frac{C_S(X) + C_C + \sum_{t=1}^{N} \frac{Oc_t + Os_t(X)}{(1+r)^t}}{\sum_{t=1}^{N} \frac{AED(X)}{(1+r)^t}} \quad (1\text{-}5)$$

where:

r is the discount rate, corresponding to the WACC (Weighted Average Cost of Capital)

N is the number of years the system is exploited

$C_S(X)$ is the CAPEX of the electrical network S

C_C is the CAPEX of the wind turbines

$Os_t(\boldsymbol{X})$ is the annual OPEX of the electrical network S

Oc_t is the annual OPEX of the wind turbines

AEP_0 is the annual energy produced by the wind turbines

$L_S(X)$ is the annual energy losses in S

$AED(X)$ is the annual energy distributed to onshore grid

In practice, the LCOE is considered as the reference objective in this work because it is stated as a reference in the offshore wind industry. Moreover, the choice for a mono-objective approach allows to take into account the available expertise in solving the optimization problem formulated in Chapter 5 and corresponding to the design optimization.

The number of years of operation and the discount rate are parameters which affect the decision. The discount rate can notably depend on the investor (between 6% and 10%). The number of years of operation can depend on the investor but also on the regulation framework.

One drawback of the LCOE objective is the obtained difficulty to analyze the impact in the choice of decision variables relative to the design of the electrical system. Indeed, for a given offshore wind farm site, modifications of the electrical network architecture concept and design do not modify substantially the LCOE. Moreover, the use of the LCOE alone makes difficult the analysis of the share in CAPEX, of reliability and dissipated losses for the various components of the system in a way that these quantities can be compared.

A new criterion is thus introduced: the Network Life Cycle Cost (NLCC), given in (1-6).

$$NLCC_{N,r}(X) = \left[\sum_{t=1}^{N} \frac{1}{(1+r)^t}.AEP_0\right].LCOE_{N,r}(X) - \left[C_C + \sum_{t=1}^{N} \frac{Oc_t}{(1+r)^t}\right] \qquad (1\text{-}6)$$

The NLCC is equivalent to the $LCOE_{N,r}(X)$ by definition because the relation between the two criteria is affine, with a strictly positive coefficient. The idea is to multiply the LCOE with a coefficient corresponding to the total discounted energy, which would be produced in N years if the electrical system was having no power losses $\sum_{t=1}^{N} \frac{1}{(1+r)^t}.AEP_0$. The obtained quantity is then homogenous to a total discounted cost that would be spent over the N years. Then, the total discounted costs, which are not affected by the design of the electrical system, $C_C + \sum_{t=1}^{N} \frac{Oc_t}{(1+r)^t}$, are subtracted to the obtained quantity, to get the NLCC. This transformation aims at keeping the new criterion equivalent to the LCOE while proposing a wider domain of variation in regard to the choice of electrical network.

Besides, it can be shown by introducing (1-5) in (1-6) and then using (1-3) that the NLCC can be written as in (1-7).

$$NLCC_{N,r}(X) = C_S(X) + \left[\sum_{t=1}^{N} \frac{1}{(1+r)^t}\right].\left[LCOE_{N,r}(X).(L_S^{dis}(X)+L_S^{cur}(X)) + Os_t(X)\right] \qquad (1\text{-}7)$$

This expression is more appropriate to the classical representation of performances that are used in power systems. Moreover, it is based on a linear weighting of several elementary criteria: the CAPEX, the levelized cost of energy losses and the levelized cost of maintenance of the electrical system. Last but not least, another advantage of the NLCC with (1-6) is the additivity property of the criterion, which allows to visualize breakdowns. It makes it a powerful objective and indicator for analysis in a complex and uncertain context.

1.4.5 Synthesis: Decision support framework methodology and tool structure

A theoretical framework for decision making in co-planning of offshore wind farms along with its grid connection is proposed, with an emphasis on the detailed network electrical architectures. The structure of the framework is depicted in Figure 1-20. It is implemented into a software developed in the Python language [78]. The flexibility of the tool is a strong requirement as the goal is the assessment of different

architecture concepts and associated technological solutions, including those presented in section 1.3. For a given **wind farm site,** the framework should quantify the above mentioned criteria and objectives for a network architecture designed on the basis of a given **technological solution**. To achieve it, several scientific developments are required to build modules of the framework structure (depicted in Figure 1-20):

- A near optimal design of the architecture is done by **design heuristics**, which solve the network design optimization problem. The latter is formalized and the heuristics for the designs are presented in Chapter 5. The obtained architecture design is mathematically described by the variable vector X. In the Python environment, the architecture is represented by a graph whose edges and vertices are components (using NetworkX library [79])
- For a given wind farm site, a **wind power simulator** computes the power produced by the wind turbines depending on the wind velocity. It is detailed in Chapter 2.
- A **load flow simulator** is used so to perform the operational simulation of the electrical network and allows, in relation with the wind power simulator, the quantification of electrical quantities and associated annual energetic quantities. The load flow simulator (associated with models and calculation method) for the coupling with the wind power simulator is presented in Chapter 2.
- A **CAPEX evaluator** is used for the computation of investment costs for the designed architecture and of the overall wind farm. It relies on cost models developed and exposed in Chapter 3.
- Then, an **aggregated objective(s) calculator** computes the decision objective(s) exposed in the previous sub-section. It makes it possible to modify the financial parameters and other costs which are subject to uncertainties.
- So to achieve a robust design of a network architecture, a **reliability simulator** computes reliability indexes (notably $L_S^{cur}(X)$). With the reliability simulator, it is possible to compute the expected value of $L_S^{cur}(X)$ or an associated empirical distribution function. These methods are exposed in Chapter 4. Accordingly, the expected values or empirical distribution of decision objectives are computed by the aggregated objective(s) calculator. It allows the provision of a decision support framework taking into account the risk as in [71], [80].

The uncertainties related to the investment costs of the components for an architecture are taken into account by the use of the NLCC, which allows a powerful visualization of the costs. The matter is also the subject of a section in the Chapter 6 in which uncertainties are taken into account.

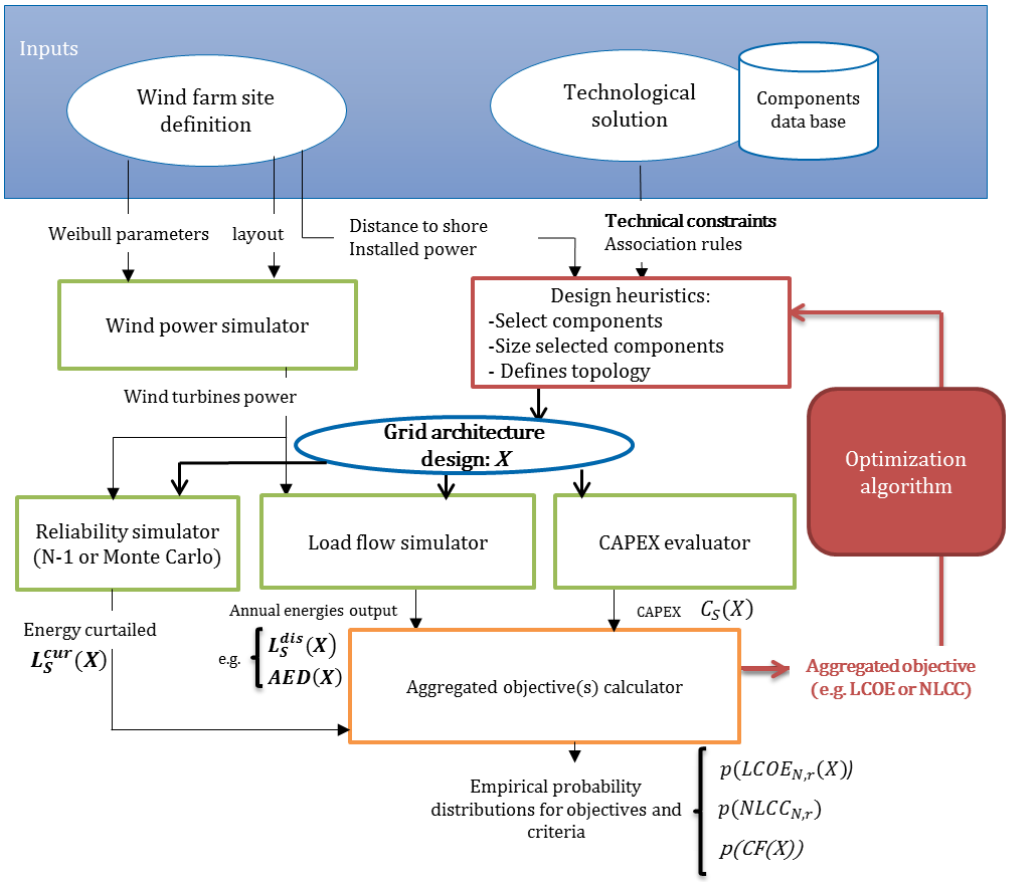

Figure 1-20: Decision support tool for the assessment of the electrical network connecting an offshore wind farm.

Chapter 2: ENERGETIC MODELS AND METHODS

2.1 Introduction

In Chapter 1, some energetic quantities, which impact the LCOE and the NLCC have been defined.

In the present chapter, the models and method to quantify them are detailed:

- The wind power simulator encompasses the model of wind turbines and allows quantifying the annual energy produced by the wind farm, AEP_0. It is presented in the section 2.2. The wind power simulator aims at quantifying the power produced by the wind turbines of a wind farm, as a function of the wind velocity. The wind turbines are in interaction with the collection electrical network. Some aerodynamic interactions can also occur between wind turbines: the phenomenon is referred to the wake effects.
- The load flow simulator and associated models and methods are exposed in the section 2.3. The static electrical models of the power components along with their integration into load flow calculations are presented. Electrical quantities for different operational points are calculated and associated constraints (in voltage, apparent power and current) are checked.
- The coupling method, allowing the quantification of energetic quantities (e.g. $AED(X)$ and $L_S^{dis}(X)$), is exposed in the section 2.4.

2.2 Wind power simulator and energetic modeling

In the next section 2.2.1, the probabilistic modeling of the wind resources is exposed. Then, in the section 2.2.2 , a brief state of the art of wake effect models is exposed. The retained approach to take into account the wake effect in the present PhD is proposed. Finally, in the section 2.2.3, a high level model of wind turbines is exposed.

2.2.1 Probabilistic modeling of the wind resource

To estimate the annual energy yield, the local wind resource probability distribution must be known. Wind resource is classically modeled through a probabilistic Weibull distribution [81]. The Weibull density of probability is given by equation (2-1) where v is the probability variable (wind velocity in m/s in the present case), k and λ are respectively shape and scale parameters of the Weibull law.

$$f_{WB}(v) = \frac{k}{\lambda}\left(\frac{v}{\lambda}\right)^{k-1} e^{-\left(\frac{v}{\lambda}\right)^{k}} \quad (2\text{-}1)$$

For offshore wind farms, classical values for k and λ are respectively in the order of 2 (no unit) and 10 m/s.

If wake losses are quantified by using computational models, the related losses need to be estimated for each wind direction. In that case, to estimate the annual expected yield energy, it would thus be necessary to have information on the wind resource angular distribution. This information can be described by a "wind rose", which takes wind directions into consideration and is represented by a set of Weibull distributions. Each distribution is associated to an angular sector (for instance 12 sectors for the Borssele wind farm in [82]).

In the present work, a macro approach is used to quantify the wake losses (see section 2.2.2). Thus, a single Weibull distribution per wind farm site is required. The methodology to estimate the annual energetic quantities by using the Weibull probability distribution function and to couple the wind power simulator and the load flow simulator is exposed in the section 2.4.

2.2.2 Wake effect phenomenon and existing models

Upstream turbines disturb the air stream thus downstream turbines see turbulences and wind velocity drops, resulting in a lower harvested energy level. This wake effect will depend on inter-locations of wind turbines and the wind direction.

The estimation of wake losses is subject of a high uncertainty, which affects the LCOE of a wind farm project. Wake effects losses are difficult to quantify; as fluid mechanics phenomena are complex, especially considering turbulences. The quantification requires very advanced models from fluid mechanics. The basis of these models is the Navier Stokes equation [83]. The scale of the system to take into account can include the whole wind farm. Besides, as the phenomenon depends on the limit conditions related to the actual wind turbines, it is very challenging to perform an accurate simulation.

Researchers from the electrical engineering field commonly use a simpler model, the Jensen model [84], [85] in order to:

- Optimize the wind farm layout or assess a concept by taking into account wake effects [44], [56], [68], [70], [86], [87]. A slight modification of the Jensen model to take multiple interactions into account is commonly used. It is referred as being the “multi-wakes” model.
- Optimize the electrical power management of the wind farm by taking into account wake effects [21], [88].

The advantages of the Jensen model is that it is simple and is not costly in computation effort, which is the main reason why it is used in the above mentioned cases where it must be used many times. However, its accuracy depends on the identification of its parameters, based on the fitting of experience data. For example, Horn Rev experience data have been used extensively [85]. Of course, the model would have different parameters for another wind farm.

Walker and al. [89] present a study on wake effect models involving industrial stakeholders of the offshore wind power industry[6]. The article evaluates the accuracy obtained with different models embedded within some commonly used softwares allowing to simulate the wake effect (OpenWind [90], based on Ainslie eddy viscosity model, WindFarmer [91], based on eddy viscosity model, WindModeller [92], based on Reynolds-Averaged Navier-Stokes and Fuga [83], based on Reynolds-Averaged Navier-Stokes). The evaluation is done on a number on wind farms for which there are some quantitative feedbacks.

[6] The Carbon Trust, DONG Energy, E.ON, SPR-Iberdrola, Mainstream Renewable Power, RWE, SSE Renewable, Statkraft, Statoil, Vattenfall.

It is thought that existing accurate models are beyond the scope of this PhD due to their complexity and to the level of expertise required in fluid mechanics. The Jensen model is simpler but it still introduces a complexity, which does not necessarily come with the benefit of a good accuracy. In 2016, Feijoo and Villanueva [93] proposed to adapt the Jensen model so to obtain a probabilistic distribution for the production of a wind farm. Still, this macro approach relies on the Jensen model parameters which are the subject of higher uncertainties.

It was thus chosen to quantify the wake losses by means of a macro factor based on industrial data:

- The UK study from The Crown Estate [10] considers annual wake energy losses of 10% of the gross annual energy produced.
- The German study from Prognos and Fichtner [14] considers an annual wake energy losses of 14% of the gross annual energy produced. They justify this higher level of wake losses by a higher density of wind farms in comparison with the UK. In particular, the inter wakes (interactions and perturbations between different wind farms) losses are thought to be higher in Germany.

The wake factor W_{fa} defined in the present PhD corresponds to the rate of annual energy, which is actually produced by the wind turbines divided by the power that they would produce without wake losses. W_{fa} is in the range of 0.9 to 0.85 as corresponding to the 10% and 15% ([10], [11]) wake losses stated above. For a given simulation, W_{fa} is fixed to a given value.

2.2.3 Wind turbine modeling

Physically, the wind turbine converts kinetic power into rotating mechanical power thanks to the blades. The efficiency of this first conversion is often named Cp (power coefficient). Theoretically, Cp cannot exceed $16/27$ (Betz law [81]). The blades are associated to a pitch system allowing to regulate the pitch angle of the blades to get the highest value of Cp for a given wind velocity. The design of the blades themselves is a specific problem in itself and is considered to be optimized; there are still significant variations of performances between manufacturers. This should be considered in order not to interfere with technical and economic analysis [56].

One could think of an analytical model of a wind turbine [21], [70], [94]. In the present PhD, the operation of each wind turbine is considered in MPPT (Maximum Power Point Tracking) for a given wind velocity. The considered model is an industrial data driven model: power curves depending on wind velocity as done by Dahmani [25]. Figure 2-1 depicts the Cp and associated power curve for an Enercon E126 wind turbine. The choice of modeling granularity, defining the level of details in the modeling, is the result of a compromise between available data and required outputs. In practice, in the present work, a large granularity for the model of the wind turbine is retained, where the power curves are loaded based on samples in a Python environment. Then, the Scipy library [95] is used for interpolation.

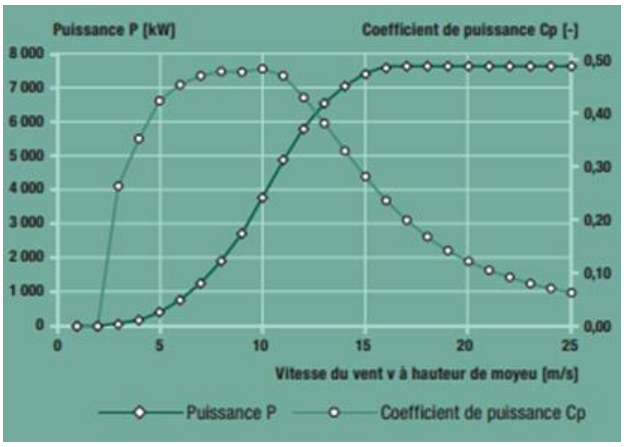

Figure 2-1: C_p and power curves for an Enercon E126 wind turbine

The mechanical rotating power is converted into electrical power thanks to a generator, being a doubly fed induction generator or a synchronous generator with permanent magnets (PMSG). Basically, the generator is connected to the network by using a converter and a transformer to adapt the voltage level. Due to its performances (efficiency among others), PMSG are preferred today [96]. This technology is considered for the present work due to the adequacy with potential adaptation of wind turbines for their participation to the management of MVDC collection network.

As a result, the power electronic conversion chains for DC and AC output wind turbines are depicted in Figure 2-2 and Figure 2-3.

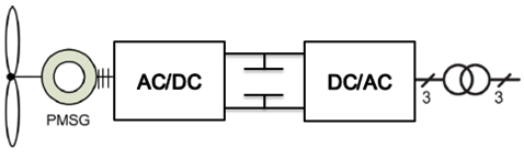

Figure 2-2: PMSG structure for 33kV or 66kV network connection.

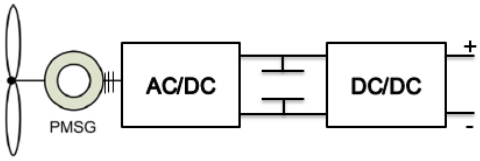

Figure 2-3: Considered structure for a DC network connection

Unless stated otherwise throughout the PhD thesis, it is assumed that the power conversion in these two cases has the same efficiency. As a result, each individual wind turbine is modelled by means of a power curve from industrial sources such as The Crown Estate (see Figure 2-4) or the paper from Ederer [56]. Ederer uses an advanced modeling for upscaling wind turbine curves so to obtain some prospective power ratings up to 20MW. To do so, he uses the methodology from Engel [97].

If there is a need to discriminate the wind turbines with AC and DC output from an efficiency perspective, a simple engineering methodology considering an industrial power curve for an AC wind turbine is preferred. It consists in using an AC wind turbine power curve to build a corresponding power curve for a DC wind

turbine. To do so, modeling characteristics of losses of the components are subtracted. The power produced by a DC wind turbine is thus computed for each wind velocity. The required electrical models of losses are available in the literature with an acceptable level of accuracy. For instance: Egrot and al. [24] for LVAC/MVAC transformer, Madariaga and al. [98] for LVDC/LVAC converters and Lagier and al. [51] for LVDC/MVDC converter.

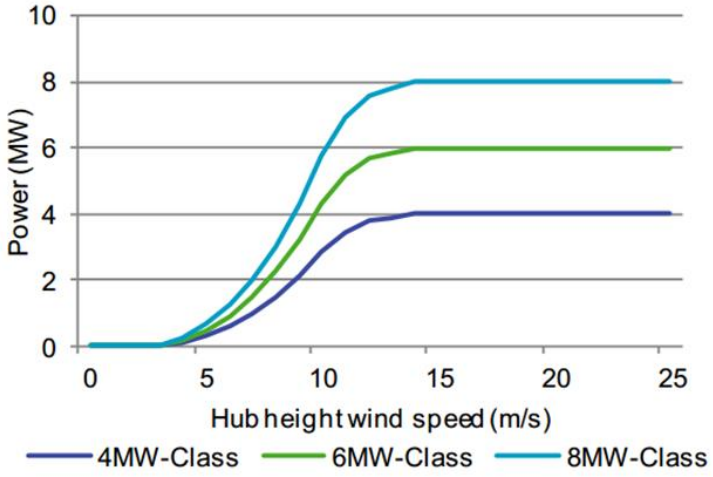

Figure 2-4: Generic power curves for overall wind turbines (The Crown Estate [10]*)*

2.3 Load flow simulator

The load flow simulator encompasses the static electrical models of power components and integrates them into load flow calculations. The latter is used to quantify the electrical quantities (current, voltage, active power, reactive power) of the electrical network. It makes it possible to quantify energetic quantities, which have an economic impact, as introduced in the Chapter 1. Additionally, it allows the checking of operational constraints such those related to maximum voltages or currents.

In sections 2.3.1, 2.3.2 and 2.3.3, the static models of power components are exposed.

These models are necessary to compute impedances to be used as parameters of the load flow calculations. Moreover, some of the exposed models, namely the cable model, are useful for their design.

For power electronic components (the MMC and MVDC/HVDC converter), models of losses are given. In such case, their integration into load flow calculations relies on a sequential approach similar to what is proposed by Beerten and al. [99].

The model of AC and DC cables is presented in the section 2.3.1. The model of transformer is presented in the section 2.3.2. Finally, the models of MMC and MVDC/HVDC converter stations are presented in the section 2.3.3.

In the section 2.3.4, the power management condition of the electrical network for various architecture concepts is exposed. Finally, the load flow calculation methods are developed in section 2.3.5.

2.3.1 Modeling of cables

Cables represent a key component in the assessment of the complete system connecting offshore wind farms to the shore. Cabling system is the main driver in favor of DC. Indeed, the savings in losses and CAPEX obtained with DC cables compared with AC cables can overcome the over costs associated to additional auxiliary systems required for the DC technology to operate.

We can cite three main sources for cable modeling, which are: IEC 60287 standards [100], [101], a model proposed by H. Brakelmann [102] and a simplification, considering a constant maximal temperature in the cable.

The objective of the IEC 60287 standard is to compute the ampacity of a cable. The ampacity is the current which does not induce a temperature in the conductor higher than the maximal acceptable value (for example 90°C for XLPE AC cables and 70°C for XLPE DC cables) [103]. For that purpose, models are proposed in that standard to compute losses of an extensive set of cables and laying conditions. Unless stated otherwise, the models here are extracted from this standard.

In section 2.3.1.1, a synthesis of the electrical model is proposed with input and output parameters. Similarly, in section 2.3.1.2, a synthesis of the thermal model of cable is provided. The thermal model is required, either to calculate the ampacity of the cable, or to calculate the resistance for a given steady state current. This is done by using a power coupling involving both the electrical and thermal models.

The extended modeling of cables based on this standard is proposed in APPENDIX A.

2.3.1.1 Synthesis of the electrical model of cable

The electrical model of cables is detailed in section A.2.of the appendix A.

Figure 2-5 and Figure 2-6 give synthesis of electrical cable models in regard to parameters, inputs and outputs.

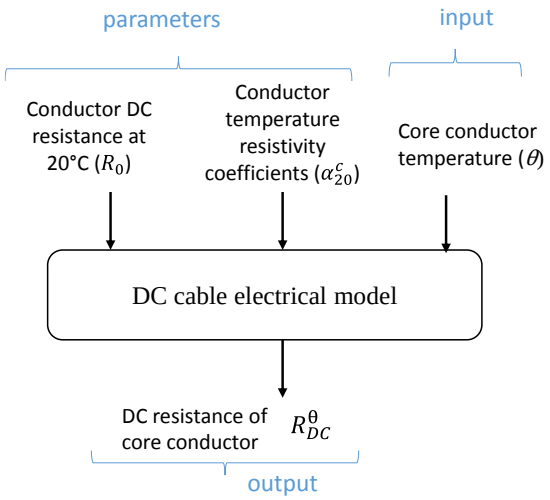

Figure 2-5: Synthesis schematic for electrical model of DC cable

It is noteworthy that the electrical DC cable model does not need as many parameters and inputs as the AC cable model. For both AC and DC electrical cables models, the DC resistance at 20°C is a parameter, which is obtained from tables of the IEC standard 60228 [104] depending on the normalized cross section (which does not necessarily corresponds to the actual core cross section of the cable). This table from the standard is implemented in Python as a look-up table using the standard values.

For an AC cable, in a load flow computations, the resistance will be considered as an equivalent AC resistance $R_{AC,eq}$, which takes into account the power losses in the metallic sheaths and in the armor. It is calculated by using equation (2-2).

$$R_{AC,eq} = R_{AC}^{\theta}(1 + \lambda_{sheath} + \lambda_{armour}) \quad (2\text{-}2)$$

where:

λ_{sheath} is the ratio between the losses in one metallic sheath and the power losses in the associated core conductor (see section A.2)

λ_{armor} is the ratio between the third of the power losses in the armor and the power losses in one core conductor(see section A.2)

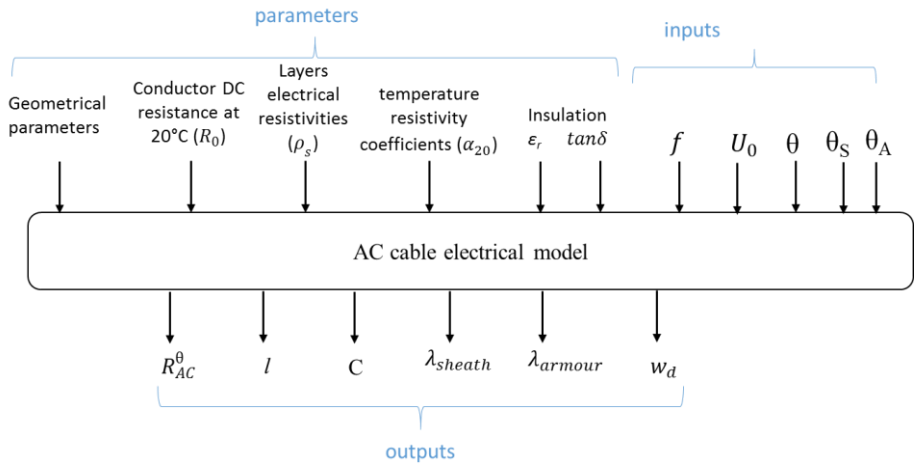

Figure 2-6: Synthesis schematic for electrical model of AC cable

where:

f is the operating frequency (50 Hz is the present work)

U_0 is the RMS phase to ground voltage (V)

θ is the temperature of the core conductor (°C)

θ_S is the temperature of the cable sheath (°C)

θ_A is the temperature of the cable armor (°C)

w_d is the per unit length dielectric losses (W)

l is the per unit length phase equivalent inductance of the cable (H/m)

C is the per unit length phase equivalent capacitance of the cable (F/m)

2.3.1.2 Thermal model synthesis

The thermal model of cables, based on IEC 60297, is detailed in section A.3 of appendix A.

Figure 2-7 gives a general view of the cable thermal model, generic for AC and DC cable models. The differences in models between the two are described in detail in section 2.3.1.1 .

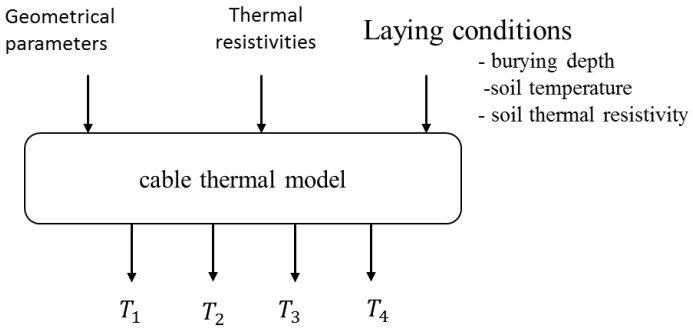

Figure 2-7: Schematic synthesis of cable thermal model

where:

T_1 is the thermal resistance of the insulation of one core conductor (see section A.3)

T_2 is the thermal resistance between the sheath and the armor of the cable (see section A.3)

T_3 is the thermal resistance of the outer layer of the cable (see section A.3)

T_4 is the thermal resistance of the sea bed at the proximity of the cable (see section A.3)

2.3.1.3 Validation of the cable model

Implemented models are validated on the basis of ampacity results. This is because:

- Ampacities of cables are easily found in manufacturer's data sheets.
- The calculation of the ampacity relies on both the electrical and thermal models. Thus the ampacity calculation can be considered to validate the two models at once.

The calculation of the ampacity is done as exposed in appendix section A.4.3 of appendix A, based on the IEC 60287.

2.3.1.3.1 Validation of DC cable model

For DC cables, results of calculated cable ampacity are given in Table 2-1 and can be compared with ABB cable ampacities [105].

Table 2-1: Validation of DC cable model on the basis of ampacity [105]

Section (mm^2)	Ampacity from ABB datasheet (A)	Ampacity from model at 150kV (A)	Ampacity from model at 320 kV (A)	Maximal relative error in comparison to ABB data (A)
1200	1458	1442	1415	2.9 %
1500	1644	1624	1595	3.0 %
1800	1830	1801	1770	3.3 %
2000	1953	1923	1889	3.3 %

Errors can be explained by approximate values used for the thickness of different layers and by interpretation of what corresponds to "close laying". Besides, the same ampacity is given by ABB for all voltages, which, of course, is an approximation. In any case, obtained results are close to data provided by manufacturers. Corresponding losses can be found very close to real losses.

2.3.1.3.2 AC cable model validation

As public field measurements are very difficult to get, IEC 60287 standards are considered to be the reference. Ampacities and losses calculated according to standards are provided in Nexans public catalogue for 33kV submarine cables [106] (used for 630 mm^2) and in non-public sheets from Nexans (used for 185 mm^2 and 300 mm^2). These data serve as validation references for implemented models. Results are presented in Table 2-2.

Table 2-2: Validation of AC cable model on the basis of ampacity

Section (mm^2)	Soil thermal resistivity (W.K/m)	Burying depth (m)	Water temperature (°C)	Ampacity from Nexans data (A)	Ampacity from model (A)	Relative error in ampacity
185	1.0	1.0	32	390	394	1.0 %
300	0.7	0.3	25	670	674	0.6 %
630	1.0	1.0	20	721	715	0.8 %

Once again, obtained results are very close to manufacturer data, with errors below 1%. Corresponding losses can be found very close to real losses as well.

2.3.1.4 Comparison with state of art scientific literature

2.3.1.4.1 Model proposed by H. Brakelmann

A mathematical development allowing not to use the iterative algorithm (refer to appendix section A.4.3) was proposed by H. Brakelmann to calculate power losses [102]. The main assumptions are similar to the standard, in particular, a thermal steady state is considered to be always reached, making possible the use of thermal resistances only. Thus, the conductor's resistances will depend on their operating temperature. The calculation of the conductor's temperatures each time for all currents would make the computation process quite heavy. Therefore, a model was provided to directly take into account currents as input parameters to quantify resistances.

To do so, H. Brakelmann defines equivalent thermal resistance of cables T_{Ers} in (2-3) by taking into account all layers and even heating in different layers due to losses.

$$T_{Ers} = T_1 + n(1 + \lambda_{sheath}).T_2 + n(1 + \lambda_{sheath} + \lambda_{armor})(T_3 + T_4) \quad (2\text{-}3)$$

where:

n is the number of core conductors of the cable (3 in AC, 1 in DC).

λ_{sheath} is the ratio between the losses in one metallic sheath and the power losses in the associated core conductor (see section A.2)

λ_{armor} is the ratio between the third of the power losses in the armor and the power losses in one core conductor(see section A.2)

The temperature rises in conductors $\Delta\theta_L$ in comparison with the external temperature θ_u, as reference for any current I, using T_{Ers}, as expressed in (2-4) and (2-5).

$$\Delta\theta_L = T_{Ers}.R_{AC}^{\theta}(\alpha_T.\Delta\theta_L + c_\alpha)I^2 \quad (2\text{-}4)$$

$$c_\alpha = 1 - \alpha_T(20°C - \theta_u) \quad (2\text{-}5)$$

where:

θ_u is the external temperature (°C)

α_T is the factor of the conductor resistivity rise

Even if not expressed in [102], it should be noted that, when writing equation (2-4), several errors are introduced:

1. Proximity and skin effects factors depend on the actual DC resistance of the conductor and thus on its temperature.
2. The influence of dielectric losses on the temperature is neglected.

By using equation (2-4), for $I = I_{max}$ and assuming that T_{Ers} is constant, equal to its value for the maximal current, it appears that $\Delta\theta_L$ is only depending on constant parameters and the current I, as expressed in equation (2-6) and (2-7).

$$\Delta\theta_L = \Delta\theta_{Lmax}.\frac{c_\alpha\left(\frac{I}{I_{max}}\right)^2}{c_m - \Delta\theta_{Lmax}.\alpha_T\left(\frac{I}{I_{max}}\right)^2} \quad (2\text{-}6)$$

$$C_m = 1 + \alpha_T.(\Delta\theta_{Lmax} + \theta_u - 20°C) \quad (2\text{-}7)$$

Note that, in reality, λ_{sheath} and λ_{armor} are not constant and thus T_{Ers} neither. This is not considered in Brakelmann's work. Finally, the ratio between losses for any current I and maximal losses for I_{max} (respectively $P_{losses,I}$ and $P_{losses,Imax}$, without dielectric losses w_d) can be written by taking into account the increase in resistivity due to the temperature, as written in (2-8).

$$\frac{P_{losses,I}}{P_{losses,Imax}} = \frac{1 + \alpha_T(\Delta\theta_L + \theta_u - 20°C)}{1 + \alpha_T(\Delta\theta_{Lmax} + \theta_u - 20°C)}\left(\frac{I}{I_{max}}\right)^2 * \left(\frac{1 + \lambda_{sheath} + \lambda_{armor}}{1 + \lambda_{sheath,max} + \lambda_{armor,max}}\right) \quad (2\text{-}8)$$

Thus, by making the assumption that the term $\lambda_{sheath} + \lambda_{armor}$ is constant and that skin and proximity effects factor are also constant (these assumptions are not clearly expressed in [102]), by replacing $\Delta\theta_L$ with (2-6) in (2-8), (2-9) can be obtained, with ν_θ expressed in (2-10).

$$P_{losses,I} = P_{losses,Imax}\left(\frac{I}{I_{max}}\right)^2.\nu_\theta + w_d \quad (2\text{-}9)$$

$$\nu_\theta = \frac{c_\alpha}{c_\alpha + \alpha_T.\Delta\theta_{Lmax}.\left[1 - \left(\frac{I}{I_{max}}\right)^2\right]} \quad (2\text{-}10)$$

Finally, ν_θ can be used to calculate the parametric resistance of conductors at the temperature θ_L, with equation (2-11).

$$R_{AC}^{\theta} = R_{AC}^{\theta_{max}} . \nu_{\theta} \quad (2\text{-}11)$$

To sum up, H. Brakelmann solves the equations of lines with a non-corrected resistance to deduce the evolution of the voltage and the current along a long transmission cable. Then, he uses current as an input to get the corresponding temperature correction factor.

2.3.1.4.2 Quantitative validation and electric resistances

By assuming that implemented models coming from IEC 60287 standards are valid for AC and DC, power losses are calculated for different loads. It is done for AC cables, on the one hand, with a complete calculation by iteratively quantifying temperature of the conductor (see section A.4) and, on the other hand, by using the analytical factor ν_{θ} for each loading current, having calculated once the cable ampacity The calculations are done with the following laying conditions: $\theta_u = 20°C$, $T_4 = \text{K.m/W}$, and $L = 1m$. It will be the case for the remaining of the PhD thesis.

A "real" interpolated ν_{θ} set could then be built and used in AC cables models as it would use an analytical version of ν_{θ}. For DC cables, the analytical ν_{θ} can be used directly without errors.

With the assumptions formulated in [102], the skin and proximity effects factors are constant and computed for the maximum admissible temperature. [102] also assumes that shield and armor resistances are constant. In reality, for lower temperatures (for example at the core of the cable where charging currents are smaller), the conductivity is greater thus the skin depth decreases. In that case, the equivalent AC resistance increases. This can be explicated by using Bessel equations as expressed in [100],(see A.2), or more simply by considering the physical action of induction phenomena on the equivalent resistance.

For illustration, Figure 2-8 proposes the per unit length resistance in function of the current in:

- Two 220kV AC cables with sections of respectively 500 mm² and 1000 mm².
- A 66kV AC cable, with a section of 185 mm².
- A DC ±320kV cable, with a section of 1000 mm².

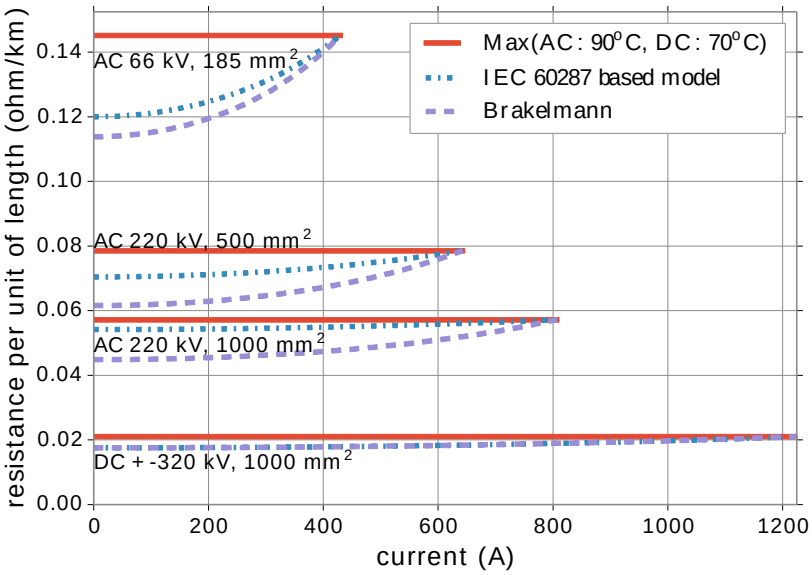

Figure 2-8: Core conductor resistances depending on the current. Comparison of the models on various AC and DC cables.

Based on the Figure 2-8, we can propose some analyses, which are also a guidance for the choice of a model to be used. For an AC cable, the more you increase the section the more the difference between the standards and the model proposed by H. Brakelmann is significant. This is confirmed for a smaller section of 185mm², where the model proposed by H. Brakelmann has a lower relative error compared to the actual resistance.

Also, for large sections, the adequacy of the constant-temperature model (which is used a lot in the literature as it is given in data sheets) with the standards is more relevant. Finally, for DC cables (and any cross section), there is no difference anymore between the standards and the model proposed by H. Brakelmann.

2.3.1.5 Synthesis for the cable model

As seen in the previous section, the cable model can be used either for the ampacity calculation, or for the quantification of impedances to be used in a load flow. Figure 2-9 and Figure 2-10 give an overview of the cable model to be used for integration into load-flows.

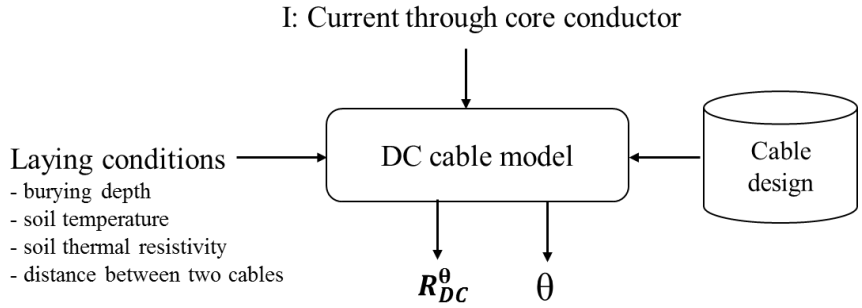

Figure 2-9: Synoptic diagraph of the DC cable model

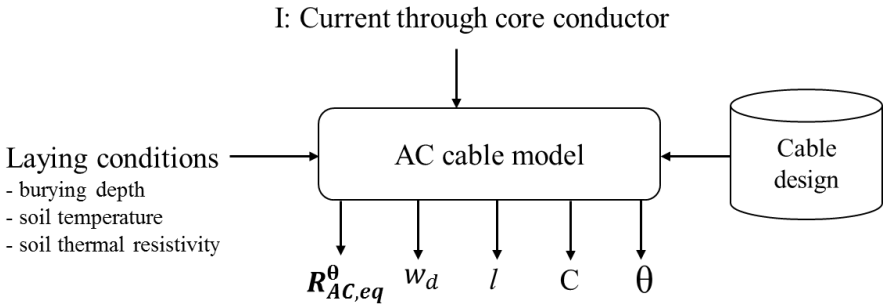

Figure 2-10: Synoptic diagram of the AC cable model

The parameters of a single phase equivalent π electrical circuit (Figure 2-11) can be calculated with obtained AC cable parameters. The parameter g is given by the equation (2-12).

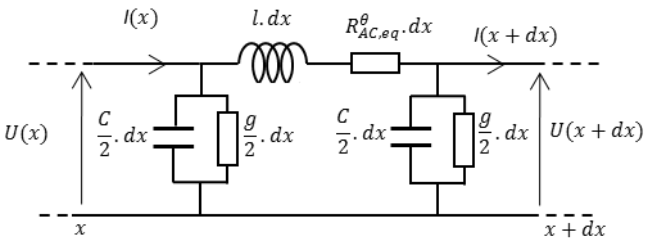

Figure 2-11: PI model of an AC cable with parameters of the model exposed.

$$g = \frac{3.w_d}{U_0^2} = 2\pi f.C.tan\delta \qquad (2\text{-}12)$$

2.3.2 Modeling of transformers

An AC power transformer model is required to take into account interfaces between collection (33 kV or 66 kV) and export (typically 150 kV or 220 kV) networks. They are modeled by using a per unit equivalent electrical circuit as in Figure 2-12. Dahmani [25] detailed equations showing equivalence between this model and a transformer per unit model with "real" values. The main objective of using per unit system is to make easier the integration into load flow studies.

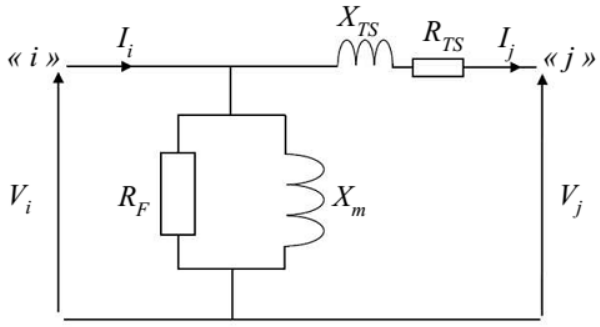

Figure 2-12: Transformer per unit model [25]

Classic values for parameters are given by Dahmani: $X_{TS} = 0.1$ p.u, $Xm = 50$ p.u. Reference [24] gives values for no-load and on-load losses in offshore export transformers (respectively 0.05% and 0.27% of the rated power). Obtaining R_{TS} and R_F from these values is straightforward if the used base power corresponds to the rated power of the transformer. Used values are R_{TS}=0.003 p.u and R_F=+∞ (meaning no-load losses are neglected).

Alternatively, in its ten years statement [26], the National Network report gives, as order of magnitude for load losses 0.5 %, corresponding to R_{TS}=0.005 p.u for transformers from 33 kV to145 or 245 kV. The latter values are in accordance with internal knowledge in SuperGrid Institute.

2.3.3 Models of transmission converter stations

2.3.3.1 MMC station model

Nowadays, half bridge MMC converters (see Figure 2-13 and Figure 2-14 for examples of submodules) are a key technology for high voltage AC/DC VSC conversion.

2.3.3.1.1 MMC station in wind power transmission context

From the point of view of the AC offshore network, the offshore MMC station (including transformers) must perform the DC to AC voltage inverting function and thus imposes the AC voltage. It also performs the current rectifying function and is a power source seen from the HVDC network.

The onshore MMC station imposes the DC voltage at its DC side. These assumptions relies on an appropriate control of the MMCs but dynamic aspects are not studied in the present work. As a result, whilst satisfying

the constraints coming from maximal apparent powers and voltages, a MMC station can be modelled for steady state load-flow calculation as:

- an AC slack bus and a P bus (DC power source) for offshore rectifier applications (see Figure 2-15).
- A DC slack bus and a PQ bus (active and reactive) source for onshore inverter applications (see Figure 2-16)

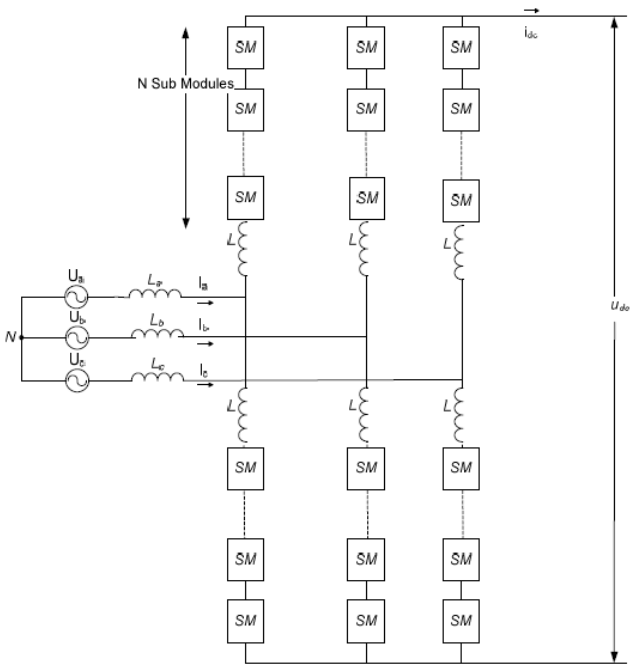

Figure 2-13: Schematic representation of a MMC converter [107]

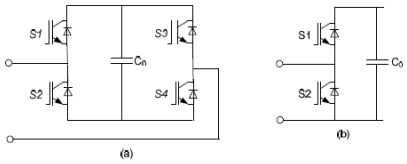

Figure 2-14: Main types of sub-modules for MMC converters: (a) Full Bridge submodule and (b) Half Bridge submodule [108]

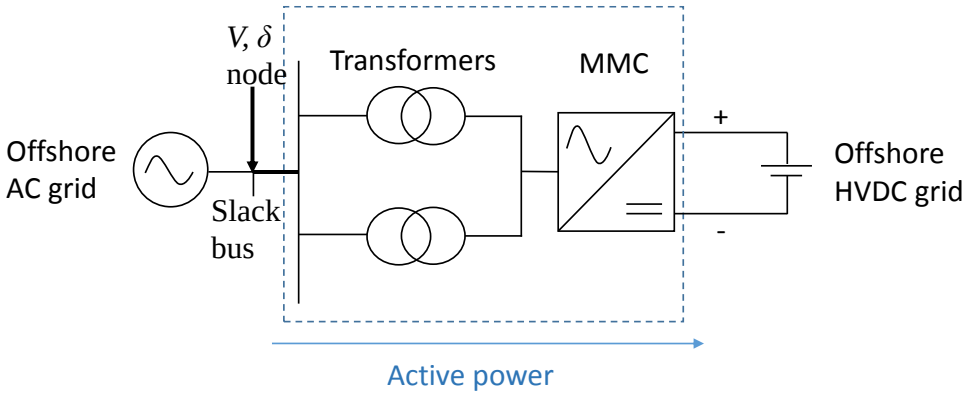

Figure 2-15: Offshore MMC converter station schematic

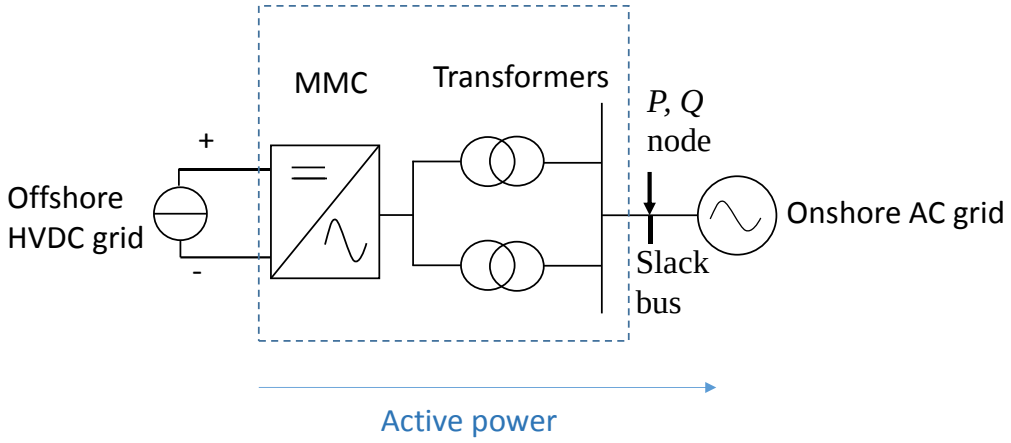

Figure 2-16: Onshore MMC converter station schematic

2.3.3.1.2 Modeling of power losses for a MMC station

The total power losses are the sum of losses in the converter transformer(s) ($P_{losses,transformers}$), in the MMC itself ($P_{losses,MMC}$) and in the auxiliaries ($P_{losses,auxilliaries}$). As a result, in the rectifier mode, when the MMC component is offshore, the AC active power from the wind farm P_{AC} must be extracted and P_{DC} is deduced from power losses in MMC station by using equation (2-13).

$$P_{DC} = P_{AC} - (P_{losses,MMC} + P_{losses,transformers} + P_{losses,auxilliaries}) \quad (2\text{-}13)$$

In inverter mode, when the MMC station is onshore, the DC power from the wind farm P_{DC} must be extracted and P_{AC} is deduced from power losses in MMC station by using equation (2-14).

$$P_{AC} = P_{DC} - (P_{losses,MMC} + P_{losses,transformers} + P_{losses,auxilliaries}) \quad (2\text{-}14)$$

Power losses of the components are determined by means of dedicated models:

- of the converter transformers, based on (2-15) [109]. The classical transformer(s) associated to a MMC have on-load and no-load losses parameters which can be taken from the National Network technology report [26] corresponding to secondary voltages of 400 kV/ 132 kV in the range of 180 MVA to 240 MVA. In practice, these parameters tend to be lower as the power rating of the converter transformer increases.
- of converter station auxiliaries, especially cooling system [110] (see equation (2-16)) of the converter
- of the MMC converter itself, due to conduction and switching losses (detailed in 2.3.3.1.3).

$$P_{losses,transformers,p.u} = P_{0,t} + S_f^2 . (P_{k,t} - P_{0,t}) \quad (2\text{-}15)$$

where: $P_{0,t}$= 0.03% [26], $P_{k,t}$= 0.39 % [26] and S_f is the per unit apparent power.

$$P_{losses,Auxilliaries,p.u} = P_{0,a} . S_f \quad (2\text{-}16)$$

where: $P_{o,a}$ = 0.05 %.

2.3.3.1.3 Losses model in MMC

Power losses in a MMC converter can be separated into three categories:

- Conduction losses in switches (either IGBT or diodes, two of each by half bridge submodule, see Figure 2-14).
- Switching losses (hard switching losses of IGBTs and soft switching losses of diodes). These power losses depend on submodules voltage balancing algorithms.
- Power losses in passive components.

Power losses in the MMC depend on both AC and DC RMS currents respectively I_{AC} and I_{DC}. These currents are estimated while neglecting power losses in the MMC. I_{DC} can so be calculated from line to ground DC voltage V_{DC} and AC active power of the converter P_{AC} by using the equation (2-17).

$$I_{DC} = \frac{P_{AC}}{2.V_{DC}} \tag{2-17}$$

I_{AC} can be calculated from the AC apparent power of the converter S and phase to ground RMS AC voltage V_{AC} by using equation (2-18).

$$I_{AC} = \frac{S}{3 * V_{AC}} \tag{2-18}$$

V_{AC} is itself calculated by using equation(2-19), where M is the mean modulation index of the converter. To ensure a sufficient operation margin, M is typically between 0.8 and 0.9.

$$V_{AC} = M.\frac{V_{DC}}{\sqrt{2}} \tag{2-19}$$

Several methods exist in the literature to estimate the power losses in a MMC converter. One widespread approach is to perform temporal simulations based on a detailed model and to use the obtained current waveforms to estimate losses in diodes and IGBTs based on manufacturer datasheets that provide steady state characteristics and switching energies [111], [112].

Conduction and switching losses depend of course on the number of switches, thus on the number of submodules. On average, a submodule with IGBTs of 3.3kV peak withstands a voltage V_S close to 1600 V (choice coming from reliability considerations). The number of submodules per arm N_a can then be obtained with equation (2-20). The factor 2 is used because the maximum voltage inserted in one arm is $2.V_{DC}$. With V_S close to 1600 V, the number of submodules per arm is 400 for an industrial MMC of ±320 kV.

$$N_a = \frac{2.V_{DC}}{Vs} \tag{2-20}$$

Rodrigues and al. [110] and Jones [113] use a similar approach where analytical models are used to estimate currents in diodes and IGBTs. However, the model developed in [110] remains complex as uses a discretization of an ideal sinusoidal wave form to determine current in each diode and each IGBT for all sample periods.

Jones [113] proposed a simplified model of losses of the MMC based on physical considerations and advanced knowledge of industrial applications. This modeling approach has been retained to estimate conduction and switching power losses in the present work.

Conduction losses in switches of the MMC

For conduction losses, Jones et al. [113] propose a simplified model by using a piecewise-linear approximation of switch characteristics (see Figure 2-17).

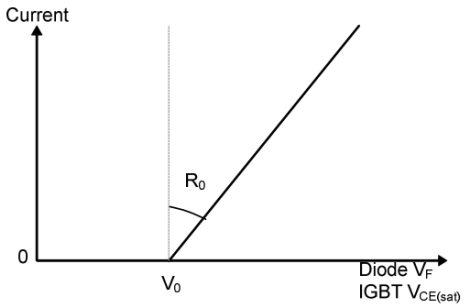

Figure 2-17 : Piecewise-linear approximation of I-V characteristics for switches (diode or IGBT) [113]

Jones then observes that with voltage balancing algorithms used in the industry (see [112] for comparison of balancing algorithms) applied to half bridge MMC, it is possible to approximate the equivalent characteristic of a submodule based on characteristics of diode and IGBTs. In the rectifier mode, where diodes are conducting most of the time, equations (2-21) and (2-22) can be used. In the inverter mode, a good approximate is obtained with equations (2-23) and (2-24). V_{0D} and V_{0T} are respectively diode and IGBT constant voltage drops. R_{0D} and R_{0T} are respectively diode and IGBT on state resistances.

$$V_{0Rec} = 0.8.V_{0D} + 0.2.V_{0T} \quad (2\text{-}21)$$

$$R_{0Rec} = 0.8.R_{0D} + 0.2.R_{0T} \quad (2\text{-}22)$$

$$V_{0Inv} = 0.2.V_{0D} + 0.8.V_{0T} \quad (2\text{-}23)$$

$$R_{0Inv} = 0.2.R_{0D} + 0.8.R_{0T} \quad (2\text{-}24)$$

Then, to calculate conduction losses, RMS current flowing in a MMC valve arm must be calculated. The RMS current flowing in one arm $I_{a,rms}$ of the MMC is given by equation (2-25).

$$I_{a,rms} = \sqrt{\frac{{I_{AC}}^2}{4} + \frac{{I_{DC}}^2}{9}} \quad (2\text{-}25)$$

As the MMC has two legs and therefore six arms, AC and DC components of the current in each arm are therefore respectively $I_{AC}/2$ and $2.I_{DC}/6$ [113].

The current in a submodule is either flowing in a diode, or in an IGBT and then, losses are related to V_0 of the switch generic characteristic of Figure 2-17. These losses are relative to the mean value of the absolute value of I_{arm} (current in one arm). The so called "rectified mean arm current" I_{aavr} *is* calculated with

equation (2-26), where θ_z angle corresponds to its zero crossing current, which can be calculated with equation (2-27).

$$I_{aavr} = \frac{1}{\pi}.[\frac{I_{DC}}{3}.(2.\theta_z - \pi) + I_{AC}.\sqrt{2}.\sin(\theta_z)] \quad (2\text{-}26)$$

$$\theta_z = cos^{-1}\left[\frac{-I_{DC}.\sqrt{2}}{3.I_{AC}}\right] \quad (2\text{-}27)$$

Finally, conduction power losses per submodule can be calculated with equation (2-28) in the rectifier mode and equation (2-29) in the inverter mode.

$$P_{cond} = V_{0Rec}.I_{aavr} + R_{0Rec}.{I_{a,rms}}^2 \quad (2\text{-}28)$$

$$P_{cond} = V_{0Inv}.I_{aavr} + R_{0Inv}.{I_{a,rms}}^2 \quad (2\text{-}29)$$

Switching losses in switches of the MMC

With voltage balancing algorithms, switching losses are very low. Jones [113] proposes to calculate them with an approximate model. It is done by assuming that switching events are uniformly distributed over a cycle. In that case, Jones shows that I_{aavr} can be considered to be the constant current flowing though the switches when the switchings occur. As a consequence, per half-bridge submodule, switching losses P_{sw} can be calculated with equation (2-30), where f_{sw} is the switching frequency for each submodule. With voltage balancing algorithms used industrially, f_{sw} is typically around 150 Hz.

$$P_{sw} = f_{sw}.(E_{on}(I_{aavr}) + E_{off}(I_{aavr}) + E_{rec}(I_{aavr})) \quad (2\text{-}30)$$

where:

$E_{on}(I_{aavr})$ is the IGBT turn-on energy for current I_{aavr},

$E_{off}(I_{aavr})$ is the GBT turn-off energy for current I_{aavr},

$E_{rec}(I_{aavr})$ is the diode turn-off energy for current I_{aavr}.

In practice, polynomial approximation of switching energies depending on current is derived from manufacturer's data sheet. For the present work, the data sheet of IGBT module Infineon FZ1500R33HL3 is used.

The analytical approximate for switching losses is reported to be within ±10% compared to results with detailed simulations. It is acceptable for present work because the share of switching losses is around 25 % of the total power electronic losses in the MMC [112].

Passive losses in MMC arms

As stated by Zama et al. [112], the passive losses can be summarized in ohmic losses of arm inductors and equivalent series resistor of submodule capacitors. The latter is very small and can be neglected. A typical value for arm resistance R_{arm} is 50 mOhm. Total passive losses of the MMC, $P_{passive}$, can finally be calculated with the equation (2-31).

$$P_{passive} = 6.R_{arm}.{I_{a,rms}}^2 \quad (2\text{-}31)$$

Synthesis of losses in the MMC

Total power losses in the MMC is the sum of conduction and switching losses in all half bridge submodules plus losses in passive elements of the arms. Because there are N_a submodules per arm and six arms per MMC, equation (2-32) can be used to calculate total power losses in one MMC.

$$P_{losses,MMC} = P_{passive} + 6.N_a.(P_{cond} + P_{sw}) \quad (2\text{-}32)$$

2.3.3.1.4 MMC converter station model synthesis

Synoptic schemes are given for MMC station model in inverter mode and rectifier mode respectively in Figure 2-18 and Figure 2-19. For the present work, switches (IGBTs and diodes of half bridge submodules) data are for Infineon FZ1500R33HL3 power module [114]. Conservative values corresponding to a temperature of junction of 150°C are used.

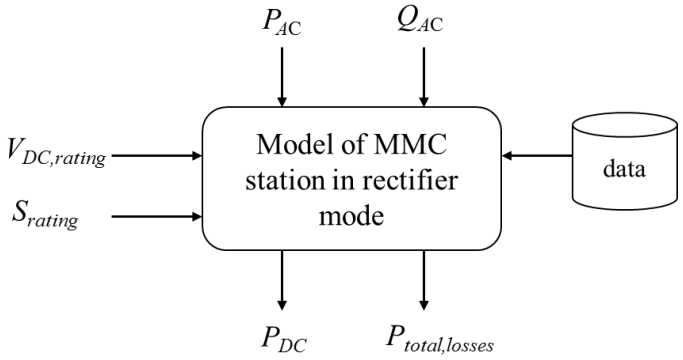

Figure 2-18 : Synoptic for the model of MMC station in rectifier mode (offshore)

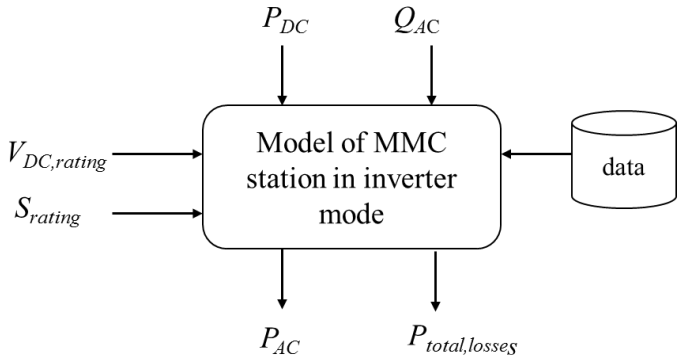

Figure 2-19 : Synoptic for the model of MMC station in inverter mode (onshore)

2.3.3.2 MVDC/HVDC converter modeling

As stated in Chapter 1, there is a high uncertainty on the actual technological solution to perform the MVDC/HVDC conversion.

2.3.3.2.1 Functional requirements for the offshore MVDC/HVDC station

As stated by Monjean and al [115], viewed from the DC collection offshore network, the offshore MVDC/HVDC station must impose the MVDC voltage . It must also behave as a current source, seen from the HVDC transmission network. The onshore MMC station imposes the DC voltage at its DC side. The MVDC/HVDC converter(s) station(s) must satisfy the constraints coming from their maximal apparent powers and voltages. An offshore MVDC/HVDC converter station can be modeled in a load-flow as a DC slack bus and an output P bus (DC power source) as depicted in the Figure 2-15. The practical integration to a load flow calculation based on a sequential approach is detailed in the section 2.3.5.

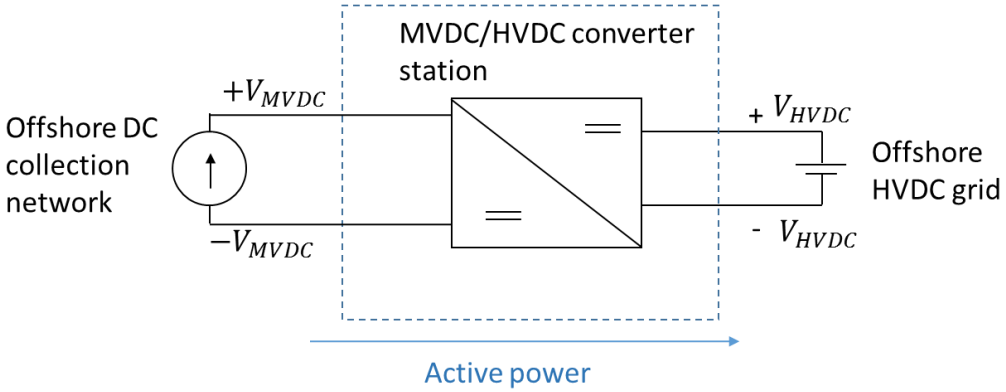

Figure 2-20: Offshore MMC converter station schematic

2.3.3.2.2 Required model structure

The electrical model of a given technological solution for the MVDC/HVDC conversion should have the structure depicted in Figure 2-21. The (active) power from the wind farm cluster collection network P_{MVDC} is extracted by the MVDC/HVDC converter. The active power injected to the HVDC transmission network by the MVDC/HVDC converter P_{HVDC} is deduced from power losses in the MVDC/HVDC converter station by using (2-33).

$$P_{HVDC} = P_{MVDC} - P_{losses,DC-DC} \tag{2-33}$$

The Figure 2-21 shows that any model of losses for a given technological solution depends on some data.

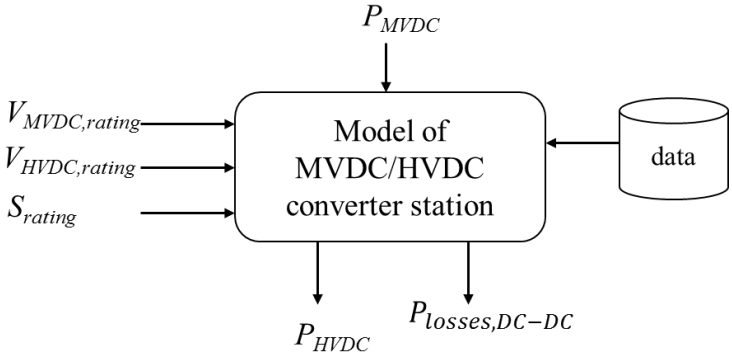

Figure 2-21 : Synoptic for model of MVDC/HVDC station (offshore)

These data include, at least, the physical parameters for power electronic switches. In addition to the power rating of the converter S_{rating}, the model depends a priori on the input voltage V_{MVDC} and on the output voltage V_{HVDC}. As there is no reactive power in DC systems, the apparent power corresponds to the active power of the converter.

2.3.3.2.3 Example of meta-modeling for a technological solution based on single active bridge converter.

Lagier and al. [51] detail a model of losses for a MVDC/HVDC converter whose topology is based on a series/parallel association of single active bridge modules. The data results have been processed in the present work so to obtain a meta-model whose structure corresponds to the above exposed specification.

A polynomial approximation of the results given by Lagier et al. is implemented. The polynomial approximation of equation (2-34) is based on the observation that, due to the use of SiC switches, the commutation losses are low. Therefore, the power losses are dominated by conduction losses in the linear region of operation of the switches and, consequently, are mainly proportional to the square of the current in each switch.

$$P_{losses,DC-DC} = S_{rating} \cdot \left[R_{s,p.u} \cdot \left(\frac{P_{MVDC}}{S_{rating}} \right)^2 + L_{p.u}^{com} \right] \quad (2\text{-}34)$$

where:

P_{MVDC} is the active power at the input of the MVDC/HVDC converter (in MW).

S_{rating} is the power rating of the MVDC/HVDC converter (in MW).

$R_{s,p.u}$ is a parameter to be identified. It can be seen as an equivalent series per unit resistance of the converter.

$L_{p.u}^{com}$ is a parameter to be identified. It can be seen as the per unit commutation losses.

The fitting of the parameters of this meta-model (equation (2-34)) is done whilst assuming that in per unit, the losses remain the same. In other words, it is assumed that $R_{s,p.u}$ does not depend on S_{rating}. It is consistent with the series/parallel association of the elementary DC/DC Single Active Bridge modules (SAB) [51]. Figure 2-22 gives fitting results. The meta-model provides correct results. The parameters are identifies as: $R_{s,p.u}$=6.0.10^{-3} (p.u.); $L_{p.u}^{com}$=1.2.10^{-3} (p.u.).

The fitting results could possibly be improved by adding a first order dependency to $\frac{P_{MVDC}}{S_{rating}}$ in (2-34).

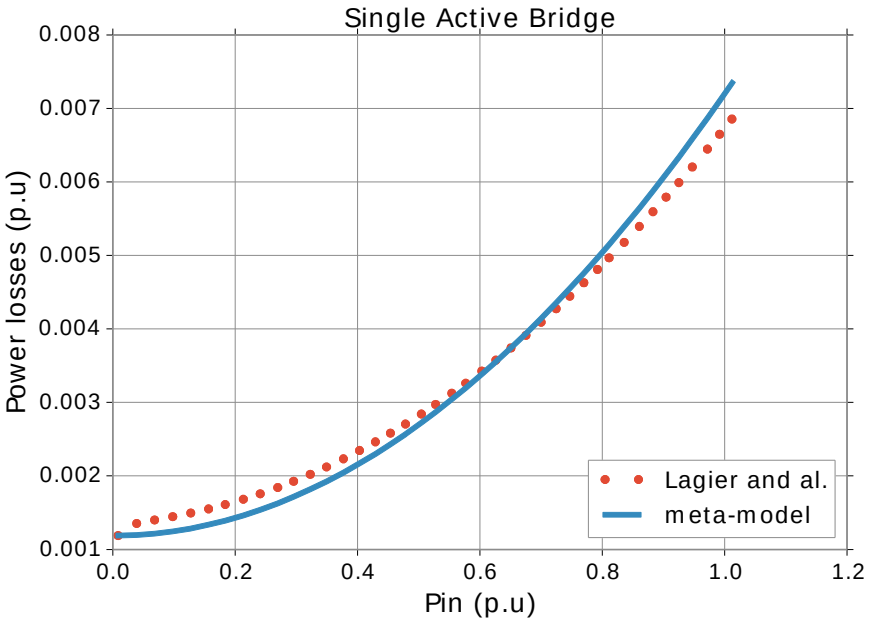

Figure 2-22: Comparison of losses obtained with model of Lagier and al. [51] and with the metamodeling. SAB based DC/DC converter topology (10 kV SiC mosfets).

It must be noted that any model of losses for a MVDC/HVDC converter depends on the actual technological solution. The results given above should therefore not be considered valid for any case. However, the methodology employing a meta-model (whose parameters are fitted) based on a detailed model of losses can obviously be applied to various topologies of DC/DC converters.

2.3.4 Power management of the electrical network and design of cables

The power management of the electrical network depends on the considered architecture concept.

Figure 2-23 depicts the presented architecture concepts, in the Chapter 1. The figure puts an emphasis on the different network functions (collection, export and transmission) for each architecture concepts. It also defines a Point of Common Coupling (PCC) PCC_{seq}, which is used in the sequential load flow (refer to section 2.3.5.1).

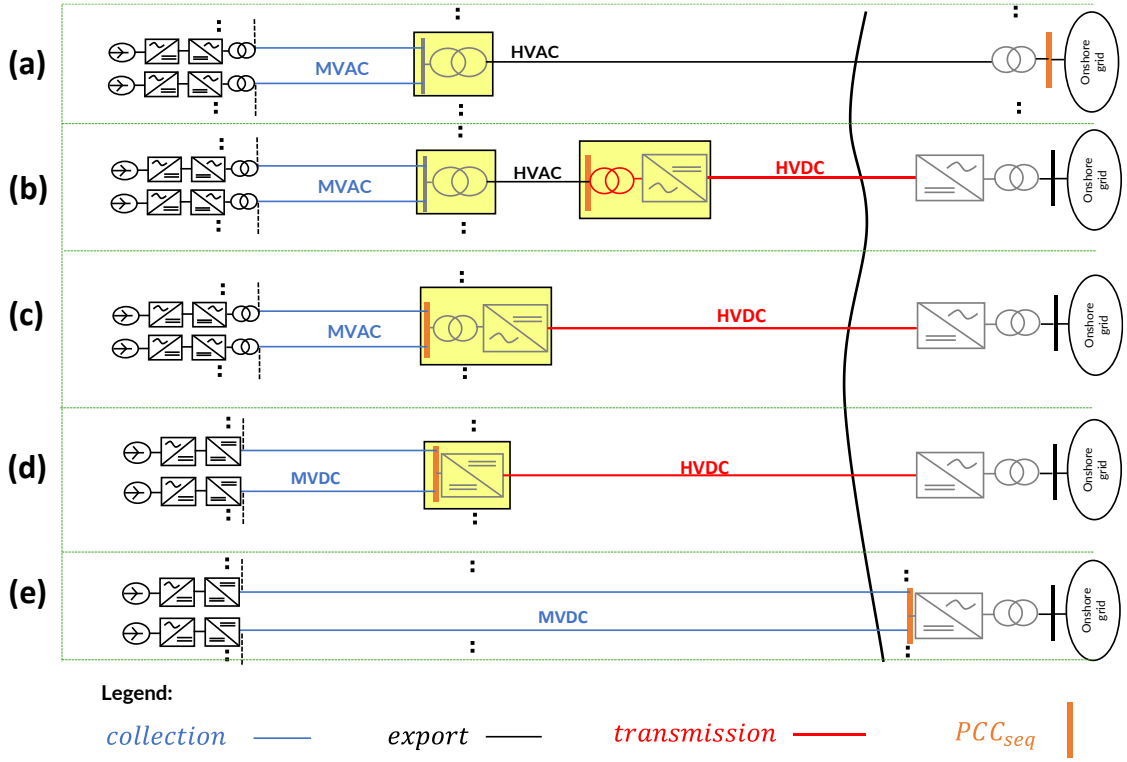

Figure 2-23: Architecture concepts considered in the PhD with an emphasis to network functions.

In the next sub-sections, the power management conditions are detailed for each of the network portions. Beyond the operational conditions, the relation with the sizing of the power components is tackled, notably for HVAC cables whose design highly depends on operational conditions due to the reactive power impact.

2.3.4.1 Power management of collection network(s)

As stated previously, the primary function of the collection network is to collect the power, which is injected by the wind turbines.

In case of MVAC collection networks, Schönleber et al. [88] show that the power factor of each wind turbine can be subject to an optimization aiming at minimizing the power losses in the collection (and export) network(s). However, the associated quantitative reduction of power losses is very low. In the present work, the wind turbine therefore has a unitary power factor (no reactive power injected or extracted). This is consistent with the current industrial practices and norms [88].

The voltage is imposed downstream of the collection network, or by a converter station (principles (b), (c), (d), (e)), which compensates the required reactive power when necessary ((b) and (c)). For the concept

(a), where the export HVAC cable(s) ensure(s) the export and transmission functions, the voltage is imposed by the onshore network. However, in the latter case, the network code can impose that the connection at the onshore PCC is done whilst providing ancillary services in relation with the reactive power.

In Chapter 5, the design of each collection cable, along with the choice of individual cables cross sections is done on the basis of the maximal active power flowing through the cable whilst neglecting the voltage drop down the feeder:

- In case of a MVDC collection network, the small voltage drop assumption is primarily justified as there is no reactive power. Moreover, the voltage being imposed downstream, the design assumption can only lead to a moderate overrating (in current) for the MVDC cables, which are at the end of a feeder. As the voltage drop is low for these short distances involved in a collection network (typically below 1% of the nominal voltage), the corresponding sub-optimality is acceptable.
- In case of MVAC collection network, this simplification is also justified due to the MVAC voltage level (up to 66kV MVAC) which does not induce a high charging current. Indeed, the shunt charging current is proportional to the voltage.

The neglecting of the reactive power in the design of MVAC cables (based on the above mentioned operational condition) can be justified quantitatively. To do so, the example of a 66kV three core MVAC cable is considered. A distance of 10km is considered as it is an upper order of magnitude for distances of collection feeders. A 630mm² cable is considered. The latter has an ampacity of 720 A, which corresponds to an apparent power rating of 82MVA (at 66kV). A multiple pi sections model, 1 km for each section (Figure 2-24), is integrated into the numerical load flow calculation by using the Pylon library [116] (a Python equivalent of Matpower) similarly as what is proposed in [117] (detailed in the section 2.3.5 for the load flow itself and 2.3.4.2 for HVAC cables).

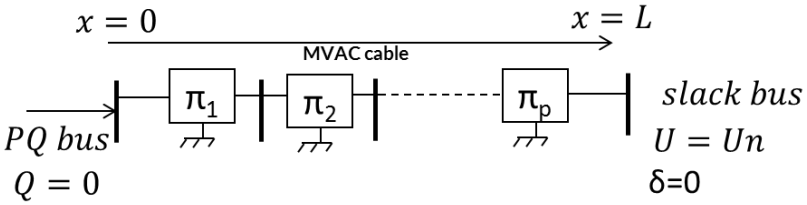

Figure 2-24: Load flow model and power management conditions for the MVAC cable

The active power losses (resulting from the load flow calculation) are worth 0.92 MW. The electrical parameters of the cable are calculated as defined in the section 2.3.1. The reactive power upstream equals zero (in accordance with the operational condition which is considered for a wind turbine). The PQ bus upstream is set with a negative P=-80MW due to the classical conventions: it means that a positive active power of 80MW is injected to the MVAC cable (at location *x=0*).

The reactive power at the slack bus is -2.3 MVAr, which means that overall, the MVAC cable produces a positive reactive power. These reactive power quantities can be calculated and checked by assuming constant voltage and current along the cable:

$$Q_{inductive} = 3.(2.\pi.f.l.I^2.L) = -1.50 \text{ MVAr (for 10 km)} \quad (2\text{-}35)$$

$$Q_{capacitive} = 2.\pi.f.C.{U_N}^2.L = 3.7 \text{ MVAr (for 10 km)} \quad (2\text{-}36)$$

where:

I is the current assumed constant along the cable (692 A, corresponding to 80 MW for 66 kV with a unitary power factor);

U_N is the phase to phase nominal voltage (66 kV here);

l is the inductance of the cable;

C is the capacitance of the cable (see section 2.3.1.1);

L is the length of the cable (see section 2.3.1.1);

f is the operating frequency.

Figure 2-25 is showing results of the load flow calculation and explains why the assumption that the voltage and current are constant along the cable is valid. This is because the voltage drop resulting from the current flowing through the distributed inductance and resistance along the cable is moderate and because the charging current is relatively low (compared to an HVAC cable).

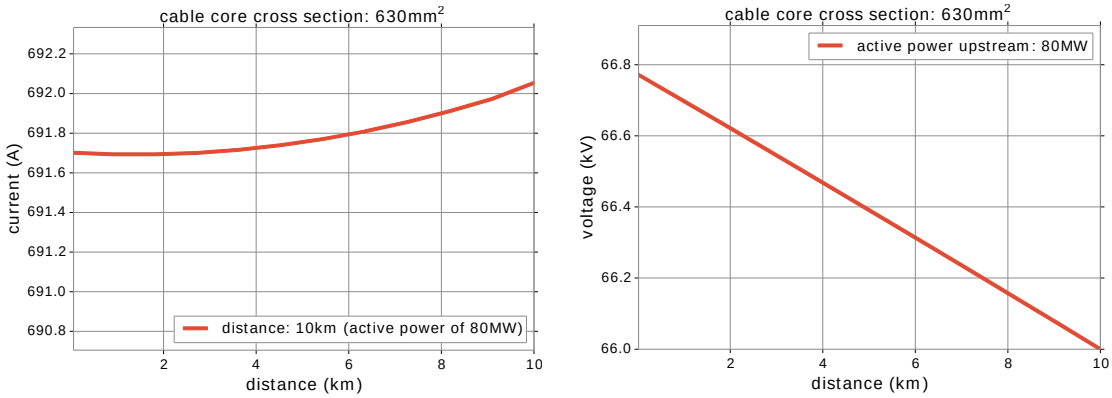

Figure 2-25: Load flow results for a 66kV with voltage imposed downstream and no reactive power injected or extracted upstream. (a): current and (b): voltage.

The voltage drop in DC are lower than in AC. The above given results therefore validate the assumption regarding the moderate voltage drop of MVDC collection cables. For the specific case of the architecture concept (e), where MVDC voltage is employed for transmission up to the shore, the distances can be high.

In conclusion, a unitary power factor is acceptable. Moreover, the voltage drop and reactive power contributions can be neglected for the collection cables design.

2.3.4.2 Sizing of reactive power compensation and maximum active power in HVAC network(s)

What is designated as export network is always based on HVAC cables in the present PhD. Unlike the case of MVAC cables, the reactive power plays a significant role in the power management and sizing of a HVAC cable. Indeed, as stated by Gustavsen and Mo [118], due to the distributed capacitances of HVAC cables with high voltage, there is a high charging current injection. As a result, the current is not uniform along the cable. Due to the distributed resistances and inductances, the voltage also evolves along the cable.

The Figure 2-26 and the Figure 2-27 propose for different distances, current and voltage distributions along the cable for a 220kV, 500mm² cross section cable instance; with reactive power compensation on both sides. As for the MVAC cable in the previous section, a distributed pi model of the cable is retained (see Figure 2-28). It gives a sufficient accuracy if the sections are small enough (1km per pi section).

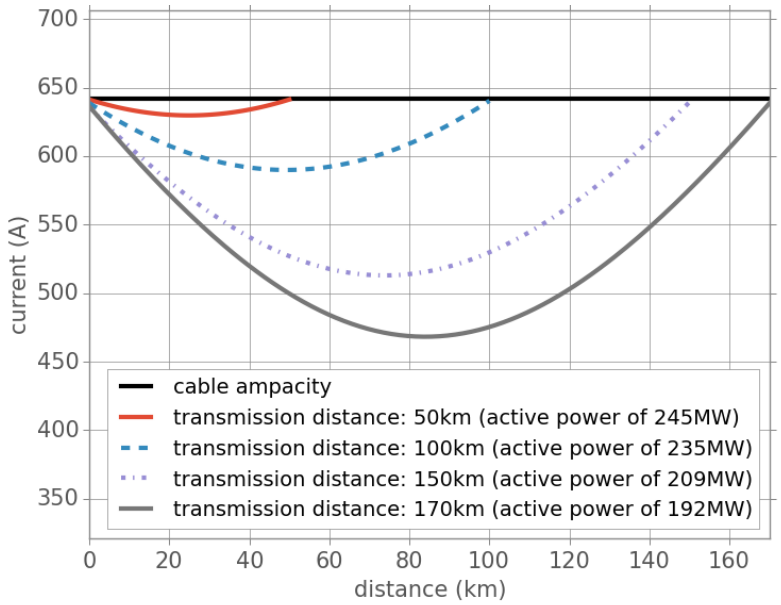

Figure 2-26: Currents distribution. Example of a 220kV and 500mm² cable

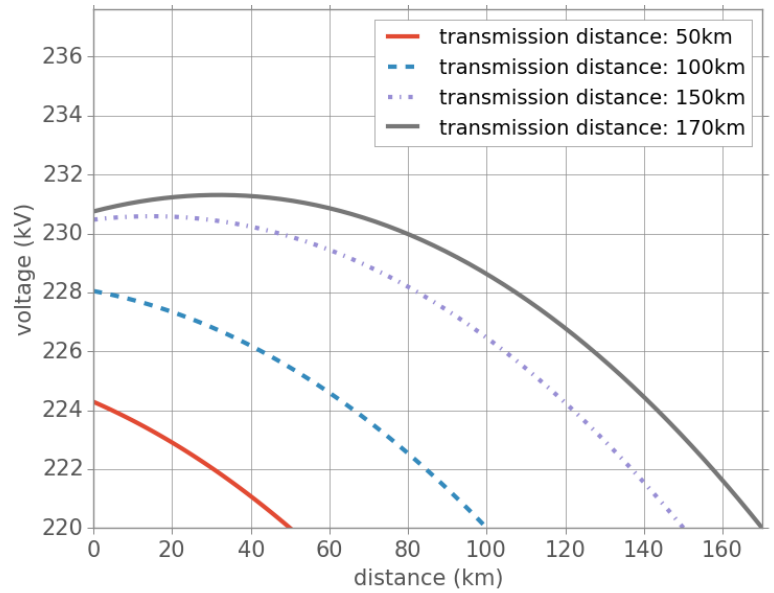

Figure 2-27: Voltages distribution. Example of a 220kV and 500mm² cable

In the present work, the power management and compensation of the cable has been determined by using the following objectives and constraints:

- Maximizing the active power, which can be transmitted (by imposing equality between offshore and onshore currents, which are at the bottlenecks).
- 2) Minimize voltage drop along the line.

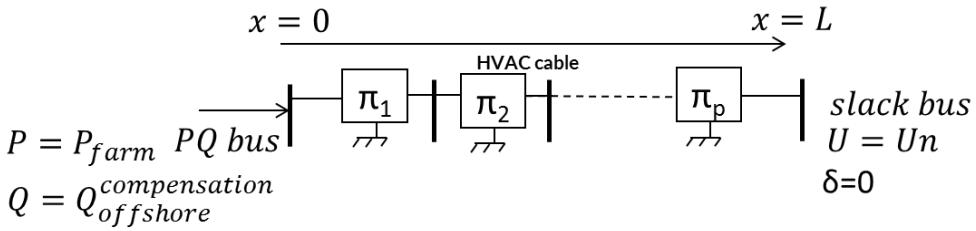

Figure 2-28: Load flow case used for the determination of optimal power management for a HVAC cable for a given distance.

The maximum current I_{max} transmitted by the cable comes from the ampacity model. It provides a first physical constraint to operational conditions of the cable. Another constraint is given by the maximal permanent voltage U_{max}. It is taken equal to $1.07 * U_n$ [119] (which is not an active constraint with the chosen reactive compensation configuration for 220 kV cables).

The used strategy is to compensate the reactive power of the cable at both sides. One optimization variable is the proportion of the reactive power which is compensated offshore, α_{share}. Figure 2-29 shows the flow chart, which presents the proposed methodology. It is verified that, for 220 kV HVAC cables, the constraint relative to the voltage is always respected if the one relative to the current is respected.

The maximal active power that can be transmitted from the wind farm must respect the onshore and offshore current constraints, which are at the critical points when the current can be maximal. These two current boundaries lead to equations (2-37) and (2-38).

$$P_{max}^{farm} = \sqrt{[U(0).I_{max}]^2 - Q_{offshore}^{compensation^2}} \quad (2\text{-}37)$$

$$P_{max}^{farm} = \frac{\sqrt{[U(L).I_{max}]^2 - Q_{onshore}^{compensation^2}}}{\eta} \quad (2\text{-}38)$$

With $U(L)$ imposed to U_n and η is the efficiency of the cable at maximal transmitted power. η is given by equation (2-39), where $P_{max}^{onshore}$ is the active power onshore, transmitted through the HVAC cable. In practice, $P_{max}^{onshore}$ is obtained as a result of a load flow calculation (refer to Figure 2-29).

$$\eta = \frac{P_{max}^{onshore}}{P_{max}^{farm}} \quad (2\text{-}39)$$

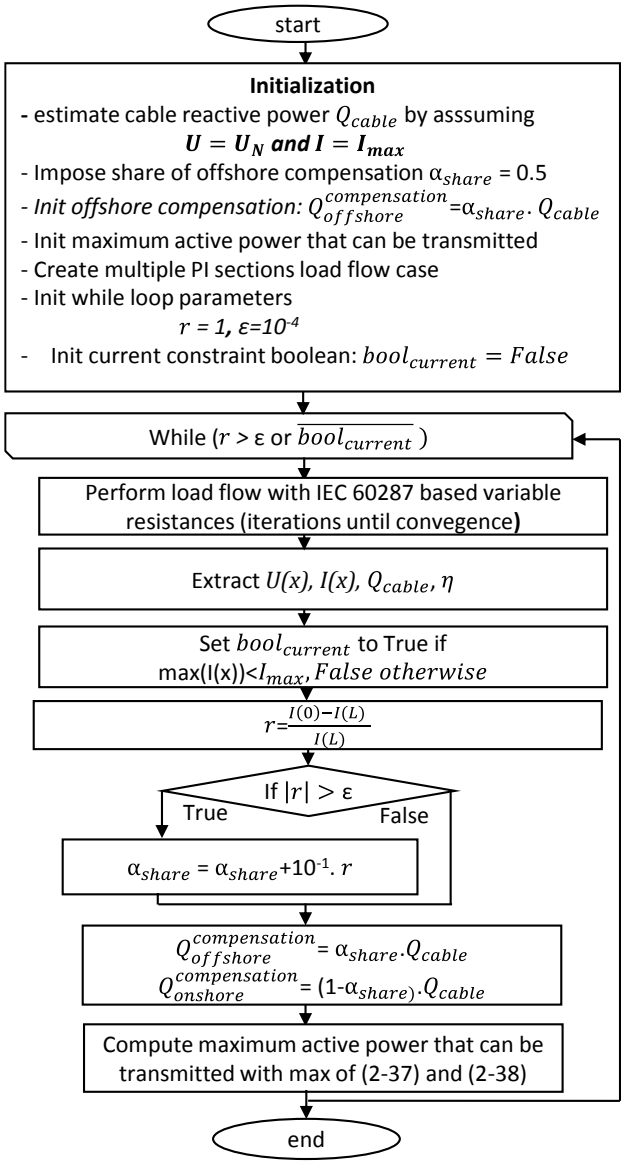

Figure 2-29: Chart flow of the cable design, with reactive power compensation for a given distance and cable cross section.

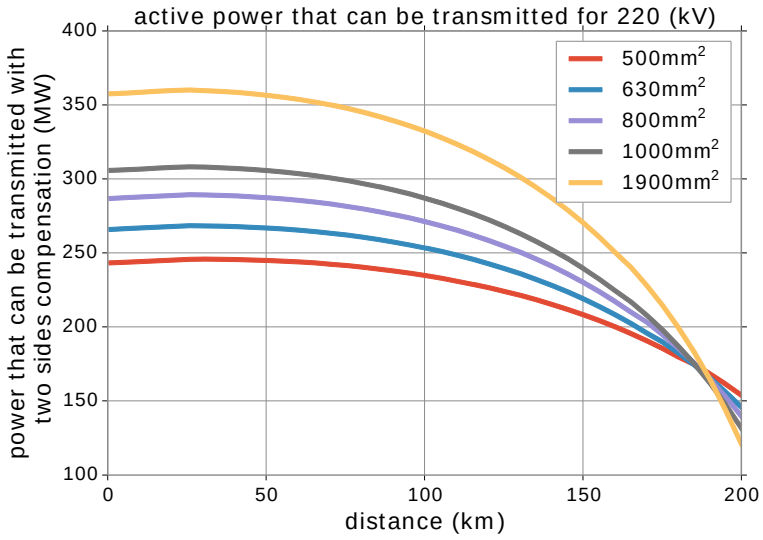

Figure 2-30: Maximum active power that can be transmitted from an offshore wind farm with optimal compensation at both sides.

Figure 2-30 shows the maximum active power transmitted obtained with the methodology for various distances and HVAC (220 kV) cables cross sections. An inflexion point can be observed in this figure, which corresponds to a distance of around 190 km. After this distance, the active power that can be transmitted collapses. In Chapter 5, this methodology is employed for the sizing of the HVAC cables, either for the connection of a cluster up to the shore (concept (a)) or to a HVDC converter station (concept (b)). In practice, the curves of Figure 2-30 are saved once. They are then loaded during a network design optimization, so to reduce the computational burden.

A typical installation consists in an offshore and onshore reactor of comparable size. Reactors can be sized to fully or partially compensate the cable capacitance depending on network code requirements. This point is further detailed by Dahmani [25]. If necessary, additional onshore compensation devices (such as shunt reactor or STATCOM) can be employed.

In practice, the compensation of long submarine cable is achieved with multiple shunt reactors. The size and location of these reactors is a tradeoff between utilization of the capacity for power transmission and the additional cost for installing several reactors [22]. The present heuristic approach is relevant in regard to the cost of the compensation as calculated with the models of Chapter 4. For 150kV HVAC cables, the same methodology can be applied. In this case, unlike for the case of 220 kV cables, the voltage constraint can be active for long distances. As 150kV cables are employed for moderate distances, this is not a major constraint.

2.3.4.3 Power management of the HVDC transmission network

As stated in the section 2.3.3 dedicated to HVDC converters, seen from the HVDC transmission network (concepts (b) to (d)), the HVDC offshore converter station(s) behave as current sources. This is similar as the case where the wind turbines connected to a MVDC collection network.

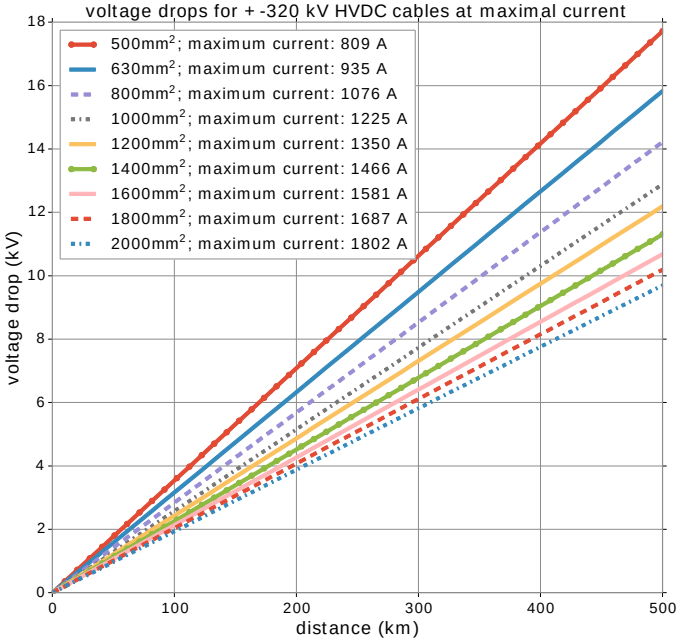

Figure 2-31: Voltage drops along a ±320kV cables at their maximal current

The HVDC voltage is imposed by the onshore MMC at the nominal voltage: standardly ±320kV.

In the same way as for collection cables, in Chapter 5, the HVDC transmission cables are designed whilst neglecting the voltage drop. The voltage drop along 320 kV HVDC cables operating at their maximal current are depicted in the Figure 2-31. The voltage drop remains below 5% for distances up to 500 km for the various cross-sections, which validates the assumption.

2.3.4.4 Synthesis of power management

Table 2-3 synthesizes the power management conditions imposed for the various networks.

Table 2-3: power management conditions for the network

Network function	Voltage type	Concepts	Power management assumption
Collection	MVAC	(a), (b), (c)	• Wind turbines inject only real power (with unitary power factor for MVAC network)
	MVDC	(d), (e)	
Export	HVAC	(a), (b)	• AC nominal voltage imposed downstream at $U_{AC,N}$ (by the converter station offshore or by the onshore network). • Shunt reactive power compensation upstream so to have currents upstream and downstream equal at maximal power.
Transmission	HVDC	(b), (c), (d)	• DC Nominal voltage imposed downstream at $U_{DC,N}$ by the onshore MMC.

A particularity of the architecture concepts (a) and (b) is that they have collection and export networks whose voltages are coupled. As a consequence, the reactive power compensation of the HVAC cables must be done whilst taking into account the reactive power of the collection network and of the transformer ensuring the interface between the two networks. In practice, the reactive power from the collection cables can be neglected, but the leakage reactance of the transformer must be taken into account as its value in per unit is high (see section 2.3.2 about the model of transformer).

2.3.5 Load flow calculations

A load flow is used to calculate the steady state of the electrical network after imposing power management operational conditions as those exposed in the section 2.3.4.

The integration of the presented models of power components into a load flow as done in the present PhD is illustrated in the Figure 2-32. The scheme shows that the impedances (resistances) calculated with the cable model as exposed in the section A.2 depends on the current flowing through the cable. To perform this coupling, in practice, several iterations of load flow calculations with updates of cables resistances are used. This is detailed and validated in A.2.

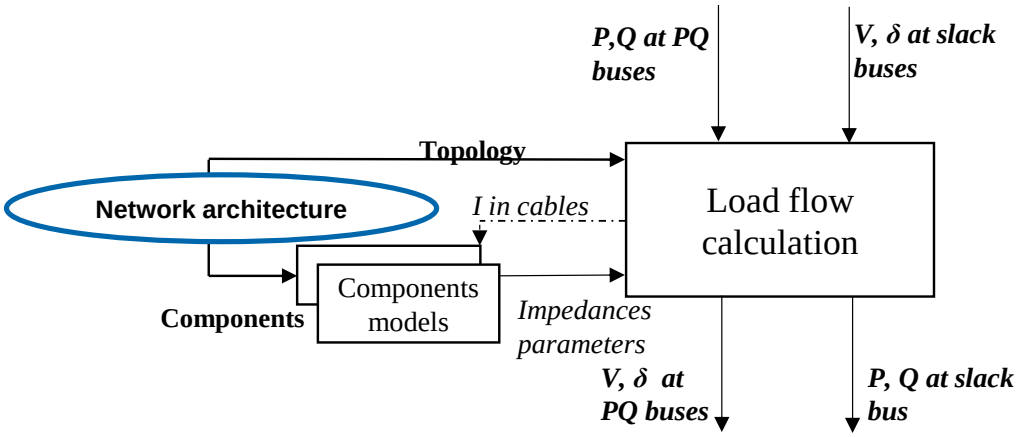

Figure 2-32: Generic scheme of load flow methods

The difficulty of the load flow calculation in the present work is the required genericity in regard to the various architecture concepts. Besides, as the architecture concepts include power converters between network portions, a method must be found to integrate them into a load flow. This challenge is very similar to the so called AC/DC power flow, which is discussed currently in the literature.

In the present work, a sequential approach similar to what is proposed by Beerten is al. [99] is used. Basically, the sequential approach consists in solving load flows for each portions of network separated by converters and sequentially couple them. It is detailed in the next sub-section (2.3.5.1).

In the sections 2.3.5.2 and 2.3.5.3, the solving methods/libraries employed for AC and DC load flows are presented.

2.3.5.1 Sequential/Meta load flow

A cluster network designates a collection network of a given cluster of wind turbines and, when applicable, the associated export network.

As defined in the Figure 2-33 for all the architecture concepts, each cluster network is connected to a Point Of Common Coupling PCC (PCC_{seq}) which is the cornerstone of the sequential load flow.

In this section, the expression "elementary load flow" is used to designate a load flow associated to one network portion: either a cluster network or a transmission network, calculated with methods in sections 2.3.5.2 (for AC networks) and 2.3.5.3 (for DC networks).

As in any classic load flow method, interfaces of an elementary load flow are based on three kinds of buses:

- *PQ bus*: Injected active power and reactive power (for AC) are imposed at this bus. A load flow computation calculates the resulting voltage magnitude V and angle δ at PQ buses. A PQ bus always corresponds to a power injection, which represents either a wind turbine (case where the network is a cluster network) or a wind farm PCC_{seq} (case where the network is a transmission network).
- *Slack bus*: The voltage magnitude V and the angle δ (excepted in DC) are imposed in general to 1 p.u and 0° respectively. P and Q are balanced and obtained by a load flow computation at the slack bus. A *slack bus always corresponds to an electrical extraction*, which is necessarily located downstream of a

network and represents either a PCC_{seq} (case where the network is a cluster network) or an onshore PCC (case where the network is a transmission network).

- *PV bus*: The active power and the voltage magnitude are imposed. They are supposed to model generators but this kind of bus is not used in the present work.

Figure 2-33 gives a schematic and generic representation of the system for the various architecture concept. In Figure 2-33, the power injections (PQ buses) corresponding to the wind turbines are not represented for the sake of simplicity.

The architecture concept (a) (where HVAC export is employed for the power transmission up to the onshore network) does not have a dedicated transmission network, neither transmission converters. Therefore, in that case, a simple AC load flow based on the solver exposed in the section 2.3.5.2 is applied to the whole electrical network.

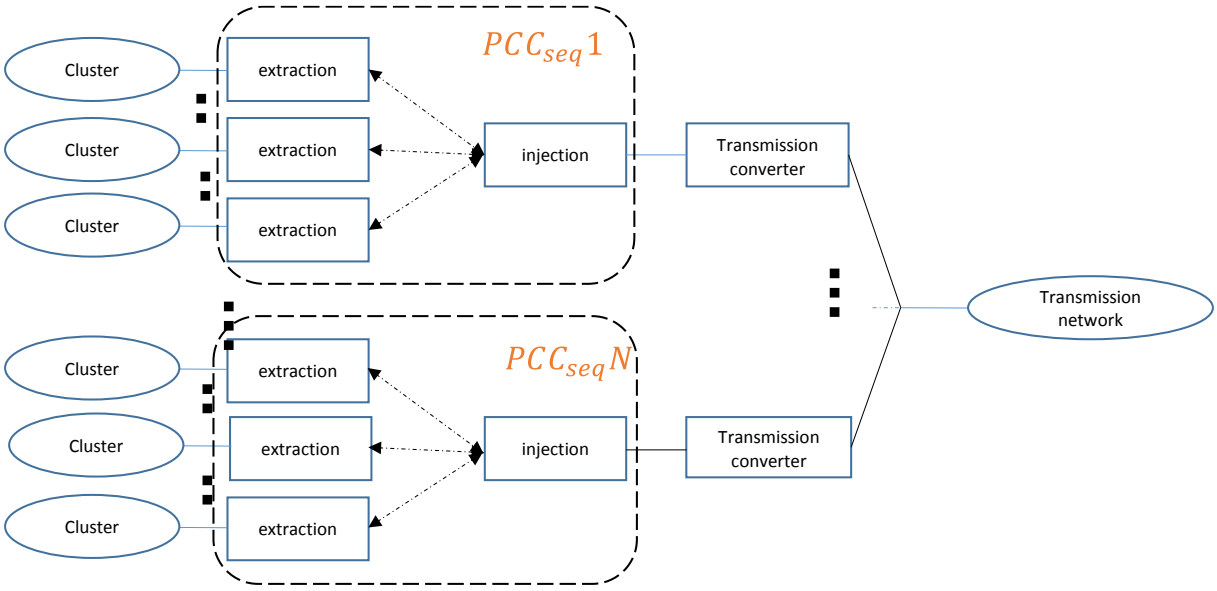

Figure 2-33: Schematic generic representation of the electrical network

The meta-load flow (or sequential load flow) handles the coupling between the different load flow calculations of the various network portions. The coupling consists in adding all powers (calculated from elementary load flows of clusters) to feed the load flow calculation of the transmission network, and to distribute the resulting calculated voltages to all clusters.

Figure 2-34 details the process for a given calculation of the overall electrical network state. The naming is the following:

- N_i is the number of cluster networks connected to PCC_{seq} i,
- Index j_i is one cluster network among the N_i cluster networks connected to PCC_{seq} i,
- $P_{extraction j_i}$, $Q_{extraction j_i}$ and $V_{extraction i_i}$ are respectively active power, reactive power and voltage magnitude of the cluster network extraction j_i connected to PCC_{seq} i. $P_{extraction j_i}$, $Q_{extraction j_i}$ are

results of the cluster network j_i power flow calculation while $V_{extraction i_i}$ is imposed as stated in the section 2.3.4. However, the methodology makes it possible to take into account technological solutions of HVDC converters, which induce a voltage drop; in that case, $V_{extraction i_i}$ is the result of the load flow for the transmission network.

- $P_{injection_{PCCi}}$, $Q_{injection_{PCCi}}$ and $V_{injection_i}$ are respectively active power, reactive power and voltage magnitude of the transmission injection point corresponding to PCC_{seq} of index *i.*

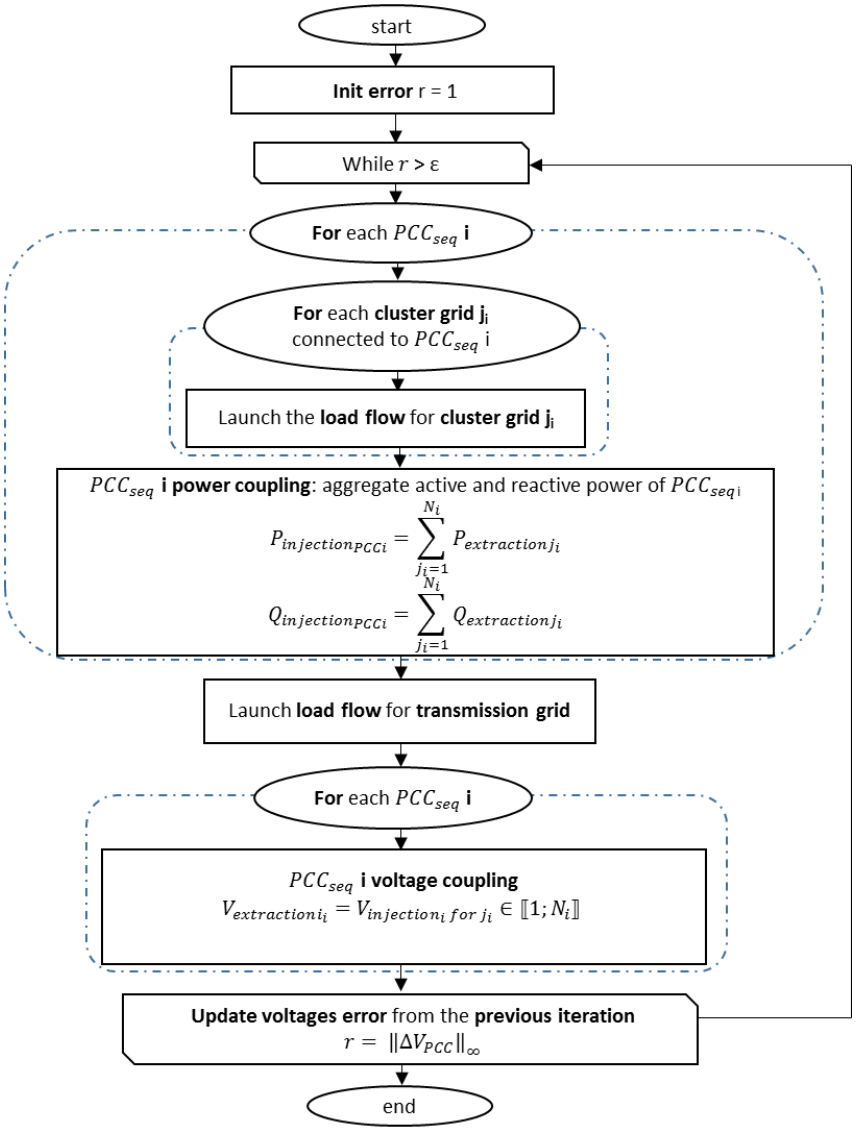

Figure 2-34: Meta-load flow chart flow

It should be noted that the cluster load flow calculations could be executed in parallel, which could allow to increase the computational speed. Another advantage of this sequential approach is that it is agile in terms of theoretical and software development. It is easier to adapt to new technological solutions as only load flows for networks portion need to be (re)developed.

2.3.5.2 AC load flow

2.3.5.2.1 AC load flow model with pylon library

The AC load flow method is based on a Python library "pylon" [116], a Python implementation of the Matpower Matlab library. Pylon lacks a detailed documentation but as it strictly reproduces Matpower, the associated documentation [120] can be used: indeed, though a case definition and its format are different (Matpower uses matrixes to define buses and branches while pylon uses definition of buses and branches objects), the formal representation of models and parameters are identical.

As mentioned, the definition of a load flow case is based on the specification of buses and branches of the network to be simulated:

- A *bus* can classically be a PQ bus, a PV bus or a slack bus. To define values of P, Q or V, per unit quantities must be used, by using a base power defined for the load flow case and by using a base voltage associated to the bus.
- A *branch* is an electrical connection between two buses and is modelled as shown in Figure 2-35. The generic branch model is used to model a cable or a transformer. Impedance related parameters (r, x_s or b_c) must be defined by normalizing them with the base impedance (where the base impedance is obtained by using equation (2-40)).

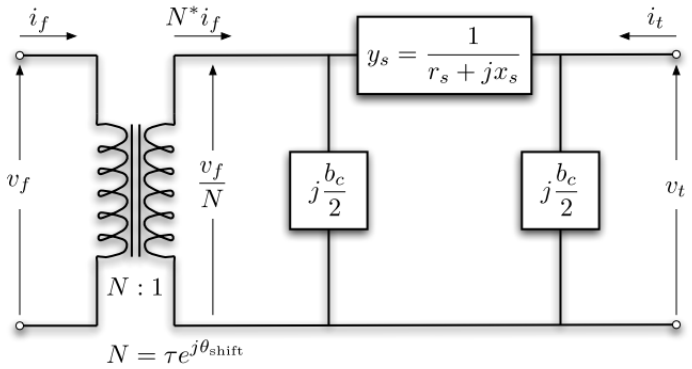

Figure 2-35: Branch model in pylon or Matpower [54]

$$base_{impedance} = \frac{\left(base_{voltage}\right)^2}{base_{power}} \qquad (2\text{-}40)$$

As Pylon solves an AC one phase problem, buses and branches must be defined on the basis of a one-phase equivalent circuit. In practice:

- RMS phase to phase voltage must be used,
- P and Q three-phase values must be used,
- It is consistent because:
  - Of the $\sqrt{3}$ factor between phase to phase and phase to ground voltages;
  - One phase P or Q is a third of the three phase value;

- The obtained $base_{impedance}$ consequently equals the value it would have if one phase power and phase to ground voltage values are used: it means that used impedances are per phase impedance values.

With Pylon, once a load-flow case is defined, the user (or the program) calls the solver and results are retrieved in branches and buses instances.

AC cable modeling with pylon

The pylon branch model is used by setting the appropriate values of its parameters. It is done by using the physical parameters as presented in the section 2.3.1. Then, these cable physical quantities are converted in per unit by using equations (2-41), (2-42), (2-43) and (2-44); where d is the cable length.

$$N = 1 \quad (2\text{-}41)$$

$$x_s = \frac{2\pi f.l.d}{base_{impedance}} \quad (2\text{-}42)$$

$$b_c = 2\pi f.C.base_{impedance} \quad (2\text{-}43)$$

$$r_s = \frac{\mathrm{R_{total,eq,T}}.d}{base_{impedance}} \quad (2\text{-}44)$$

So, to take cables dielectric losses into account, Pylon branch model cannot be used. However, buses have shunt active and reactive admittances parameters, respectively g_{shunt} and b_{shunt}. They are specified in MW (respectively Mvar) equivalent consumption (respectively injection) at a nominal voltage of 1 p.u. The AC cable model is therefore used to calculated dielectric losses w_d, given in section dedicated to the cable model (2.3.1.1). In practice, for each cable, g_{shunt} the value of the upstream connected bus, is used to take dielectric losses into account.

Transformer modeling by using branch model

As the transformer model presented in section 2.3.2 is a per unit model, it is similar to a branch model, which can thus be used. However, the base power of the load flow case must correspond to the transformer rating. Otherwise, per unit parameters of branch must be calculated following equations (2-45), (2-46) and (2-47), where S_r is the transformer apparent power rating and $base_{voltage}$ and $base_{impedance}$ are associated to the same connected bus (either the two at the primary or the two at the secondary).

$$r_s = R_{TS}.\frac{\left(base_{voltage}\right)^2}{base_{impedance}.S_r} \quad (2\text{-}45)$$

$$x_s = X_{TS}.\frac{\left(base_{voltage}\right)^2}{base_{impedance}.S_r} \quad (2\text{-}46)$$

$$b_c = -\frac{1}{X_m}.\frac{base_{impedance}.S_r}{\left(base_{voltage}\right)^2} \quad (2\text{-}47)$$

If no load losses should be considered, g_{shunt} of connected buses should be modified to take these losses into account. But as mentioned in section 2.3.2 no-load losses in transformers are very low and can be neglected.

2.3.5.3 DC load flow

2.3.5.3.1 DC radial load flow algorithm

For DC load flow calculations, an algorithm is developed for any DC radial network having only one voltage level. The philosophy comes from sweep backward forward load flow principle [121] used for AC radial distribution networks: a sweep is done in one direction to propagate the power through the network and in the other one to propagate the resulting voltage drops in branches. Implemented model and algorithm take advantages of the knowledge of active power (no reactive power in DC) direction in studied networks. Parameters of the model are:

- Resistances: R is a column vector, whose elements are branch resistances. D_R is a diagonal matrix corresponding to R.
- Topology: M is the matrix whose elements $a_{i,l} = 1$ if there is a connection in the downstream direction from bus j to branch i., 0 otherwise. M is given in equation (2-48) for the network example of Figure 2-36.

The inputs of the model are:

- Slack bus voltage magnitude: V_0 is a column vector whose elements have identical values corresponding to the slack bus voltage magnitude. V_0 is used as an initialization voltage vector.
- Bus power: P_{buses} is a column vector, whose elements are the power injected at the buses.

Outputs of the model are:

- Buses voltage magnitude: V is a column vector, whose elements are buses voltages.
- Power in branches: $P_{Branches}$ is a column vector, whose elements are power outputs of branches.
- Losses in branches: P_{losses} is a column vector, whose elements are power losses in branches.
- Currents in branches: I is a column vector, whose elements are currents in branches.

Branches and buses of the radial network are numbered so that a bus and the directly downstream associated branch have the same index as for the example of Figure 2-36. In this context, the slack bus is not part of the matrixes and of the vectors, but its voltage is imposed and is thus known; the output power of the connected branch corresponds to its power.

$P_{losses,cum}$ is an internal column vector whose element of index i corresponds to power losses in the upstream branches of branch i, including the branch itself. It is required inside algorithm to compute branches power outputs (represented by $P_{branches}$) taking into account losses in upstream branches.

$$M = \begin{matrix} 1 & 1 & 1 & 1 & 1 & 1 \\ 0 & 1 & 1 & 0 & 0 & 0 \\ 0 & 0 & 1 & 0 & 0 & 0 \\ 0 & 0 & 0 & 1 & 0 & 0 \\ 0 & 0 & 0 & 0 & 1 & 1 \\ 0 & 0 & 0 & 0 & 0 & 1 \end{matrix} \quad (2\text{-}48)$$

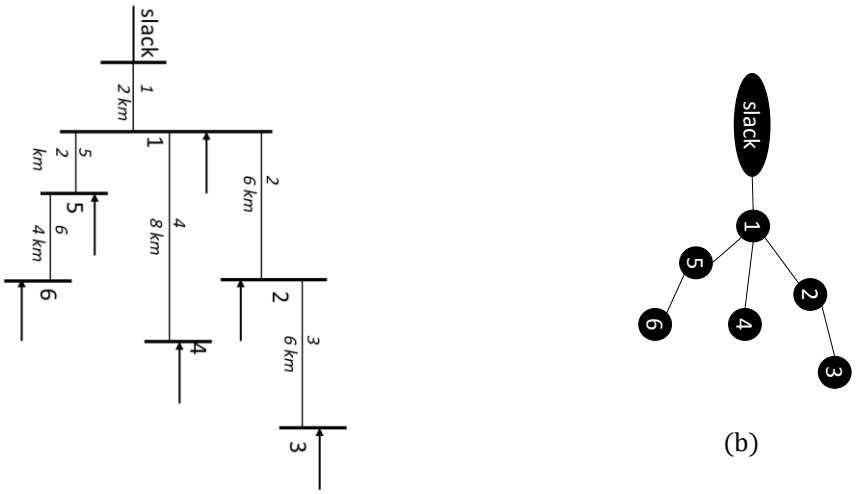

Figure 2-36: Branches and buses numbering example of a simple radial network. (a) Classical representation. (b) Graph representation.

The algorithm is shown in the chart flow of Figure 2-37, where * is a matrix product.

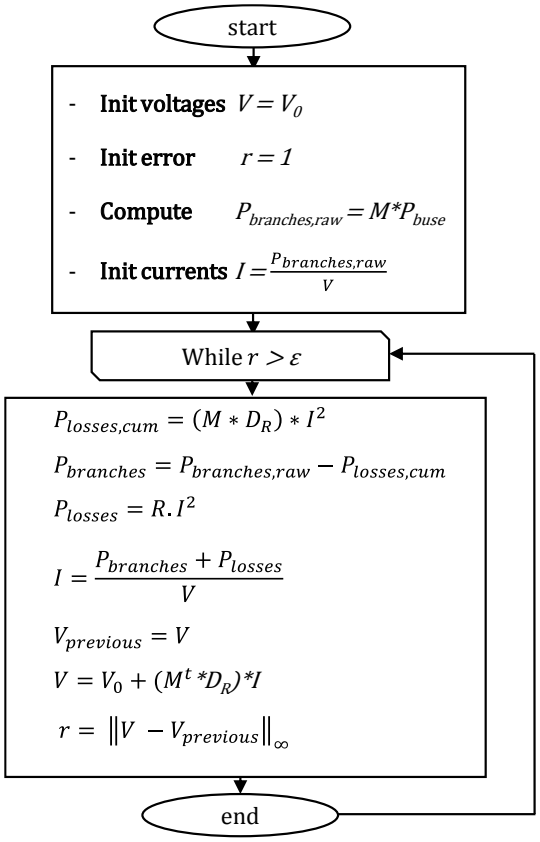

Figure 2-37: Developed radial DC load flow chart-flow algorithm

Other operators are always term to term operators. ε is a convergence criterion based on the voltage convergence. The DC radial load flow model parameters are basically cable resistances. All calculations are done per conductor. The load flow can thus be applicable to a monopolar network with a positive DC voltage and the ground.

2.3.5.3.2 Radial DC load flow validation

The study case for validation is based on seven buses (including the slack bus) network of Figure 2-36.

It is considered that each bus from 1 to 6 produces a power of 3.5 MW. The base power of the per unit system is 3.5 MW. The base voltage is 25 kV. The base impedance is consequently 179 ohms. The resistance of each branch is a multiple of resistance of one km of 300 mm^2 copper core at 20°C, 0.0601 ohm. The slack bus has a voltage fixed at 1 p.u. Parameters used for the load flow study case are summed up in the Table 2-4. ε used is fixed to 10^{-6}.

Table 2-4: DC radial load flow case study

Index	Bus injected power (MW)	Bus injected power (p.u)	Branch length (km)	Branch resistance (ohm)	Branch resistance (p.u)
1	3.5	1	2	0.1202	0.000673
2	3.5	1	6	0.3606	0.002019
3	3.5	1	6	0.3606	0.002019
4	3.5	1	8	0.4808	0.002692
5	3.5	1	2	0.1202	0.000673
6	3.5	1	4	0.2404	0.001346

The validation of the algorithm is done on the basis of:

- The voltage drop (or rise, in production case) adequacy with currents and impedances,
- The power conservation; in particular, the power extracted by slack bus must be equal to the sum of power injected at buses minus losses in branches,
- The current conservation at buses.

The load flow algorithm converges with three iterations. Results are given in Table 2-5, where recalculated bus voltages and branches losses are obtained from currents calculated by the load flow algorithm.

Table 2-5: DC radial load flow case study results

Index	Branch power output (p.u)	Branch losses (p.u)	Branch current (p.u)	Bus voltage (p.u)	Bus voltage error (%)
1	5.9595	0.0239	5.9595	1.0040	0
2	1.9901	0.0079	1.9821	1.0080	0
3	0.9980	0.0020	0.9901	1.0100	0
4	0.9973	0.0027	0.9934	1.0067	0
5	1.9960	0.0027	1.9880	1.0054	0
6	0.9987	0.0013	0.9934	1.0067	0

The voltage rise obtained from the load flow algorithm is consistent with currents and resistances in branches, which is not surprising as the voltage is used as a convergence criterion.

The power conservation is also verified as the sum of losses in branches (third column of Table 2-5) equals to 0.04046 p.u and the total injected power is 6.0 p.u. The difference corresponds to power extracted by the slack bus, which is the power output of branch 1: 5.95953 p.u. It is not surprising to verify that currents at nodes are retrieved: the example of bus 1 shows that the downstream current equals to 5.9595 p.u. While the sum of upstream currents (in branches 2, 4 and 5, respectively) added with the current corresponding to bus 1 injection (1.0040 x 1.0040) equals to 5.9595 p.u, which means that the error is smaller than 10^{-4} p.u (in fact even smaller than 10^{-6}).

2.4 Coupling of the wind power simulator with the load flow simulator

Physically, for a given wind velocity, each of the N_{WT} wind turbines produces a power that is injected to the collection network and which is then exported, transmitted up to the onshore PCC, where it is distributed.

As a consequence, as depicted in the Figure 2-38 (a), the wind power simulator provides the power produced by the wind turbines of the wind farm for a given velocity (by using the wind turbine model exposed in section 2.2.3).

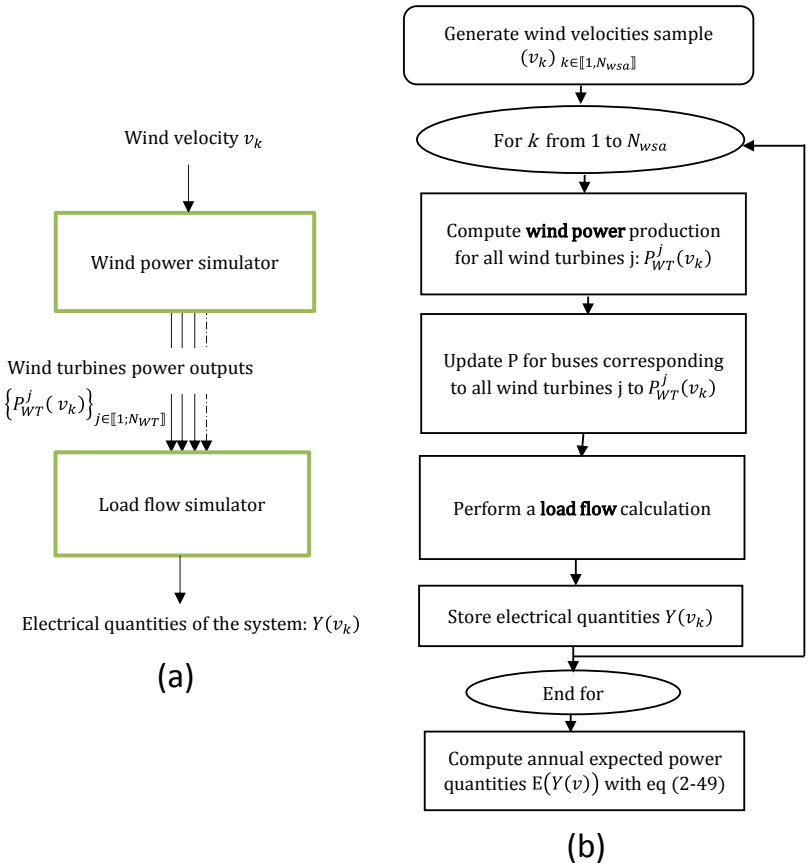

Figure 2-38: Schematic representation of the coupling methodology. (a) Calculated and exchanged quantities for given velocity sample. (b) Chart flow of the quantification method.

The active power of the buses corresponding to the wind turbines are modified accordingly in the wind power simulator. A load flow calculation for the electrical network is then performed for the given wind velocity.

The chart flow of Figure 2-38 (b) details the procedure. It consists first in sampling wind velocities. Then, the produced power are computed for each discrete wind velocity. Load flow calculations are performed for all the discrete wind velocities The results are various physical quantities, which are stored for each wind velocity of the sample $(v_k)_{k\in[\![1,N_{wsa}]\!]}$ are:

- Power injected by each wind turbine $P_{WT}^{j}:(v_k), j \in [\![1; N_{WT}]\!]$;
- Active power for each bus of the electrical network;
- Reactive power for each bus of the electrical network;
- Voltages for each bus of the electrical network;
- Active power transmitted by the branches (cables, transformers or converters) of the electrical network;
- Reactive power transmitted by the branches (cables, transformers or converters) of the electrical network.

Each of these above mentioned quantities can be calculated in a deterministic manner depending on the wind velocity v because:

- the power characteristic of wind turbines associates a deterministic produced power to any wind velocity (refer to section 2.2)
- the electrical state of the network for a given production of wind turbines is deterministic (calculated by means of a load flow calculation as exposed in section 2.3).

The wind velocity v is a probabilistic variable: obeying a Weibull probabilistic distribution as presented in the previous sub-section. Thus, let one of the mentioned variables depending on v be written $Y(v)$. As a consequence of the probabilistic transfer theorem, the expected value of Y, $E[Y]$ can be calculated by using (2-49).

$$E[Y] = \int_{v_{min}}^{v_{max}} Y(v).f_{WB}(v)dv \qquad (2\text{-}49)$$

where:

f_{WB} is the Weibull distribution function introduced in section 2.2.1.

v_{min} is the cut in speed of the wind turbines

v_{max} is the cut off speed of the wind turbines

In practice, the Simpson integration method, which is readily implemented in the Scipy library [95], is used for the numerical integration. A sample of 30 velocity values is standardly employed in this work as it gives a sufficient accuracy.

If $Y(v)$ corresponds to a power quantity, $E[Y]$ corresponds to the associated annual mean power. As a consequence, it can be used to estimate the associated expected energy. The latter is given by the value $T_{year}.E[Y]$, where T_{year} is the duration of one year. This is how, among others, the energetic indexes introduced in the Chapter 1 are quantified by following this principle:

- The annual energy produced by the wind turbines AEP_0, calculated with (2-50).
- The annual energy losses dissipated by the electrical network, calculated with *(2-51)*.
- The annual energy losses within a given component. It is calculated similarly as for the overall electrical network above. It consists in considering $Y(v)$ as being the power losses dissipated by the power components (from the network portion) and computing $T_{year}.E[Y]$ (by using equation (2-49)).

$$AEP_0 = W_{fa}.T_{year}.\int_{v_{min}}^{v_{max}} \sum_{j=1}^{N_{WT}} P_{WT}^{j}(v)\,.f_{WB}(v)dv \tag{2-50}$$

where Wfa is the wake factor which takes into account the wake losses. It is in the range of 0.9 to 0.85 as stated in section 2.2.2 [10], [11].

$$L_S^{dis}(X) = T_{year}.\int_{v_{min}}^{v_{max}} \left[\sum_{j=1}^{N_{WT}} P_{WT}^{j}(v) - P_{onshore}^{PCC}(v)\right].f_{WB}(v)dv \tag{2-51}$$

where $P_{onshore}^{PCC}(v)$ is the power distributed by the electric network at the onshore PCC for a given wind velocity.

As, for the sake of a limited computational duration and accuracy of the wake losses, the macro wake factor W_{fa} is employed for quantification of AEP_0 (see section 2.2.2), the wind power simulator and load flow simulator do not take into account the wake losses for a given wind velocity. The consequence is that the power, which is assumed to be injected to the electrical network by the wind turbines, is higher that it would actually be. It thus leads to a minor overestimation of the power losses and consequent annual energy dissipated in the electrical network $L_S^{dis}(X)$. What matters is that, when calculating $LCOE_{N,r}(X)$ or the capacity factor *CF(X),* the wake losses are taken into account because they have a more significant impact on the results. The error on the dissipated losses does not present the same order of magnitude.

The estimation of the annual energy distributed must be done as stated in Chapter 1, following an energetic conservation principle by using *(2-52)*.

$$AED(X) = AEP_0 - \left[L_S^{cur}(X) + L_S^{dis}(X)\right] \tag{2-52}$$

where $L_S^{cur}(X)$ is the annual curtailed energy (refer to Chapter 1) estimated by means of the methodology exposed in Chapter 4.

2.5 Conclusion

In this chapter, models and methods are proposed with the objective to quantify the energetic indices required for the assessment of an electrical network.

The section 2.2 presents the wind simulator the quantification of the annual energy produced by a wind farm AEP_0. The intermittence of the wind power production is taken into account by means of a probabilistic approach. The wake effects and associated wake losses are taken into account by a macroscopic approach.

A coupling with the wind power simulator presented in the section 2.3 makes possible the computation of the expected energies. The coupling methodology is presented in the section 2.4. Section 2.3 firstly presents the model of power components of the network (cables in section 2.3.1, transformers in section 2.3.2 and converters in the section 2.3.3).

Then, in section 2.3.4, the power management conditions are discussed for the collection, export and transmission networks. This is done for all the architecture concepts, which are presented in the Chapter 1. Beyond its technical necessity, this discussion justifies the optimization formulation, which is proposed in Chapter 5. Notably, it justifies that for the design of a collection network, the reactive power and voltage drop can be neglected (valid for MVAC and MVDC networks). Conversely, due to the capacitive reactive power, the power management and operation of a HVAC export network must mandatorily be taken into account in its design. A design method for a HVAC export network is proposed accordingly in the section 2.3.4.2. This design method is used in Chapter 5.

Finally, the integration of these static electrical models of power components into load flow methods is proposed in the section 2.3.5. A sequential load flow method makes it possible to calculate a steady state for any of the architecture concepts presented in the Chapter 1. It allows:

- The computation of the energetic indices relative to the performance of the network such as the expected annual energy dissipated by the electrical network $L_S(X)$. This is done thanks to the coupling with the probabilistic wind power simulator.
- The analysis of the cases where the operational technical constraints of the electrical network are respected (voltage, current, apparent power etc.). These constraints are imposed in the formulation of the electrical network design optimization, which is proposed in Chapter 5

The models and methods of this chapter do not make it possible to assess the reliability of the electrical network. Some method allowing to estimate the annual curtailed energy $L_S^{cur}(X)$ is presented in Chapter 4.

In Chapter 3, the modeling of the component of costs is proposed. The CAPEX is indeed necessary to compute the decision criteria (NLCC and LCOE)

Chapter 3: MODELING OF INVESTMENT COSTS

3.1 Introduction

The main goal of this research project is to compare various electrical network architectures in order to identify the best one regarding cost and reliability criteria. From available data in the bibliography, economic models of required power components are proposed in this chapter. They are used to quantify the investment costs (CAPEX: $C_S(X)$) of different architectures. As introduced in Chapter 1, the CAPEX models of the components are used to quantify the CAPEX of the electrical network $C_S(X)$, within the CAPEX calculator. The CAPEX of the network connection system $C_S(X)$ has a major impact on the assessment of the different architecture concepts (Figure 3-1).

After a state of the art regarding the CAPEX modeling of power components, a method is proposed to derive mathematical models integrating cost uncertainties. Hence, this method is applied to current power components in offshore electrical networks.

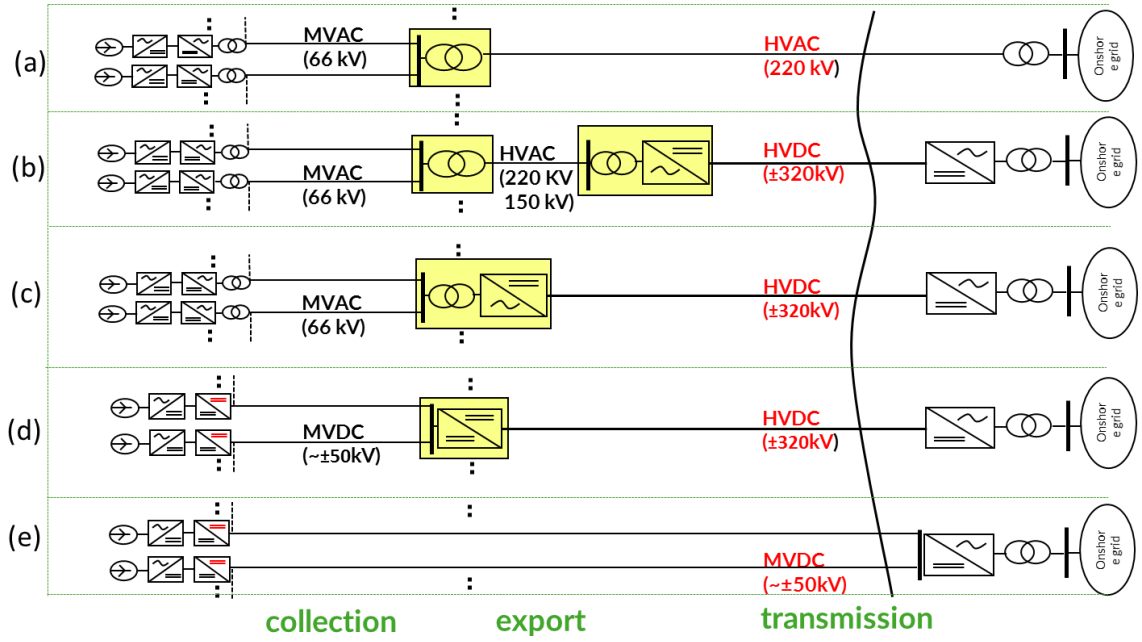

Figure 3-1: Architecture concepts

3.2 Calculation of the CAPEX of the electrical network

As the studied system is made of power components and potential associated support structure (offshore platforms, wind turbines support), it is necessary to have CAPEX models available for the following components of the system:

- High power electronic converters (MMC or MVDC/HVDC), in the section 3.5.1.
- HVDC platforms housing the offshore HVDC substations, in the section 3.5.2.1.
- AC platforms housing the offshore AC substations, in the section 3.5.2.2.
- Switchgears (MVAC, HVAC, MVDC, HVDC), in the section 3.5.1.4.

- Reactive power compensation components (MVAC and HVAC shunt reactors). These components have intrinsic costs but also induce indirect costs related to the AC offshore platform volumes, footprints and weights. The model is given in the section 3.5.1.3.
- Power transformers, in the section 3.5.1.2.
- Cables (three core MVAC and HVAC, the single core MVDC and HVDC), whose CAPEXs depends on their sizing (see section 3.5.3) but also on their installation (see section 3.5.4).
- Wind turbines, including the nacelle with the power conversion chain, the tower and the support structure. The supply and investment cost models are given in the section 3.5.5.

The cost, which are taken into account in the present work, includes supply and installation costs when no precision is given.

3.3 State of the art for CAPEX modeling of power components

As written in Chapter 1, Lazaridis and Ackermann [65], [66] (2005) and Lundberg [122] (2009) are pioneers in the assessment and comparison of network architectures connecting offshore wind farms. They provide CAPEX models for most of the items, which are listed above. However, the technology itself along with market costs has obviously evolved until today.

More recently, other authors studied the offshore wind farm connection problem and provide with CAPEX data and models [24], [25], [42], [43], [48], [65], [66], [68], [69], [71], [72], [74], [123]. Some of them propose new CAPEX models by using fitting approaches [66], [69], [124] when these authors are related to manufacturers or use cost data from real projects. Others use models or data already presented in the literature. Among others, Dahmani [25] provides a very good synthesis of the CAPEX models, which exist in the scientific literature but restricted to AC collection and HVAC transmission.

The ideal case would be to have manufacturers cost data from which a modeling would be possible. But, for confidentiality reasons, it is obviously not always possible. However, in the present work, unless stated otherwise, the proposed CAPEX models are built with a fitting approach based on the existing public industrial data, thought reliable:

- For transmission system items: the National Grid report [26],
- For the MV cables: the DNV GL report on 66 kV voltage level for collection cables [125],
- For wind turbines and other macro-economic factors associated to the offshore wind power plants: the Crown Estate [10] (UK, 2012) and Prognos and Fichtner [11] (Germany, 2013) reports on offshore wind power cost reduction.

When necessary, some alternative sources might be used. If so, it will be explicitly written. The analytical models used for the fitting will be justified case by case: either by citing some sources presenting these models or, if possible, with a technical justification.

An alternative major source of data is the very complete review of cost data for components of an offshore wind farm by Gonzalez-Rodriguez [126] (2017). It can be used for further improvement of the model

exposed in the present document. The two reasons why the data from this source are not used in the present work are:

- Some factors such as the inflation, and the market conditions are subject to high uncertainties. The data from Gonzalez-Rodriguez [126] are sometimes old but he does a very valuable processing of the data by taking inflation into account. However, the learning curves for the various components are not taken into account. Therefore, it appears that the cost of some items is over-estimated in [126]. The fact that some costs are from the US can also affect the consistency, because the market conditions are very different between the US and Europe.
- Integrating these data for improving the model requires a very rigorous analysis (in relation with the point above). As the reference was found late during the PhD (during the final writing), no sufficient time was remaining to integrate the data.

3.4 Methodology for CAPEX modeling

For various reasons including the confidentiality associated to some cost data, the required CAPEX models are subject to important uncertainties. As for a risk analysis, the CAPEX uncertainty associated with one item depends on its CAPEX impact (percentage of the total CAPEX of the system) and on the confidence associated to the model. The model itself is described by an analytical expression, a set of parameter values and a domain of validity.

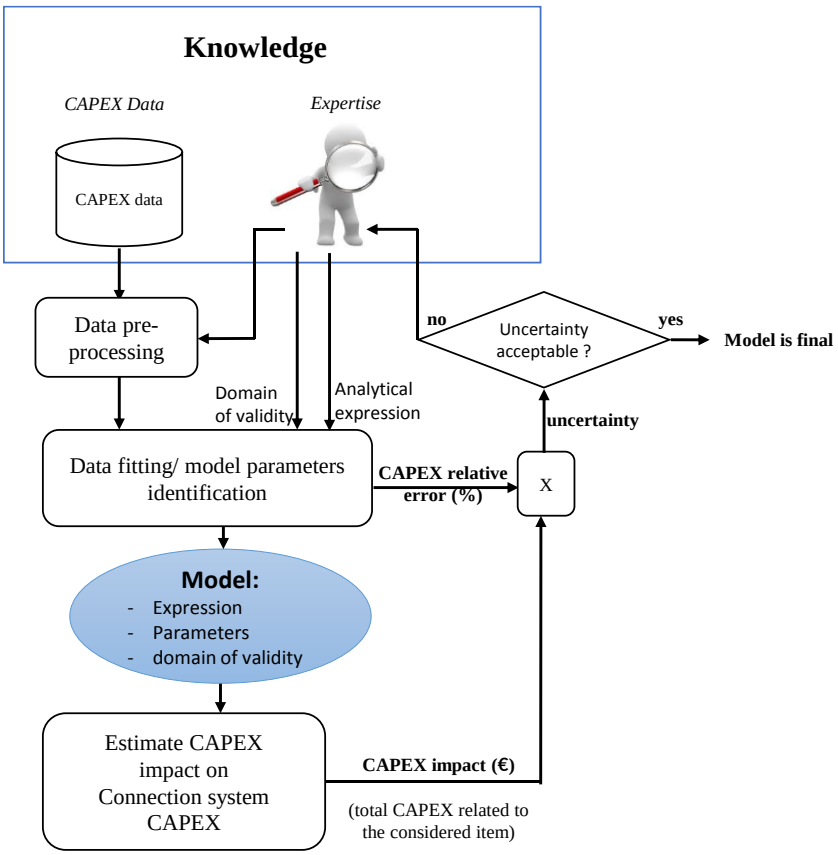

Figure 3-2 : Conceptual methodology for CAPEX modeling for a given item

As shown in Figure 3-2, the proposed CAPEX modeling follows an iterative process including the following phases:

1. Gather and prepare recent CAPEX public data [10], [11], [26], [125], which will be used for the determination of a model.
2. Propose an analytical expression of the model. One important aspect to highlight is that the data are not the only form of available knowledge. The technological expertise is important to be taken into account in the modeling process (see for instance the Cross industry Standard Process for Data Mining document [127]). In particular, the analytical expression should, as far as possible, be based on technological justifications. It is particularly crucial when the resulting model is used to extrapolate data: the expert not only provides the analytical expression but also gives technical boundaries, which form the domain of validity (e.g. the achievable apparent power rating of a HVDC converter for a given nominal voltage). In case where the data are the only form of knowledge, the analytical expression should remain simple enough and extrapolations should be avoided.
3. Fit the prepared data with the proposed analytical expression. This step is done by means of a particular least squares method exposed below (see identification function of equation (3-1)).
4. Perform CAPEX assessment of the architectures in order to quantify the order of magnitude in cost impact for each item. The main CAPEX data available are made of pessimistic and optimistic values. This is in particular the case with data from National Grid [26], which is a major data source for power components. It is also a classical case because the CAPEX of a product depends on market conditions (e.g. the copper price impact to the cost of power insulated cables, supply and demand etc.). As a result, a proposed least squares method is used for the identification of parameters P of a CAPEX model and is associated to the function f_P which is based on an objective function J to minimize (see the equation (3-1)). The objective function is the sum of squared differences with the optimistic values $C_{min,i}$ and with pessimistic values $C_{max,i}$. Weights w_{min} and w_{max} (taken in the domain $[0, 1]$) aim at extracting different sets of parameters depending on the scenario. In practice, for each CAPEX model f_P, three sets of parameters are identified:
   - Optimistic parameter set (where $(w_{min}, w_{max}) = (1,0)$)
   - Pessimistic parameter set ((where $(w_{min}, w_{max}) = (0,1)$)
   - "Mean" parameter set ((where $(w_{min}, w_{max}) = (1,1)$)

$$J(P) = \sum_{i \in E} w_{min}\left(f_P(X_i) - C_{min,i}\right)^2 + w_{max}\left(f_P(X_i) - C_{max,i}\right)^2 \quad (3\text{-}1)$$

where:

P is the set of parameters to identify;

J is the identification objective function to minimize;

f_P is the function associated to the analytical cost model, depending on the parameters set P;

E is the set of data point indices;

X_i is the vector of model inputs for data point i;

$C_{min,i}$ is the optimistic cost value associated to the data point i;

$C_{\max,i}$ is the pessimistic cost value associated to the data point i;

w_{min} is the weight given to the minimum cost ($wmin \in [0,1]$);

w_{max} is the weight given to the maximum cost ($wmax \in [0,1]$).

When the cost data available do not have min and max values, a relative error is imposed on the data used for the fitting of an analytical model. It is thought that, due to market conditions, the relative error cannot be below 10%. This is an arbitrary prior assumption, which is made when no more information is available. In practice, the minimization of the least square function (3-1) is done by using the module "optimize" of the Python library Scipy [95]. The "Nelder Mead" solver is used. The obtained optimum is taken as an initial solution for a second optimization by using the "CG" (Conjugate Gradient) algorithm when it is necessary.

For a given item, once an identification of parameters is determined, the maximum relative error in percentage with the extreme points can be determined. Then, an uncertainty in regard to the CAPEX can be estimated as shown in Figure 3-2: The total CAPEX of a considered component kind is multiplied by the relative error in percentage, which corresponds to the total maximum error in CAPEX in relation with this component. The higher is the obtained value, the higher is the uncertainty in regard to the CAPEX of this component kind. This measure of uncertainty is necessary because the relative error is not meaningful by itself. Indeed, for a component kind with a low total CAPEX (low in term of share of the total CAPEX of the electrical network), it does not really matter that its relative error is high.

In the present chapter, an indicative relative error is given for the component models. An indication of the qualitative share of the total CAPEX is also given for the various components. A more advanced way of handling CAPEX uncertainties in proposed in Chapter 6, which is based on the scenarios parameters identified in the present chapter, used within a probabilistic approach.

3.5 CAPEX modeling

3.6 Conclusion

In the present chapter, some cost models are presented for items involved in the offshore wind farm system including the electrical network(s).

The found investment cost models of the studied architectures $C_S(X)$ are given in Table 3-1. For the sake of simplicity, a synthetic formulation are retained, similarly as what is proposed in Serrano Gonzalez and al. [71].

Table 3-1: Calculation of electrical network CAPEX for the different architecture concepts

concepts	Formulation of electrical network CAPEX	
(a)	$C_S(X) = \sum C_{platform}^{AC} + \sum C_{tran} + \sum C_{comp} + \sum C_{breaker}^{AC} + \sum C_{cable,tot}^{MVAC} + \sum C_{cable,tot}^{HVAC}$	(3-2)
(b)	$C_S(X) = \sum C_{MMC} + \sum C_{platform}^{HVDC} + \sum C_{cable,sup}^{HVDC} + \sum C_{platform}^{AC} + \sum C_{tran} + \sum C_{comp} + \sum C_{breaker}^{AC} + \sum C_{cable,tot}^{MVAC} + \sum C_{cable,tot}^{HVAC}$	(3-3)
(c)	$C_S(X) = \sum C_{MMC} + \sum C_{platform}^{HVDC} + \sum C_{cable,sup}^{HVDC} + \sum C_{breaker}^{AC} + \sum C_{cable,tot}^{MVAC}$	(3-4)
(d)	$C_S(X) = \sum C_{MMC} + \sum C_{MVDC/HVDC} + \sum C_{platform}^{HVDC} + \sum C_{cable,sup}^{HVDC} + \sum C_{breaker}^{DC} + \sum C_{cable,tot}^{MVDC}$	(3-5)
(e)	$C_S(X) = \sum C_{MMC} + \sum C_{breaker}^{DC} + \sum C_{cable,tot}^{MVDC}$	(3-6)

where :

$C_{cable,tot}^{MVAC}$ is calculated as the sum of supply and installation cost of MVAC cables, by using the models of sections 3.5.3.2 and 3.5.4.

$C_{cable,tot}^{MVDC}$ is calculated as the sum of supply and installation cost of MVDC cables, by using the models of sections 3.5.3.4 and 3.5.4.

$C_{cable,tot}^{HVAC}$ is calculated as the sum of supply and installation cost of HVAC cables, by using the models of sections 3.5.3.1 and 3.5.4.

$C_{cable,tot}^{HVDC}$ is calculated as the sum of supply and installation cost of HVDC cables, by using the models of sections 3.5.3.3 and 3.5.4.

The models are based on a data driven approach with useful prices and costs that are needed to deduce the LCOE. However, the analytical formulation of the models are justified with physical/expert understanding. They provide the most economic data to enable the programming of the proposed framework (refer to Figure 1-20) and the application of the optimization algorithms.

To take into account the uncertainty onto the costs, for each model, three set of parameters are given, depending on “optimistic”, “pessimistic” and “mean” scenarios. These scenarios allow to capture the uncertainties related to cost models. These uncertainties are present in the public available data, which are used for the fitting for each item model.

After detailing how to calculate investment costs, next chapter will propose two methodologies to assess the reliability of the electrical network.

Chapter 4: RELIABILITY ASSESSMENT

4.1 Introduction

In previous chapters, the electrical modeling and the cost modeling have been presented. In the present chapter, methods to quantify a measurement of the electrical network reliability (the annual energy curtailed), required for the calculation of the LCOE and NLCC, are proposed.

In section 4.2, a state of the art of existing method for the assessment of the architecture reliability is presented. In section 4.3, a method dedicated to wind power context to calculate the expected power curtailed due to the network unavailability is presented. In section 4.4, the method of section 4.3 is used on a benchmark case for quantifying the expected curtailed power in N-1 states. Then, it is used within two methods allowing the estimation of the annual energy curtailed. In section 4.5, a method to estimate the expected value of the annual energy curtailed is proposed. In section 4.6, a Monte Carlo simulation based method is proposed; it allows the determination of an empirical probability distribution of the annual energy curtailed.

After a collection of required reliability data is done in section 4.7, a validation of the proposed reliability assessment methods is given in section 4.8.

4.2 Existing indices and methods for the reliability assessment

There are two main scientific challenges for assessing a power electrical network:

- The first one is to define meaningful quantitative indices;
- The second one, but not the least, is to define efficient estimators and associated algorithms/methods to quantify the previous defined indices. The performances of these methods can be measured by their accuracy and their computational cost.

On that subject, Billinton, [135], [136], is a well-known reference, notably for the definition of reliability indexes among which are:

- The Loss of Load Expectation (LOLE).
- The Expected Energy Not Supplied (EENS).

EENS is a quantity adapted to our problem. Indeed, an offshore wind power plant injects its produced power whatever the consumption is and also because the power which is not supplied, affects the profitability of the plant. It corresponds to $L_S^{cur}(X)$, defined in Chapter 1 of the present thesis and is depending on the electrical network architecture. Its quantification must take into account the particularity of wind power production, notably the intermittence of the wind.

To compute the different indices, Billinton proposes in addition a Capacity Outage Probability Table (COPT), which associates power capacity levels to probabilities. These probabilities can be used to compute the various reliability indices. A state space Markov diagram to compute the COPT is also used, and applied to a three terminal DC system having two LCC stations and one VSC station [137]. But as the complexity of a system grows, the computational cost associated to the calculation of this indicator increases.

In the context of offshore wind power systems, some authors aim at developing analytical models or efficient algorithms so to reduce the computational burden. Notably, Dahmani translates the topology of the studied electrical system (limited to the collection grid) into a reliability graph [138]. Then he applies simplifications to compute the EENS but does not take into account the intermittent nature of wind power production. Moreover, since he does not take into account the rating constraints of the components, it means that he assumes that any power path is enough rated to transmit any amount of power. In particular, a system including parallel components with partial power rating cannot be taken into account by using that method.

Also, Ackermann et al. [65] quantify the EENS for transmission networks for offshore wind farms by considering the different associated failure modes. As for a COPT, each mode is defined depending on the maximum power than can be transmitted. Simple probabilistic formula to calculate the probability of each mode are proposed. When the size of the network increases (number of components), notably when the collection network is included, the complexity of analytical formula grows. De Prada et al. [19], [21], [139] propose analytical formula to calculate the expected EENS for the electrical network connecting an offshore wind farm, including the collection, export and transmission networks. The computational cost decreases with such analytical formula, but the formula are not generic in regard to architecture concepts and topologies. For instance if a branched topology is employed for the collection network, the formula proposed by de Prada in [139] are not applicable.

Several authors use Monte Carlo simulations to estimate indices assessing the reliability of the electrical system. In a general context, Zio [140] exposes and uses Monte Carlo Simulation methods. He shows that this term comprises various methods, especially depending on the sampling methodology. Monjean [42] uses a Monte Carlo simulation to quantify the EENS of the electrical system connecting offshore wind farms. To do so, Monjean samples the wind velocities given by a Weibull probability distribution and the states of the electrical network. In the context of offshore HVDC networks, MacIver et al. [141], [142] use a Monte Carlo simulation to compute some reliability indices whilst taking into account the weather conditions. Jaramillo et al. [80] use a similar method to assess the EENS associated to the export network. They use the method to optimize the rating of export transformers as the compromise between the CAPEX and the EENS.

Any approach aiming at calculating the EENS (named $L_S^{cur}(X)$ in the present work) requires to know the unavailability U of each component (i.e. the probability that the component is unavailable during a given time lapse). These data can either be obtained by using mean unavailability durations based on surveys (as in [65]) or from the knowledge of failure rates λ and repair rates μ. λ and μ are related to the Mean Time To Failure (MTTF) and to the Mean Time To Repair (MTTR) by using the equations (4-1) and (4-2).

$$\mu = \frac{1}{MTTR} \tag{4-1}$$

$$\lambda = \frac{1}{MTTF} \tag{4-2}$$

These data are obtained thanks to experience and are thus subject of high uncertainties, particularly for novel components. To take these uncertainties into account, Gonzalez et al. [71] consider a Gaussian probabilistic law for the MTTR (standard deviation of 10% of the mean value). The dependency of the system reliability to these data associated to the components shows that the system inherits the reliability of its components.

The unavailability U can be calculated by using the equation (4-3), which is the result of a steady state Markov process as depicted in the Figure 4-1.

$$U = \frac{\lambda}{\mu + \lambda} \tag{4-3}$$

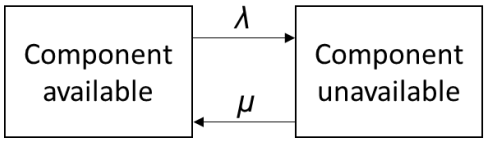

Figure 4-1: Two states Markov model for the unavailability of a component

In the section 4.3, a method allowing the determination of the impact in the case of an expected power curtailment (taking wind intermittence into account) for a given state of the electrical network system is exposed. The method is based on constrained max flow calculations. It does not require reliability data such as the MTTR and the MTTF of the power components.

The method of section 4.3 is the cornerstone of the calculation of the annual curtailed energy ($L_S^{cur}(X)$) within methods exposed in the sections 4.5 and 4.6. These methods and associated estimators are based on the use of μ and λ (refer to equations (4-1) and (4-2)) whose values for the different components of the electrical networks are collected from the literature and processed as exposed in the section 4.7.

4.3 Quantifying the expected power curtailed with a max flow algorithm

The studied offshore electrical network has a specific function, which is to collect, export and transmit wind power from the wind turbines to the shore. The expected power produced is therefore an important criterion. As presented in Chapter 2, it is the consequence of:

1) The wind resources modeled by a Weibull distribution function $f_{WB}(v)$.
2) The wind generator power characteristics giving the electrical power produced as a function of the wind velocity.

It is also the consequence of the availability of the electrical network, which must be able to collect, export and transmit the produced power. If, one or several components are unavailable, it can appear that some transmittable power must be curtailed.

One consideration used in the present work is that the stochasticity in relation with the wind velocity is not correlated to the state of the electrical network SS (where the state SS defines the availabilities of

components). The two phenomena are independent from a probabilistic point of view. They are considered for the quantification of their impact on the annual curtailed energy. Thus, to accelerate the calculation and to ease the analysis of the results, the asymptotic impact (expected curtailed power) of phenomenon associated to the wind velocity is considered for a given state of the system.

For a given wind velocity v, the wind powers are determined in a deterministic way by using the power characteristics of the wind turbines. Moreover, for a given state of the system, the power curtailment for a given wind velocity v is deterministic and depends on the power ratings of available components. Thus, for a given state of the system, the expected power not distributed (or "curtailed") due to components unavailabilities can be calculated as the expected value of the power curtailed. It is done by using the transfer theorem of the probability theory.

The probabilistic transfer theorem can be used to compute the expected value of a random variable Y so that $Y=\varphi(X)$, where X is a random variable with a density function f_X on an interval I. In such case, the expected value of Y, $E[Y]$, can be calculated by using (4-4).

$$E[Y] = \int_{x \in I} \varphi(x).f_X(x).dx \tag{4-4}$$

The asymptotic annual mean power not distributed (or "curtailed") due to component failures for the system state SS is analytically calculated as a consequence of the transfer theorem:

$$E[P_{curtailed}(SS)] = \int_{v_{min}}^{v_{max}} P_{curtail}(SS)(v).f_{WB}(v).dv \tag{4-5}$$

where :

SS is the state of the electrical network system. $SS = \{s_i\}_{i \in C}$, C being the set of power component indexes and s_i the state of the component i (see (4-6)).

$P_{curtail}(SS)(v)$ is the random power, which cannot be transmitted to the onshore grid due to component(s) unavailability(ies) for a power production corresponding to a wind velocity v.

$$s_i = \begin{cases} 0 \text{ if the component i is not available} \\ 1 \text{ if the component i is available} \end{cases} \tag{4-6}$$

$E[Y]$ is the mathematical expected value of a probabilistic variable Y. In the present case, $E[P_{curtailed}(SS)]$ is the expected value of the probabilistic variable $P_{curtailed}(SS)(v)$ in regard to the wind velocity, which is modeled as a probabilistic variable following a Weibull probabilistic distribution. The relationship between $P_{curtailed}(SS)(v)$ and v is deterministic. Formally, the method proposed below allows the calculation of the deterministic function φ_{SS} so that for a given system state SS, $P_{curtail}(SS)(v)=\varphi_{SS}(v)$.

The proposed method aims at taking advantage of an existing solving algorithm based on operational researches and the graph theory. It is the capacity constrained maximum flow. The general procedure to compute $E[P_{curtailed}(SS)]$ is presented in the Figure 4-2.

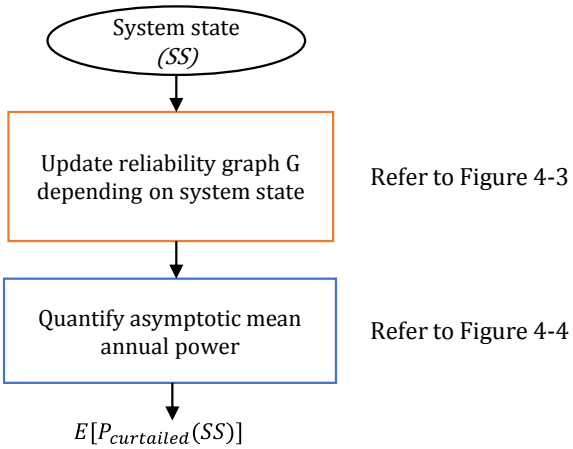

Figure 4-2: General procedure for calculation of the expected mean power curtailed

The studied electrical network is represented as a graph. This representation is then used to calculate constrained max flows. To do so, each component is represented by an edge, which has a "capacity" attribute corresponding to the power rating of the power component in its available state. The electrical buses are nodes of the graph. The wind turbines are edges whose, "capacity" attributes correspond to the production level. The wind turbines are then connected to a single "source" node and the onshore Point of Common Coupling (PCC) to a "sink" node. Figure 4-3 shows on an example how the "source" is connected to wind generator outputs by edges representing the wind turbines: this approach then allows, if necessary, various production levels by setting the capacities of the different wind turbines edges to different values.

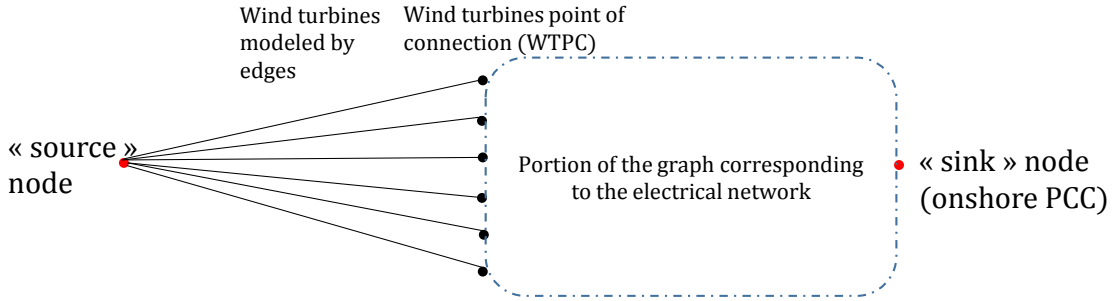

Figure 4-3: Example of reliabity graph describing the connection of the "source" to six wind turbines outputs

Knowing a system state with defined available components, the "capacity" of each edge representing a component is modified to be set to zero if the component is down, as presented in Figure 4-4. For the sake of simplicity, the portion of the graph corresponding to the electrical network is not represented. It can have any topology, in relation with the actual architecture of the electrical network.

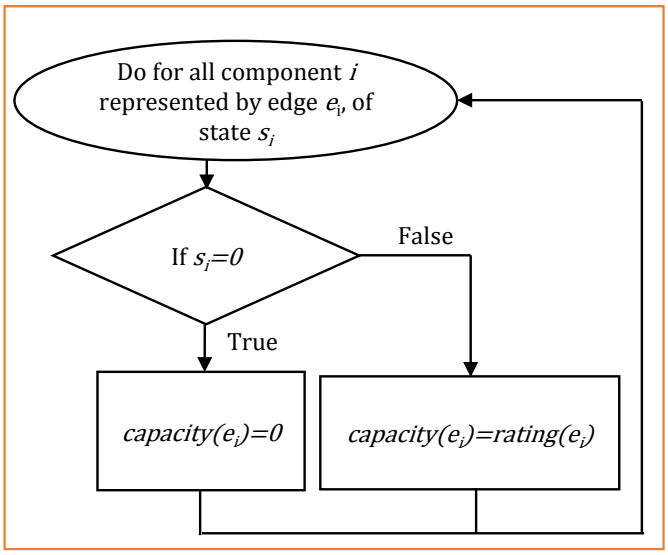

Figure 4-4: Chart flow showing the translation of the system state into a graph with appropriate attributes.

Once the attributes of the reliability graph are updated following the process of Figure 4-4, the calculation of $E[P_{curtailed}(SS)]$ is done following the method depicted in Figure 4-5.

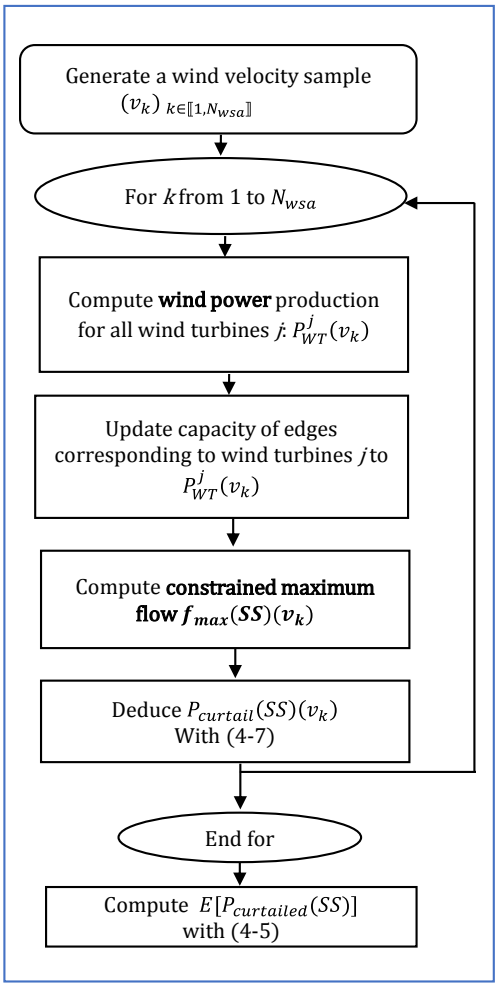

Figure 4-5: Chart flowsshowing the method for the quantification of the asymptotic annual mean power.

The power produced by the N_{WT} wind turbines for a wind velocity is obtained from the wind turbine power characteristic as presented in Chapter 2 and depicted in Figure 4-6 (taken from The Crown Estate study [10]). A sample from N_{wsa} wind velocity points ($(v_k)_{k\in N_{wsa}}$) is used in the procedure of Figure 4-5. This sample is determined in a deterministic manner in order to then, perform the numerical integration required for the calculation of the expected value $E[P_{curtailed}(SS)]$ (refer to equation (4-5)). In practice, the numerical integration is done with the Simpson method, which is readily implemented in the Scipy library [95].

It should be emphasized that the wind velocity sampling is not stochastic. It is only done so to perform the numerical integration corresponding to equation (4-5). Simpson discrete integration is done based on the knowledge of discrete values of the quantity $P_{curtail}(SS)(v_k).f_{WB}(v_k)$ for $k \in N_{wsa}$.

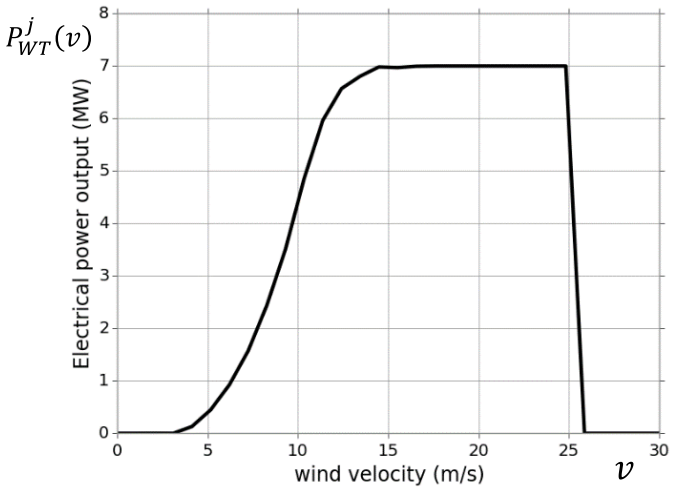

Figure 4-6: Wind turbine power characteristic

For a given wind velocity v_k, the power curtailed $P_{curtailed}(SS)(v_k)$ is calculated by using (4-7): it is the difference between the total power produced if all components are available and the result of the max flow calculation ($f_{max}(SS)(v_k)$). The calculation of the constrained max flow $f_{max}(SS)(v_k)$ for a given wind velocity v_k is done with a max flow algorithm. The latter finds the maximum power from the "source" to the onshore PCC. The constrained max flow calculation is done by using the function readily implemented in the Networkx Python library [79].

$$P_{curtailed}(SS)(v) = \sum_{j=1}^{N_{WT}} \left[P_{WT}^{j}(v)\right] - f_{max}(SS)(v) \qquad (4\text{-}7)$$

where:

$P_{WT}^{j}(v)$ is the power produced by the wind turbine $P_{WT}^{j}(v)$ for a wind velocity v.

$f_{max}(SS)(v)$ is the max flow through the reliability graph from the "source" node to the "sink" node (onshore PCC), for a given system state SS.

4.4 Application of the impact based method to a N-1 analysis

Figure 4-7 depicts an illustrative architecture with a hypothetic topology and 7 MW wind turbines. In this section, the method for the quantification of the expected power curtailed (exposed in the section 4.3) is applied to an *N-1* analysis of the electrical system. The export transformers have a power rating of 14 MVA each (half the total rating of one export station). The converter transformers have a power rating of 28 MVA each. The power rating of the other components does not affect the results because they have no partial redundancy.

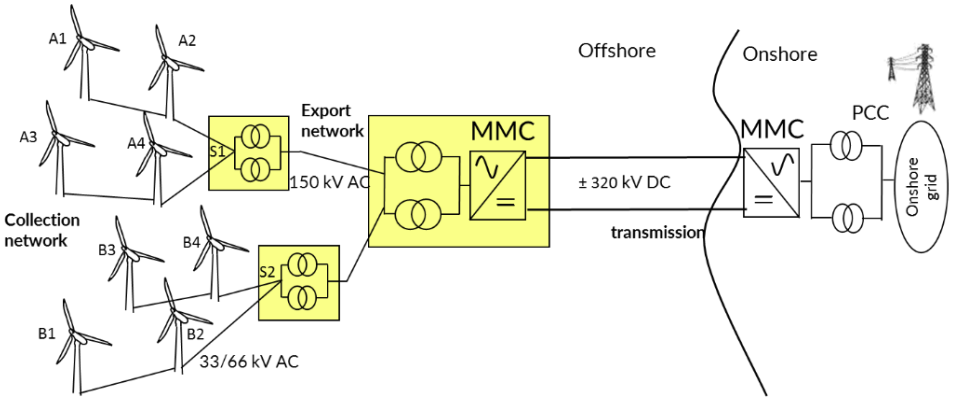

Figure 4-7: Electrical network with MMC based HVDC transmission

Figure 4-8 depicts the reliability graph associated to the network of Figure 4-7.

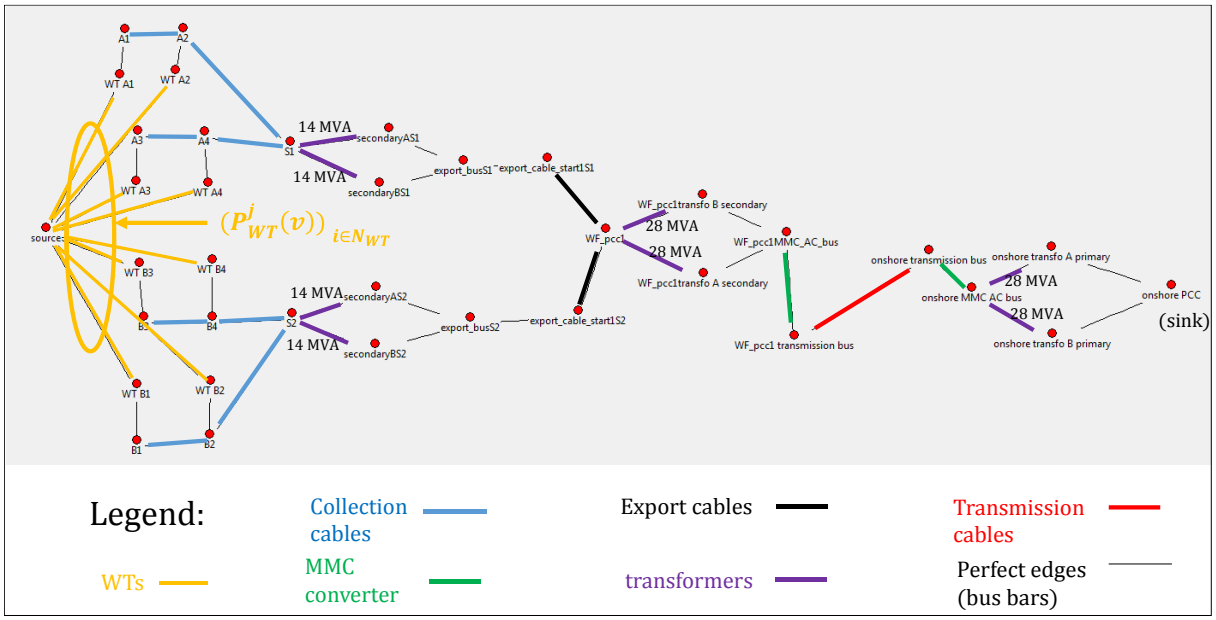

Figure 4-8: Reliability graph of the benchmark system

The capacities (power ratings) of each edge (representing a components) are given. MMC converters and cables are not depicted because if they are well rated for normal operation, and so they do not affect the max flow if the electrical system is degraded. Yellow edges have capacities corresponding to the power production of associated wind turbines as explained in section 4.3.

Nodes of the reliability graph are perfect nodes. The graph of Figure 4-8 could have less perfect edges and nodes and is then not optimized. This is because it is automatically generated by the tool developed in the Python environment in a generic way in regard to the various architecture concepts which are considered in the present work.,

The N-1 analysis consists in enumerating all the system states where one and only one component is down and then in quantifying the impact on the overall operation of the infrastructure in steady state. There are as many N-1 states as the number of electrical components of the system

The methodology exposed in section 4.3 to compute the asymptotic annual mean power for a given degraded mode relies on the calculation of the power curtailed as a function of the wind velocity. Figure 4-9 and Figure 4-10 show the variation of the following quantities for some "N-1 state" examples:

- The total power curtailed $P_{curtailed}(SS)(v)$,
- The power that would be produced if there were no failed components $\sum_{j=1}^{N_{WT}}\left[P_{WT}^{j}(v)\right]$,
- The constraint max flow $f_{max}(SS)(v)$.

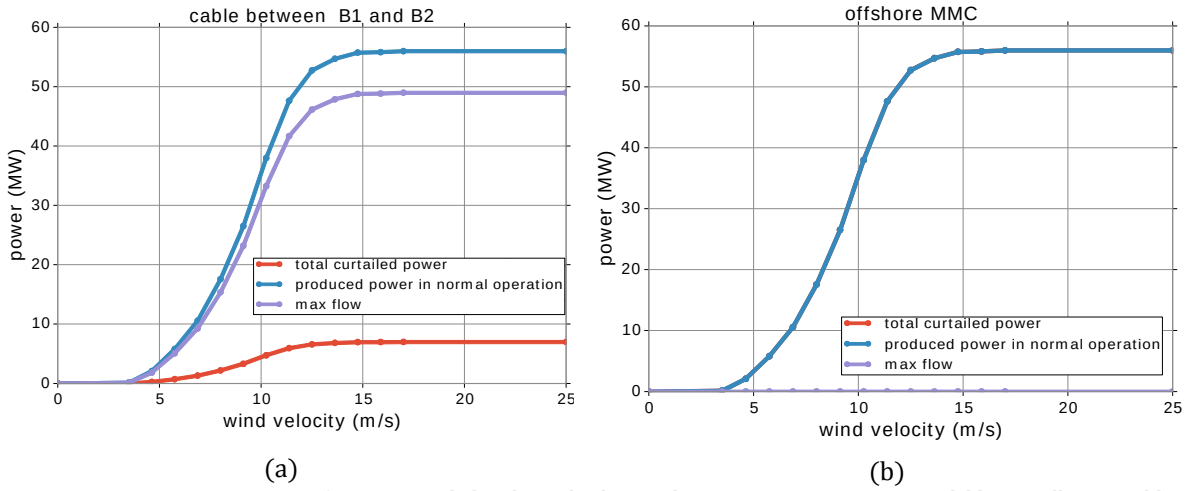

(a) (b)

Figure 4-9:Variation of power curtailed with wind velocity when one component is not available (a) collection cable between wind turbines buses B1 and B2. (b) offfshore MMC.

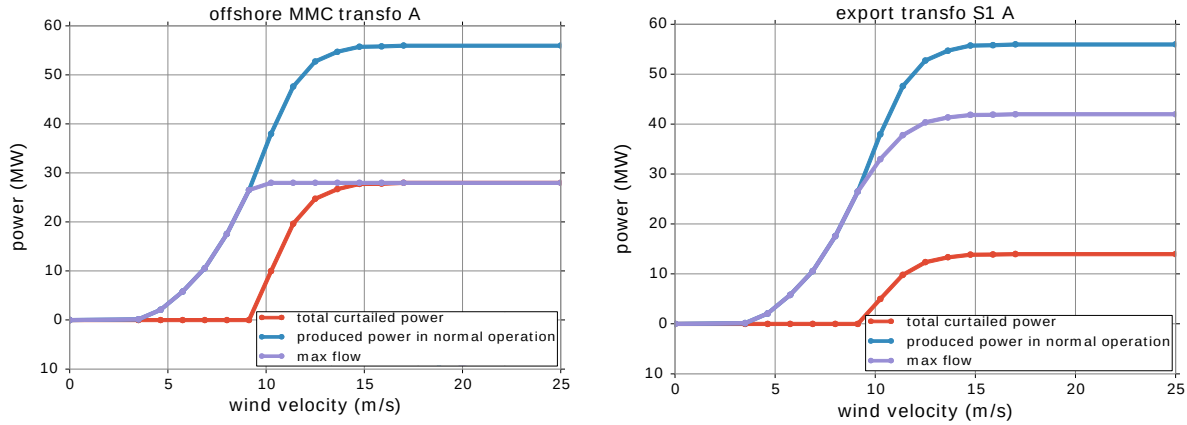

(a) (b)

Figure 4-10:Variation of power curtailed with wind velocity when one component is not available (a) one converter transformer of offshore MMC (b) one export transformer.

The Weibull probability density function (pdf) $v \rightarrow f_{WB}(v)$ with shape and scale parameters of 2.2 and 10.57 m/s respectively [82] is depicted in Figure 4-11. These parameters of the Weibull distribution are used in the remaining of this chapter.

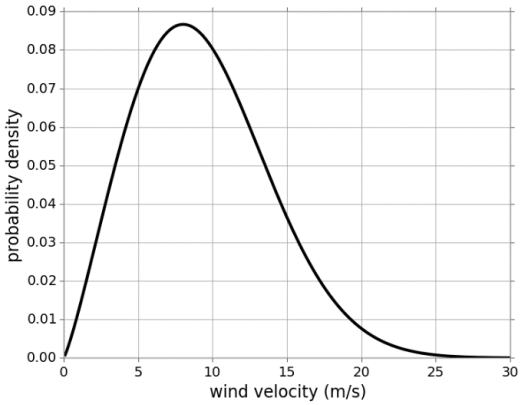

Figure 4-11: Weibull probability density function

Figure 4-9 shows the evolution of the quantities for two extreme cases. On Figure 4-9 (b) it can be seen that without surprise, the loss of the offshore MMC means that no power can be transmitted and thus, the totality of the power must be curtailed. The same figures could be depicted for the pair of transmission cable and for the onshore MMC. Figure 4-9 (a) shows that when the cable between B1 and B2 is not available, the power produced by the wind turbine B1 cannot be collected and thus, has to be curtailed.

Figure 4-10 shows the quantities for one export transformer and one converter transformer. The specificity of these components in the benchmark architecture is that they are each associated to a parallel transformer. Thus, when they are not available, up to 50% of the cluster peak power (export transformer) or 50% of the total peak power (MMC converter transformer) can be transmitted. Thus, after the total power reaches 50% of the peak power, the exceeding power must be curtailed.

The impact of a given N-1 state is measured by the asymptotic annual mean power not injected for the N-1 states of the system (states with one and only one component down, of index i):

$E[P_{curtailed}(\{1-\delta ij\}_{j\in C})]$, where δij is the Kronecker delta (refer to equation (4-8))

The results showing $E[P_{curtailed}(\{1-\delta ij\}_{j\in C})]$ for all $i \in C$ are presented in Figure 4-12.

$$\delta ij = \begin{cases} 1 \; if \; i = j \\ 0 \text{ otherwise} \end{cases} \tag{4-8}$$

Though it was predictable, the MMC converter and the transmission cables (considered as one component as both equipment must be available to transmit power) have the highest impact on the infrastructure availability. It should be noted that single collection cable failures have a relatively low impact in comparison to the other power components even for this study case. This trend is accentuated for a realistic, large wind farms. As a consequence, most of collection networks on real wind farms do not include any redundancies.

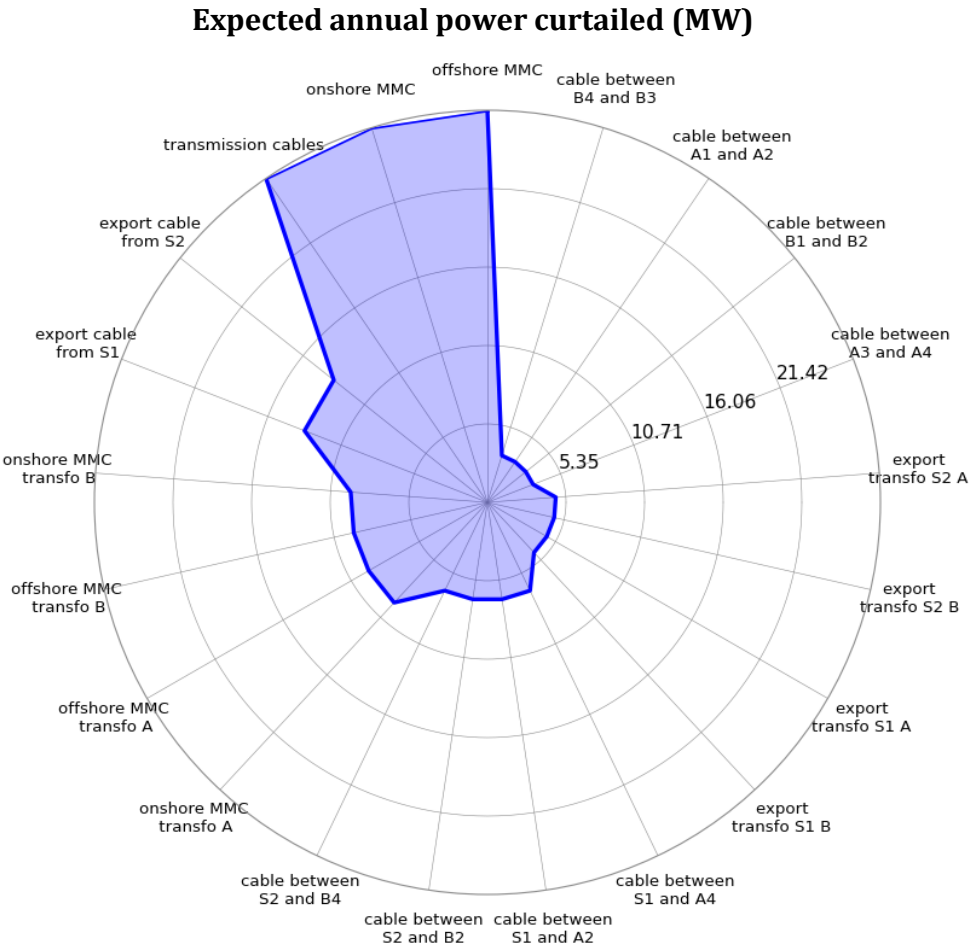

Figure 4-12: N-1 results of some power components of the illustrative system

It also explains why industrials study the impact of the export transformer on the reliability of the system [80] and why the export transformers have, most of the time, at least partial redundancies (two transformers of at least half the power rating of the cluster rather that one with the total rating), as imposed by the National grid's NETS Security and Quality of Supply Standard (SQSS) [143] in the UK for offshore substations of power ratings above 90MW.

4.5 Estimator based on a first order expected curtailed power

Once $E[P_{curtailed}(\{1-\delta ij\}_{j\in C})]$ is obtained for each component i, it is possible to multiply it by the unavailability U_i (refer to equation (4-3)), to obtain indices taking into account the probabilistic aspect. In other words, the loss of a component can have a low impact but be so frequent that the quantity of the annual energy curtailed, $L_S^{cur}(X)$, is high. Following this idea, an estimator $\widehat{L_S^{cur}(X)}$ of $L_S^{cur}(X)$ is proposed:

$$\widehat{L_S^{cur}(X)} = T_{year}.\sum_{i\in C} U_i.\ E[P_{curtailed}(\{1-\delta ij\}_{j\in C})] \qquad (4\text{-}9)$$

One advantage of this estimator is that it eases the analysis and makes the problem simpler. On the one hand the impact (mean annual curtailed energy $E[P_{curtailed}(\{1-\delta ij\}_{j\in C})]$) of the loss of one component is

considered and also on the other hand, the probability of occurrence of such event (the unavailability U_i). It can thus ease the decision making based on a quantitative support.

Another advantage of this estimator is that once $E[P_{curtailed}(\{1-\delta ij\}_{j\in C})$ is known for all the components of the system, it can be recalculated with various unavailability values (U_i) with minor additional computational costs. In other words, it allows performing a sensitivity analysis in regard to reliability data (MTTR and MTTF of the components) without a major computational burden.

However, there are two main drawbacks with the estimator of equation (4-9):

- The estimator allows the computation of the expected annual curtailed energy, which is not necessarily the better choice. Stochastic methods such as Monte Carlo could bring more information.
- The estimator is numerically biased for estimating the expected annual curtailed energy. Indeed, it takes into account only the states of the system with one component down. This limits the computational burden and makes easier the analysis but modifies the quantitative result. An exact estimator could be used.

The exact estimator of (4-10) is obtained by application of the inclusion exclusion principle (refer to [144] as a reminder).

$$\widehat{L_S^{cur}(X)} = T_{year}. \sum_{k=1}^{card(C)} (-1)^{k-1} \sum_{\substack{J\subset C \\ card(J)=k}} \left(\prod_{i\in J} U_i\right). E[P_{curtailed}(SS_J)] \qquad (4\text{-}10)$$

where:

C is the set of indexes associated to power components of the electrical network system,

SS_J is given by equation (4-11):

$$SS_J = \{s_i \ / i \in C \ and \ s_i = 0 \ if \ i \in J, \ 1 \ otherwise\} \qquad (4\text{-}11)$$

The index k of the outer sum can be interpreted as the number of unavailable components in the system. This estimator could be very costly to compute (though some analytical simplifications taking into account the topology of the system could be derived similarly as in [21]).

The estimator is a sum of expected power curtailed corresponding to all possible states. A given state has a probability of occurrence corresponding to the product of unavailabilities of unavailable components of the state (because they are assumed to have independent unavailabilities). For some values of k, the quantity $(-1)^{k-1}$ is positive and for others, it is negative. In this way, in accordance with the inclusion exclusion principle, the events with intersections are handled (refer to [144] as a reminder).

The reason why the estimator $\widehat{L_S^{cur}(X)}$ of equation (4-9) gives quantitative results not so far from (4-10) is because (4-9) neglects the cases with more than one component unavailable, corresponding to the orders $k>1$ in (4-10). Thus associated terms have low values. Indeed, a component i should be reliable and thus,

hopefully, U_i <<1. Thus for $k>1$, as $card(J)=k$, $\prod_{i\in J} U_i$ should give very small values in comparison with individual values of U_i.

To go further, it could be shown by using the probabilistic Bonferroni inequalities that the estimator $\widehat{L_S^{cur}(X)}$ with (4-9) gives a value of $L_S^{cur}(X)$, which is higher than the value obtained with (4-10).

In section 4.6, an estimator based on a Monte Carlo simulation is presented. It is complementary to the estimator exposed in the present section. A cross validation of the numerical methods of the present section and of the section 4.6 is presented in section 4.8.2.

4.6 Stochastic estimator based on a Monte Carlo Simulation

The Monte Carlo simulation allows computing $L_S^{cur}(X)$ whilst taking into account the stochastic nature of the occurring process. In other words, it allows the calculation of an empirical probability distribution of $L_S^{cur}(X)$ and not only its expected value. It is complementary to the previous *N-1* analysis (section 4.4) and to the estimator of section 4.5 because a Monte Carlo simulation does not easily identify the causes of deteriorated quantities affecting the long term profitability of a project.

The general methodology of Monte Carlo simulations is exposed by Zio [140]. The applied methodology is very similar to the one exposed by McIver and al. [141], [142], who apply it to the reliability assessment of HVDC transmission networks.

To do so, a simulation time window corresponding to the operation life of the system (N years) is considered. Failure and repair events are generated for the different power components independently. The events in regard to one component are sequentially generated.

From a healthy state, the next time of failure TTF is deduced from the function generated through equation (4-12). Equation (4-12) is the consequences of the exponential distribution law (refer to McIver and al. [141], [142] and to Zio [140] for the general formulation for any distribution law).

$$TTF = -\frac{1}{\lambda} ln(Rf) \qquad (4\text{-}12)$$

Where:

λ is the failure rate of the considered component.

Rf is a generated random number obeying a uniform law in [0,1].

From a down state, the next time of repair is determined in a similar manner by using the equation (4-13) to calculate the time to repair TTR. A constant time to repair is used as it is thought more realistic than an exponential law but more advance probabilistic laws could be used. For instance, McIver and al. [141], [142] include offshore weather conditions to determine TTR.

$$TTR = MTTR \qquad (4\text{-}13)$$

Once the events are generated for all the power components, they are sorted in regard to their time of occurrence. L intervals between events are thus obtained and each interval j has a duration τ_j. For each

interval *j*, the system has a system state SS^j. Figure 4-13 shows the obtained events and intervals (L=7) for an illustrative system having three components C={1, 2, 3} for a single Monte Carlo simulation over N years.

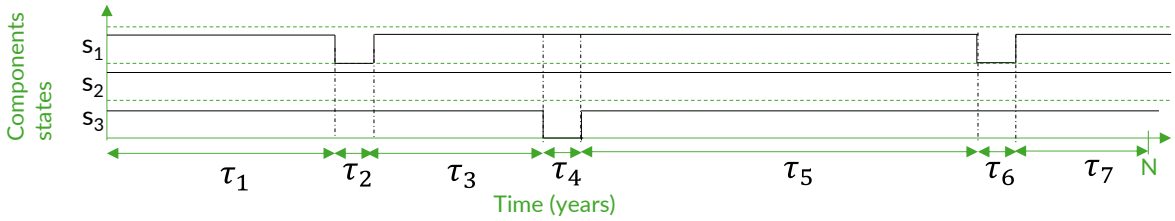

Figure 4-13: Time line for one simulation over N years for an illustrative system with 3 components.

This general method of reliability analysis is exposed in [140] and it is called "direct simulation method". With this Monte Carlo method, an estimator $\widehat{L_S^{cur}(X)}$ of $L_S^{cur}(X)$ is given by the equation (4-14). Equation (4-14) does not give the expected value of $L_S^{cur}(X)$ but it gives the value associated to one occurrence of the stochastic process. To estimate the expected value of $L_S^{cur}(X)$ in regard to the states of the system, a large number of Monte Carlo Simulations must be performed. Such simulations can then also be used to determine an empirical probability distribution of the annual energy curtailed $L_S^{cur}(X)$.

$$\widehat{L_S^{cur}(X)} = \frac{1}{N}\sum_{j=1}^{L} \tau_j .\ E[P_{curtailed}(SS^j)] \qquad (4\text{-}14)$$

where:

N is the number of years of operation;

$E[P_{curtailed}(SS^j)]$ is calculated for the system state SS^j of each interval j with the method exposed in the section 4.3 (refer to equation (4-5)).

In practice, a large number of Monte Carlo simulations has to be performed in order to build an empirical distribution of the estimator $L_S^{cur}(X)$. It can also be used to compute the expected value of $L_S^{cur}(X)$ but it is likely to be computationally more costly than the method of section 4.5 without bringing more information (see the calculation of the confidence interval at 95% in the section 4.8.2).

4.7 Data collection and processing for MTTR and MTTF

This section details the collection and processing of the used numerical data for the MTTR and MTTF. As stated previously, their values for the various components highly affect $L_S^{cur}(X)$.

For a review of the existing data for MTTR and MTTF, Dahmani (2014) performs a comprehensive survey for components of the HVAC transmission architecture [25], [145]. For components of a HVDC transmission network, MacIver et al. [141], [142] provide consistent data.

The study on behalf of Ofgem (from the company GHD) for calculating target availability figures for HVDC interconnectors [146] (Update of the study by the company SKM [147]) is thought to be legitimate for components related to HVDC networks (converters, power cables etc.). It is preferably used when it is applicable.

In the present work, the switchgears are assumed to be perfectly reliable. As a consequence, bus bars are assumed to be ideal nodes. As a consequence, no MTTR or MTTF are associated to switchgears.

Table 4-1 (failure rates) and the Table 4-2 (repair durations) gather raw data, which are collected and used in the present work for the various power components. Values associated to "mean", "optimistic" and "pessimistic" are given, along with associated references. It is reminded that the MTTF is straightforwardly calculated as the inverse of the failure rate of the component (λ, see section 4.2).

It must be noted that the failure rates for high power converters in Table 4-1 are rather pessimistic but that the associated failure mode is minor and thus, the repair times are acceptable. However, it illustrates the difficulty of gathering accurate reliability data.

Table 4-1: Failure rate data for components (in occurrence per year)

Items	Optimistic scenario failure rate (occ/year)	Mean scenario failure rate (occ/year)	Pessimistic scenario failure rate (occ/year)	Data source reference (Optimistic| Mean| Pessimistic)
HVDC converter	0.5	1.0	3.0	Monjean [42] | GHD [146] | GHD GHD [146]
transformer	$1.3.10^{-2}$	$2.0.10^{-2}$	$2.9.10^{-2}$	Dahmani [25] | Dahmani [25] | Canadian association [148]
MVAC cables	See section 4.7.2: Calculating MTTF for power cables for external and internal failures			GHD [146]
HVAC cables				
MVAC cables				
HVDC cables				

Table 4-2: Mean Time to Repair (MTTR) data for components

Items	Optimistic MTTR (hours)	Mean scenario MTTR (hours)	Pessimistic scenario MTTR (hours)	Data source reference (Optimistic| Mean| Pessimistic)
HVDC converter	6	24	72	MacIver [142] | GHD [146] | Monjean [42]
transformer	48	72	240	MacIver [142] | MacIver [142] | Dahmani [25]
MVAC cables	840			GHD [146]
HVAC cables				
MVAC cables				
HVDC cables				

In practice the MTTR of a given component is calculated differently depending on whether components are installed onshore or offshore. This is detailed in the section 4.7.1.

Power cables can fail for various reasons, some are internal and others are external. Knowing this, the calculation of the MTTF actually used in the reliability simulation is exposed in the section 4.7.2.

4.7.1 Calculating MTTR for onshore and offshore components

Some of the components which are part of the electrical network, are installed on offshore platforms. This is the case of some of the offshore HVDC converters and transformers (export transformers or converter transformers). The associated repair time must thus take into account the offshore environment. In addition to the repair duration (such as those given in Table 4-2), some fixed duration, related to the access to offshore locations, are proposed by MacIver et al. [141]. MacIver et al. consider various scenarios taking into account weather conditions.

The reason why the procurement duration for converters equals zero is because the failure mode for these components is such that a priori, spares are available (e.g. MMC sub-modules). In practice, the MTTR, which is used within a reliability study is the sum of:

- The repair time, which is intrinsic to the component to repair (see Table 4-2),
- The procurement duration (see Table 4-3),
- The duration to access offshore equipment (see Table 4-3).

Table 4-3: Procurement and offshore shift repair time for components

Items	Procurement duration (hours)	Shift duration related to offshore environment (hours)	Data source reference
Onshore converter	0	15	MacIver [142]
Offshore converter	0	15	MacIver [142]
Onshore transformer	1440	15	MacIver [142]
Offshore transformer	1440	15	MacIver [142]
Power cable	1440	720	GHD [146]

4.7.2 Calculating MTTF for power cables for external and internal failures

The CIGRE report 379 [149] gives reliability data for underground and submarine HV cables. It is the result of a comprehensive study on service experience. It shows that an important part of the failures is due to external damages.

As stated by GHD in its report for OFGEM [146], to calculate the availability of HVDC interconnectors, new practices of risk assessment and for protection of submarine cables have been improved and the external damages are reduced. Accordingly, the data from the CIGRE TB 379 [149] have been processed by the SKM company [147] and reused by GHD [146]. They are depicted in Table 4-4.

Table 4-4: MTTF for submarine cables considering internal and external failure modes [146], [147]

Items	Optimistic failure rate (occ/year/km)	Mean failure rate (occ/year/km)	Pessimistic failure rate (occ/year/km)
Internal failure	$2.0.10^{-4}$	$2.7.10^{-4}$	$4.1.10^{-4}$
External failure	$1.6.10^{-4}$	$2.1.10^{-4}$	$3.2.10^{-4}$

Table 4-4 depicts the per unit length failure rates (in number of occurrence per year per meter) for mean, optimistic and pessimistic scenarios.

A cable branch between two nodes is defined as:

- A three core cable in AC in case of a MVAC or HVAC network,
- One pair of single core cable in DC (case of a MVDC or HVDC network). The pair of DC cables can be bundled or simply laid together in one trench.

To calculate the MTTF for a cable branch, the method differs depending on the cable kind:

For MVAC and HVAC cables, it is assumed that the internal failures affect the three cores and associated insulations all together. $MTTF_{total}^{AC}$ is the MTTR associated to a AC cable branch (one three core cable):

- $$MTTF_{total}^{AC} = \frac{1}{(\lambda_{internal} + \lambda_{external}).L_{branch}} \quad (4\text{-}15)$$

where:

L_{branch} is the length of the cable branch;

$\lambda_{internal}$ is the failure rate related to an internal electrical failure of the cable, values of 4.7.2 are used;

$\lambda_{external}$ is the failure rate related to a failure due to an external damage, values of 4.7.2 are used.

- For MVDC and HVDC cables, it is assumed that a failure related to an external damage (e.g. due to an anchor) affects the two cables as a group. This is because they are laid very closely or are bundled and thus, there is a common mode of external failure. $MTTF_{total}^{DC}$ is the MTTR associated to a DC branch (a pair of DC cables):

$$MTTF_{total}^{DC} = \frac{1}{(2.\lambda_{internal} + \lambda_{external}).L_{branch}} \quad (4\text{-}16)$$

4.8 Validation of the methods

In this section, the validation of the methods is presented and is related to the numerical accuracy of the methods. These methods will be used for the assessments of architecture concepts including the reliability in Chapter 5.

In section 4.8.1, the validation of the corner stone method, which is based on a max flow algorithm (section 4.3) and allows the computation of the expected power curtailed for a given state of the electrical network system, is presented.

In the section 4.8.2, a cross validation of the methods allowing the estimation of $L_S^{cur}(X)$ is exposed.

These validations are made on the virtual benchmark case study with eight wind turbines of 7 MW (section 4.4). The choice of this architecture concept with MVAC collection, HVAC export and MMC based HVDC

transmission networks, depicted in the Figure 4-7, is driven by the fact that it is the only one, which includes all the components. Indeed, in regard to the reliability, the DC/DC converters behave as a MMC converter whose behavior is determined by its MTTR, MTTF and power rating. The same validation could be done on any of the architecture concepts introduced in the Chapter 1. The methods are implemented for all the concepts introduced in the Chapter 1.

4.8.1 Validation of the calculation of the expected power curtailed

The objective is to set and validate the size of the wind velocity samples, which are required for an accurate numerical calculation of $E[P_{curtailed}(SS^j)]$ for any system state SS^j. The validation is based on a N-1 analysis as in Figure 4-12 of the section 4.4. In Figure 4-12, for each N-1 state, $E[P_{curtailed}(\{1-\delta ij\}_{j\in C})]$ is calculated for all components i of the system with a sample of 30 wind velocities by using a Simpson numerical integration (second order interpolation of the points). The Simpson method is supposed to have a lower error than rectangular or trapezoidal methods.

The results are calculated on the benchmark case for various velocity sample sizes: 5, 10 and 15 points. The velocity values of a sample are chosen to be uniformly spaced.

The obtained values of energies with these sample sizes are compared with the sample of 30 velocities, which is considered to be the reference in regard to which the errors are calculated. The error is computed as the maximum absolute value of the error in estimation (via Simpson numerical integration) of the expected values of power curtailed as in equation (4-17).

$$error = max_{i\in C}(\left|E^n[P_{curtailed}(\{1-\delta ij\}_{j\in C})] - E^{n_{ref}}[P_{curtailed}(\{1-\delta ij\}_{j\in C})]\right|) \qquad (4\text{-}17)$$

where:

n is the number of wind velocity points of the sample set;

n_{ref} designates the sample size of the reference set (n_{ref} =30 points);

$E^n[P_{curtailed}(\{1-\delta ij\}_{j\in C})]$ is an estimation of the expected value with a sample of n points;

$E^{n_{ref}}[P_{curtailed}(\{1-\delta ij\}_{j\in C})]$ is an estimation of the expected value of power curtailed with a sample of n_{ref} points (30 points).

Table 4-5 shows that a sample of 5 wind velocities is not sufficient. A sample of 10 wind velocities is a good compromise and is retained for the remaining work in the PhD (for the quantification of the reliability).

Table 4-5: Errors in quantification of expected curtailed power in N-1 states for various sizes of wind velocity sample set

	n=5 points	n=10 points	n=15 points	n_{ref}=30 points (ref)
Max absolute value of relative error	5.4%	0.15%	0.14%	0%

4.8.2 Cross validation of N-1 and Monte Carlo based estimators

In this section, a cross validation of the estimators of $L_S^{cur}(X)$ exposed in the sections 4.5 (first order approximation) and 4.6 (Monte Carlo) is proposed.

It is noteworthy that with the reliability data exposed in the section 4.7 and with a cable length of a few kilometers (see geographical layout of the benchmark architecture in Figure 4-14), the maximum component unavailability $max_{i \in C}(U_i)$ is worth $3.6.10^{-3}$. It validates the main numerical hypothesis, which is made when writing the estimator considering only first order failure states (section 4.5). For the benchmark architecture and associated cable length, the unavailabilities of the transmission cables have a similar order of magnitude as the unavailabilities of other components. Thus, if the cable length is more than 100 km long, their unavailabilities dominate. However, cables unavailabilities remain individually below 10^{-1} even for length of a few hundred kilometers.

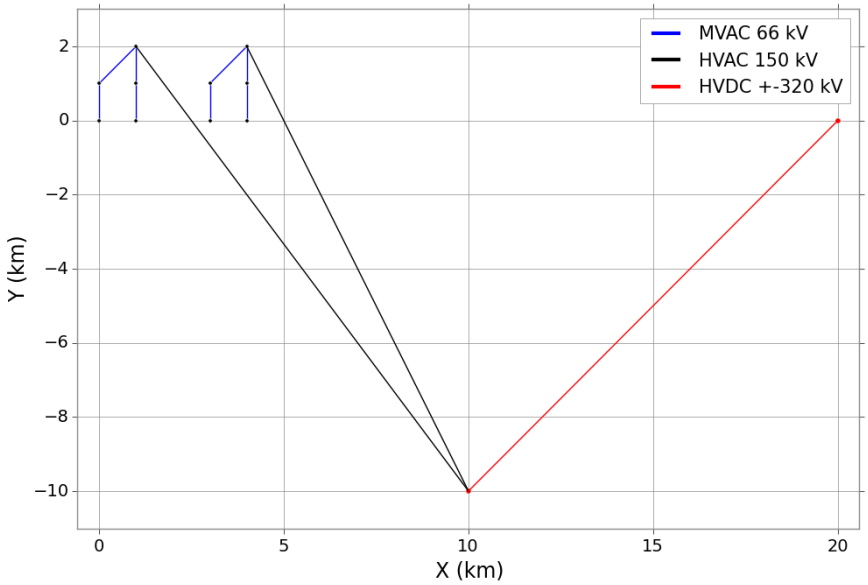

Figure 4-14: Geographical layout of the benchmark architecture

Table 4-6 depicts the values of $L_S^{cur}(X)$ obtained with the two estimators, which are proposed in the present work. In particular, the value with the Monte Carlo method is obtained with 1000 Monte Carlo simulations over a period of 20 years each. The value proposed in Table 4-6 for the Monte Carlo estimation is the average value of the 1000 obtained values. As predicted, the first order estimator is more pessimistic than the real estimation (which is assumed to be closed to the expected value obtained with 1000 Monte Carlo Simulations).

Table 4-6: Comparison of estimators of $L_S^{cur}(X)$ on the benchmark architecture

First order estimator (section 4.4)	Monte Carlo based estimator (section 4.6)
4.59 GWh	4.51 GWh

The first order estimator requires fewer computational resources but it is complementary to the Monte Carlo simulations. Indeed, the latter allows obtaining an empirical probabilistic distribution of $L_S^{cur}(X)$, as depicted in Figure 4-15.

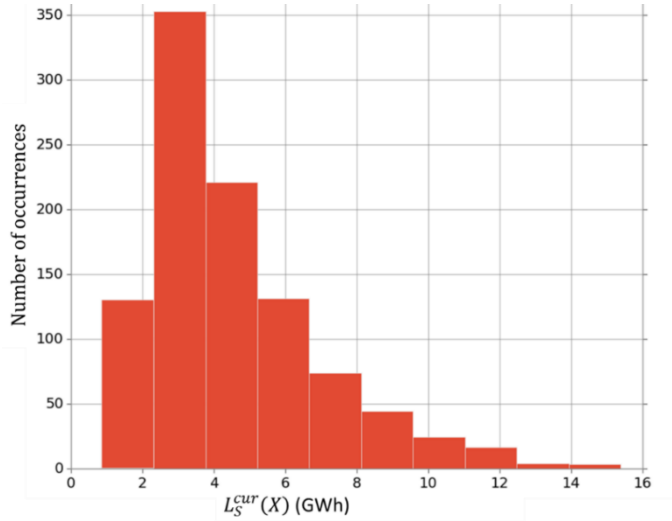

Figure 4-15: Empirical probabilistic distribution of $L_S^{cur}(X)$ for the benchmark architecture

As reminded by Dutrieux [150], from the central limit theorem, a confidence interval can be calculated for the Monte Carlo estimator. For a 95% confidence interval, the margin of error δ_{err} is given:

$$\delta_{err} = 1.96.\frac{\sigma}{\sqrt{M}} \tag{4-18}$$

where:

σ is the standard deviation of $L_S^{cur}(X)$ over its sample obtained with the 1000 Monte Carlo Simulations.

M is the size of the sample (1000 in the present case).

The corresponding confidence interval for the 1000 Monte Carlo simulation is [4.36 GWh, 4.66 GWh].

The simulations are performed with Python 2.7 on a 4 core, 64-bit DELL PC with Intel ® Core TM i5-4310U CPU, 2.6 GHz and RAM 8 Giga-byte. The 1000 Monte Carlo simulations take around 900 seconds in total. However, it can be noticed that during a Monte Carlo simulation as presented in the section 4.6, it can happen that $SS^j = SS^i$ for $i \neq j$. In other words, the same system state can occur for various intervals of the Monte Carlo simulations. Thus, the quantification of $E[P_{curtailed}(SS^j)]$ can be done only once for a given state of the system. Accordingly, a "memorization" technique is used: In computer science, the "memorization" technique, which consists in storing in memory a result that could be reused later in an algorithm (refer to [151]). The practical implementation is simply done by testing for each interval of index j if the state has been encountered previously:

- If the state was not encountered, no value is available in memory, thus $E[P_{curtailed}(SS^j)]$ is calculated and the value is put in memory.
- If the state was encountered, the value $E[P_{curtailed}(SS^j)]$ has already been calculated and is available in memory.

The simulations with "memorization" on the benchmark case resulted in a total computation duration of about 35 seconds for the 1000 Monte Carlo simulation. Compared to the simulation without "memorization", the speed is increased with a factor of 25. It turns out to be an important improvement, particularly valuable for a reliability assessment of a large scale system such as those of Chapter 5.

4.9 Conclusion

In this chapter, some existing studies for the assessment of electrical networks connecting an offshore wind farm are briefly exposed (see section 4.2). The dependency to reliability data (MTTR and MTTF) for any assessment method is highlighted. In the present work, it is proposed to use the annual energy curtailed (corresponding to the classical EENS) as a reliability measure because from a wind farm planner, it is directly related to the profitability of the project (refer to the LCOE). Other indexes such as the LOLE is more adapted to other contexts such as distribution networks where the reliability should be measured by its impact on the consumption side.

Then, a method allowing the assessment of the expected power curtailed for a given state of an electrical network is proposed (see section 4.3). The originality of the method is the use of a classical constrained max flow algorithm within a formalized method. In the section 4.4, it is shown that this method can be used within an N-1 analysis of the electrical network. Such a N-1 analysis is useful to determine the critical components without requiring any reliability data.

Two methods allowing to estimate the retained reliability criterion (the annual curtailed energy $L_S^{cur}(X)$) are presented.

In the section 4.5, a first order approximation method can be used to estimate the expected value of $L_S^{cur}(X)$ with a reduced computational burden and a correct accuracy. It is in the continuity of the N-1 analysis and has the advantage to ease the analysis. Indeed a method similar as for a risk analysis can be applied: it allows associating to each component an impact (mean curtailed power if it is down) and a probability (unavailability U). Hence, the dependency to the components reliability data to the associated uncertainties can be mitigated.

In the section 4.6, a Monte Carlo simulation based method to estimate $L_S^{cur}(X)$ is presented. It is complementary to the first order estimation method as it can be used to build an empirical probability distribution of $L_S^{cur}(X)$. The decision on the design of the electrical network in regard to the reliability can thus be done not only based on the expected values but taking into account the complete stochastic process. A drawback of the Monte Carlo based method is that it requires high computational resources. However a memorization technique, as often used in computer science is employed, highly reducing the computational cost. This method is used in the section 4.8.2.

In the section 4.7, reliability data collection and pre-processing is presented. In the section 4.8, a validation of the methods is done.

The methods proposed in the present work are developed with the ambition to be a generic method allowing to accurately assess EENS in offshore wind farm context, with an acceptable computational cost.

Further improvements including the use of analytical formula are perspectives of the work, notably to reduce the computational costs.

In Chapter 5, the models and methods developed in Chapter 2, 3 and 4 are used for the design and assessment of architectures.

Chapter 5: DESIGN OPTIMIZATION FOR OFFSHORE ELECTRICAL NETWORKS

5.1 Introduction

The present chapter aims at developing an optimization tool to design and size various electrical architectures for the connection of large wind farms to the onshore grid. The targeted task is the minimization of the Network Life Cycle cost, including investment costs but also operating costs over the duration of the project. Hence, models of investment costs (Chapter 3) and the models of energetic conversion and losses (Chapter 2) must be integrated in the optimization process.

As exposed in Chapter 1, architectures of electrical networks are complex to design because of the various required functionalities under different technical constraints. To break these difficulties, a serialization into five sub problems that can be solved separately and quickly is proposed.

The objective is to optimize the NLCC of the electrical architecture (refer to Chapter 1 or to section 5.4.2), equivalent to the LCOE of a complete wind farm project (proof of equivalence in Chapter 1).

In the section 5.2, a nomenclature of the parameters and variables is exposed. In section 5.3, a state of the art regarding the optimization of offshore wind farm networks is given. In the sections 5.4 and 5.5, a formulation of the optimal design problem is detailed. In the section 5.6, the proposed framework is applied to various architecture concepts and wind farm sites. Obtained performances are presented.

5.2 NOMENCLATURE

5.2.1 Indices, sets and parameters

P_{WT}^{peak}	Single wind turbine peak power used for normalization (MW)
g_{t_i}	Normalized peak power produced of wind turbine t_i (p.u.)
N_{WT}	Number of wind turbines of the complete wind farm
$T = \{t_i\}_{i \in [\![1;N_{WT}]\!]}$	Set of wind turbine indexes
$(x_t, y_t)_{t \in T}$	Locations of wind turbines
s_O	Index of the onshore substation O
(x_{s_0}, y_{s_0})	Location of the onshore substation
N_C^{max}	Max number of cluster substations
$S_C = \{s_k\}_{k \in [\![1;N_C^{max}]\!]}$	Set of cluster substation indexes
N_T^{max}	Max number of transmission substations
$S_T = \{s_k\}_{k \in [\![1;N_T^{max}]\!]}$	Set of transmission substations indexes
$Q^C_{\max\_WT}$	Max number of wind turbines per cluster
$Q^C_{\max\_cable}$	Max number of cables per wind turbines

$Q^T_{\max\_cable}$	Max number of transmission cables per transmission station
A_C	Set of collection cable cross sections
A_E	Set of export cable cross sections
A_T	Set of transmission cable cross sections
$\{P_l^C\}_{l\in A_C}$	Set of collection cable maximal normalized active power (calculated thanks to the ampacity model of Appendix A) (p.u.)
$\{P_l^E\}_{l\in A_E}$	Set of export cable maximal normalized active power (calculated thanks to the ampacity model of Appendix A) (p.u.)
$\{P_l^T\}_{l\in A_T}$	Set of transmission cable maximal normalized active power (calculated thanks to the ampacity model of Appendix A)
$\{c_l^C\}_{l\in A_C}$	Set of collection cable per unit length investment costs (calculated thanks to cost model in Chapter 3) (€)
$\{c_l^E\}_{l\in A_E}$	Set of export cable per unit length investment costs (calculated thanks to cost model in Chapter 3) (€)
$\{c_l^T\}_{l\in A_T}$	Set of transmission cable per unit length investment costs (calculated thanks to cost model in Chapter 3) (€)
X_{cross}	Set of quaternion defining crossing potential connections for the collection network
$d_{u,v}$	Euclidian distance between u and v
N	Number of years of the project life span
r	Discount rate

5.2.2 Variables (encompassed into the X vector variable)

$\{Z_s^C\}_{s\in S_C}$	Binary variable, = 1 if the cluster substation *s* is installed
$\{Z_s^T\}_{s\in S_T}$	Binary variable, = 1 if the transmission substation *s* is installed
$S_C^A = \{s \in S_C / Z_s^C = 1\}$	Set of active cluster substation indexes
$S_T^A = \{s \in S_T / Z_s^T = 1\}$	Set of active transmission stations indexes
$N_C = card(S_C^A)$	Number of active cluster stations
$N_T = card(S_T^A)$	Number of active transmission stations
$(x_s, y_s)_{s\in S_C^A}$	Locations of cluster substations

$(x_s, y_s)_{s \in S_T^A}$	Locations of transmission stations
$\{Y_{t,s}^C\}_{(t,s) \in T \times S_C^A}$	Set of binary variables for wind turbines clustering, = 1 if wind turbine *t* is associated to the cluster station *s*, *0* otherwise
$\{X_{u,v,l}^C\}_{(u,v,l) \in (T \cup S_C^A)^2 \times A_C}$	Set of binary variables, = 1 if the node *u* is connected to node *v* with collection cable of index *l*, 0 otherwise
$\{Y_{u,v}^E\}_{(u,v) \in S_C^A \times S_T^A}$	Set of binary variables for wind turbines clustering, = 1 if cluster station *u* is associated to the offshore transmission station *v*, *0* otherwise
$\{X_{u,v,l}^E\}_{(u,v,l) \in S_C^A \times S_T^A \times A_E}$	Set of binary variables, = 1 if the node *u* is connected to node *v* with export cable of index *l*, 0 otherwise
$\{X_{u,v,l}^T\}_{(u,v,l) \in (S_T^A \cup \{s_O\}) \times (S_T^A \cup \{s_O\}) \times A_T}$	Set of binary variables, = 1 if the node *u* is connected to node *v* with transmission cable of index *l*, 0 otherwise
$\{p_{u,v}^C\}_{(u,v) \in (T \cup S_C^A)^2}$	Normalized peak active power flow in collection cable from the node u to v (p.u.)
$\{p_{u,v}^E\}_{u \in S_C^A, v \in S_T^A}$	Normalized peak active power flow in export cable(s) from the node u to v (p.u.)
$\{p_{u,v}^T\}_{(u,v) \in (S_T^A \cup \{s_O\}) \times (S_T^A \cup \{s_O\})}$	Normalized peak active power flow in transmission cable from the node u to v (p.u.)
$\{S_s^{rating}\}_{s \in S_C^A \cup S_T^A \cup \{s_O\}}$	Sizing of power components of substations (VA)
$\forall s \in S_C^A, T_s = \{t \in T / Y_{t,s}^C = 1\}$	Set of wind turbines associated to the cluster substation station *s*
$\forall s \in S_C, K_s = T_s \cup \{s\}$	Set of nodes of the cluster associated to the cluster substation *s*

5.3 Existing contributions

The economic optimal design of offshore wind farm networks is a highly complex problem. In the literature, only few authors propose an optimization of the overall system including collection, export and transmission networks altogether at once.

For example, Rodriguez and al. [68], in addition to the design of the network, consider wind turbine numbers, ratings and locations as decision variables. Dahmani [145] proposes the optimization problem of the transmission from offshore to onshore, but only by considering an AC collection with HVAC export up to the onshore network; Banzo and Ramos [152] propose a Mixed Integer Non Linear Programming (MINLP) model of the complete network system considering two slightly different models, one with a HVAC transmission to shore and the other with a HVDC transmission. The decision variables are the cable connections between the wind turbines and the single substation, whose location is fixed a priori.

Banzo and Ramos [152] take into account the wind intermittence via a discretization of the Weibull distribution function, and the reliability. Banzo and Ramos achieve this goal with an optimization objective by taking into account the Capital Expenditure (CAPEX), the energy not distributed and the energy losses. The model is holistic but at the price of a high computational burden. The required time to solve it is 26 hours on a PC with a 2 GHz single core and 2 GB of RAM, for a problem instance with 30 wind turbines only. Lumbreras and Banzo [153] improve the model by using decomposition strategies. For a problem instance having 75 wind turbines, the computational duration remains high if we consider the relatively low size of the instance (around 3.75 hours with a 2.80 GHz single core and 4 GB of RAM).

To decrease computation times, Pillai and al. [154] propose a method to solve one after the other two problems: First the wind turbines clustering problem, then the collection networks design problem. This serialization of sub-problems is promising. Chen and al. [155] also propose to solve the problem via a similar serialization by using a Benders' decomposition. The computational requirements are still significant though.

To reduce the computation time, most of the studies in the literature are thus dedicated to the optimization of a part of the electrical system:

- The transmission network**,** from the offshore station to the onshore network. Some studies regarding the transmission network to connect wind farms are advanced analysis, which do not use optimization methods but an expert and quantitative approach [72]. Ergun and al. [123] solve the non-explicit model of offshore transmission network design by using a dedicated genetic algorithm. González and al. [71] perform a quantitative comparative analysis of enumerated possibilities for the offshore wind power transmission by taking into account the risk of non-transmission.
- The collection network design problem is tackled in numerous studies. Pioneering studies assessed the comparative performance of different topologies, namely the star topology [62], [156] the ring topology [96], [156], [157], the strictly radial topology [48], [62] (see Figure 5-1 (a)) or the branched/dendrite topology [157] (see Figure 5-1 (b)). Other studies formulate optimization models for the collection design problem in line with one of these topologies. Some solving methods are based on metaheuristics [158–161], others on heuristics [145], [162–164] while last ones use CPLEX or equivalent solver to solve their Mixed Integer Programming (MIP) formulation [154], [162], [164–166].

(a) (b)

Figure 5-1: Schematic difference between fully radial and branched topologies. (a) purely radial (b) branched

The literature review shows that the design optimization of the complete electrical network comprises many decision variables. Due to the problem complexity, both the formulation of the problem and its solving raise challenges. In addition, the calculation of the objective function requires not only the calculation of the investment costs but also energetic quantities such as the annual curtailed energy and annual energy dissipated. Thus, a methodological approach must be proposed to reduce the complexity of the problem. In this way, the problem can be solved with acceptable computation durations so to obtain near optimal designs for which detailed assessments are then possible.

5.4 Overall problem of robust design optimization

5.4.1 Problem statement

The problem consists in designing an optimal electrical network performing the collection, export and transmission functions of a wind farm production, from offshore to onshore. In a first approach, the architecture concept (refer to definition of Chapter 1) is supposed to be an input of the problem. An important lock is to make generic the problem definition in regard to the considered architecture concepts.

This optimization problem is complex with a significant number of variables, which can be classified into integer variables and continuous variables. An instance of an optimization problem defines the parameters of the problem and their values. The instance depends on the considered architecture. With a single MIP formulation of the complete problem in its simplest form, the number of variables would be high (formulation and definition of variables detailed in sections 5.4.3 and 5.5).

The number of binary variables is:

$$N_C^{max} + N_T^{max} + (N_{WT} + N_C^{max})(N_{WT} + N_C^{max} - 1).card(A_C) + N_C^{max}.N_T^{max}.card(A_E) + N_T^{max}(N_T^{max} + 1).card(A_T)$$

Corresponding to:

- $N_C^{max} + N_T^{max}$ binary variables defining if offshore stations are active (variables Z_s^C and Z_s^T);

- $(N_{WT} + N_C^{max})(N_{WT} + N_C^{max} - 1).card(A_C)$ binary variables defining the collection cable connections between cluster substations and wind turbines, with cable choices among the set A_C (refer to $X_{u,v,l}^C$);

- $N_C^{max}.N_T^{max}.card(A_E)$ binary variables defining export cable connections between cluster and transmission stations, with cables among the set A_E(refer to variables $X_{u,v,l}^E$);

- $N_T^{max}(N_T^{max} + 1).card(A_T)$ binary variables defining transmission cable connections between transmission substations (refer to variables $X_{u,v,l}^T$).

The number of continuous variables is:

$$2(N_C^{max} + N_T^{max}) + N_C^{max} + N_T^{max} + 1 + (N_{WT} + N_C^{max})(N_{WT} + N_C^{max} - 1) + N_C^{max}.N_T^{max} + N_T^{max}(N_T^{max} + 1)$$

Corresponding to:

- $2(N_C^{max} + N_T^{max})$ scalars defining the offshore substation locations (refer to variables (x_s, y_s));

- $N_C^{max} + N_T^{max} + 1$ scalars defining the power rating of offshore cluster and transmission substations, plus the onshore substation (variables $\{S_s^{rating}\}_{s \in S_C^A \cup S_T^A \cup \{s_O\}}$);

- $(N_{WT} + N_C^{max})(N_{WT} + N_C^{max} - 1)$ power flows between wind turbines and cluster substations (variables $p_{u,v}^C$);

- $N_C^{max}.N_T^{max}$ export power flows between cluster and transmission substations (variables $p_{u,v}^E$);

- $N_T^{max}(N_T^{max} + 1)$ power flows between transmission stations ($p_{u,v}^T$).

The number of variables is quickly increasing with the size of the instance, as shown in the Table 5-1 (architecture concept (b) for which there are a MVAC collection, HVAC export and MMC based HVDC transmission networks). As a result, optimization methods used for medium sized instances can be difficult to apply to large instances corresponding to industrial wind farms.

Table 5-1: Number of variables depending on instance size

Instance size				Nb of binary variables	Nb of continuous variables
$card(A_C)$	3	N_{WT}	30	2799	940
$card(A_E)$	3	N_C^{max}	1		
$card(A_T)$	2	N_{WT}	200	121819	40616
N_T^{max}	1	N_C^{max}	2		

To reduce the number of variables, a sequential approach is proposed (details in section 5.5). The proposed formulation is based on the formulation of sub-problems. In the present implementation of the proposed framework, heuristic methods are used to solve the sub-problems. This is justified by the uncertainties coming from the reliability, CAPEX models and associated parameters (refer to Chapter 3 and Chapter 4):

- Taking into account these uncertainties can require a sensitivity analysis for which the reduction of the computation duration is a major advantage.
- Improving the optimality of a solution by a few percent, while the models have higher uncertainties, does not seem to be justified.

Hopefully, a reduction of the uncertainties can appear, notably in regard to the CAPEX for real projects. For this reason, in the section 5.5, a MIP formulation is given for all sub-problems. A global optimization solver can then be used; such as CPLEX in perspective of the present work.

5.4.2 Optimization objective

As it is introduced in the Chapter 1, the LCOE criterion is a reference for industrial shareholders [9–11] and assessments of power infrastructures. It can be used at the system level, including the production, collection/export and transmission networks

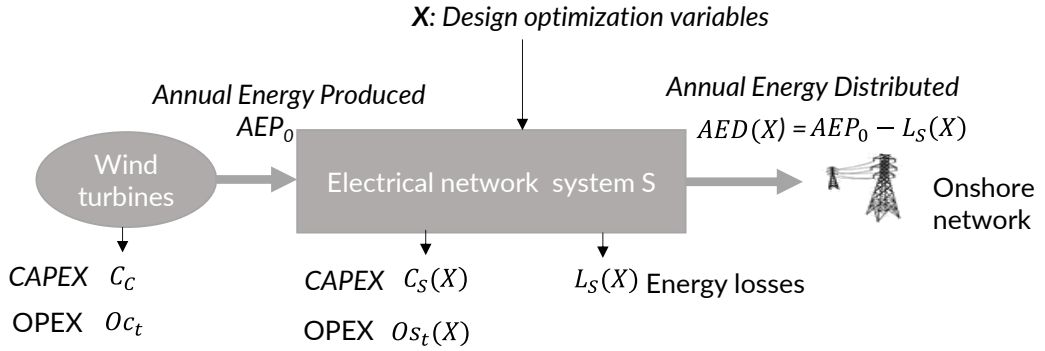

Figure 5-2: Associated technico economic variables to the studied electrical network system.

As written in Chapter 1, the minimization of the LCOE is thus the optimization objective of the present work. The LCOE is calculated by using the equation (1-5), with indexes depicted in Figure 5-2

$$LCOE_{N,r}(\mathrm{X}) = \frac{C_S(X) + C_C + \sum_{t=1}^{N} \frac{Oc_t + Os_t(X)}{(1+r)^t}}{\sum_{t=1}^{N} \frac{AED(X)}{(1+r)^t}} \tag{5-1}$$

where:

$C_S(X)$ is the CAPEX of the electrical network architecture S, calculated with models from Chapter 3;

C_C is the CAPEX of the wind turbines;

$Os_t(X)$ is the annual OPEX of the electrical network architecture S, due to its maintenance;

Oc_t is the annual OPEX of the wind turbines, due to their maintenance;

$AED(X)$ is the annual energy distributed to onshore network, given by the equation (5-2);

r is the discount rate;

N is the number of years the project is exploited.

$$AED(X) = AEP_0 - L_S(X) \tag{5-2}$$

where AEP_0 is the annual energy produced by the wind turbines.

The losses in the electrical network $L_S(X)$ are calculated by using the equation (1-2). Electrical losses dissipated in the electrical network, $L_S^{dis}(X)$, are calculated with the models and methods of the Chapter 2. In the present chapter, the annual curtailed energy due to electrical network unavailability $L_S^{cur}(X)$ is calculated by using the first order estimator, which is defined in Chapter 4.

$$L_S(X) = L_S^{cur}(X) + L_S^{dis}(X) \tag{5-3}$$

The Network Life Cycle Cost (NLCC), calculated by using equation (1-6), is introduced in the Chapter 1.

$$NLCC_{N,r}(X) = C_S(X) + \left[\sum_{t=1}^{N} \frac{1}{(1+r)^t}\right] . \left[LCOE_{N,r}(X) . (L_S^{dis}(X) + L_S^{cur}(X)) + Os_t(X)\right] \tag{5-4}$$

It is shown in the Chapter 1 that it is equivalent to the LCOE in terms of optimality. Moreover, it eases the analysis of the results such as in the section 5.6.

To calculate the economic indexes ($C_S(X)$, $Os_t(X)$, $L_S^{cur}(X)$, $+L_S^{dis}(X)$) and resulting criteria ($LCOE_{N,r}(X)$ and $NLCC_{N,r}(X)$) a fixed design X of the electrical network must be determined. Section 5.4.3 exposes the general methodology to determine the design X.

5.4.3 Formulation based on serialization of sub problems

The optimization framework follows the synoptic depicted in Figure 5-3.

Some variables named metavariables (X_{meta}) are imposed by the Meta-optimizer. It is the case of the number of offshore substations in the formulation of the present work.

The meta-optimizer defines the number of active offshore substations:

- N_T is the number of active transmission stations;
- N_C is the number of active cluster stations.

To determine the values of N_C and N_T, the meta-optimizer performs an enumeration whilst following the rules corresponding to the considered architecture concept (refer to Table 5-2).

Table 5-2: Constraints for enumeration of N_T and N_C depending on the architecture concept

Architecture concept	Collection	export	Transmission	N_C	N_T
(a)	MVAC	HVAC	/	$N_C \in [\![1; N_C^{max}]\!]$	/
(b)	MVAC	HVAC	HVDC	$N_C \in [\![1; N_C^{max}]\!]$	$N_T < N_C$ $N_T < N_T^{max}$
(c)	MVAC	/	HVDC	$N_C \in [\![1; N_C^{max}]\!]$	$N_T = N_C$
(d)	MVDC	/	HVDC	$N_C \in [\![1; N_C^{max}]\!]$	$N_T = N_C$
(e)	MVDC	/	MVDC	$N_C \in [\![1; N_C^{max}]\!]$	$N_T = N_C$

As a consequence of N_T and N_C, the values of binary variables Z_s^C and Z_s^T define the active cluster stations and transmission stations. It is then possible to define the sets of cluster and transmission substations, which are active:

- Active cluster substations $S_C^A = \{s \in S_C / Z_s^C = 1\}$;
- Active transmission substations $S_T^A = \{s \in S_T / Z_s^T = 1\}$.

It should be noted that $N_T = card(S_T^A)$ and $N_C = card(S_C^A)$. In the general definition of the decision variables, there are more possibilities (refer to nomenclature of section 5.2). Thus, the use of a meta-optimizer highly reduces the number of variables of the complete problem.

Then, the network architecture is designed by solving the followings sub-problems (refer to Figure 5-3, Figure 5-4 showing the application with an example):

- (P1) Grouping each wind turbine t into a cluster, then setting ($\{Y_{t,s}^C\}_{s \in S_C^A}, t \in T$) and locating the cluster power stations (x_s, y_s)
- (P2) Designing the collection network inside each cluster, including the choice of cross sections for collection cables, with a single set of binary variables $\{X_{u,v,l}^C.\}$ (refer to [154])

- (P3) Only if the considered architecture concept includes MVAC collection network(s), HVAC export network(s) and a HVDC transmission network: Locate offshore transmission substations ((x_s, y_s)) and associate the (AC) cluster power stations to transmission power station(s) ($\{Y^E_{u,v}\}$).
- (P4) Sizing of power components (excluding the collection cables and the HVDC transmission cables, including power converters and transformers), (i.e. choice of export cables cross sections when the connection exists $\{X^E_{u,v,l}.\}_{(u,v,l)\in S^A_C\times S^A_T\times A_E}$, number of parallel export cables when the connection exists $\{m^E_{u,v}\}_{(u,v)\in S^A_C\times S^A_T}$ and sizing of power substations $\{S_s^{rating}\}_{\forall s\in\forall s\in S^A_C\cup S^A_T\cup\{s_O\}}$).
- (P5) Designing the HVDC transmission network when applicable. It means defining the topology and the cables cross sections ($\{X^T_{u,v,l}\}$).

With the proposed formulation:

- The collection network(s) can have either purely radial or branched topologies;
- An export cable can only connect a single cluster substation to a single offshore transmission substation (or onshore PCC if the architecture, which is considered employs HVAC transmission up to the shore);
- Branched topologies for the HVDC network are possible (but not meshed).

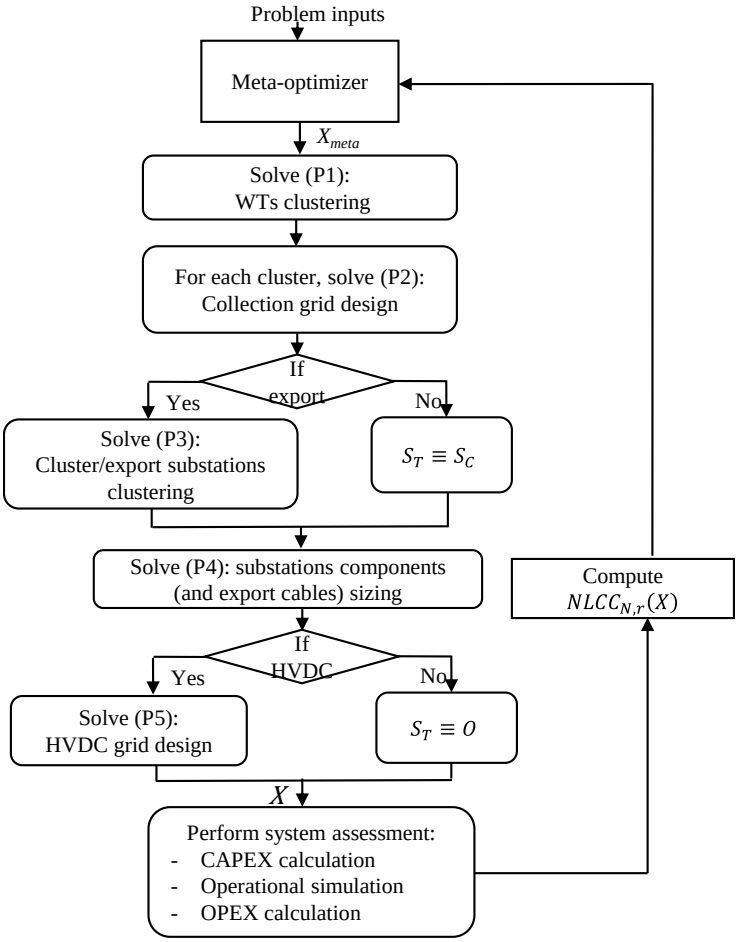

Figure 5-3: Heuristic serialization of sub-problems including highly impacting variables (number of substations as metavariables)

In the present work, to solve the general problem of electrical network optimization, the sub-problems ((P1) to (P5)) are solved sequentially until the network architecture is obtained. Then, the system assessment allows the computation of the LCOE (equation (1-5)) and the NLCC (equation (1-3)) by a CAPEX calculation and an operational simulation based on a wind power simulator and on the Python load flow library "pylon" [116] (refer to Chapter 2). A reliability assessment is also performed, by using the first order estimator and associated method as presented in section 4.5 of Chapter 4.

The MIP formulations of the sub-problems (P1)-(P5), are an extension of the formulation proposed by Pillai and al. [154] and are detailed in sections 5.5. The latter is indeed limited to the wind turbines clustering and to the design of the collection networks (thus limited to (P1) and (P2)).

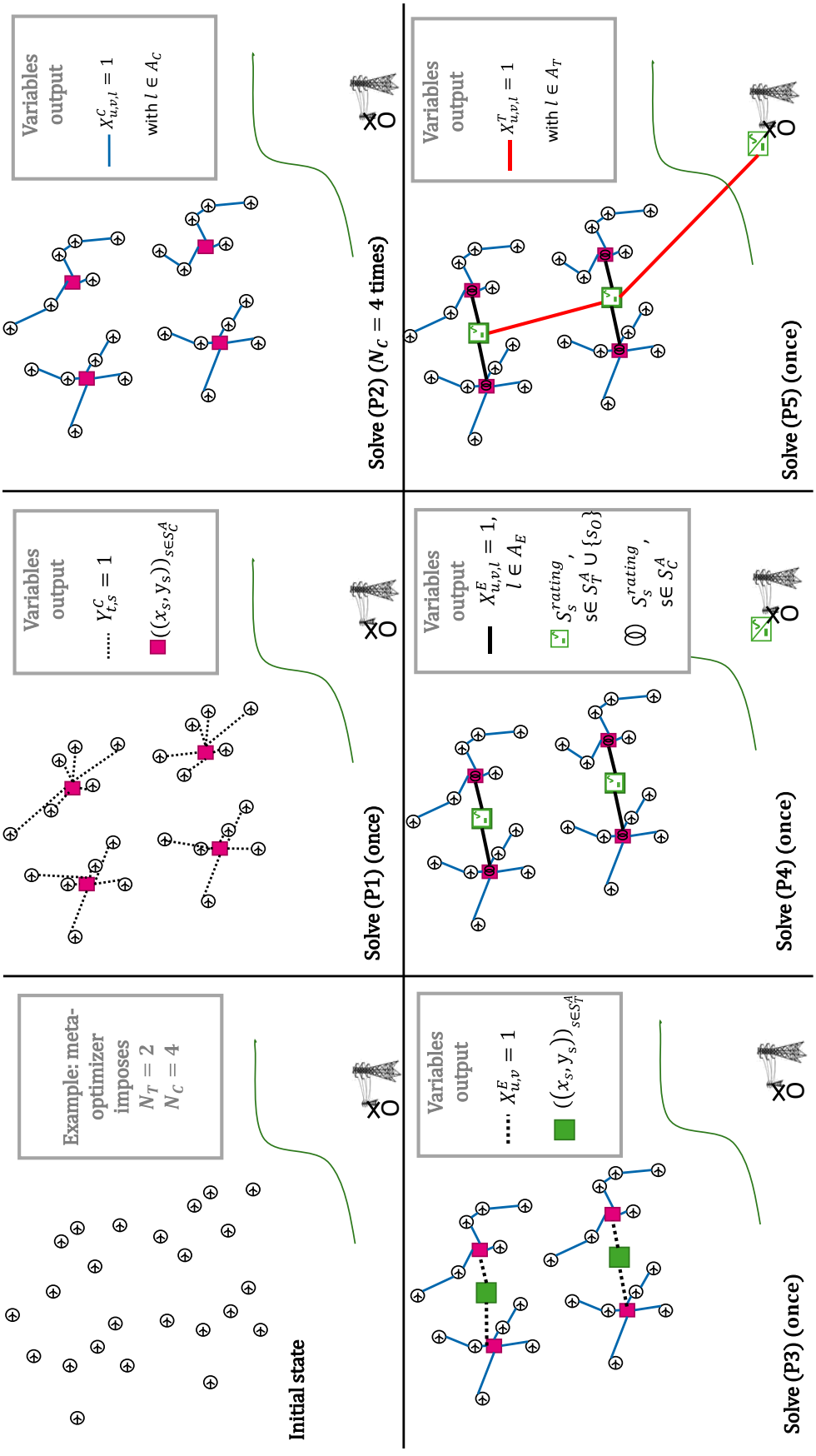

Figure 5-4: Illustrative process to solve an architecture with MVAC collection, HVAC export and HVDC transmission networks ($N_C = 4$ and $N_T = 2$)

5.4.4 Respect of the electrical constraints

The technical constraints relative to cable ampacities and apparent power ratings of transformers, power electronic converters and voltages are checked during the load flows corresponding to the "operational simulation" (see Figure 5-3). The voltage constraints are considered to be $\pm 5\%$ of the nominal values. In practice, these technical constraints are always satisfied when the operational simulation is performed because the obtained design from the resolution of the problems (P2), (P4) and (P5) ensures the respect of these constraints. The collection cable choice (in (P2)) is done while neglecting the voltage drops and the reactive power. However, the assumption relative to voltage drops is valid because the distances are short (refer to section 2.3.4 of Chapter 2).

5.5 Formulation of sub-problems

5.5.1 Clustering problem (P1)

It should be reminded that in the present work, the locations of wind turbines are fixed a priori. To decouple (P1) and (P2) problems, some variables have to be introduced:

- The association of wind turbines to offshore cluster substations is quantified by a binary function:

$$Y_{t,s}^{C} = \begin{cases} 1 \text{ if the wind turbine } t \text{ is associated to the cluster substation } s \\ 0 \text{ otherwise} \end{cases}$$

$$\forall t \in T \times, \forall s \in S_C^A;$$

- The number of wind turbines associated to one cluster station $s \in S_C^A$: $n_s^C \leq Q_{\max\_WT}^C$.

5.5.1.1 Formulation of (P1)

Parameters and variables of the nomenclature and the preamble of section 5.5.1 are used. The input parameters of (P1) are the following:

- (x_t, y_t) are the fixed location coordinates of the wind turbine $t \in T$;

- Q_{max}^C is the maximum number of wind turbines which can be connected to a given cluster substation $s \in S_C^A$. If wind turbines are homogenously allocated among the given cluster stations, then: $Q_{max}^C = \left\lceil \frac{card(T)}{N_C} \right\rceil$, where $\left\lceil \frac{card(T)}{N_C} \right\rceil$ is the superior integer part of the integer $\frac{card(T)}{N_C}$.

The output variables of (P1) are the following:

- (x_s, y_s) are the location coordinates of the cluster substation $s \in S_C^A$;

- $Y_{t,s}^C$ defines if the wind turbine $t \in T$ is associated to the cluster substation of index $s \in S_C^A$. All wind turbines connected to a cluster substation constitute a subset of T. It aims only at clustering wind turbines, not at defining the cable connections, which is done in (P2);

- n_s^C is the number of wind turbines associated to the cluster substation $s \in S_C^A$.

  $n_s^C \leq Card\ (T)$, $n_s^C \leq Q_{max}^C$.

The goal of the problem (P1) is to find the locations of cluster power stations $(x_s, y_s)_{s\in S_C^A}$ that minimize the squared distance between the clustered wind turbines $(x_t, y_t)_{t\in T}$ and the cluster power stations, with the following objective function:

$$\sum_{t\in T}\sum_{s\in S_C^A}[(x_t - x_s)^2 + (y_t - y_s)^2].Y_{t,s}^C \quad (5\text{-}5)$$

Constraint (5-6) imposes that each wind turbine is associated to one and only one cluster substation.

$$\sum_{s\in S_C^A} Y_{t,s}^C = 1 \ , \ \forall t \in T \quad (5\text{-}6)$$

Constraints (5-7) and (5-8) impose that each cluster station is placed at the barycenter of its associated wind turbines.

$$\sum_{t\in T} x_t.Y_{t,s}^C = n_s^C.x_s^C \quad ,\forall s \in S_C^A \quad (5\text{-}7)$$

$$\sum_{t\in T} y_t.Y_{t,s}^C = n_s^C.y_s^C \quad ,\forall s \in S_C^A \quad (5\text{-}8)$$

Constraint (5-9) imposes that the number of wind turbines associated to a cluster substations remains below Q_{max}^C.

$$\sum_{t\in T} Y_{t,s}^C \leq Q_{\max\_WT}^C \quad ,\forall s \in S_C^A \quad (5\text{-}9)$$

Constraint (5-10) captures the number of wind turbines per cluster substation; it is necessary for the closure of problem.

$$\sum_{t\in T} Y_{t,s}^C = n_s^C \quad ,\forall s \in S_C^A \quad (5\text{-}10)$$

An enhancement of this formulation could be proposed where the positions of cluster substations are input parameters of the problem (P1) and not variables. It means that the problem then consists in associating each wind turbine to one cluster station (variable $Y_{t,s}^C$). In such case, the meta-optimizer would be in charge of optimizing these positions, which would be meta-variables.

5.5.1.2 Solving (P1)

The clustering problem is NP (Nondeterministic Polynomial time) hard. Using a solver such as CPLEX could lead to very long calculation durations when the size of the instance becomes too large. A possible heuristic algorithm to solve the problem is the "capacitated k-means ++", presented by Pillai et al. [154]. It consists in applying the k-means ++ algorithm and then to achieve the constraint given in equation (5-9) by balancing the wind turbines between clusters. So, the output of (P1) problem is the locations $(x_s, y_s)_{s\in S_C^A}$ of the N_C cluster substations and their associated wind turbines $(Y_{t,s}^C)$. For simplification in the remaining of the chapter, the set of wind turbines associated to station s *is* $T_s = \{t \in T / Y_{t,s} = 1\}$. The set of nodes of the cluster associated to s is defined by $K_s = T_s \cup \{s\}$.

5.5.2 Design of the collection network (P2)

The problem (P2) is to define the connection of wind turbines, which have been previously associated to cluster substations (solution of (P1)) and to choose the cross section of each cable. The problem must be solved for each cluster substation among S_C^A. It is similar to a Capacitated Minimal Spanning Tree (CMST), applicable when branched topologies are allowed and when only one single cross section is considered.

The reactive power is assumed not to impact the sizing of the collection cable due to the moderate voltage level and distances of collection cables (this is justified in section 2.3.4 of the Chapter 2).

A non-crossing cables constraint must be added. When several cross sections are considered, the problem complexity increases. In [154], an extensive mixed integer formulation is proposed but the terminology CMST is used. Gamvros et al. [167], [168] use the terminology "Multi Level Capacitated Minimal Spanning Tree" (MLCMST) for the same problem in the telecommunication field. The formulation of the present work is similar to the one proposed by Pillai et al. [154]. The formulation of the MLCMST uses the total CAPEX of the collection cables as objective function. It does not give the same solution as CMST, whose goal is the minimization of the total length of the cables.

To respect the power conservation, an intermediate quantity, corresponding to the total normalized peak power "injected" by substation is introduced:

$$g_s = -card(T_s) \quad , \forall s \in S_C^A \tag{5-11}$$

5.5.2.1 Formulation of (P2)

The definitions of parameters and variables from the nomenclature and the preamble of section 5.5.1 are used.

The input parameters of (P2) are the following:

- c_l^C is the cost per unit length for a collection cable of section corresponding to the index $l \in A_C$;
- $d_{u,v}$ is the Euclidian distance between two nodes u, v;
- P_l^C is the maximum normalized active power that can be transmitted by a cable of index $l \in A_C$;
- $Q_{\max\_cable}^C$ is the maximum number of collection cables connected to a single wind turbine. For strictly radial topologies, $Q_{connect}^C = 2$ (one cable upstream and one cable upstream);
- $n_s^C = g_s$ is the total number of wind turbines connected to the cluster substation s.

The output variables of (P2) are the following:

- $X_{u,v,l}^C$ defines if two nodes u and v are connected together with a collection cable, whose cross section corresponds to the index $l \in A_C$;
- $p_{u,v}^C$ is the normalized active power transmitted from the node u to the node v, in p.u.

The problem (P2) minimizes the total cost of required collection cables with the following objective:

$$\sum_{v\in K_s}\sum_{u\in K_s\setminus\{v\}}\sum_{l\in A_C} c_l^C . d_{u,v} . X_{u,v,l}^C \tag{5-12}$$

under constraints. The quantity $c_l^C . d_{u,v}$ is the cost of the collection cable of cross section, corresponding to the index $l \in A_C$. If there is a connection with the cable l between u and v, then $X_{u,v,l}^C$=1 and thus, $c_l^C . d_{u,v} . X_{u,v,l}^C$ corresponds to $c_l^C . d_{u,v}$. Summing over the couples (u and v) and possible cross sections (l) gives the total cost of collection cables.

Constraint (5-13) stipulates that a wind turbine can have only one downstream connection.

$$\sum_{u\in K_s}\sum_{l\in A_C} X_{u,v,l}^C \leq 1 \quad , \forall v \in K_s \tag{5-13}$$

Constraint (5-14) states that the peak power flowing upstream a given wind turbine t minus the peak power flowing downstream necessarily equals the peak power produced by the wind turbine.

$$\sum_{u\in K_s}\sum_{l\in A_C} p_{v,u}^C . X_{v,u,l}^C - \sum_{u\in K_s\setminus\{v\}}\sum_{l\in A_C} p_{u,v}^C . X_{u,v,l}^C = g_v \quad , \forall v \in K_s \tag{5-14}$$

The peak power transmitted between two nodes u and v cannot exceed the maximum power rating of the collection cable of index l, and is expressed as the following constraint:

$$p_{u,v}^C - \sum_{l\in A_C} P_l^C . X_{u,v,l}^C \leq 0 \quad , \forall (u,v) \in K_s^2 \tag{5-15}$$

Constraint (5-16) imposes that, for two nodes u and v, only one cable is installed at most.

$$\sum_{l\in A_C} X_{u,v,l}^C \leq 1 \quad , \forall (u,v) \in K_s^2 \tag{5-16}$$

Collection cables cannot cross each other. This constraint is expressed by the equation (5-17).

$$\sum_{l\in A_C} X_{u,v,l}^C + X_{w,z,l}^C \leq 1 \quad , \forall (u,v,w,z) \in X_{cross} \tag{5-17}$$

In practice, this constraint is checked only for connections, which are created by the solution.

Constraint (5-18) expresses that a maximum of $Q_{\max\_cable}^C$ cables can be connected to a single wind turbine. For a purely radial topology, $Q_{\max\_cable}^C$=2.

$$\sum_{u\in K_s}\sum_{l\in A_C} X_{u,t,l}^C + X_{t,u,l}^C \leq Q_{\max\_cable}^C \quad , \forall t \in T_s \tag{5-18}$$

$$\forall (u,v) \in K_s^2, p_{u,v}^C \geq 0 \tag{5-19}$$

5.5.2.2 Solving (P2)

Heuristics methods have the advantage to be quick and robust. Several studies have constructed a Minimal Spanning Tree by using Prim algorithm [145], [160]. In some cases, the collection network routing itself is only based on this method [145], which turns out to be ineffective for large instances with around 100 wind

turbines or beyond. Bauer and al. [162], [164] propose methods to solve the problem by imposing a strictly radial topology by using Planar Open Saving (POS) heuristics. When a branched topology is allowed, the problem can be seen as a CMST problem for which the Esau William (EW) heuristic [169] can be applied by imposing non-crossing constraints as done by Katsouris [163]. Katsouris [163] modifies and proposes a hybrid version of EW and POS heuristics to solve the Capacitated Minimal Spanning Tree (MLCMST named by Gamvros and al. [167]) and obtain good performances, but with a maximum of three types of cables per problem. In the present work, similar heuristics are developed while extending it to any number of types of cables:

- The heuristic developed in the present work (to obtain purely radial topologies) is called POS MLCMST.
- The heuristic developed in the present work to obtain branched topologies is called EW MLCMST.

5.5.3 Association of cluster stations to transmission stations (P3)

Some intermediate variables have to be introduced to solve this problem.

- The connection variable for $(u, v) \in S_C^A \times S_T^A$, $Y_{u,v}^E$. If an active cluster substation of index u is connected to a transmission substation of index u, $Y_{u,v}^E$=1, 0 otherwise.

- The number of wind turbines associated to one transmission station: $\forall v \in S_T^A,\ n_v^T$;

The formulation of (P3) is similar to the one of (P1). Instead of clustering wind turbines, now, cluster substations are clustered. The input parameters of (P3) are the following:

- (x_u, y_u) are the location coordinates of the cluster substation $u \in S_C^A$;

- g_u is the number of wind turbines associated to the cluster substation $u \in S_C^A$;

The output variables to be found are the following:

- (x_v, y_v) are the location coordinates of the transmission substation $v \in S_T^A$;

- $Y_{u,v}^E$ defines if a cluster substation u is connected to a transmission substation v;

- n_v^T is the total number of wind turbines associated to the transmission substation $v \in S_T^A$.

The problem (P3) is similar to the problem (P1) (refer to section 5.5.1.1). It must minimize the sum of squared distances between cluster substations and associated transmission substations:

$$\sum_{u \in S_C^A} \sum_{v \in S_T^A} [(x_v - x_u)^2 - y_v - y_u)^2] \,.\, X_{u,v}^E \qquad (5\text{-}20)$$

Under constraints.

Equation (5-21) stipulates that each cluster substation $u \in S_C^A$ can be connected to only one transmission substation.

$$\sum_{v \in S_T^A} Y_{u,v}^E = 1 \quad , \forall u \in S_C^A \tag{5-21}$$

Constraints (5-22) and (5-23) impose the location of each transmission substation $\forall v \in S_T^A$ to be in the gravity center of the cluster substation:

$$\sum_{u \in S_C^A} x_u^C . Y_{u,v}^E = n_v^T . x_v^T \quad , \quad \forall v \in S_T^A \tag{5-22}$$

$$\sum_{u \in S_C^A} y_u^C . Y_{u,v}^E = n_v^T . y_v^T \quad , \forall v \in S_T^A \tag{5-23}$$

Equation (5-24) is a closure equation imposing the power balance for the peak power produced by wind turbines in fine connected to a given transmission substation:

$$\sum_{u \in S_C^A} Y_{u,v}^E . |g_u| = n_v^T \quad , \forall v \in S_T^A \tag{5-24}$$

To solve the problem (P3), a method similar to the one proposed for (P1) is used.

An enhancement of this formulation could be proposed where the position of transmission substations are parameters of the problem (P3). In such case, the meta-optimizer would be in charge of optimizing these positions, which would be meta-variables. Alternatively, the positions of the transmission substations could be imposed by the user.

5.5.4 Sizing of substations and export components (P4)

The problem (P4) consists in sizing the components of the cluster and transmission substations and in sizing the export cables. The sizing of power components is a complex problem in itself; depending on the reliability (refer to [80] for export transformers design), CAPEX etc. The proposed formulation allows the choice of various options including base cases.

5.5.4.1 Formulation of problem (P4)

The formulation of the problem is given below.

The input parameters of the problem (P4) are the following:

- $Y_{u,v}^E$ is the result of problem (P3) and defines if there is an export connection between the cluster substation u and the transmission station v;
- n_s^C is the result of the problem (P1) and corresponds to the number of wind turbines connected to the cluster substation $s \in S_C^A$;
- n_s^T is the result of the problem (P3) and corresponds to the number of wind turbines connected to the offshore transmission substation $s \in S_T^A$;

- P_l^E is the maximum normalized apparent power that can be transmitted with an export cable of cross section corresponding to the index $l \in A_E$.

The output variables, to be found, are the following:

- $X_{u,v,l}^E$ (only when there is are dedicated export connection(s)) defines if there is an export cable connection between the cluster substation $u \in S_C^A$ and the offshore transmission substation $v \in S_T^A$ with cables cross section corresponding to $l \in A_E$. It is must respect the choice of connections done in (P3) and thus, corresponds only to defining the cable cross sections;

- $m_{u,v}^E$ is the number of export cables in parallel between the cluster substation $u \in S_C^A$ and the transmission substation $v \in S_T^A$;

- $p_{u,v}^E$ is the active power to be transmitted by a group of export cables between the substations of indexes $(u, v) \in S_C^A \times S_T^A$;

- $\left|cos\varphi_{u,v,l}^{maxprod}\right|$ is the min absolute value of the power factor at extremities of export cables between a cluster substation u and a transmission substation v. In practice, a load flow calculation is required. This is executed offline for various distances and wind farm peak powers with the methodology of section 2.3.4 in Chapter 2. With the mentioned methodology, a compensation at both sides of the export cable(s) is calculated;

- S_s^{rating} is the normalized apparent power rating of the substation $s \in S_C \cup S_T \cup \{s_O\}$ (p.u.);

- $\left|cos\varphi_s^{maxprod}\right|$ is the absolute value of power factor, corresponding to the peak production, at the interface of the substation of index s with their networks, $s \in S_C \cup S_T \cup \{s_O\}$.

Thus, for the problem (P4), the objective is to minimize the power ratings of the power components (S_s^{rating}), implicitly minimizing the associated investment costs:

$$\sum_{u \in S_C^A} \sum_{v \in S_T^A} \sum_{l \in A_C} m_{u,v}^E . P_l^E . X_{u,v,l}^E + \sum_{s \in S_C^A \cup S_T^A \cup \{s_O\}} S_s^{rating} \qquad (5\text{-}25)$$

while respecting the following constraints.

Constraint (5-26) corresponds to the fact that some export cables can be installed between a cluster station and a transmission station only if they are associated together (result of (P3)):

$$X_{u,v,l}^E \leq Y_{u,v}^E \quad , \forall (u, v, l) \in S_C^A \times S_T^A \times A_C \qquad (5\text{-}26)$$

Constraint (5-27) ensures that only one kind of export cables (cross section) is used to connect a cluster station to a transmission station:

$$\sum_{l \in A_E} X_{u,v,l}^E \leq 1 \quad , \forall (u, v) \in S_C^A \times S_T^A \qquad (5\text{-}27)$$

Constraint (5-28) imposes that all the peak active power is extracted from cluster stations to transmission stations. Equation (5-29) is necessary to impose a consistent power balance:

$$\sum_{u \in S_C^A} \sum_{l \in A_T} p_{u,v}^E . X_{v,u,l}^E = n_v^T \quad , \forall v \in S_T^A \tag{5-28}$$

$$p_{u,v}^E \geq 0 \quad , \forall (u,v) \in S_C^A \times S_T^A \tag{5-29}$$

Constraint (5-30) ensures that the HVAC export cables (when applicable) are sized so that the constraint in apparent power is respected. This is more detailed in Chapter 2:

$$p_{u,v}^E \leq \sum_{l \in A_C} m_{u,v}^E . \left| cos\varphi_{u,v,l}^{maxprod} \right| . P_l^E . X_{u,v,l}^E \quad , \forall (u,v) \in S_C^A \times S_T^A \tag{5-30}$$

Constraints (5-31), (5-32) and (5-33) impose that the constraint in regard to the apparent power through the power stations is respected for the peak production.

$$n_s^C \leq \left| cos\varphi_s^{maxprod} \right| . S_s^{rating}, s \in S_C \tag{5-31}$$

$$n_s^T \leq \left| cos\varphi_s^{maxprod} \right| . S_s^{rating}, s \in S_T \tag{5-32}$$

$$\sum_{v \in S_T^A} n_v^T \leq \left| cos\varphi_{s_O}^{maxprod} \right| . S_{s_0}^{rating} \tag{5-33}$$

5.5.4.2 Solving (P4)

In the present implementation of the design framework, considered architectures concepts include only HVAC export networks (refer to section 1.3.of Chapter 1). Integrating DC export would be a simplification (no reactive power).

To solve the part of (P4) related to HVAC export cables, power management assumptions (as detailed in the section 2.3.4 of Chapter 2) are used to increase the active power that can be transmitted by a given cable. It is based on the following approximations:

- The reactive power due to the collection network(s) are neglected;
- The power losses due to the collection network(s) are neglected;
- The export transformer takes 0.1 p.u. of the peak active power in reactive power (corresponding to leak reactance of the transformer in Chapter 2, refer to Dahmani [25]).

For the design of substations, a moderate level of granularity is employed:

- An absolute power factor $\left| cos\varphi_s^{maxprod} \right| = 0.95$ is considered for the power stations. Then, the problem is solved by applying equalities for equations (5-31), (5-32) and (5-33) to determine S_s^{rating} for $s \in S_C^A \cup S_T^A \cup \{s_O\}$
- Transformers of the substations (MMC based HVDC substations and cluster power substations) are always associated in pairs, in parallel. Each transformer is sized at half the total rating of the power station S_s^{rating}. The rate of power rating associated to one transformer $\lambda_{transfo}$ (50% in present case) can be considered a decision variable for which the reliability must be considered as in Almiray et al. [80].

When applicable, the MVDC/HVDC converter of a single substation is assumed to be a single component with the total rating.

A posteriori when the load flow computations are performed, operational constraints are checked (refer to Figure 5-3).

A perspective for the proposed formulation is to consider a priori values of power factor for substations $\left|cos\varphi_s^{maxprod}\right|$ and the rate of power per transformer $\lambda_s^{transfo}$ as meta-variables. The present formulation and associated implementation is a compromise between the complexity of the problem and the level of details for the results.

5.5.5 Design of the HVDC transmission network (P5)

To make possible the power conservation from the offshore transmission substations to the onshore transmission substation, an intermediate quantity corresponding to the maximum power "injected" (therefore negative) in DC must be defined. It is called n_O^T and corresponds to the total number of wind turbines (if they have the same rated power in p.u.) in the wind farm that are connected to the offshore transmission substations.

$$n_O^T = -\sum_{v \in S_T^A} n_v^T \tag{5-34}$$

The formulation of (P5) is similar to the formulation of (P2). Thus, the proposed formulation includes only branched topologies for the HVDC transmission network. Meshed transmission networks are not considered a priori. Meshed topologies can be interesting for reliability issues. As the design of transmission substations is obtained from (P4), the solution of (P5) defines only the connections between offshore and onshore transmission stations and associated cable choices.

The definitions of parameters and variables of the nomenclature and the preamble of section 5.5.5 are used. The input parameters of (P5) are the following:

- c_l^T is the cost per unit length for a pair of transmission cables of section corresponding to the index $l \in A_T$;
- P_l^T is the maximum normalized active power that can be transmitted by a pair of transmission cables of cross section corresponding to the index $l \in A_T$;
- $d_{u,v}$ is the Euclidian distance between two transmission substations of indexes u and v;
- $Q_{\max\_cable}^T$ is the maximum number of transmission cables pairs connected to a single transmission station. In practice, $Q_{\max\_cable}^T$ is fixed to 3;
- n_v^T is the total number of wind turbines associated to a given transmission station (including the onshore transmission station) $v \in S_T^A \cup \{O\}$.

The output variables of (P5) are the following:

- $X_{u,v,l}^{T}$ defines if two nodes u and v are connected together with a pair of transmission cables, whose core conductor cross section corresponds to the index $l \in A_T$;

- $p_{u,v}^{T}$ is the normalized active power transmitted from the node u to the node v.

The problem (P5) must minimize the total cost of transmission cables (similarly as for the problem (P2), refer to section 5.5.2.1) and corresponds to the following objective function:

$$\sum_{v \in S_T^A \cup \{s_O\}} \sum_{u \in (S_T^A \cup \{s_O\}) \setminus \{v\}} \sum_{l \in A_E} c_l^T . d_{u,v} . X_{u,v,l}^T \tag{5-35}$$

Under constraints.

Equations (5-36) and (5-37) impose the constraint that an offshore transmission substation can have only one downstream connection.

$$X_{u,u,l}^T = 0 \ , \qquad \forall u \in (S_T^A \cup \{s_O\}), \forall l \in A_T \tag{5-36}$$

$$\sum_{u \in S_T^A \cup \{s_O\})} \sum_{l \in A_T} X_{u,v,l}^T \leq 1 \ , \ \ \forall v \in S_T^A \cup \{s_O\}) \tag{5-37}$$

Constraint (5-38) states that for a given offshore transmission substation v, the peak power flowing via upstream pair(s) of transmission cables minus the peak power flowing via the downstream pair of transmission cables equals the peak power, which is produced by the wind turbines connected to the transmission station.

$$\sum_{u \in S_T^A \cup \{s_O\})} \sum_{l \in A_T} p_{v,u}^T . X_{v,u,l}^T - \sum_{u \in S_T \cup \{s_O\} \setminus \{v\}} \sum_{l \in A_T} p_{u,v}^T . X_{u,v,l}^T = n_v^T, \forall v \in (S_T^A \cup \{s_O\}) \tag{5-38}$$

Equation (5-39) corresponds to the physical constraint that the peak power transmitted between two nodes u and v cannot exceed the maximum power rating of the pair of transmission cables whose cross section corresponds to the index $l \in A_T$.

$$p_{u,v}^T - \sum_{l \in A_T} P_l^T . X_{u,v,l}^T \leq 0 \quad , \forall (u,v) \in (S_T^A \cup \{s_O\})^2 \tag{5-39}$$

Constraint (5-40) imposes that for two nodes u and v, only one pair of transmission cable is installed at most.

$$\sum_{l \in A_T} X_{u,v,l}^T \leq 1 \quad , \forall (u,v) \in (S_T^A \cup \{s_O\})^2 \tag{5-40}$$

Equation (5-41) imposes that at most $Q_{\max\_cable}^T$ pairs of HVDC transmission cables are connected to a single offshore transmission station.

$$\sum_{u \in (S_T^A \cup \{s_0\}} \sum_{l \in A_T} X_{u,v,l}^T + X_{v,u,l}^T \leq Q_{\max\_cable}^T \quad , \forall v \in S_T^A \tag{5-41}$$

Equation (5-42) is necessary to impose a consistent power convention, in order to ensure the power balance.

$$p^{C}_{u,v} \geq 0 \quad ,\forall (u,v) \in (S^{A}_{T} \cup \{s_O\})^2 \tag{5-42}$$

To solve (P5), the heuristic used to solve (P2) is modified in order to take into account non-unitary injected power nodes (the power that is injected to offshore transmission substations corresponds to several wind turbines). As the practical size of instances for (P5) is not so high, an enumeration technique could also be used.

5.5.6 Geographical obstacles and inter-networks cables crossings

Additional constraints, not naturally taken into account while solving the sub-problems (P1)-(P5), need to be satisfied in a general case:

- The cables of different networks (export, collection and transmission) should not cross each other. Otherwise, installation costs drastically increase (around 1 M€ per crossing [26]);
- The location of HVAC and HVDC cables should avoid forbidden zones.

The methodology, which is proposed to respect these constraints consists in determining non straight paths for HVAC and HVDC cables. Such paths should avoid the collection cables and the forbidden zones, which can be modelled by forbidden segments. A grid of the 2 D space is constructed with an appropriate resolution, which is a compromise between the obtained precision and the computational time (e.g. a resolution of 1 km). Each node of the network is virtually connected to neighbor points of the grid. These points along with potential connections are modeled with a weighted graph, whose edges correspond to the connections. Weights of the edges equal the corresponding Euclidian distances. If a connection crosses a forbidden segment, the connection is not considered and the edge is thus not added to the graph. Once the graph is built, the shortest path problem is solved for all HVAC and HVDC cables between their connection points. To solve the Shortest Path Problem, the Dijkstra algorithm implementation in the Networkx Python library [79] is employed.

In practice, the problems (P4) and (P5) are first solved while neglecting these geographical constraints. Once they are solved, connection bus nodes are known and the shortest path methodology is performed for all HVAC and HVDC cables. In the present implementation of the optimization methodology for the overall system, these geographical constraints are solved for each combination of metavariables.

5.6 Study cases for validation of the proposed design framework

In the present section, the models, methods and associated parameters, which are used to compute the CAPEX and to assess the reliability, correspond to the “mean” scenario in the Chapter 2 and in the Chapter 3. For the calculation of the CAPEX of wind turbines, a water depth of 30 m is used.

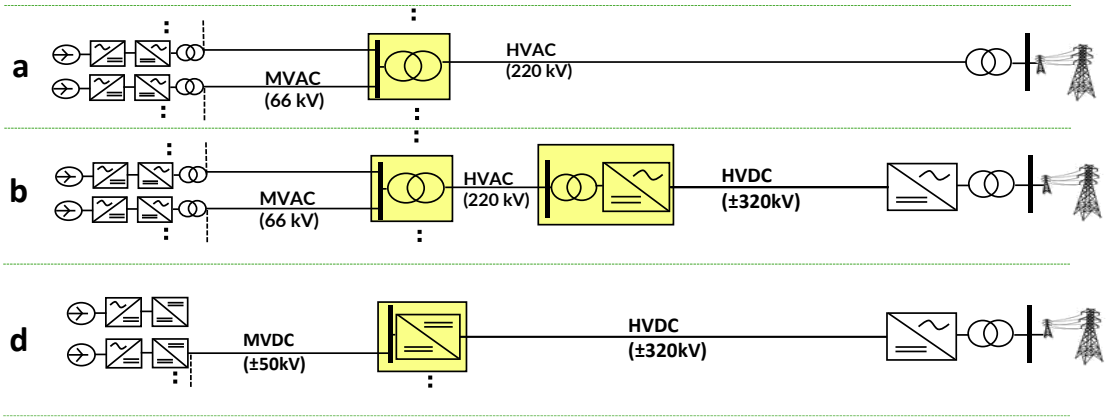

Figure 5-5: Architecture concepts considered for application of the design methodology

The objective of this Chapter is not to raise conclusion on the competitiveness of the architecture concepts, which are considered. The objective is rather to show the effectiveness of the proposed design framework (refer to Figure 1-20 of Chapter 1). Thus:

- In the section 5.6.1 an application of the framework to the design and assessment of the electrical network of a real wind farm site is done. It is done with the architecture concept by using MVAC collection networks and HVAC export networks up to the shore (refer to concept (a) of Figure 5-5). An emphasis is put on the validation of the heuristic methods solving the problem (P2) relative to the design of the collection network.
- In the section 5.6.2, the proposed framework is applied to a virtual wind farm site with the architecture employing a MMC based HVDC transmission network with dedicated HVAC export networks and MVAC collection networks (refer to concept (b) of Figure 5-5).
- In the section 5.6.2, the proposed framework is also applied to a virtual wind farm site with the architecture concept employing a HVDC transmission and MVDC collection networks (refer to concept (d) of Figure 5-5).

In other words, these applications are proposed in accordance with the framework of Figure 1-20. Accordingly, a wind farm site is selected (Borseele Wind Farm III and IV in section 5.6.1 and virtual wind farm site of section 5.6.2) along with an architecture concept, with choice of the technological solution. Then, "design heuristics" are used for the design of the electrical network, by using the external meta-optimizer ("optimization algorithm"). Once the design is obtained, the "reliability simulator", "load flow simulator" and "CAPEX evaluator" of the framework are used to calculate the various quantities so to then, calculate the LCOE and the NLCC.

The simulations are performed with Python 2.7 on a 4 core, 64-bit DELL PC with Intel ® Core TM i5-4310U CPU, 2.6 GHz and RAM 8 Giga-byte.

5.6.1 Validation on the "Borseele Wind farm III and IV" project

In this section, for a validation of the framework methodology along with cost models, a comparison with a known public LCOE of an industrial project is undertaken. To do so, an optimization is performed on the

real project "Borssele wind farm III and IV" with the wind turbine layout taken from Ecofys in [125]. It consists of 100 wind turbines of 7 MW each. The bidding process has resulted to a LCOE of 72.4€/MWh [16] including two offshore HVAC stations. The LCOE of the real project was calculated with N=25years.

In this study, the following technical and financial parameters are used:

- Actual Weibull parameters $k = 2.2$ and $\lambda = 10.57$ m/s [82].
- Wake losses of 10% as considered in [10].
- Discount rate r=8% and considered duration N=25 years.
- Constant yearly maintenance cost for wind turbines (Oc_t) in the range given by reference studies [10], [11]: 50k€/MW installed, meaning that $Oc_t = 70M€$. $Os_t(\boldsymbol{X})$ is neglected in the results of the section 5.6.

In addition to the computational durations, Table 5-3 gives the LCOE and the NLCC for various design of the collection networks.

Table 5-3: Results for BORSSELE III & IV

	Branched collection network	Strictly radial collection network	Given Ecofys layout
$LCOE$ (€/MWh)	76.71	76.79	76.79
total $NLCC$ (M€)	867.3	872.0	872.8
CAPEX (M€)	670.2	673.8	673.3
Dissipated $NLCC$ (M€)	141.7	142.5	143.4
curtailed energy $NLCC$ (M€)	55.5	55.7	55.2
Total duration (s)	504	393	Not meaningful, design of the collection network is imposed
Optimization duration (s)	390	280	
First order reliability analysis duration (s)	110	111	

The solving duration for the branched collection network is higher because the heuristic EW_MLCMST takes more time than POS_MLCMST (terminology defined in section 5.5.2.2).

With the three designs of the collection networks, the LCOEs and the NLCCs are very close. It is the main objective of our presented method to have design methods allowing the comparison of different architectures. More detailed results are given below on the case study.

The obtained layouts are given for:

- The branched design of the collection network in the Figure 5-6, where the problem (P2) is solved by using the EW_MLCMST heuristic, giving a branched topology for the collection network.
- The strictly radial design of the collection network in the Figure 5-7, where the problem (P2) is solved by using the POS_MLCMST heuristic, giving a strictly radial topology for the collection network.
- The design of the collection network given by Ecofys in the Figure 5-8, where the offshore stations are the ones given in the report written by DNV GL on behalf of the TSO TenneT [125]. The routing

of the collection cables is also imposed as given in [125] (design proposed by the company Ecofys). The problem (P4) is solved with the methods proposed in the present thesis.

It can be seen that the obtained HVAC cable routes are not straight, due to the non-crossing constraint with collection cables.

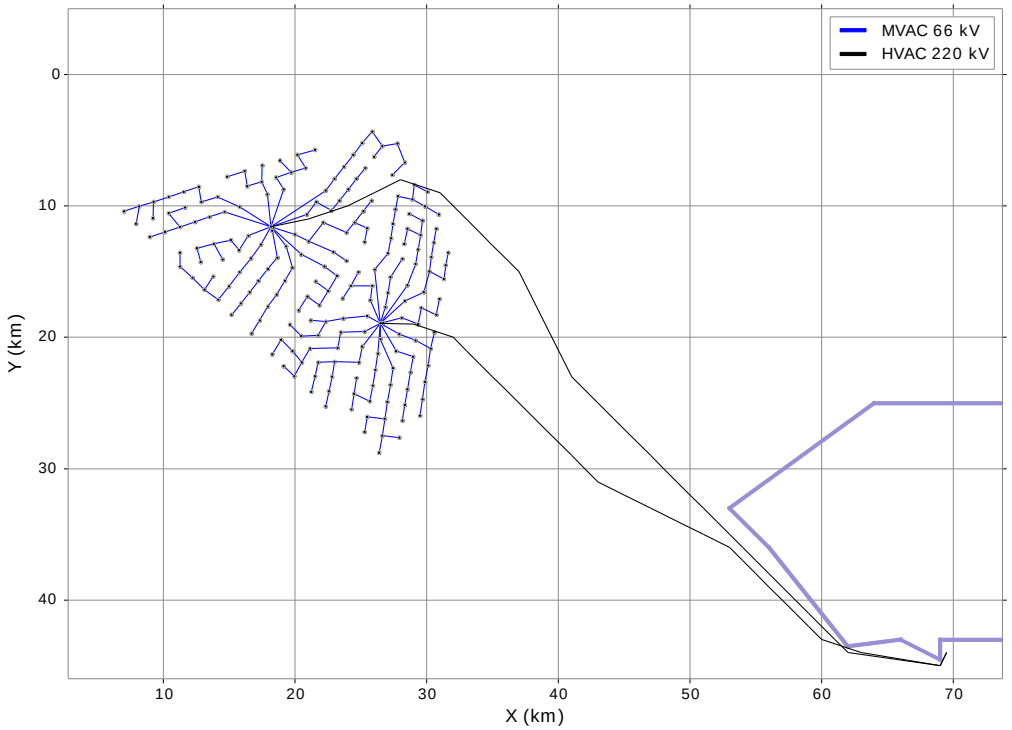

Figure 5-6: Electrical network layout for Borssele III and IV with (P2) solved with EW_MLCMS

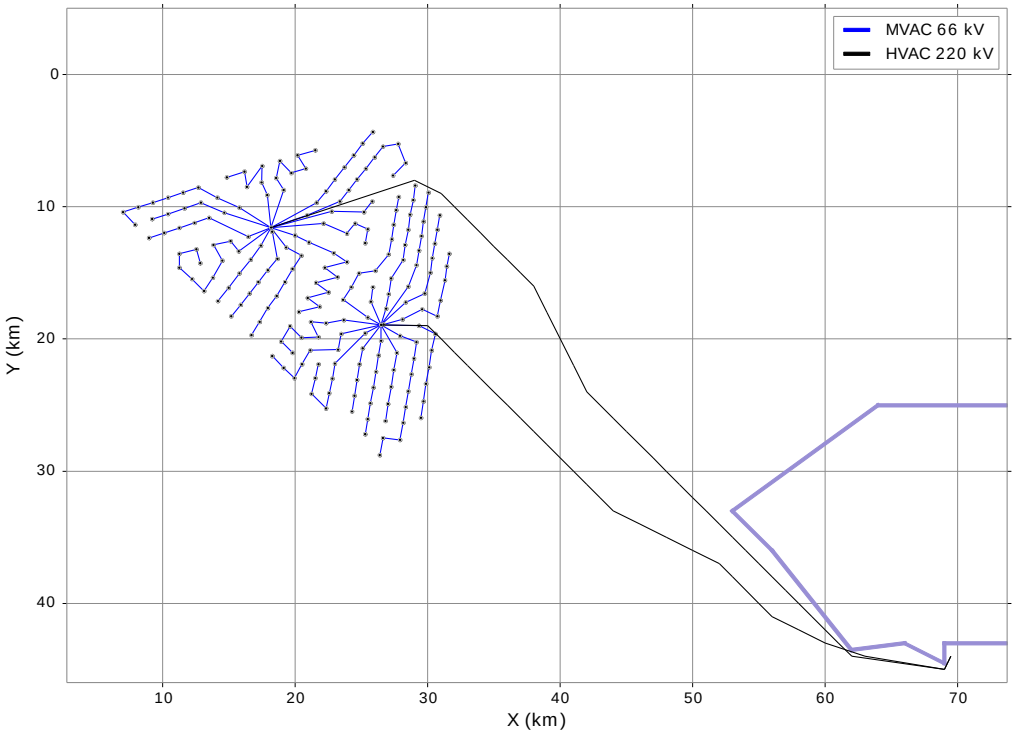

Figure 5-7: Electrical network layout for Borssele III and IV with (P2) solved with POS_MLCMST

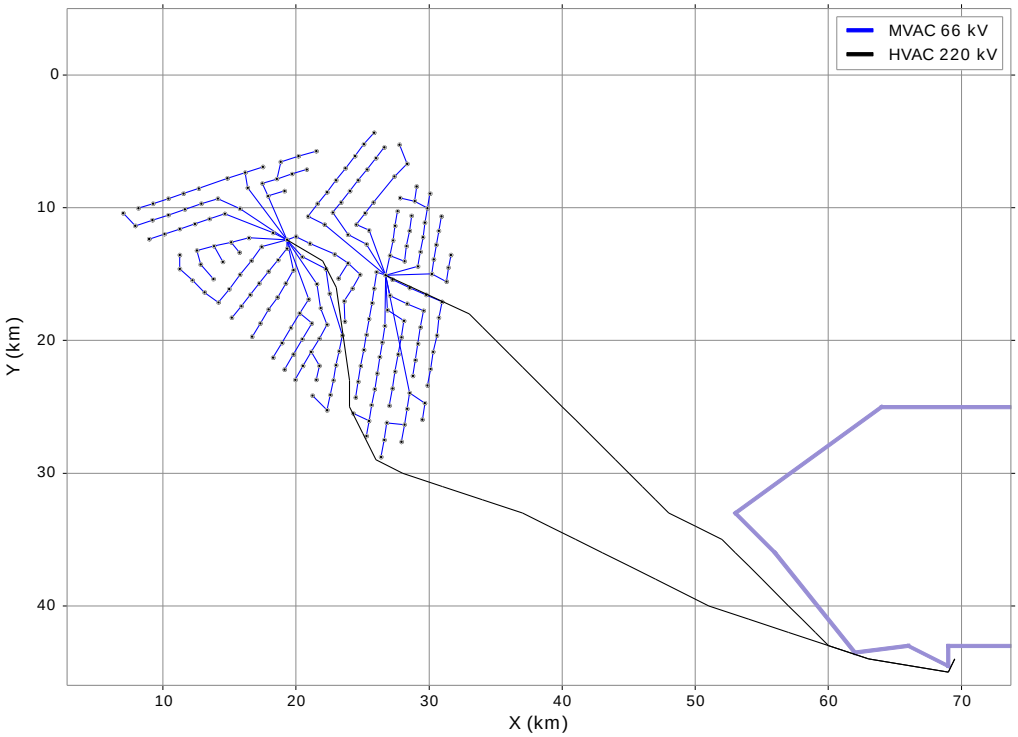

Figure 5-8: Electrical network layout for Borseele III and IV with Ecofys collection cables routing

The major geographical constraints are depicted in violet on the figures. The 220 kV HVAC cables corridors are shown in black and the 66kV MVAC collection cables in blue.

A resolution of 1km is used in the procedure to avoid the obstacles (refer to section 5.5.6) for the HVAC cable routing. The choice of the resolution therefore depends on the application. It should be different if the framework is applied to the architecture concept assessment or to the pre-project planning.

The primary discriminating factors between the three designs of the collection networks are the CAPEX and annual energy losses (dissipated and curtailed) associated to the collection cables. The Figure 5-9 gives the lengths of collection cables among the considered conductor cross sections.

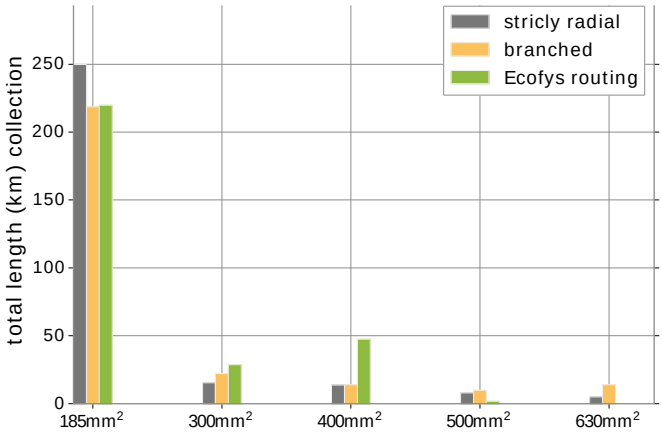

Figure 5-9: Obtained lengths of collection cables

Figure 5-10 compares the part of the NLCC, which can be associated to the collection cables for the three designs. The part of the NLCC relative to curtailed energy can be given separately for the collection cables thanks to the first order estimator, which is presented in the Chapter 3. It can be seen that with the MTTF data for the cables (as described in the Chapter 4), the impact of the curtailed energy for the collection cables is moderate. Thus, it is considered that the proposed design is cost-effective and that it is justified not to add redundant collection cables.

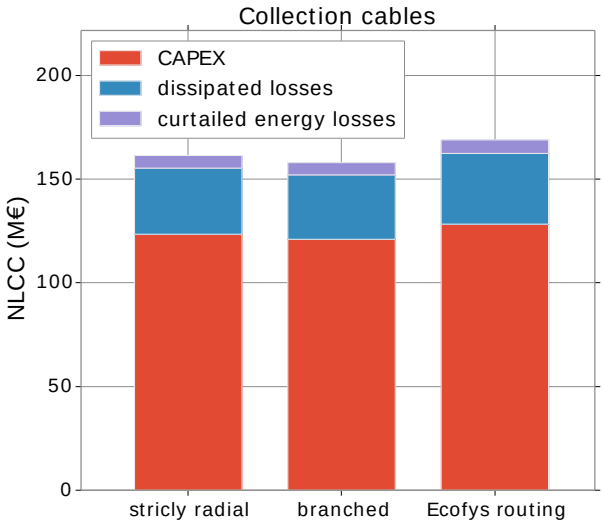

Figure 5-10: NLCC breakdowns for the collection cables for the three designs

For the remaining of this chapter and in the Chapter 6, unless stated otherwise, the heuristic EW_MLMST is used as it provides the best results. Though its computational cost is slightly higher than the one of POS_MLCMST, it remains acceptable.

After a first validation on a real project with conventional architecture (MVAC collection, HVAC export and transmission networks), section 5.6.2 defines a prospective virtual wind farm site with higher wind turbine power ratings. It is then used to design and assess two other architecture concepts in sections 5.6.3 (MVAC collection, HVAC export and HVDC transmission networks) and 5.6.4 (MVDC collection and HVDC transmission networks), thus showing the applicability of the proposed framework to various concepts.

5.6.2 Virtual wind farm site

In order to test our proposed framework for other architectures, the virtual wind farm site of Figure 5-11 is defined in accordance with industrial practices, imposing at least a minimal distance between wind turbines being eight times the wind turbine diameter (D) [56]. In the present work, the distance between two wind turbines is so that $d.D \in [9D, 11D]$. d follows a uniform probability law in the interval [9.0, 11.0] and is calculated for each wind turbine. The virtual case study allows to consider future 10 MW wind turbines, which could contribute to the reduction of the LCOE [56].

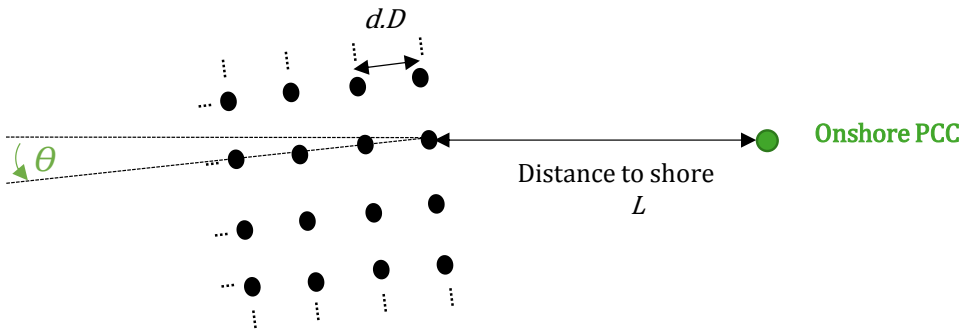

Figure 5-11: Virtual wind farm site with defined distances

The rotation angle θ is a parameter necessary to have a virtual wind farm site, which can mimic various real wind farm sites. These sites are a priori not regular and not aligned with the transmission direction. In the sections 5.6.3 and 5.6.4 where two different architectures are optimized, the virtual wind farm site is instantiated with different values of the angle. It allows emphasizing the genericity of the proposed optimization method.

The wind turbines have 10 MW peak power with a rotor diameter of 190 m, with the power characteristic given in [56]. Realistic values for shape (k) and scale (λ) parameters of the Weibull distribution are used (k =2 and λ =10 m/s). The other technical and financial parameters, which are used in the section 5.6.3 and 5.6.4 are put to the same values as in section 5.6.1.

5.6.3 Architecture with MVAC collection, HVAC export and HVDC transmission networks

In this section, the optimization framework is applied to the most complex architecture concept (b), which has a 66kV MVAC collection network, a dedicated 220kV HVAC export network and a ±320 HVDC transmission network with dissociated AC stations and HVDC station(s). An instance of the virtual case study (refer to Figure 5-11) with 100 wind turbines layout (1 GW) with 14 columns and with an arbitrary rotation $\theta = 3°$ with the transmission direction is considered. The transmission distance L is 120 km. The optimization procedure is launched with at maximum four clusters $N_C^{max} = 4$. Thus, configurations $(N_T, N_C) \in \{(1,2), (1,3), (1,4), (2,4)\}$ are considered (refer to section 5.4.3 for definition of N_T and N_C).

The optimal solution is obtained for one HVDC station and four cluster AC stations (refer to Table 5-4), and is shown in the Figure 5-12. The second and the third solutions are depicted respectively on the Figure 5-13 and the Figure 5-14. Figure 5-15 depicts the obtained topology for two offshore HVDC stations and four offshore AC stations.

The violet segments define geographical zones which cannot be crossed by the cables. It can be seen that the exposed method of section 5.5.6 is effective; the transmission cables avoid the two zones.

To avoid the obstacles a resolution of 1km presently seems to be sufficient for the present validation of the framework. A higher precision could be considered but it will induce a higher computational cost.

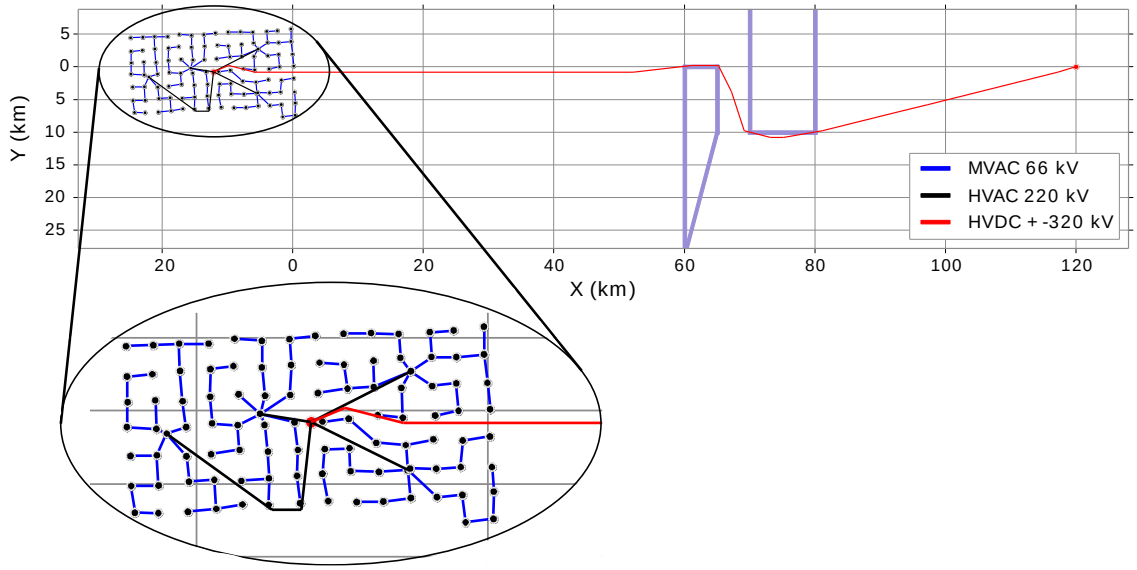

Figure 5-12: The optimal layout ($(N_T, N_C) = (1,4)$) with the architecture (b)

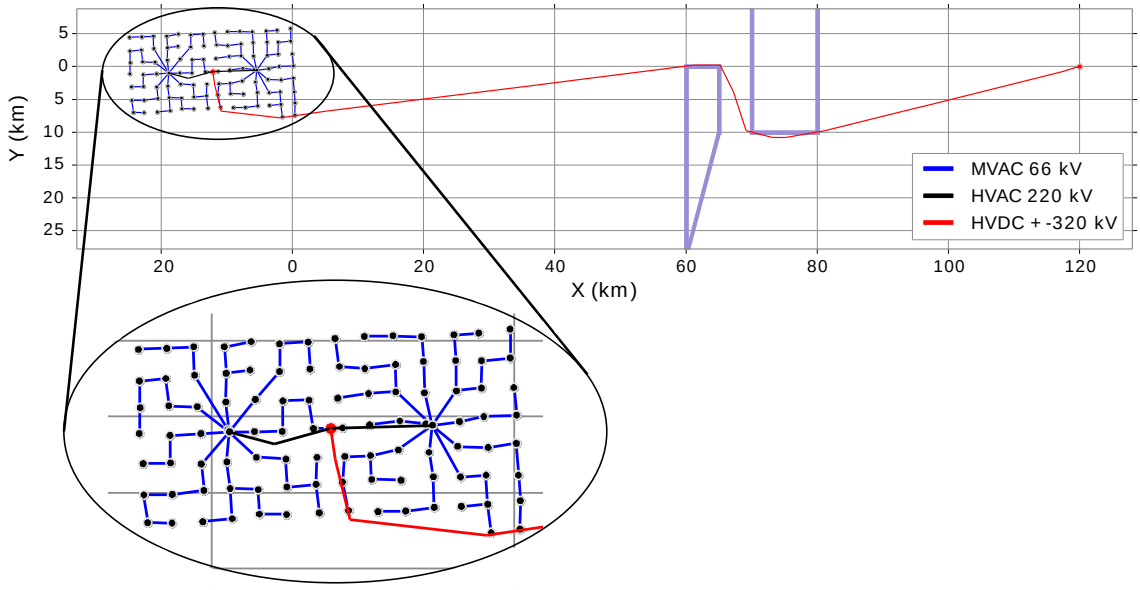

Figure 5-13: The optimal layout ($(N_T, N_C) = (1,2)$) with the architecture (b)

The macro results of the Table 5-4 give the best values of the metavariables based on a simple dominion criterion.

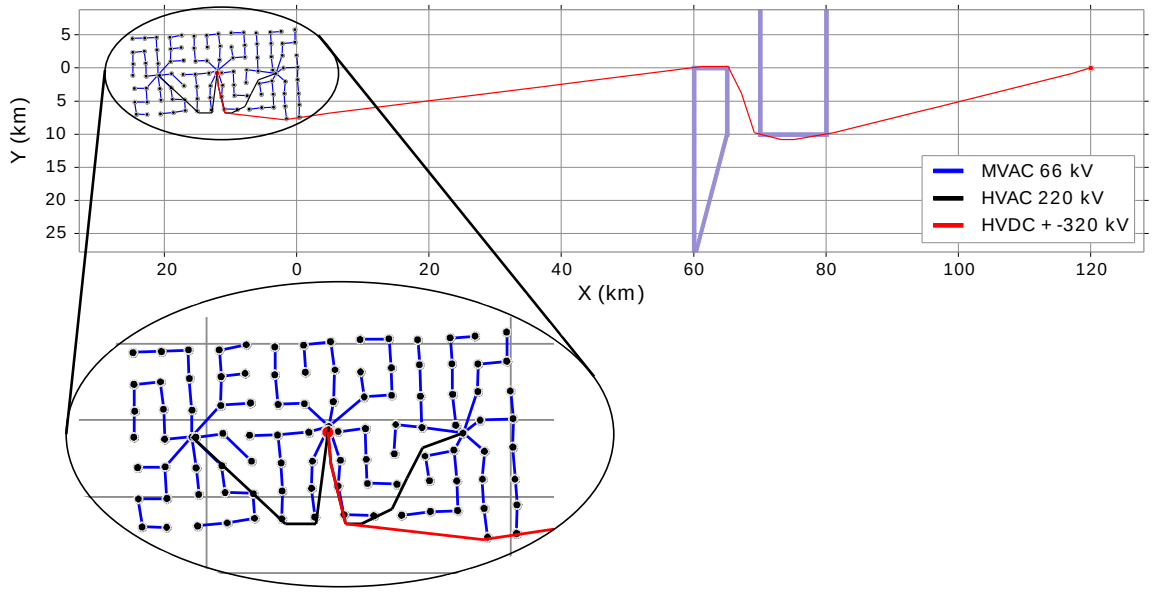

Figure 5-14: The optimal layout ($(N_T, N_C) = (1,3)$) with the architecture (b)

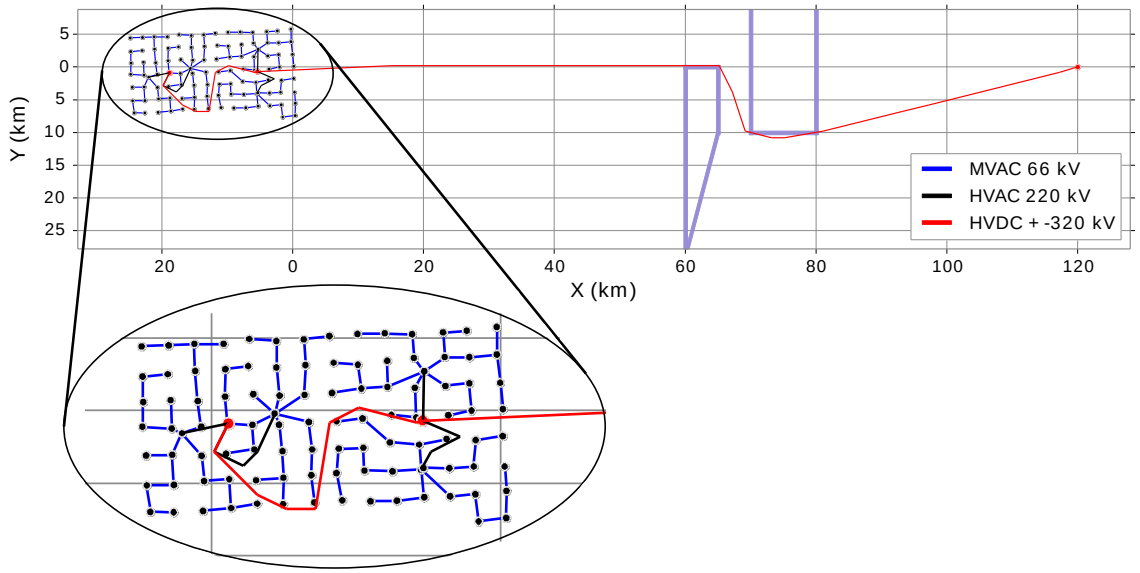

Figure 5-15: The optimal layout ($(N_T, N_C) = (2,4)$) with the architecture (b)

Table 5-4: Simulation results with MVAC collection, HVAC export and HVDC transmission networks

(N_T, N_C)	$(1,2)$	$(1,3)$	(1,4)	$(2,4)$
$LCOE$ (€/MWh)	97.3	97.6	97.1	99.4
total $NLCC$ (M€)	1727	1741	1717	1825
$CAPEX$ (M€)	1246	1252	1238	1317
Dissipated $NLCC$ (M€)	213	215	209	207
curtailed energy $NLCC$ (M€)	268	274	271	301
Total computation duration (s)	238	278	278	298
Optimization duration (s)	209	241	246	263
First order reliability analysis duration (s)	26	34	28	31

It is useful to visualize the responsibility of each item of the electrical network system to its cost-effectiveness. Thus, the Figure 5-16 depicts the NLCC breakdowns for each set of values of the metavariables.

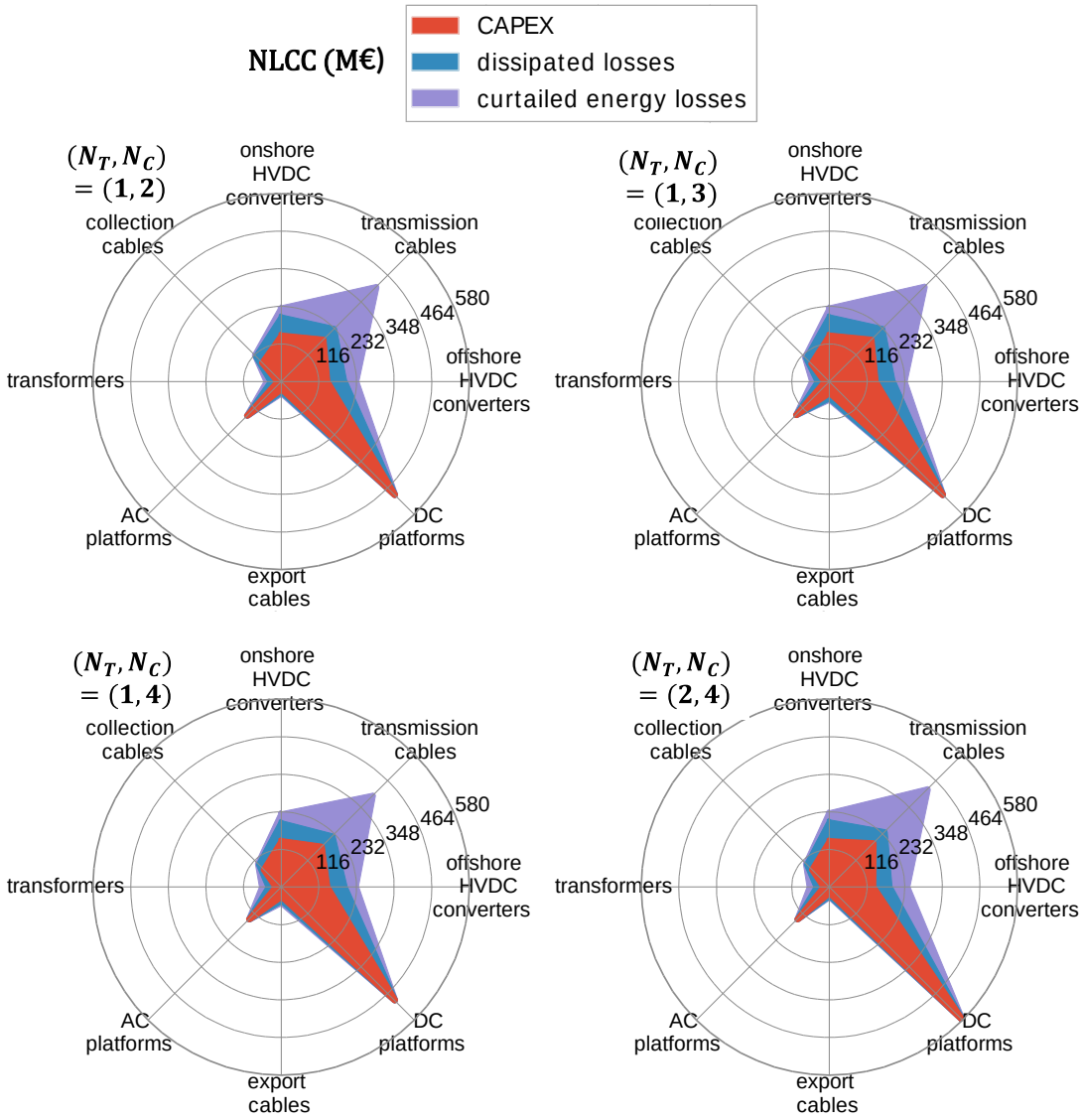

Figure 5-16: NLCC breakdowns for the designs of the MVAC/HVAC/HVDC MMC based concept

The items with the higher impact to the NLCC are the HVDC offshore platforms and the HVDC transmission cables. The NLCC of the transmission cables is due to their unavailability and to their CAPEX with about equal quantitative impacts. The NLCC related to the curtailed energy due to the HVDC transmission cables highly depends on associated reliability data. The latter are subject to high uncertainties but in the present work, the considered failure rate is relatively low compared to the one in other studies [42], [139], [152]. The failure rate for transmission cables in the present study are the one used by the British Office of Gas and Electricity Market (OFGEM) to set availability target for offshore networks interconnections [146]. Besides, because CAPEX and curtailed energy life span cost relative to the HVDC transmission cables have similar values, it seems that improving the reliability of the transmission cables system (by means of

redundancies for example) would probably not be economically justified. Indeed, the increase of the CAPEX would be in the same order of magnitude as the decrease of the NLCC due to the energy curtailed coming from HVDC cables unavailability. From a reliability point of view, the proposed design of the electrical network is thus reasonable.

Unlike the other items of the system, the NLCC of the HVDC offshore platform(s), strictly resulting from the CAPEX, is subject to a high variation depending on the metavariables (especially N_T). It is the reason why the design with two offshore HVDC stations is the one with the highest NLCC. The design obtained with the proposed optimization framework is very similar to classical designs, which are applied with this architecture concept [38], [170].

Figure 5-17 depicts the choice of the cross sections for the cables. The lengths for the DC cables correspond to pairs of conductors and associated insulation. For AC cables, the length is given per length of three core cable.

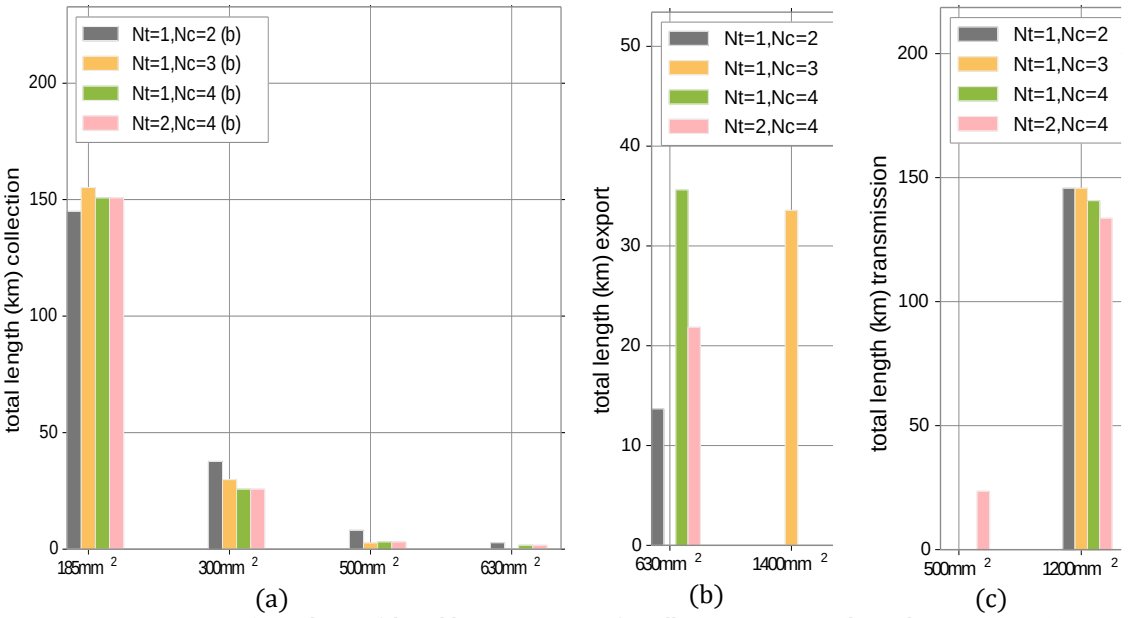

Figure 5-17: Choice of the cables cross sections for collection (a), export (b) and transmission (c) networks.

5.6.4 Architecture concept with MVDC collection and HVDC transmission networks

For the architecture concept (d), where MVDC collection network(s) (±50 kV) and a HVDC transmission network (±320 kV) are employed, there is (are) additional MVDC/HVDC converter station(s) at the interface between collection and transmission networks.

For this concept, there is no dedicated export network and thus, as depicted on the Figure 5-3, $N_T \equiv N_C$. Thus, there is one offshore transmission station per cluster (refer to Figure 5-5) and a cluster substation is also a transmission substation. Therefore, in the remaining section, only the meta-variable N_T, corresponding to the number of clusters and to the number of offshore transmission station is used.

The architecture with MVDC collection network(s) and a HVDC transmission network requires a MVDC/HVDC converter, whose technological solution is unknown. Moreover, the wind turbines technologies with DC output are not readily available. Thus, some assumptions have to be made:

- The CAPEX of a MVDC/HVDC converter station is the same as a MMC station of the same power rating (thus the cost model of MMC station from Chapter 3 is used).
- The CAPEX of the HVDC platform is the same as the one of an offshore MMC station of the same power rating (thus the cost model of MMC station platform Chapter 3 is used).
- The reliability of a MVDC/HVDC converter is the same as the one of a MMC converter. Thus, the same MTTR and MTTF are used (refer to section 4.7 of the Chapter 4).
- The power losses of MVDC/HVDC converter are given by the per unit model of losses of a Single Active Bridge converter (see section 2.3.3.2 of Chapter 2).
- The CAPEX and efficiency of wind turbines with DC outputs are the same as the ones of a wind turbine with AC output.
- The protection strategy of the MVDC collection network is fully selective after recovery. The reliability is done accordingly: the unavailability of a collection cable does not affect the availability of other collection cables.
- The MVDC switchgears of the offshore MVDC/HVDC station(s) have a cost which is given by the model proposed in Chapter 3, where the scaling factor equals 5 p.u.

An instance of the virtual case study with a 100 wind turbines rectangular layout with 14 columns and with an arbitrary rotation θ =65° with the transmission direction is considered. Figure 5-18, Figure 5-19 and Figure 5-20 give the obtained layouts for $N_T \in \{1, 2, 3\}$.

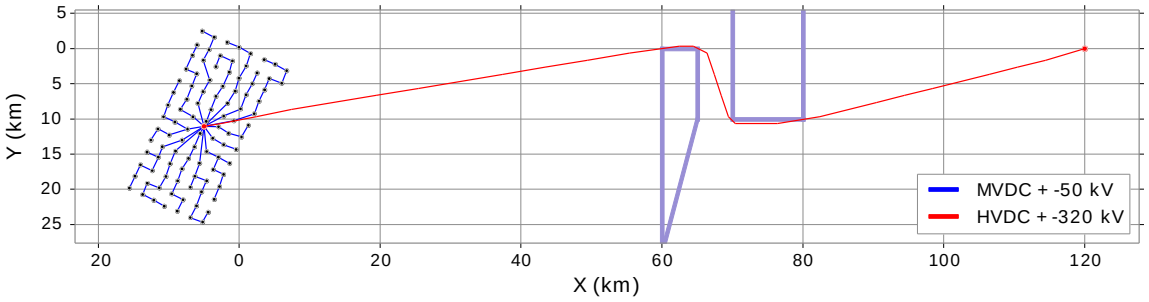

Figure 5-18: The optimal layout for $N_T = 1$ with the architecture (d)

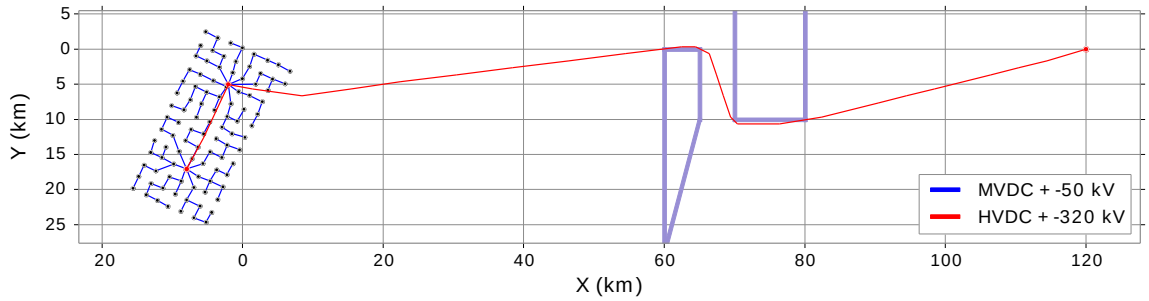

Figure 5-19: The optimal layout for $N_T = 2$ with the architecture (d)

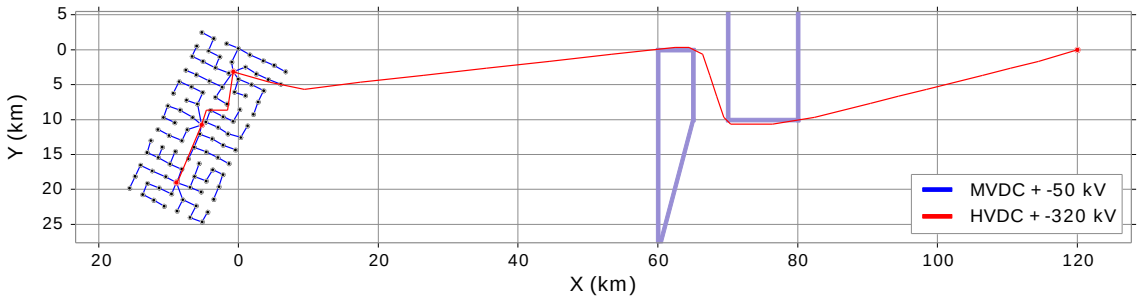

Figure 5-20: The optimal layout for $N_T = 3$ with the architecture (d)

Table 5-5 exposes macroscopic criteria for the three values of the metavariable N_T, namely the LCOE, the NLCC and associated detailed quantities. Table 5-5 also gives the duration of the simulation in each case.

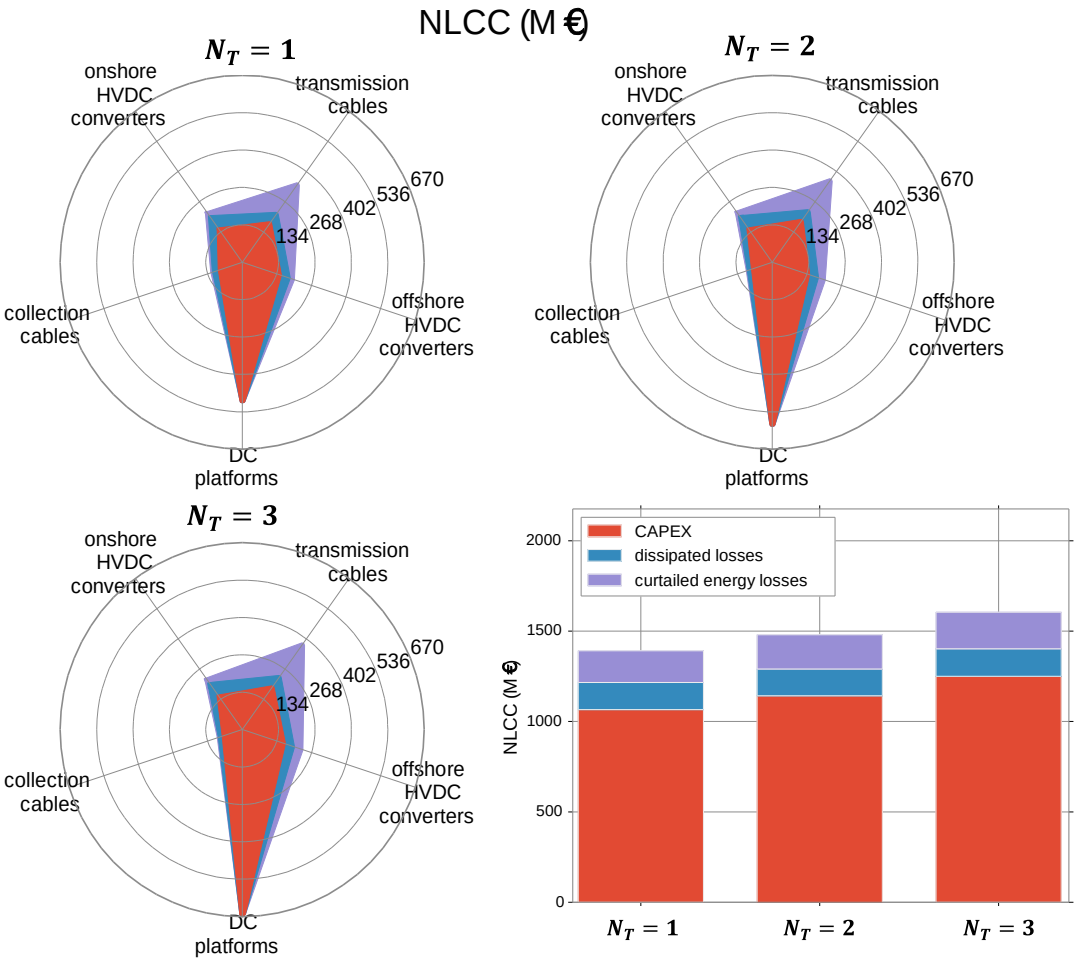

Figure 5-21: NLCC breakdowns for the designs of the MVDC/HVDC concept (d)

Figure 5-21 depicts the NLCC breakdowns for each set of values of the metavariables. It can be seen that the NLCC relative to the collection cables is lower for $N_T = 2$ and $N_T = 3$ than for $N_T = 1$. The NLCC relative to the offshore MVDC/HVDC converters also follows a similar trend. However, the NLCC relative to the offshore HVDC platforms (exclusively due to their CAPEX) increases. This conclusion is entirely dependent to the assumptions made above.

Table 5-5: Simulation results for the virtual wind farm site with MVDC collection and HVDC transmission networks

	$N_T = 1$	$N_T = 2$	$N_T = 3$
$LCOE$ (€/MWh)	90.2	92.1	94.7
total $NLCC$ (M€)	1391	1479	1604
$CAPEX$ (M€)	1066	1243	1250
Dissipated energy $NLCC$ (M€)	151	148	152
curtailed energy $NLCC$ (M€)	175	189	203
Total computation duration (s)	252	255	263
Optimization duration (s)	225	223	234
First order reliability analysis duration (s)	25	30	27

Figure 5-22 depicts the choice of the cross sections for the cables. The lengths in the Figure 5-22 correspond to pairs of conductors and associated insulation. It can be seen that in the case $N_T = 1$, the cumulated length of the collection cables is higher than for the other two values of the metavariable N_T. As it can be expected, the cumulated length of HVDC transmission cables is higher where there are several offshore stations. It increases the cost relative to HVDC cables but reduces the cumulated length and CAPEX of the collection cables.

As for the case of the architecture concept (b) with a MMC based HVDC transmission network, the major driver is the number of offshore platforms. It must be remembered though, that an actual technological solution for MVDC/HVDC conversion with a station having a lower footprint and weight, the situation could be different. In any case, the present section aims at validating and illustrating the proposed optimization framework.

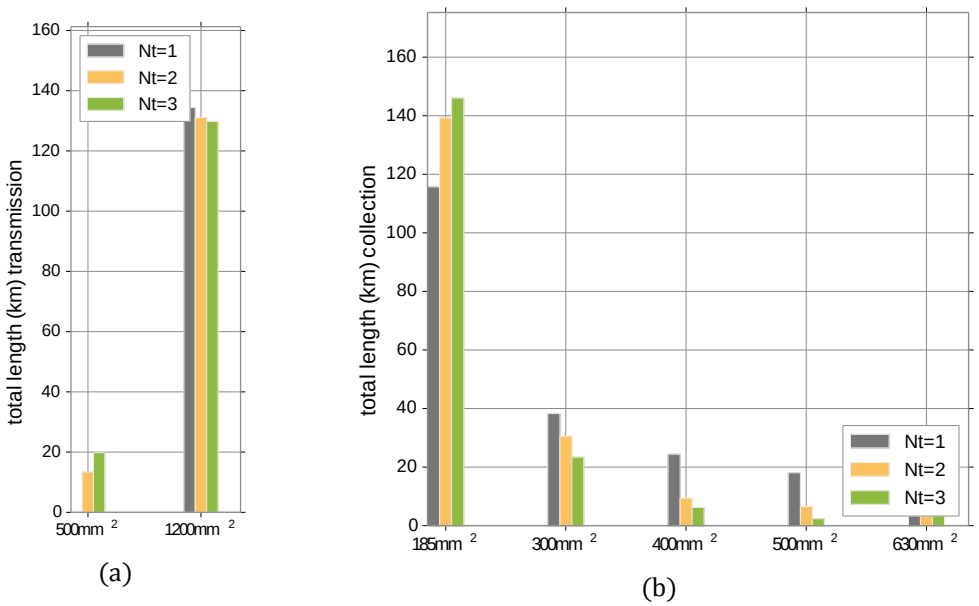

Figure 5-22: choice of the cables cross sections for collection (a) and transmission (b) networks.

5.7 Conclusion

The framework presented in this chapter is proposed in a context of investigation of the cost-effectiveness associated to innovative architecture concepts for the electrical connection of offshore wind farms (refer to Chapter 1). The proposed design formulation within the framework (refer to 5.4 and 5.5) allows obtaining near optimal designs for various architecture concepts.

When an architecture concept is assessed, associated costs are notably subject to uncertainties, particularly when the concept is innovative. Thus, searching for the global optimum for the design problem is questionable.

In section 5.6, an application of the design methodology is proposed for a representative set of architecture concepts (involving MVAC collection or MVDC collection, (HVAC) export and HVDC transmission networks). Based on the designs obtained with the methodology, a holistic assessment relying on the electrical (refer to Chapter 2), CAPEX (refer to Chapter 3) and reliability (refer to Chapter 4) models is possible.

The speed of the problem solving enables the study of several wind farm sites (wind farm peak power, distance to shore, spatial density of wind turbines). This is necessary because the cost-effectiveness of a given architecture should not be concluded on the basis of a single site.

The framework NLCC economic criterion (equivalent to the LCOE and introduced in Chapter 1) can ease the technical and economic analysis. Indeed, the NLCC sums the contributions of components of the electrical system and separates investment costs and costs of losses. Thus a breakdown of the NLCC can be visualized. It makes it possible to highlight the components of the system, which mainly impact the cost-effectiveness of an architecture concept and associated design.

In the context of mature network architecture concept(s) in planning phase of an actual project, the need for global optimization of the architecture design can be raised. A perspective to enhance the design methodology proposed in section 5.4 accordingly could be considered. To do so, the problems (P1) and (P3) should be slightly modified so that the location(s) of offshore substation(s) are parameters of these sub-problems. Then, the meta-optimizer should encompass a metaheuristic, which would be responsible for the optimization of offshore substation(s) location(s). It is achievable thanks to the quick solving of sub-problems with the methods exposed in this paper. Once an optimum is obtained for the complete connection system, the global optimums of the sub-problems can be calculated by solving the MIP formulations individually. The latter can be done by using a global optimization solver such as CPLEX.

In Chapter 6, an enhancement of the proposed decision support framework to take uncertainties into account is detailed.

Chapter 6: HANDLING UNCERTAINTIES FOR THE DECISION MAKING REGARDING NETWORK DESIGN COST

6.1 Introduction

In previous chapters, a framework for the design and assessment of electrical network architectures has been presented. However, it was emphasized in previous chapters that once an architecture design is obtained and sized (Chapter 5), uncertainties from such an assessment requiring both CAPEX models (Chapter 3) and reliability evaluation (Chapter 4).

In the present chapter, methods are proposed to handle the uncertainties associated to the design of offshore wind farm networks in the planning stage or in a context of research for innovative architecture concepts.

For the assessment of architectures, there are two main sources of uncertainties: the reliability of the network and the model parameters.

The decision making can be affected by the uncertainties in regard to the availability of the electrical network, measured by the associated annual curtailed energy. Additionally, the uncertainties in regard to the model parameters also impact the assessment of a network architecture and thus, the decision making.

To handle the uncertainties in regard to model parameters, several approaches can be considered:

- Parametric sensitivity analysis. This approach has the advantage that it can easily be applied to any models and criteria shown as black boxes. With such a method, the variations of the parameters are imposed and the output criteria are calculated. When several parameters are subject to variations, the application of the approach can suffer of a high complexity. Especially because it is then difficult to quantify the impact of simultaneous variations of several parameters. Moreover, the likelihood of occurrence of a given value for a parameter and then of the criteria are unknown.
- A probabilistic analysis where the uncertainties in regard to given parameters is handled by modeling the parameters as random variables. Then, the propagation of uncertainties associated to the parameter can be analyzed by determining the resulting random variables, which represent the decision criteria. The outcome of such an approach is both the domain of variation of the decision criterion and the likelihood associated to its possible values.

A methodology applying a probabilistic analysis can:

1) be based on a pseudo Monte Carlo approach, where a probabilistic sampling of parameters seen as random variables is generated to then calculate the empirical probability distribution of the decision criterion.

2) Be based on probabilistic analytical developments. It cannot be applied to a black box as it depends on the analytical relations between the parameters and decision criterion. The second kind of method has the advantage that the computation speed is higher.

A methodology corresponding to a probabilistic approach based on analytical developments is proposed in the present chapter. It allows the modeling and then the analysis of propagation of models uncertainty up to the decision criteria (LCOE and NLCC).

In this chapter, applications of the methods are proposed on the basis of the designs associated to the architecture concept (b) (MVAC collection, HVAC export and MMC based HVDC transmission networks) with the wind farm site and the four designs ($X_1, X_2, X_3\ X_4$) proposed in section 5.6.3 of Chapter 5. In the present section, the designs are identified by the values of the meta-variables (number of transmission stations N_T, number of cluster stations N_C) as presented in Table 6-1.

Table 6-1: Designs used for the application of the uncertainties analysis

X_i	N_T	N_C
X_1	1	2
X_2	1	3
X_3	1	4
X_4	2	4

As in section 5.6.3 of chapter 5, economical parameters are:

- Actual Weibull parameters $k = 2.2$ and $\lambda = 10.57$ m/s [82],
- Wake losses of 10% as considered in [10],
- The annual maintenance cost are calculated as in section 5.6.3 so that $Oc_t = 50M€$

In section 6.2, a brief review of methodological approaches (proposed in the literature) to take into account such uncertainties is exposed. Then, in section 6.3, the uncertainties due to the stochasticity associated to the electrical network reliability is assessed by using the Monte Carlo based method presented in Chapter 4. Then, an approach to handle the uncertainties of the model parameters is proposed in section 6.4.

6.2 Uncertainties handling for planning and design

In the literature, several sources of uncertainties for design and planning of offshore wind farm are considered.

The economic uncertainties are the one considered by an investor for wind farms. It can be measured by the LCOE or NLCC. These uncertainties can be the result of the difference between the expected energy production and the actual energy, which is produced (difference due to the network unavailability for instance). These uncertainties can also result from the cost of the hardware system.

The wind resources are subject to uncertainties [171–173] but this is more impacting for onshore farms, where the wind is not as regular as in offshore.

There are uncertainties which are inherent to the reliability associated to the life span of the system [80], [142]). Such an uncertainty is due to the fact that the failure of a component is not well known. Thus, the electrical network system reliability inherits the stochasticity of its components reliability (refer to Chapter 4 for more references taking into account these uncertainties by means of Monte Carlo simulations)

In relation with the reliability, there are also uncertainties due to the reliability, notably the MTTR and MTTF (named reliability data in the remaining of this Chapter) associated to the various components of the electrical network. Few authors considered the uncertainties in regard to these parameters. To take it into account, González et al. [71] propose to associate a normal probability distribution to the MTTF of each

component and assess the propagation of uncertainties by using a pseudo Monte Carlo approach. A pseudo Monte Carlo method consists in sampling the values of the parameters subject to uncertainties, which are then modelled as probabilistic variables in order to evaluate their propagation to the decision criteria.

Few authors consider uncertainties in regard to the CAPEX of components of the system. Most of the time, deterministic analytical models are used [65], [66], [71], [72], [74], [80], [124], [138]. As stated in Chapter 3, market conditions can highly impact the cost of the components, even for mature technologies. Cost uncertainties are even more critical for innovative technologies for which the maturity can be lower. Thus the costs for such technologies are subject to future decreases in relation with their learning curve. Thus, for the assessment of offshore DC collection networks, De Prada et al. [19] take into account the cost uncertainties for some components such as DC/DC converters or DC breakers. De Prada et al. [19] take these uncertainties by means of factors that are applied to the reference costs (obtained from analytical models).

In the present work, in section 6.3, the uncertainties related to the stochasticity of components reliability, are taken into account by using classically Monte Carlo simulations with fixed reliability data (MTTR and MTTF) and constant parameters of CAPEX models.

In section 6.4, the propagation of uncertainties of model parameters is analyzed. With a proposed analysis method the sources of uncertainties correspond to the parameters of CAPEX models (refer to Chapter 3) and reliability data (MTTR and MTTF, refer to Chapter 4). Analytical developments using a methodology for uncertainty propagation are applied to the LCOE, which is written as a ratio of normal probabilistic variables. This is a work extension of Heydt results [174], who did not apply it to the LCOE but to another ratio. Then, the relation between the LCOE and NLCC is used to analyze the propagation of uncertainties due to model parameters (CAPEX models and reliability data) to the NLCC. The method relies on analytical results and thus makes possible the assessment of the uncertainties without costly computations that a pseudo Monte Carlo approach would imply.

6.3 Uncertainties associated to electrical network availability

In Chapter 4, two methods have been provided to calculate the annual curtailed energy $L_S^{cur}(X)$ due to the electrical network unavailability. The first one allows the estimation of the expected value of $L_S^{cur}(X)$ and is used in section 5.6 has been used to compute expected values of the economic criteria (LCOE and NLCC).

The second method, based on Monte Carlo Simulations is proposed in Chapter 4. It allows reproducing the stochastic process associated to the components availability of the electrical network. In the present section, results using this Monte Carlo Simulations based method are proposed. The method is the one, which has been introduced in Chapter 4.

The discount rate r is the same as in section 5.6, where r=8% and the number of years is N=25. The CAPEX models with associated parameters and the reliability data correspond to the "mean scenarios" (refer to Chapter 3 and Chapter 4).

For each of the four different designs, 10^4 Monte Carlo simulations of 25 years are performed to compute the annual curtailed energy. With the "memorization" technique introduced in Chapter 4, 10^4 simulations for a given design last about 1400 s in total.

Figure 6-2 depicts the obtained empirical probability distributions of $L_S^{cur}(X)$ for the four designs. It can be seen that a relatively large uncertainty appears.

Table 6-2 gives the standard deviation of the annual curtailed energy. It also gives the expected value of annual curtailed energy and associated confidence interval at 95% (application of the central limit theorem, refer to Chapter 4). The confidence intervals associated to the expected values of the annual curtailed energy have reduced amplitudes. Thus, it can be considered that 10 000 simulations is a sufficient number for the considered architectures having more than 200 nodes and 200 edges.

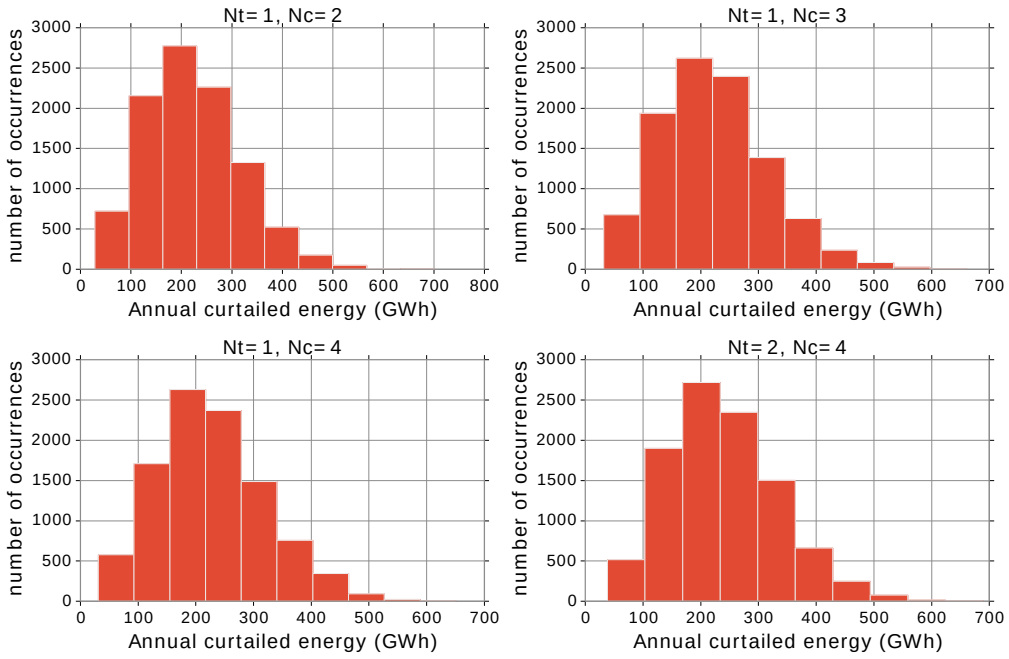

Figure 6-1: Empirical probability distibutions of $L_S^{cur}(X)$ obtained with 10 000 Monte Carlo simulations.

Table 6-2: Expected value and associated confidence interval of $L_S^{cur}(X)$ for the four designs

Design (N_T, N_C)	Standard deviation of $L_S^{cur}(X)$ (GWh)	Average value $E(L_S^{cur}(X))$ (GWh)	95% confidence interval of $E(L_S^{cur}(X))$ (GWh)
(1, 2)	93.5	221	[219.2, 222. 9]
(1, 3)	92.8	223	[221.6, 225.3]
(1, 4)	93.4	229.9	[228.0, 231.7]
(2, 4)	93.3	240.5	[238.7, 242.4]

Figure 6-2 shows that the capacity factor *CF(X)* is subject to relatively high uncertainties due to the stochasticity of the annual curtailed energy $L_S^{cur}(X)$ (refer to equation (1-4) taken from Chapter 1).

$$CF(X) = \frac{AEP_0 - L_S^{cur}(X)}{P_{peak} \cdot T_{year}} \qquad (6\text{-}1)$$

where:

T_{year} is the duration of one year, 8760 hours,

AEP_0 is the wind farm annual energy produced,

P_{peak} is the peak power of the wind farm.

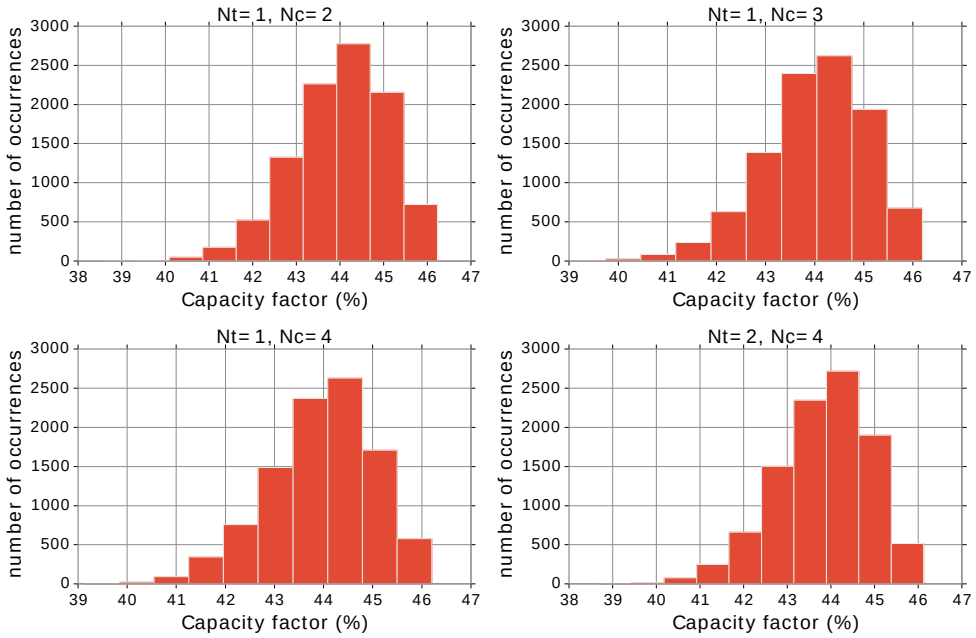

Figure 6-2: Empirical probability distibutions of the capacity factor CF(X) obtained with 10 000 Monte Carlo simulations.

On the basis of the reliability, it is difficult to discriminate the four designs because they give similar capacity factors. This is because, as it would be seen later (section 6.4.5.2), the annual curtailed energy is mainly due to the transmission cables, which have about the same length in the four designs.

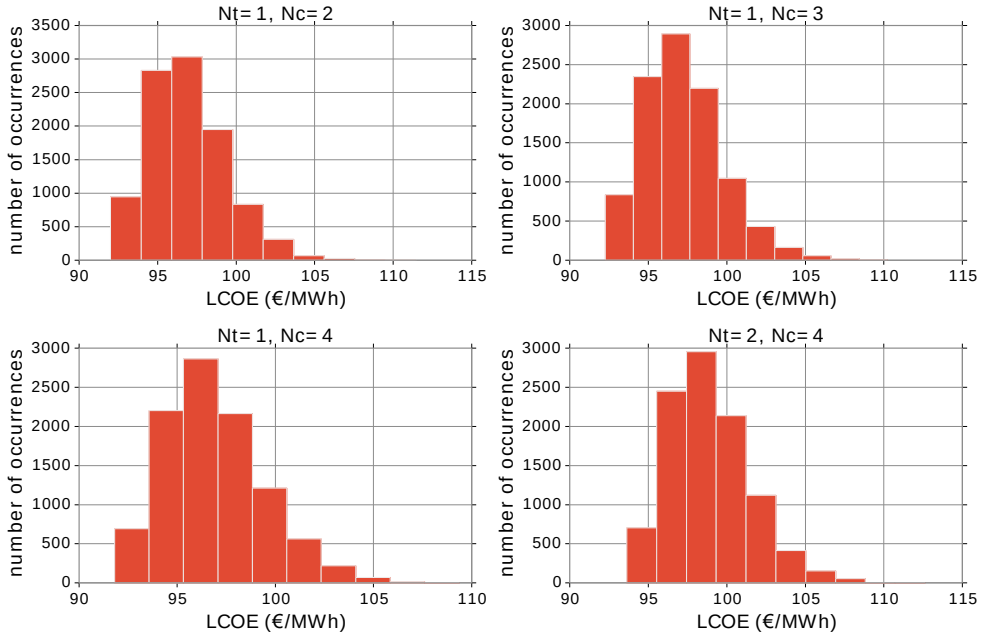

Figure 6-3: Empirical probability distibutions the LCOE obtained with 10 000 Monte Carlo simulations.

Figure 6-3 shows values of the LCOE resulting from the uncertainties associated to the annual curtailed energy (refer to equation (5-1)). It can be seen that similarly as in section 5.6.3 where the same designs are assessed, the costs and the dissipated energy are close in the four designs, excepted for the one with two offshore HVDC stations, which is clearly more expensive.

In the present section, the accuracy and details for the reliability analysis are high. However, it is not possible to analyze easily the most impacting components in the system reliability. Moreover, the distributions are given for fixed values of the CAPEX model parameters.

In section 6.4, the uncertainties related to the parameters of CAPEX models and to reliability data are considered. It is therefore complementary to the information, which has been provided in the present section, which assumes that the model parameters are perfectly known and thus constant.

6.4 Propagation of model uncertainties

6.4.1 Applied scientific method

In Chapter 3, relative to CAPEX models and their parameters, and in Chapter 4, relative to reliability assessment, some models have been proposed along with associated parameters, which are subject to uncertainties. It is assumed that the electrical models proposed in the Chapter 2 are reliable. It is justified by the facts that:

- The impact of the dissipated losses on the NLCC and LCOE criteria are moderated (refer to section 5.6).
- The confidence of accuracy associated to the electrical models is correct (below 5% relative error for the annual energy losses). This is because the physics of the phenomena, which cause the dissipated losses are well known.

In the sections 6.4.2 and 6.4.3, some methods to take into account uncertainties of the models and then associated parameters for the CAPEX and the annual curtailed energy are presented. In these sections, the concept of “components class” is used. A component class is designated by its index $l \in CL$. A component class includes all components of a given type:

- Transformers
- MMC converters
- MVAC cables
- MVDC cables
- HVAC cables
- HVDC cables
- Offshore platform(s) DC
- Offshore platform(s) AC
- Compensation unit(s)

Then, in section 6.4.4, the propagation of the uncertainties, due to the models and parameters, to the economic criteria (LCOE and NLCC), is analyzed. The proposed methodology consists in assessing the uncertainties associated to models and parameters for reliability and CAPEX for fixed designs of the architecture. Thus, in the analytical developments of sections 6.4.2, 6.4.3 and 6.4.4, the proposed probabilistic distributions depend on a fixed design vector variable *X*.

The proposed method is synthetized in Figure 6-4. It consists first in a probability assumptions regarding the level of confidence of the model parameter scenarios. The probability p_{out}^{cost}, that the actual costs are outside the region formed with the cost values obtained in a deterministic manner by using the model parameter scenarios ("mean", "pessimistic" and "optimistic"), is imposed a priori. The probability p_{out}^{cur}, that the actual curtailed energy values are not included in the values formed with the parameter scenarios, is imposed analogously. In this way, normal probability laws for the costs and annual curtailed energies associated to the components classes are determined:

- $\aleph(m_l^{cost}, \sigma_l^{cost^2})$ is the normal law of the cost of class *l*, where m_l^{cost} is the mean value of this cost and $\sigma_l^{cost^2}$ is its variance;
- $\aleph(m_l^{cur}, \sigma_l^{cur^2})$ is the normal law of the annual curtailed energy due to unavailabilities of components of class *l*, where m_l^{cur} is the mean value and $\sigma_l^{cur^2}$ is the variance.

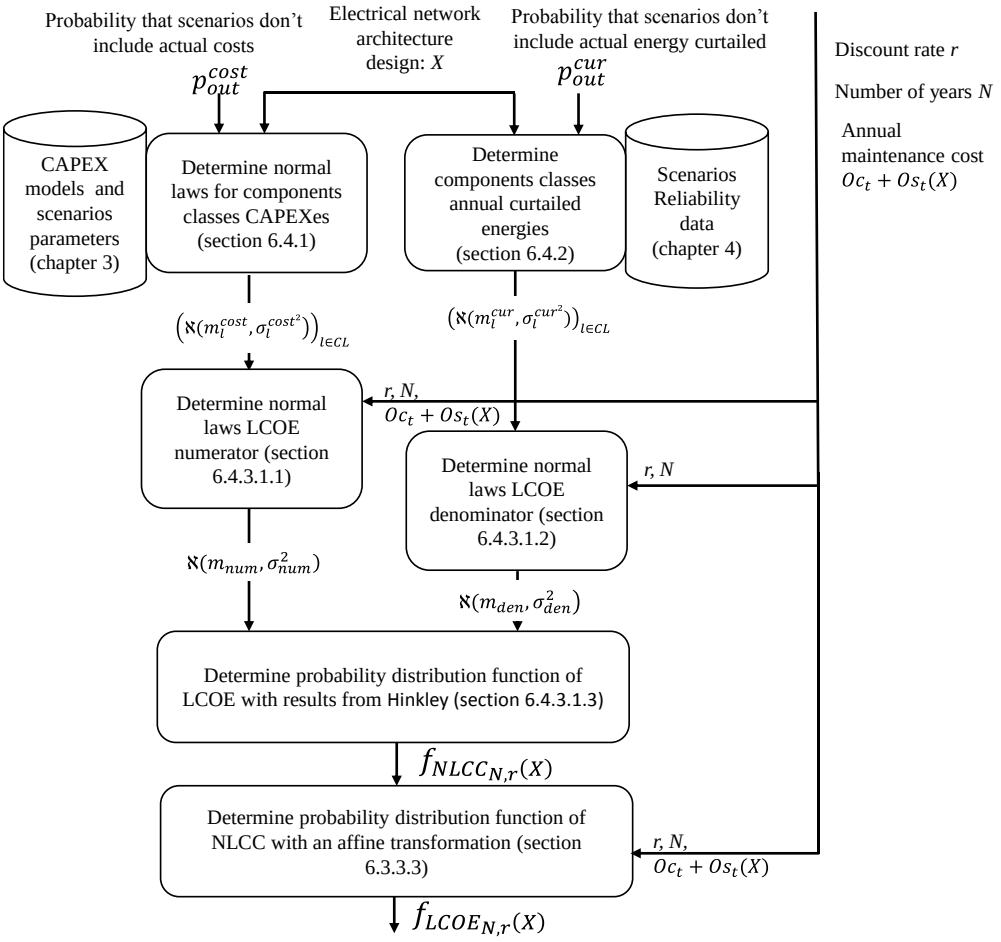

Figure 6-4: Methodological approach for the analysis of model uncertainties and propagation

Then, the LCOE is written as a ratio of normal variables by using $\aleph(m_l^{cost}, \sigma_l^{cost^2})$ and $\aleph(m_l^{cur}, \sigma_l^{cur^2})$ for the classes $l \in CL$. $\aleph(m_{num}, \sigma_{num}^2)$ is the normal law corresponding to the numerator of the LCOE and $\aleph(m_{den}, \sigma_{den}^2)$ the one of its denominator. The parameters of these probabilistic laws depend on the discount rate r; the duration of the project N and the annual maintenance costs: $Oc_t + Os_t(X)$.

Then, by using the probabilistic results from Hinkley [175] (used by Heydt [174]), the probability distribution of the LCOE is determined. The obtained probabilistic nature of the LCOE with this modeling is the result of the probabilistic nature of the costs and annual curtailed energy (taking into account model uncertainties). Therefore, the propagation of model uncertainties to the LCOE is obtained.

Finally, the determination of the NLCC probability density function is done from the knowledge of the LCOE one by using an affine transformation.

6.4.2 CAPEX model uncertainties

6.4.2.1 Goal

To take into account the uncertainties in regard to the CAPEX, normal probabilistic laws are considered. As reminded by Heydt [174], this is commonly done for the CAPEX. Heydt writes that the assumption of using a normal distribution is justified by a weak form of the central limit theorem and that the conditions of this assumption is not clearly met. However, he states that:

> " *- Engineers are familiar with the assumption of normal distribution, and consequences of this assumption may be managed*
>
> *- It is better to examine the cited assumed probabilistic formulation, albeit in an approximate way, rather than ignore the uncertainty.* "

In the present work, for a given design of the electrical network, the CAPEX of a component class corresponds to the sum of the investment costs of components of the same class. The CAPEX of a component class of index l is modelled as a normal variable (law $\aleph(m_l^{cost}, \sigma_l^{cost^2})$). This assumption is justified because the component CAPEX of a same class can be assumed to be perfectly correlated (e.g. transformers of the same system, having the same function, have almost the same cost). The CAPEX of two distinct classes are assumed to be independent.

6.4.2.2 Normal law associated to a component class

The determination of the parameters $m_l^{cost}, \sigma_l^{cost^2}$ for a given component class l depends on the prior assumption, relying on the scenario parameters of the Chapter 3 ("mean", "optimistic" and "pessimistic").

As shown in the Figure 6-5, the parameter m_l^{cost} corresponds to the CAPEX of the component class of index l in the "mean" scenario. The probability that the cost (of the considered component class) is outer the bounds given by the "optimistic" and "pessimistic" scenarios is named p_{out}^{cost} (refer to equation (6-2)). The probability p_{out}^{cost} corresponds to the hatched surface on the Figure 6-5. The higher is p_{out}^{cost}, the higher are the uncertainties.

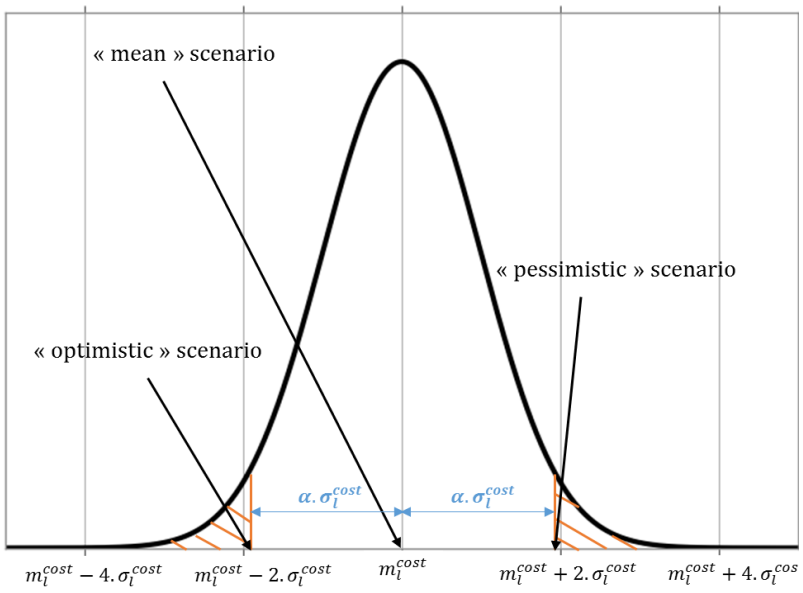

Figure 6-5: pdf of a Gaussian distribution of the studied random variable

$$\mathrm{P}(\mathrm{cost}_l \leq \mathrm{cost}_{optimistic} \text{ or } \mathrm{cost}_l \geq \mathrm{cost}_{pessimistic}) = p_{out}^{cost} \quad (6\text{-}2)$$

where:

$cost_l$ is the cost of the component class of index l modelled as a normal random variable;

$cost_{pessimistic}$ is the cost of the component class of index l in the "pessimistic" scenario of the Chapter 3;

$cost_{optimistic}$ is the cost of the component class of index l in the "optimistic" scenario of the Chapter 3.

The optimistic and pessimistic costs are considered symmetrical around the normal parameter m_l^{cost}. This can be imposed by fixing it as the mean of the cost values, obtained with the three scenarios. In practice, with the model parameters of Chapter 3, this is not required.

Equation (6-2) is equivalent to equation (6-3).

$$P\left(cost_{optimistic} \leq cost_l \leq cost_{pessimistic}\right) = 1 - p_{out}^{cost} \quad (6\text{-}3)$$

By considering a symmetrical variation of the cost (Figure 6-5), a parameter α is analytically defined so that equations (6-4) and (6-5) are respected.

$$cost_{optimistic} = m_l^{cost} - \alpha.\sigma_l^{cost} \quad (6\text{-}4)$$

$$cost_{pessimistic} = m_l^{cost} + \alpha.\sigma_l^{cost} \quad (6\text{-}5)$$

Then, the equation (6-3) is equivalent to the equation (6-6) with a symmetric variation assumption.

$$P(m_l^{cost} - \alpha.\sigma_l^{cost} \leq cost_l \leq m_l^{cost} + \alpha.\sigma_l^{cost}) = 1 - p_{out}^{cost} \quad (6\text{-}6)$$

Equation (6-6) is equivalent to (6-7).

$$P\left(-\alpha \leq \frac{cost_l - m_l^{cost}}{\sigma_l^{cost}} \leq +\alpha\right) = 1 - p_{out}^{cost} \tag{6-7}$$

Due to the a priori assumption that $cost_i \rightarrow \aleph(m_l^{cost}, \sigma_l^{cost^2})$, the random variable $y = \frac{cost_l - m_l^{cost}}{\sigma_l^{cost}}$ follows a normalized normal law $\aleph(0,1)$.

An investment decision is classically based on an acceptable risk. Here, this risk corresponds to a desirable probability p_{out}^{cost} and the goal is to determine the effect on the cost through α. Thus, classically, the value of α is depending on the wanted probability p_{out}^{cost} and can be calculated by equation (6-8).

$$\alpha = \phi^{-1}(1 - \frac{p_{out}^{cost}}{2}) \tag{6-8}$$

where ϕ^{-1} is the inverse function of the cdf (cumulated distribution function) of $\aleph(0,1)$. In practice, probability tables can be used (same tables used as for the determination of confidence intervals). Alternatively, some software tools or libraries such as Matlab or the Scipy Python library [95] can be used to calculate it by using the *erf* function so that ϕ^{-1} and ϕ are calculated by using equations (6-9) and (6-10). This is what is done in the present work.

$$\phi^{-1}(y) = \sqrt{2}.erf^{-1}(2y - 1) \tag{6-9}$$

$$\phi(x) = \frac{1}{2}.erf(\frac{x}{\sqrt{2}} + 1) \tag{6-10}$$

$$erf(\lambda) = \frac{2}{\pi}\int_0^{\lambda} \exp(-t^2)\, dt \tag{6-11}$$

In the example of the Figure 6-5, p_{out}^{cost} is imposed to 0.05 and thus, *α=1.96.*

Once α is calculated as the consequence of the choice of p_{out}^{cost}, the standard deviation σ_l^{cost} is calculated by using the inverse equations of (6-4) and (6-5):

$$\sigma_l^{cost} = \frac{1}{\alpha}\left(\text{cost}_{pessimistic} - m_l^{cost}\right) = \frac{1}{\alpha}\left(m_l^{cost} - \text{cost}_{optimistic}\right) \tag{6-12}$$

6.4.2.3 Normal law associated to an electrical architecture

The CAPEX of all component classes are assumed as independent normal variables. Then, the total CAPEX of the electrical system $C_{S(X)}$ is the sum of the CAPEX of all component classes of the system. Thus, it is a normal probabilistic variable following the law $\aleph(m_{tot}^{cost}, \sigma_{tot}^{cost^2})$, where the parameters are given by equations (6-13) and (6-14), where CL is the set of component class indexes.

$$m_{tot}^{cost} = \sum_{l \in CL} m_l^{cost} \tag{6-13}$$

$$\sigma_{tot}^{cost^2} = \sum_{l \in CL} \sigma_l^{cost^2} \tag{6-14}$$

6.4.3 Uncertainties relative to reliability parameters

As stated in section 6.2, the uncertainties relative to the annual curtailed energy can be classified as:

1. Intrinsic uncertainty, which is due to the stochastic process during the operation life of the electrical network: random sequential failures and repairs of components. In Chapter 4, such a process has been simulated by using a Monte Carlo simulation for fixed reliability parameters (MTTR and MTTF).
2. Additional uncertainty, which is due to the fuzzy/lack of knowledge of the reliability of individual components. In other words, there are high uncertainties relative to the MTTF and MTTR of the various components.

To take into account the additional uncertainties, Monte Carlo Simulations are not the most adapted method. Indeed, it is computationally costly for one set of reliability parameters. Thus, performing a sampling of parameter values is even more costly.

The first order estimator presented in Chapter 3 computes the expected annual curtailed energy straightforwardly by using the unavailability U_i of each component *i*. The estimator is reminded in equation (6-15).

$$\widehat{L_S^{cur}(X)} = T_{year}.\sum_{i\in C} U_i.\ E[P_{curtailed}(\{1-\delta_{ij}\}_{j\in C})] \qquad (6\text{-}15)$$

where:

C is the set of component indexes;

$E[P_{curtailed}(\{1-\delta_{ij}\}_{j\in C})]$ is the asymptotic expected power curtailed when the component i is not available. $\delta_{ij} = 1$ if *i=j*, else, it is 0.

In equation (6-15), the parameter uncertainties are concentrated in the U_i values. $E[P_{curtailed}(\{1-\delta ij\}_{j\in C})]$ does not depend on the MTTR nor on MTTF. Thus, the method presented below does not require to recalculate $E[P_{curtailed}(\{1-\delta ij\}_{j\in C})]$ for $i \in C$ to perform a sensitivity analysis in regard to reliability data.

Special care should be put on the choice of the elementary normal variables. Indeed, if $L_S^{cur}(X)$ is written as the sum of independent normal variables, it is then possible to calculate directly the parameters of the associated normal law $\aleph(m_{tot}^{cur}, \sigma_{tot}^{cur^2})$. It is not the case of the formula in equation (6-15) where the reliability data are a priori correlated for components of a same class (all transformers of the system are supposed to have the same reliability). Consequently, the annual energy curtailed associated to each component class (*l*,) must be distinguished:

$$L_l^{cur}(X) = T_{year}.\sum_{i\in c_l} U_i.\ E[P_{curtailed}(\{1-\delta ij\}_{j\in C})]\text{ , for } l\in C \qquad (6\text{-}16)$$

where:

c_l is the set of indexes of components of the class *l*.

CL is the set of components class indexes (NB: $\bigcup_{l\in CL} c_l = C$).

If the reliability parameters of components of a same class are assumed to be the same, then the first order estimator (6-15) will be written as in equation (6-17).

$$\widehat{L_S^{cur}(X)} = \sum_{l\in CL} T_{year}.\sum_{i\in c_l} U_i.\ E[P_{curtailed}(\{1-\delta ij\}_{j\in C})] \qquad (6\text{-}17)$$

It is then assumed that the reliability parameters of components in a same class are the same. Then, for $l \in CL$, the annual curtailed energy associated to the components class of index l, $L_l^{cur}(X) = T_{year}.\sum_{i\in c_l} U_i.\ E[P_{curtailed}(\{1-\delta ij\}_{j\in C})]$ is a normal variable. It is then assumed that the $L_l^{cur}(X)$ $(l \in CL)$ are independent normal variables $\aleph(m_l^{cur}, \sigma_l^{cur^2})$. Consequently, the parameters $m_l^{cur}, \sigma_l^{cur^2}$ are determined similarly as it is done for the CAPEX of component classes, with σ_l^{cur} depending on an a priori probability p_{out}^{cur}.

Finally, the parameters of $\aleph\left(m_{tot}^{cur}, \sigma_{tot}^{cur^2}\right)$ can be calculated by using equations (6-18) and (6-19).

$$m_{tot}^{cur} = \sum_{l\in CL} m_l^{cur} \qquad (6\text{-}18)$$

$$\sigma_{tot}^{cur^2} = \sum_{l\in CL} \sigma_l^{cur^2} \qquad (6\text{-}19)$$

The methodology for the determination of $\aleph(m_l^{cur}, \sigma_l^{cur^2})$ and $\aleph\left(m_{tot}^{cur}, \sigma_{tot}^{cur^2}\right)$ is applied to the design X_4 (refer to Table 6-1 in section 6.4.5.3).

6.4.4 Propagation of uncertainties up to the economic criteria

The LCOE is a ratio. Its numerator and its denominator can both be modelled as normal distribution by using results of sections 6.4.2 and 6.4.3. Thus, the result of Heydt [174] can be used to determine the probability density function (pdf) of the LCOE.

To achieve it, first, sections 6.4.4.1.1 and 6.4.4.1.2 detail how to obtain the parameters of the normal variables modeling the numerator and denominator of the LCOE (given by equation (1-5) as defined in Chapter 1).

$$LCOE_{N,r}(\mathrm{X}) = \frac{C_S(X) + C_C + \sum_{t=1}^{N} \frac{Oc_t + Os_t(X)}{(1+r)^t}}{\sum_{t=1}^{N} \frac{AED(X)}{(1+r)^t}} \qquad (6\text{-}20)$$

Once these probabilistic distributions of criteria are obtained, they can be used to determine probabilistic quantities such as the expected values and standard deviation of the LCOE.

6.4.4.1 Propagation of models uncertainties to the LCOE

6.4.4.1.1 Numerator of the LCOE as a normal variable

The numerator of the LCOE is a random variable, depending on a normal law and the discount rate (r):

$$num_{N,r}(X) = C_S(X) + C_C + \sum_{t=1}^{N} \frac{Oc_t + Os_t(X)}{(1+r)^t} \tag{6-21}$$

In equation (6-21), the sum $\sum_{t=1}^{N} \frac{Oc_t+Os_t(X)}{(1+r)^t}$, corresponding to the maintenance cost over the years (N), is assumed to be known, without uncertainty. In practice, an amount is locked annually to fund the maintenance. The term C_C corresponding to the total investment cost of the wind turbines can either be considered perfectly known, or it can be assumed to follow a normal law. The term $C_S(X)$, corresponding to the CAPEX of the electrical network, is modelled as a normal variable obeying $\aleph(m_{tot}^{cost}, \sigma_{tot}^{cost^2})$, which has been determined in the section 6.4.2. .

If the CAPEX of the wind turbine is assumed to be perfectly known, the numerator of the LCOE follows also a normal law $\aleph(m_{num}, \sigma_{num}^2)$, whose parameters are given by the equations (6-22) and (6-23).

$$m_{num} = m_{tot}^{cost} + C_C + \sum_{t=1}^{N} \frac{Oc_t + Os_t(X)}{(1+r)^t} \tag{6-22}$$

$$\sigma_{num}^2 = \sigma_{tot}^{cost\,2} \tag{6-23}$$

If the CAPEX of the wind turbines is uncertain, it can be modelled as a random variable following a normal law $\aleph(m_C, \sigma_C^2)$. Then, the CAPEX of the wind turbines and of the electrical network can be assumed to be independent. In this case, the numerator of the LCOE follows a normal law $\aleph(m_{num}, \sigma_{num}^2)$, whose parameters are given by the equations (6-24) and (6-25).

$$m_{num} = m_{tot}^{cost} + m_C + \sum_{t=1}^{N} \frac{Oc_t + Os_t(X)}{(1+r)^t} \tag{6-24}$$

$$\sigma_{num}^2 = \sigma_{tot}^{cost^2} + \sigma_C^2 \tag{6-25}$$

6.4.4.1.2 Denominator of the LCOE as a normal variable

The denominator of the LCOE is given by equation (6-26).

$$den_{N,r}(X) = \sum_{t=1}^{N} \frac{1}{(1+r)^t} \left[AEP_0 - L_S^{cur}(X) - L_S^{dis}(X)\right] \tag{6-26}$$

where:

AEP_0 is the annual energy produced by the wind turbines (electrical outputs)

$L_S^{dis}(X)$ is the annual energy dissipated throughout the electrical network. It is assumed to be perfectly known (ref to section 2.4 of Chapter 2).

$L_S^{cur}(X)$ is the expected annual curtailed energy due to the electrical network unavailability. It is assumed to be a random variable following a normal law $\aleph(m_{tot}^{cur}, \sigma_{tot}^{cur^2})$, whose parameters are determined in the section 6.4.3.

Thus, for fixed financial conditions, the denominator of the LCOE follows a normal law $\aleph(m_{den}, \sigma_{den}^2)$ whose parameters can be calculated by using equations (6-27) and (6-28).

$$m_{den} = \sum_{t=1}^{N} \frac{1}{(1+r)^t} \left[AEP_0 - m_{tot}^{cur} - L_S^{dis}(X) \right] \tag{6-27}$$

$$\sigma_{den}^2 = \left(\sum_{t=1}^{N} \frac{1}{(1+r)^t} \right)^2 . \sigma_{tot}^{cur^2} \tag{6-28}$$

6.4.4.1.3 Calculation of the probability distribution function of the LCOE

In 1969, Hinkley [175] has proposed an analytical exact formula to calculate the probability distribution function of a random variable resulting from the ratio of two normal variables. In 2017, Heydt [174] has applied the result to the probabilistic cost benefit analysis of transmission and distribution asset expansion projects. The ratio considered by Heydt to apply the result from Hinkley is the CAPEX of an expansion project over the savings that can obtained per year. The ratio gives thus the duration after which the expansion project is beneficial.

In the present work, the LCOE is written as a ratio of normal variables and the results from Hinkley [175] can be used.

As stated by Hinkley [175], the knowledge of the parameters of normal laws is not sufficient to obtain the distribution of the ratio. Indeed, the correlation ρ between the numerator and denominator variables is also required in the general case. In the present work, there is no correlations between the numerator and the denominator because they are assumed to be independent.

The equation (6-29) gives the probability density function of the ratio random variable *Y.*

$$\begin{aligned} f_Y(Y) = \frac{b.d}{2\sqrt{2\pi}\sigma_{num}\sigma_{den}a^3} \left[erf\left(\frac{b}{a\sqrt{2(1-\rho^2)}} \right) - erf\left(\frac{-b}{a\sqrt{2(1-\rho^2)}} \right) \right] \\ + \frac{\sqrt{1-\rho^2}}{\sigma_{num}\sigma_{den}a^2} exp\left(-\frac{c}{2(1-\rho^2)} \right) \end{aligned} \tag{6-29}$$

where:

erf is the error function, noted as in Matlab and in the scipy Python library [95] and given by equation (6-11).

a, b, c, d are coefficients given in equations (6-30), (6-31), (6-32) and (6-33).

$$a = \sqrt{\frac{Y^2}{\sigma_{num}} - \frac{2\rho Y}{\sigma_{num}\sigma_{den}} + \frac{1}{\sigma_{den}^2}} \tag{6-30}$$

$$b = \frac{m_{num}Y}{\sigma_{num}^2} - \frac{\rho(m_{num} + m_{den}Y)}{\sigma_{num}\sigma_{den}} + \frac{m_{den}}{\sigma_{den}^2} \tag{6-31}$$

$$c = \frac{m_{num}^2}{\sigma_{num}^2} - \frac{2\rho m_{num}m_{den}}{\sigma_{num}\sigma_{den}} + \frac{m_{den}^2}{\sigma_{den}^2} \tag{6-32}$$

$$d = exp\left(\frac{b^2 - ca^2}{2(1-\rho^2)a^2}\right) \tag{6-33}$$

The data from Heydt [174] have been used to validate the implementation through comparisons.

6.4.4.2 Propagation of the model uncertainties to the NLCC

Then, by using the affine relation between the LCOE and the NLCC, the pdf of the NLCC can also be obtained. Indeed, the NLCC is defined (see Chapter 1) by the equation (6-34).

$$NLCC_{N,r}(X) = \left[\sum_{t=1}^{N} \frac{1}{(1+r)^t}.AEP_0\right].LCOE_{N,r}(X) - \left[C_C + \sum_{t=1}^{N} \frac{Oc_t}{(1+r)^t}\right] \tag{6-34}$$

Thus, for N and r fixed, the terms $A_{N,r} = \sum_{t=1}^{N} \frac{1}{(1+r)^t}.AEP_0$ and $B_{N,r} = -\left[C_C + \sum_{t=1}^{N} \frac{Oc_t}{(1+r)^t}\right]$ can be assumed to be perfectly known. The $LCOE_{N,r}(X)$ has been modelled as a random variable, whose probability distribution function $f_{LCOE_{N,r}(X)}$ is determined by equation (6-29) in the section 6.4.4.1.3.

Below is a classical mathematical probabilistic theorem [176], which is used to determine the probability density function of the $NLCC_{N,r}(X)$ from the knowledge of $f_{LCOE_{N,r}(X)}$.

Hypothesis:

- Let Y following a law with a probability density function f_Y,
- Let Z be a random variable defined by $Z = \varphi(Y)$, where φ is a diffeomorphism from $\mathbb{R}$ to $\mathbb{R}$.

Then:

- Z has a density function g_Z given by equation (6-35), where φ' is the derivative of φ and φ^{-1} is its reciprocal function.

$$\forall z \in R, g_Z(z) = \frac{f_Y\left(\varphi^{-1}(z)\right)}{\left|\varphi'\left(\varphi^{-1}(z)\right)\right|} \tag{6-35}$$

This result is applied to the random variables $LCOE_{N,r}(X)$ and $NLCC_{N,r}(X)$, with the relation given by equation (6-36) where φ, is the affine function given by the equation (6-37).

$$NLCC_{N,r}(X) = \varphi(LCOE_{N,r}(X)) \tag{6-36}$$

$$\forall y \in R, \varphi(y) = A_{N,r}.y + B_{N,r} \tag{6-37}$$

φ is affine from $\mathbb{R}$ to $\mathbb{R}$ and is thus a diffeomorphism. Therefore, it can be shown by mere application of the above exposed proposition (and equation (6-35)) that the probability density function of $NLCC_{N,r}(X)$ is given by the equation (6-38), which is equivalent to equation (6-39).

$$\forall z \in R, f_{NLCC_{N,r}(X)}(z) = \frac{1}{A_{N,r}} f_{LCOE_{N,r}(X)}\left(\frac{z - B_{N,r}}{A_{N,r}}\right) \tag{6-38}$$

$$\forall z \in R, f_{NLCC_{N,r}(X)}(z) = \frac{1}{\sum_{t=1}^{N} \frac{1}{(1+r)^t}.AEP_0} f_{LCOE_{N,r}(X)}\left(\frac{z + C_C + \sum_{t=1}^{N} \frac{Oc_t}{(1+r)^t}}{\sum_{t=1}^{N} \frac{1}{(1+r)^t}.AEP_0}\right) \tag{6-39}$$

6.4.5 Practical studies of the uncertainty propagation

The methodology to analyze the propagation of the uncertainties in regard to the models is applied to the architecture concept (b) (MVAC collection, HVAC export and MMC based HVDC transmission networks) with the wind farm site and the four designs ($X_1, X_2, X_3\ X_4$) proposed in section 5.6.3. These designs are identified by the values of the meta-variables $(N_T, N_C) \in \{(1,2),\ (1,3), (1,4), (2,4)\}$.

This is done in the context of the general framework of Figure 1-20 (Chapter 1). For a given "wind farm site" and with the choice of an architecture concept with "technological solution", a design is obtained with the "design heuristics" and "optimization algorithm" detailed in Chapter 5. The proposed method to take uncertainties into account enhances the "CAPEX evaluator" (with results of section 6.4.2) the "reliability simulator" (with results of section 6.4.3) and the "aggregated objective(s) calculator" (with results of section 6.4.4).

As in the 5.6, the economical parameters used are:

- Actual Weibull parameters $k = 2.2$ and $\lambda = 10.57$ m/s [82];
- Wake losses of 10% as considered in [10];
- The annual maintenance cost are calculated as in section 5.6 so that $Oc_t = 50M€$;
- A modification of the values of r and N is proposed below.

The CAPEX of wind turbines is known. It is justified in the context where the decision support aims at analyzing the cost-effectiveness associated to the network architecture. Including the uncertainties in regard to the CAPEX of the wind turbines implies higher uncertainties for the LCOE and can be valuable for a holistic wind farm project planning.

For the determination of the normal parameters for the CAPEX classes of components (constituting the electrical network), we consider a risk of p_{out}^{cost}=5% onto CAPEX regarding the electrical infrastructure (refer to section 6.4.2.2). Similarly, a risk p_{out}^{cur}=5% (refer to section 6.4.3) is considered regarding reliability uncertainties onto the annual curtailed energy.

The discount rate r and the number of years of operation N have an impact on the LCOE of the project and also on the NLCC. Thus, the probabilistic distributions of the NLCC and LCOE are calculated for various values of r and N. The longer the duration of exploitation, the lower should be the LCOE. The lower the

discount rate, the lower should be the LCOE. Extreme cases are retained where $(r, N) \in \{(6\%, 25 \text{ years}), (8\%, 20 \text{ years})\}$.

With the application of the methodology, in section 6.4.5.1, the calculated pdf (probability distribution function) of the NLCC and LCOE are exposed. Then, in section 6.4.5.2, a more detailed analysis of the uncertainties due to the reliability data is proposed for one of the designs. In section 6.4.5.3, an analysis of the uncertainties related to the CAPEX models uncertainties is done for one of the same designs.

These detailed analysis (sections 6.4.5.2 and 6.4.5.3) make possible the characterization of the uncertainties observed on the economic criteria (NLCC and LCOE) with the sources of uncertainties. Finally, in section 6.4.5.4, a discussion of the impact of N and r onto the NLCC and LCOE is exposed.

6.4.5.1 Uncertainties of NLCC and LCOE due to model uncertainties

In this section, it is shown how the uncertainties due to the models affect the NLCC and the LCOE.

The results are calculated:

- for one case by taking into account the cumulated impact of reliability data and CAPEX models uncertainties.
- for another case by taking into account only the uncertainties relative to the CAPEX model uncertainties.

Table 6-3 sums up the case studies for the application of the method to the architecture designs, which are presented in the introduction of section 6.4.5. When the uncertainties due to reliability data are not taken into account, reliability data are fixed to the values corresponding to the "mean" scenario of Chapter 4.

Table 6-3: Case studies to study model uncertainties propagation to NLCC and LCOE

Economical parameters	Criterion	Source of uncertainties	
		Reliability data and CAPEX	CAPEX models only
r=8%, N=20	LCOE	Figure 6-6 (a)	Figure 6-6 (b)
	NLCC	Figure 6-8 (a)	Figure 6-8 (b)
r=6%, N=25	LCOE	Figure 6-7 (a)	Figure 6-7 (b)
	NLCC	Figure 6-9 (a)	Figure 6-9 (b)

The same x scales are used for Figure 6-6 and Figure 6-7 for an easier comparison of the results depending on r and N. In the same way, the same scales are used for Figure 6-8 and Figure 6-9.

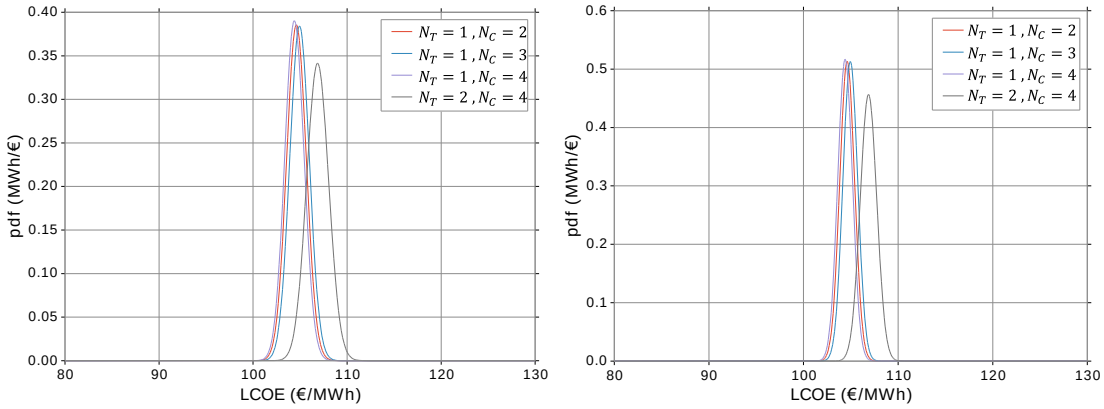

Figure 6-6: Probability density functions of the LCOE with fixed wind turbines CAPEXs (r=8% and N=20 years). (a) with variation of reliability data. (b) "mean" scenario reliability data

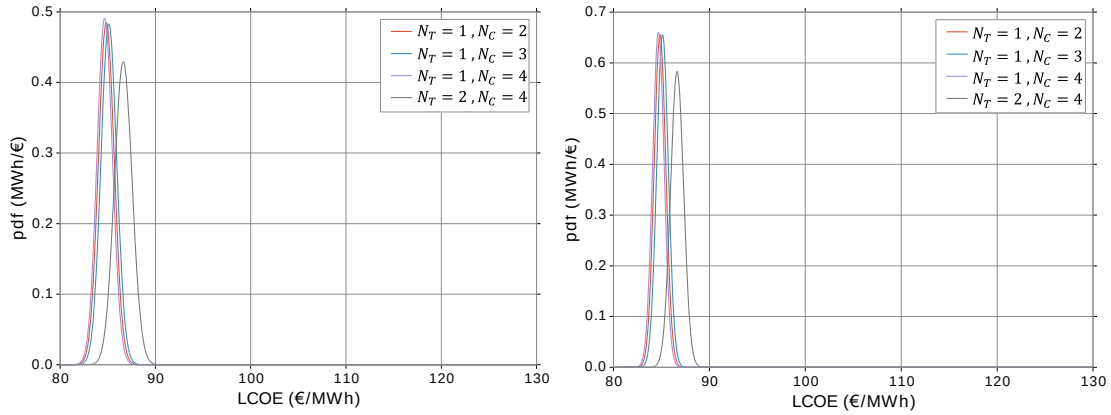

Figure 6-7: Probability density functions of the LCOE with fixed wind turbines CAPEXs (r=6% and N=25 years). (a) with variation of reliability data. (b) "mean" scenario reliability data

Moreover, by comparing the obtained distributions of the NLCC and of the LCOE with CAPEX and reliability model parameter uncertainties or only with the uncertainties related to the CAPEX models (by comparing (a) and (b) of Figure 6-6, Figure 6-7, Figure 6-8 and Figure 6-9). The specific impact of reliability data uncertainties on NLCC and LCOE can be understood. It can be seen that variation amplitude of the criteria is not highly increased when the uncertainties associated to the reliability data are taken into account. Therefore, it can be said that the uncertainties associated to the CAPEX models are higher than the one due to reliability data. It must be highlighted that the uncertainties due to CAPEX models are mainly due to the market (supply and demand, raw hardware cost etc.)

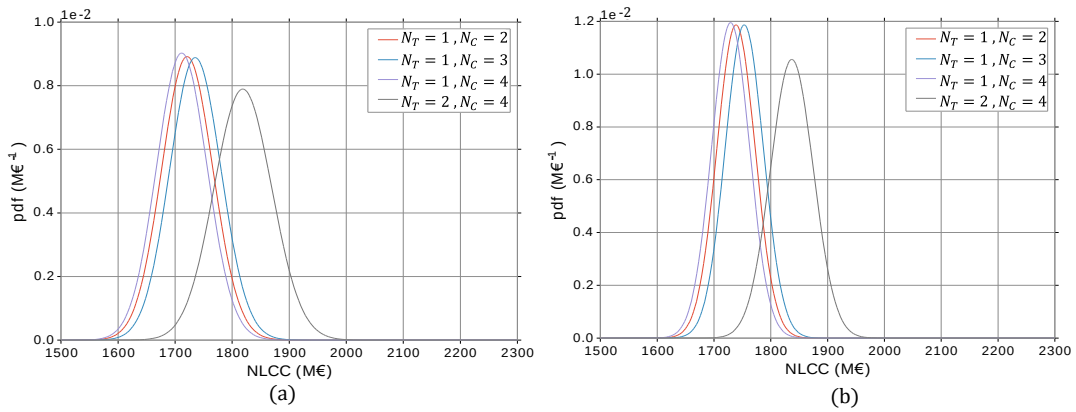

Figure 6-8: Probability density functions of the NLCC with fixed wind turbines CAPEXs (r=8% and N=20 years). (a) uncertainty of reliability data. (b) "mean" scenario reliability data

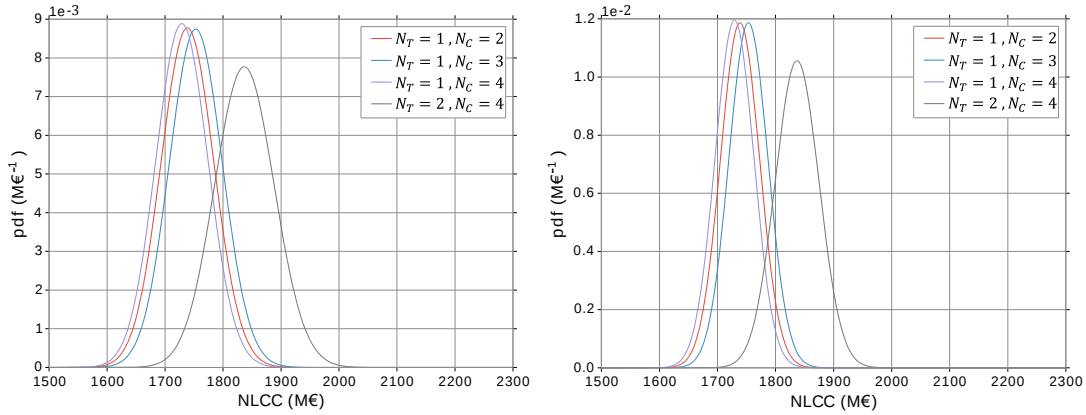

Figure 6-9: Probability density functions of the NLCC with fixed wind turbines CAPEXs (r=6% and N=25 years). (a) uncertainty of reliability data. (b) "mean" scenario reliability data

Table 6-4 gives the expected values and standard deviations of the LCOE and NLCC for the various designs, and for the different sets of values $(r, N) \in \{(6\%, 25 \text{ years}), (8\%, 25 \text{ years}), (8\%, 20 \text{ years})\}$. The standard deviations are given for the distributions, where all models uncertainties are considered (reliability data and CAPEX models). It can be seen that the expected values of NLCC and LCOE, calculated from the probability density functions, are the same as in section 5.6.3 for r=8% and N=25 years.

Table 6-4: Expected values and standard deviation of LCOE and NLCC for various cases

		LCOE (€/MWh)		*NLCC* (M€)	
Economical parameters	(N_T, N_C)	**Expected value**	**Standard deviation**	**Expected value**	**Standard deviation**
r=8%, N=20	**(1, 2)**	104.6	1.0	1722	44.8
	(1, 3)	104.9	1.0	1736	44.9
	(1,4)	104.4	1.0	1712	44.2
	(2, 4)	106.9	1.2	1819	50.5
r=8%, N=25	**(1, 2)**	97.3	1.0	1727	45.0
	(1, 3)	97.6	1.0	1741	45.1
	(1,4)	97.1	1.0	1717	44.4
	(2, 4)	99.4	1.1	1825	50.8

		LCOE (€/MWh)		*NLCC* (M€)	
***r*=6%, *N*=25**	**(1, 2)**	84.8	0.8	1739	45.5
	(1, 3)	85.1	0.8	1753	45.6
	(1,4)	84.7	0.8	1729	44.9
	(2, 4)	86.6	0.9	1837	51.4

It can be noticed that the dominion based on the expected values of the LCOE and NLCC (refer to Table 6-4) for the various designs remains the same whatever the values of r and N. This is because the CAPEX, mainly impacts the LCOE and the NLCC, and is the primary discriminating criterion between the designs. Indeed, the CAPEX is not affected by N and r in the LCOE and NLCC.

6.4.5.2 Determination of components with the main contribution to the annual curtailed energy

Figure 6-10 shows the normal cumulated distribution functions associated to the expected annual curtailed energy (first order estimation, refer to section 6.4.3) of component classes for the design $(N_T, N_C) = (2,4)$. This latter design is the one with the higher cost (measured by the LCOE or NLCC) and annual curtailed energy. Thus, this is the design for which the uncertainties of the models result to the higher uncertainties.

On Figure 6-10, the horizontal dotted lines corresponds to the limit of the 95% probability, which is used. Thus, the values given by the intersections of these lines with the cdf (cumulated distribution function) for the various components correspond to the "optimistic" and "pessimistic" values of annual curtailed energy.

The proposed method enables the determination of the components, mostly responsible the uncertainties due to reliability data. It allows assessing the critical components of the network. In the present case, it helps to determine that long transmission cables are the weak components of the network in regard to the reliability (because of the obtained highest lost energy). It explains why for real projects, studies of risk assessments are done before validating the routing of a submarine cable [147]. In such studies, an acceptable level of risk (notably due to external damages) can be imposed a priori and protection methods are deployed accordingly (e.g. deeper burying of cables in sand or rock dumping above cables in case the sea bed soil is not soft).

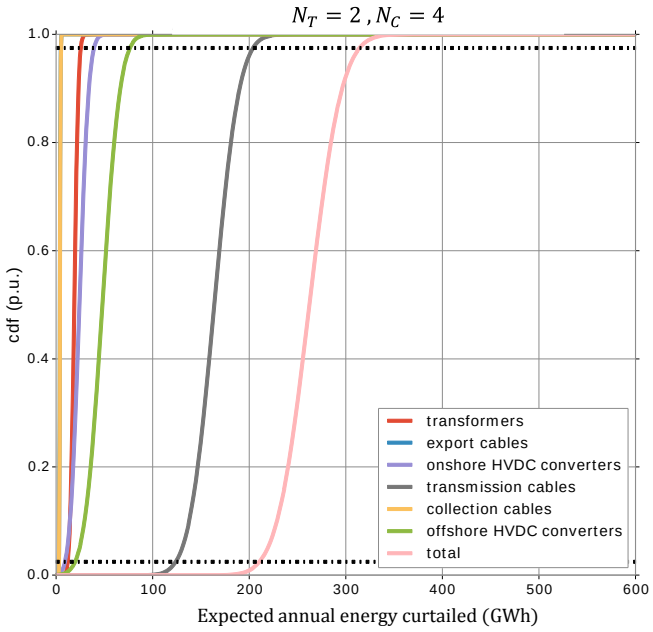

Figure 6-10: Cumulated distribution functions for the normal expected curtailed energy (first order estimator) showing the uncertainties related to reliability data $(N_T, N_C) = (2,4)$.

6.4.5.3 Determination of component with the main contribution to the CAPEX

Figure 6-11 shows the cumulated distribution functions for the CAPEX of the different component classes for the design with $(N_T, N_C) = (2,4)$. This is the design for which the uncertainties of the LCOE and NLCC, measured by their standard deviations, are the highest. This is because there are two offshore HVDC platforms.

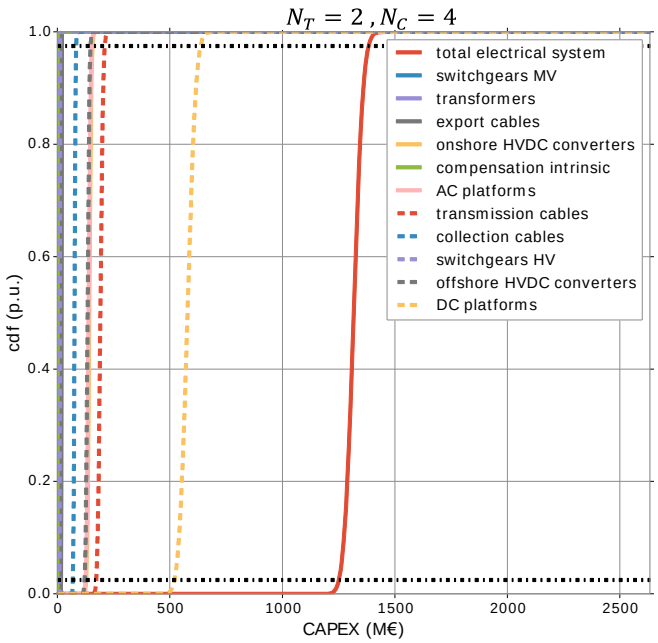

Figure 6-11: Cumulated distribution functions for the normal CAPEX showing the uncertainties of the CAPEX models. Example of $(N_T, N_C) = (2,4)$.

Figure 6-11 shows that this class of components (DC platforms) is the one with the higher CAPEX and also higher CAPEX uncertainties. This illustrates that the present method allows the analysis of the model uncertainty propagation and also the mitigation of these uncertainties by determining the items (e.g. offshore HVDC platform) and indexes (e.g. CAPEX) causing these uncertainties.

This is complementary to the visualization of the NLCC breakdown (refer to section 5.6). It can help to decide where some improvements in accuracy are required in models.

6.4.5.4 Analysis of NLCC and LCOE behaviours with variation of financial parameters

In the present sub-section, a discussion of the impact of N and r on the economic criteria (LCOE and NLCC) is proposed.

One could find surprising that when N increases and r decreases, the NLCC increases while the LCOE decreases as expected (refer to equation (6-40)).

$$LCOE_{N,r}(\mathrm{X}) = \frac{C_S(X) + C_C + \sum_{t=1}^{N} \frac{Oc_t + Os_t(X)}{(1+r)^t}}{\sum_{t=1}^{N} \frac{AED(X)}{(1+r)^t}} \tag{6-40}$$

Analytically, the term $\left[\sum_{t=1}^{N} \frac{1}{(1+r)^t}\right] . LCOE_{N,r}(X) . (L_S^{dis}(X) + L_S^{cur}(X))$ of the NLCC written as in equation (6-41) is the one which depends on N and r:

$$NLCC_{N,r}(X) = C_S(X) + \left[\sum_{t=1}^{N} \frac{1}{(1+r)^t}\right] . \left[LCOE_{N,r}(X) . (L_S^{dis}(X) + L_S^{cur}(X)) + Os_t(X)\right] \tag{6-41}$$

It does not necessarily follow the same direction of variations as $LCOE_{N,r}(X)$ because when the term $\left[\sum_{t=1}^{N} \frac{1}{(1+r)^t}\right]$ increases, $LCOE_{N,r}(X)$ decreases (refer to equation (6-40)). Thus, determining the variations direction of $\left[\sum_{t=1}^{N} \frac{1}{(1+r)^t}\right] . LCOE_{N,r}(X)$ is not trivial. From an economical view point, the direction of variation of the NLCC can be explained by the fact that the term $\left[\sum_{t=1}^{N} \frac{1}{(1+r)^t}\right] . LCOE_{N,r}(X) . (L_S^{dis}(X) + L_S^{cur}(X))$ is not actually a cost but rather a loss of income, which depends on the LCOE.

This being explained, the NLCC remains a powerful criteria for assessment and comparison of architectures. In particular, Figure 6-6, Figure 6-7, Figure 6-8 and Figure 6-9 show that the NLCC is not as strongly impacted by the variations of N and r as the LCOE is. It means that in addition to the advantage of the NLCC related to its capacity to be represented as a breakdown (refer to Chapter 5), it has the second advantage to mitigate the impact of the financial parameters on the decision regarding the assessment or comparison of architectures.

6.5 Conclusion

In this Chapter, methods are proposed to take into account the uncertainties, which can affect the decision making in relation with the choice of offshore wind farm network architecture. Two sources of uncertainties

are taken into account: 1) the stochasticity associated to the reliability 2) the uncertainties related to the model parameters.

The Monte Carlo simulation based method to assess the reliability proposed in Chapter 4 is applied to some architectures obtained with the optimization design method of Chapter 5. Thus, a propagation of the uncertainties inherent to the reliability stochasticity is quantified by means of the LCOE.

The present Chapter also proposes a method to take into account uncertainties in regard to the model parameters (CAPEX and reliability). Classically, the assessment of model uncertainties and propagation are based on systemic sensitivity analysis. The proposed novel approach takes into account the uncertainties of the models and study their propagation to the decision criteria (LCOE and NLCC in the present work) by using analytical results. The proposed method is based on analytical results of the probability theory and thus allows handling the model uncertainties at low computational cost. The approach is applied to one architecture concept designed in Chapter 5.

The application of the method shows that the proposed method allows the understanding and determination of the source of uncertainties, thus making it possible to mitigate them. Such a mitigation can consist in a future enhancement of the proposed models, which cause the highest uncertainties. Additionally, the application cases highlight other advantages of the NLCC than those presented in Chapter 5: the use of the NLCC mitigates the impact of the financial parameters (discount rate and number of years the infrastructures are exploited) on the decision making. Indeed, it is barely affected by the variations of these parameters. In a research and development context when the financial behavior of the final investor is not always known, it can be valuable to reduce the uncertainties in this regard.

GENERAL CONCLUSION AND PERSPECTIVES

Offshore wind power is a promising renewable source. It is currently the subject of a fast expansion, especially in Europe where it reached 12 GW of installed capacity. The cost-effectiveness of offshore wind power in comparison with other sources of electricity (measured with the standard LCOE) highly depends on the architecture of the electric connection to the onshore grid.

The electric connection infrastructure impacts the profitability of offshore wind farm projects, particularly when the distance for the electric connection increases. A substantial number of architecture concepts and associated technologies can be considered for the electric connection network design.

In this manuscript, a detailed review of the available architectures is proposed with an emphasis on the technologies considered to perform the required functions (voltage transformation, current rectifying or inversion etc.). A selection of architecture candidates is made.

The scientific problem addressed in this work is to know *what is the best electric network architecture* from an economic perspective for a given wind farm site (with a fixed distance to onshore grid point of connection, total peak power, number of wind turbines and spatial density)

Answering this question requires the development of a comprehensive decision support framework. Specifying such a decision framework is the primary objective of this PhD thesis. Therefore, a review of methodological approaches for assessing or comparing architecture concepts and associated technologies is exposed. This literature review raises the need for decision support framework dedicated to the assessment of offshore wind farm networks architectures, which must include models and methods for the calculation of:

- Energy dissipated losses;
- Investment costs;
- Annual curtailed energy;
- Maintenance costs.

To calculate these indexes, the chosen architecture must be designed. Thus, there is a need for a methodology to design the electric network, in a generic way in regard to the various architectures which can be considered.

The choice between a multi-objective and mono-objective approaches for the assessment is justified in the context of the present work by the existence of the standard LCOE criterion. The LCOE allows aggregating the elementary indexes, which affect the cost-effectiveness of an architecture (CAPEX, annual energy dissipated or curtailed and annual maintenance costs). **A novel criteria, the NLCC (Network Life Cycle Cost), equivalent to the LCOE in terms of optimality is also proposed in Chapter 1**. The NLCC is legitimate due to its

relation with the LCOE and also allows a more powerful analysis of the assessment of some electric network architectures. This is shown in details in Chapter 5 and Chapter 6.

In Chapter 2, models and methods to compute energetic quantities are proposed. The wind resources are modelled by means of a Weibull probabilistic distribution and the wind turbines are modelled by their power characteristics. Wake effects are taken into account by using a "wake macro factor" whose value depends on the actual wind farm site. Then, an extensive static electric modeling of power components of electric networks for the selected architectures is proposed. A special effort is made for the modeling of power cables by using the IEC standard 60287. This is because power cable is a key component, whose physical behaviour affects both its design and operation. These static electric models are used to compute parameters of load flow calculations, which are used to quantify the electric steady states of the electric network. The load flow calculation is based on a sequential approach, which has both the advantages of being generic in regard to the various architectures and being compatible with hybrid architectures (AC and DC).

Also in Chapter 2, an analysis of power management of the electric network in various cases (MVAC or MVAC collection, HVAC or HVDC transmission) is done. The resulting quantitative analysis of voltage drops and reactive power conditions is used later to justify simplifications in the formulation of the electric design optimization problem (in Chapter 5). In particular, it is shown that the network design can be done whilst neglecting the reactive power for MVAC, while it must be taken into account for the design of HVAC networks.

Finally, still in Chapter 2, the methodology to link the wind resources and wind turbines models with the load flow calculations encompassing the component electric models is detailed. It is based on the probabilistic transfer theorem, which allows the estimation of energies (such as the annual energy distributed or dissipated) with a quick convergence.

Chapter 3 proposes an approach for the modeling of component costs. It takes into account cost uncertainties, which are due to market conditions, cost of raw materials etc. For each component, an analytical model is justified by expertise when possible and its parameters are identified based on cost data. The parameter identification for each kind of components is done for three sets of cost data, each corresponding to a scenario ("mean", "optimistic" and "pessimistic"). The set of parameters associated to the scenarios are used later to study the propagation of model uncertainties.

Chapter 4 study the network reliability, also impacting its cost effectiveness. The reliability of the electric network inherits the ones of its components, depending on the topologies, which connect them (e.g. level of redundancies etc.). A state of the art of existing contributions for the assessment of the reliability of the electric networks connecting offshore wind farm is exposed. It confirms that the annual curtailed energy is an appropriate index to be calculated. The annual curtailed energy depends on both the wind resources and on the electric network system state of availability. **A novel approach to compute the annual curtailed energy is proposed, with two objectives, being 1) to give accurate results 2) with as low computational durations as possible**. To achieve this, the wind resources are modeled by assuming that the wind velocity follows a

Weibull probabilistic law, which is a classical assumption. Then, a state of availability defines what components of the electric network are available. Based on these considerations, a cornerstone method based on the constrained max flow problem from the graph theory is proposed. The cornerstone method consists in calculating the expected annual power, which is curtailed for a given state of the system.. In comparison with the classically used Monte Carlo simulations (where the wind velocity would be randomly generated) the proposed method improves the estimation speed of power expected values.

A mere application of this method allows the determination of the components of the electric network whose failure is the most critical.

Then, the cornerstone method to compute the expected power curtailed for a given state of the system is used in two complementary methods to estimate the annual curtailed energy:

- One allows the computation of the expected value of the annual curtailed energy by using the unavailability index of the components.
- The second, based on Monte Carlo Simulations, where the sampled variable is the state of the system, consists in generating a stochastic process of failures and repairs of components. The second methods allows the calculation of an empirical distribution of annual curtailed energy and thus, give an information regarding the risk. Compared to a simultaneous sampling of the system states and wind velocity, with the proposed Monte Carlo based method, the computational performances are highly improved. This is due to the facts that: 1) As mentioned above in relation with the use of the transfer theorem, the estimation of curtailed power expected value is quicker. 2) A so called memorization technique can be used to calculate expected power curtailed corresponding to a given state of the system only once, even if it appears several time during the sequences generated during the Monte Carlo simulations.

The application of both methods for the calculation of the annual curtailed energy requires a collection of reliability data, the MTTR (Mean Time To Repair) and MTTF (Mean Time To Failure). In the present work, these data, which are gathered from the literature, are classified into three sets of parameters, each corresponding to a scenario (“optimistic”, “pessimistic” and “mean”). The two proposed estimators are compared and cross-validated by using “mean” scenario reliability data and by comparing them to a benchmark of electric network architecture.

As stated above, before assessing any architecture, its near optimal design must be determined. Thus, a formulation of the design problem is proposed accordingly in Chapter 5. First, a review of existing contributions for the optimization of electric network(s) associated to offshore wind farms is done. **A formulation of the complete electric network, from the wind turbines up to the point of common coupling with the onshore network is then proposed. To the author’s knowledge, it was not done before, especially as the proposed formulation is generic in regard to many architectures concepts (MVAC collection or MVDC collection, HVAC transmission or HVDC transmission, with or without AC platforms etc.)**. Due to the complexity of the problem, the proposed formulation splits the problem into five sub-problems. A meta-optimizer is in charge of handling major optimization variables (number of clusters of the wind farms and

number of offshore transmission substations). Then, a MIP (Mixed Integer Programming) formulation of each sub-problem is detailed. The sub-problems are the (P1) clustering of wind turbines, (P2) design of collection network(s), (P3) association of cluster substations to transmission substations, (P4) design of power components and (P5) design of the HVDC transmission networks.

The solving of the sub-problems is done by using very well performing heuristic methods, providing near optimal solutions. It is justified in a context where, as shown in Chapter 3 and Chapter 4, there are uncertainties in regard to parameters of cost and reliability models/methods.

An application of the design optimization formulation is done for three architectures concepts. One with MVAC collection and HVAC transmission networks. Another with MVAC collection, HVAC export and HVDC transmission networks. A third with MVDC collection and HVDC transmission networks. Once the designs are obtained, the assessment framework based on models from Chapter 2 and "mean" scenario models parameters from Chapter 3 and Chapter 4 is done. It leads to the calculation of various indexes and criteria including the LCOE and NLCC.

These applications in Chapter 5 highlight the added value of the NLCC for which a breakdown over the components of the system can be given. It helps determining the components, which impact the most the cost-effectiveness of an architecture. Thus in a R&D context, it is a powerful tool for cost driven innovations.

In Chapter 6, novel methods to take into account the uncertainties related to the assessment of an architecture are proposed. They are based on analytical results from probability theory and allow the reduction of the computational burden, compared to pseudo Monte Carlo methods. The uncertainties in assessing architectures of the electric network connecting offshore wind farms can have several causes. In the present work, two main causes are considered: 1) the uncertainties intrinsic to the reliability, 2) the uncertainties associated to the various models and their parameters (investment costs models parameters and reliability data).

First, for handling the uncertainties due to the reliability, an application of Monte Carlo simulations as proposed in Chapter 4 is done by using the reliability data corresponding to the "mean" scenario. This is using a design obtained in Chapter 5. An empirical probability distribution of annual curtailed energy, corresponding to 10.000 simulations, is calculated. A propagation of the risk associated to the annual curtailed energy, which can actually occur in real projects, is analyzed by calculating the empirical distribution of the LCOE. It shows that even with a perfect knowledge of the costs and reliability of the components, the LCOE of a real project can be substantially far from its expected value (up to 5% with the studied case).

Secondly, an analytical method is proposed to analyze the propagation of uncertainties in the models. To do so, a classification of components into consistent classes of component is proposed. Components of a same class have consistent costs and reliability. Then, it is shown how to consider the costs and annual energies curtailed (based on the first order estimator) as normal probabilistic variables (whose probabilistic nature is due to the uncertainties of the model parameters).

The method to determine parameters of the corresponding normal laws is based on the scenarios for model parameters and is detailed for both the CAPEX and the annual curtailed energy. Then, it is shown that the LCOE can be written as a ratio of normal variables. It allows a novel application of a result from the probability theory regarding the probability distribution function of the ratio of two normal variables. Therefore, with the proposed method, it is possible to determine the probability density function for the LCOE, whose probabilistic nature is the consequence of the uncertainties of the model parameters. Finally, the affine relation between the LCOE and the NLCC is used to show that the probability density function of the NLCC can be determined analytically.

The method for analyzing the propagation of model uncertainties is applied to a fixed architecture obtained in Chapter 5. It shows the impact of model uncertainties to the decision criteria. The quantitative results are given for several sets of values of discount rate and duration of operation. The results help determining the components of the system for which the models require further improvements. Additionally, the handling of these uncertainties justifies the choice of near optimal methods for the design of the electric network.

In conclusion, with the proposed framework (refer to Figure 1-20), for a given wind farm site, an architecture concept is selected (among many choices) and the design heuristics and optimization algorithm of the framework are used to design the network. Then, the holistic assessment of the architecture can be done with modules of the framework ("wind power simulator", "load flow simulator", "CAPEX calculator" and "reliability simulator"), so to calculate decision criteria (with "aggregated objectives evaluator").

Therefore, the two main scientific contributions are:

- The proposal of a consistent holistic framework, which brings a decision support through assessment of electric connections of offshore wind farms to shore. The framework mainly aims at managing the complexity, which is the main barrier that a person faces when making a decision. In this regard, the proposed NLCC criterion is valuable to ease the analysis of the results.
- The possibility to analyze and mitigate uncertainties, which affect the decision criteria and to put them in relation with their origins (model parameters, reliability, etc.). The small computational time for analysis of uncertainties, thanks to the novel use of analytical results, is particularly valuable in an industrial context.

Perspectives

Short term

In the present thesis, the emphasis is put on the methodological developments encompassed in the proposed assessment framework. The proposed applications of the framework in Chapter 5 and Chapter 6 aim at showing the possibilities and potential constraints of the framework. The framework should obviously be further exploited for the assessment and comparison of architectures. This is a major perspective of this research for SuperGrid Institute and its Partners.

Another perspective is to enhance the proposed framework so that it can cope with requirements for a global optimization. It would be justified in a project oriented context where the costs are notably subject to much lower uncertainties. To achieve this goal, one approach would be to consider the locations of offshore substations as metavariables. In such case, a mere modification of sub-problems (P1) and (P3) is required so to have the substations locations as input parameters of these two sub-problems. The meta-optimizer would then have to comprise an optimization algorithm such as a meta-heuristic (e.g. a popular genetic algorithm), which would have to handle a reduced number of variables. Doing this is possible thanks to the quick methods, which are used to solve the sub-problems. Once such a systemic optimization is performed, an improvement of the optimality for each of the sub-problems can be achieved individually by using a global optimizer such as CPLEX.

Medium term

An extension of the framework to architectures comprising meshed HVDC networks is a perspective, which is natural in the context of SuperGrid Institute, which studies such networks. In this context, the level of granularity of the problem formulation must be carefully determined.

In this regard, the reliability can be a major driver. Therefore, considering the level of redundancies as additional decision variables of the proposed decision support framework seems promising. With the formulation proposed in Chapter 5, it seems possible to consider such decision variables as meta-variable and to cascade them to the sub-problems. For instance, the power rating of parallel transformers designed within the sub-problem (P4), can be such a decision variable.

However, it seems unrealistic or even risky to leave entirely the decision regarding the reliability to algorithms. Particularly in a context where reliability data are subject to high uncertainties. The decision maker must have the last word, guided by the decision support framework and by the expert. It is thought by the author that the main added value of the framework must be to handle the complexity, which can be a barrier for decision making by a person.

Long term

Providing a single formulation of the complete electric network, which can be solved at once with reasonable durations, is still pending. Several scientific locks are associated with this objective:

- Providing a generic formulation, in regard to the architecture concept is always a challenge. A higher level of abstraction could ease the process of modifying the problem formulation to cope with the introduction of a new architecture concept.
- Solving such a problem with reasonable computational duration depends on the performance of the solver but also of the quality of the mathematical formulation. For instance, some MIP formulations of a given problem are stronger than others even though they give the same solutions. With a weaker formulation, the solving time would be higher.

- Even with the first order method proposed in the present thesis, the calculation of the annual curtailed energy for a given design is time consuming and remains a major lock against the design optimization problem taking into account the reliability.

Thanks to the NLCC (Network Life Cycle Cost) criteria, which is equivalent to the LCOE, but which can be written as a sum of CLCC (Component Life Cycle Cost), the target cascading method, which has successfully been applied in an electric context, could also be considered. The target cascading can be applied to optimization of systems of systems. It could require an in-depth modification of the formulation but could be a promising direction to investigate.

BIBLIOGRAPHY

[1] "renewable energy technologies: cost analysis series – wind power," IRENA, 2012.

[2] [online] visited the 10/04/2017 https://ec.europa.eu/clima/policies/strategies/progress/kyoto_1_e/, "Kyoto 1st commitment period (2008–12) in the European Union."

[3] [online] visited the 10/04/2017 https://ec.europa.eu/clima/policies/strategies/progress/kyoto_2_en, "Kyoto 2nd commitment period (2013–20). European Union."

[4] "Trends and projections in Europe 201 6 - Tracking progress towards Europe's climate and energy targets," European Environment Agency, 2016.

[5] "Europe's onshore and offshore wind energy potential. An assessment of environmental and economic constraints.," European Environment Agency, 2009.

[6] A. Nghiem, A. Mbistrova, I. Pineda, P. Tardieu, and L. Miró, "Wind in power, 2016 European statistics (published in February 2017)," WindEurope, 2017.

[7] "The European offshore wind industry. Key trends and statistics 2016.," Wind Europe, 2016.

[8] ENTSO-E, "Offshore Grid Development in the North Seas ENTSO-E views," 2011.

[9] A. Dhabi, "Innovation Outlook: Offshore Wind," International Renewable Energy Agency, 2016.

[10] B. Associates, "Offshore wind cost reduction pathways Technology work stream," prepared for The Crown Estate, 2012.

[11] A. Gerken, P. Heinrich, M. Richter, F. Peter, L. Krampe, and J. Hobohm, "Cost Reduction Potentials of Offshore Wind Power in Germany," Prognos and Fichtner for the german offshore wind energy fundation and partners, 2013.

[12] B. O'Kelly, M. Arshad, C. Ng, and L. Ran, "Chapter 20: Offshore wind turbine foundations—Analysis and design," *Offshore wind farms: technologies, design and operation*. Woodhead Publishing, Cambridge, UK, pp. 589–610, 2016.

[13] Y. Liu, S. Li, Q. Yi, and D. Chen, "Developments in semi-submersible floating foundations supporting wind turbines: A comprehensive review," *Renewable and Sustainable Energy Reviews*, vol. 60, pp. 433–449, 2016.

[14] "Offshore wind cost reduction statement: Offshore wind can reduce costs to below €80," Adwen, EDP Renewable, Eneco Energie, E.ON Climate Renewables, GE Renewable Energy, Iberdrola Renovables, MHI Vestas Offshore Wind, RWE Innogy, Siemens Wind Powe, Statoil, Vattenfall, 2016.

[15] "Cost Monitoring Framework," Catapult, Offshore Renewable Energy.

[16] [online] and G. Hundleby, "www.offshorewind.biz/2016/10/28/borssele-tender-revealed/, visited the 16/03/2017. BORSSELE TENDER REVEALED."

[17] [online], "http://analysis.windenergyupdate.com/offshore/tender-design-output-gains-key-dongs-record-low-borssele-12-offshore-bid-price, visited the 10/04/2017. Tender design, output gains key to DONG's record-low Borssele 1&2 offshore bid price."

[18] [online], "https://corporate.vattenfall.com/press-and-media/press-releases/2016/vattenfall-wins-tender-to-build-the-largest-wind-farm-in-the-nordics/, visited the 10/04/2017. Vattenfall wins tender to build the largest wind farm in the Nordics."

[19] M. D. P. Gil, J. Domınguez-Garcıa, F. Dıaz-González, M. Aragüés-Peñalba, and O. Gomis-Bellmunt, "Feasibility analysis of offshore wind power plants with DC collection grid," *Renewable Energy*, vol. 78, pp. 467–477, 2015.

[20] M. Liserre, R. Cardenas, M. Molinas, and J. Rodriguez, "Overview of multi-MW wind turbines and wind parks," *IEEE Transactions on Industrial Electronics*, vol. 4, no. 58, pp. 1081–1095, 2011.

[21] M. de Prada Gil, O. Gomis-Bellmunt, and A. Sumper, "Technical and economic assessment of offshore wind power plants based on variable frequency operation of clusters with a single power converter," *Applied Energy*, vol. 125, pp. 218–229, 2014.

[22] I. E. Davidson and N. K. Amaambo, "Comparative Analysis of Wind Turbine Technologies for Harsh Environments," *13th wind integration workshop: International Workshop on large-scale integration of wind power into power systems as well as on transmission networks for offshore wind power plants*, 2014.

[23] O. S. Senturk, L. Helle, S. Munk-Nielsen, P. Rodriguez, and R. Teodorescu, "Medium voltage three-level converters for the grid connection of a multi-MW wind turbine," in *Power Electronics and Applications, 2009. EPE'09. 13th European Conference on*, 2009, pp. 1–8.

[24] P. Egrot, P. Monjean, and G. Tremouille, "Key parameters for the optimization of a Wind Farm: Impact on the offshore substation," *CIGRE 2014*, 2014.

[25] O. Dahmani, "Modélisation, optimisation et analyse de fiabilité de topologies électriques AC des parcs éoliens offshore," PhD thesis, STIM, 2014.

[26] N. Grid, "Appendix E: Technology," in *Electricity Ten Years Statement*, 2015.

[27] H. Liu and J. Sun, "Voltage Stability and Control of Offshore Wind Farms With AC Collection and HVDC Transmission," *Emerging and Selected Topics in Power Electronics, IEEE Journal of*, vol. 2, no. 4, pp. 1181–1189, 2014.

[28] P. Menke, "New Grid access solutions for offshore wind farms," in *EWEA*, 2015.

[29] P. Bresesti, W. L. Kling, R. L. Hendriks, and R. Vailati, "HVDC connection of offshore wind farms to the transmission system," *Energy Conversion, IEEE Transactions on*, vol. 22, no. 1, pp. 37–43, 2007.

[30] W. G. B4.55, "HVDC connection of offshore wind power plants," Cigré, 2015.

[31] C. Barker, C. Davidson, and al., *HVDC -Connectiong to the future*. Alstom Grid (Firm), 2010.

[32] U. Axelsson, A. Holm, C. Liljegren, M. Åberg, K. Eriksson, and O. Tollerz, "The Gotland HVDC Light project-experiences from trial and commercial operation," in *Electricity Distribution, 2001. Part 1: Contributions. CIRED. 16th International Conference and Exhibition on (IEE Conf. Publ No. 482)*, 2001, vol. 1, p. 5–pp.

[33] A. Lesnicar and R. Marquardt, "An innovative modular multilevel converter topology suitable for a wide power range," in *Power Tech Conference Proceedings*, 2003.

[34] H. Liu and J. Sun, "Small-signal stability analysis of offshore wind farms with LCC HVDC," in *PowerTech (POWERTECH), 2013 IEEE Grenoble*, 2013, pp. 1–8.

[35] W. G. B4-46, "Technical brochure 492: Voltage Source Converter (VSC) HVDC for Power Transmission – Economic Aspects and Comparison with other AC and DC technologies," in *GIGRE*, 2012.

[36] E. Joncquel, "Fonctionnement des liaisons à courant continu haute tension," *Techniques de l'ingénieur*, 2006.

[37] N. Mahimkar, G. Persson, and C. Westerlind, "HVDC Technology for large scale offshore wind connections," *Smartelec*, 2013.

[38] H. kirkeby, "Nowitech Reference wind farm electrical design."

[39] W. G. B3.36, "Special considerations for AC collector systems and substation associated with HVDC-connected wind power plants," Cigré, 2015.

[40] S. Bernal-Perez, S. Ano-Villalba, R. Blasco-Gimenez, and J. Rodriguez-D'Derlee, "Efficiency and fault ride-through performance of a diode-rectifier-and VSC-inverter-based HVDC link for offshore wind farms," *Industrial Electronics, IEEE Transactions on*, vol. 60, no. 6, pp. 2401–2409, 2013.

[41] S. Seman, R. Zurowski, and T. Chirst, "Investigation of DC converter nonlinear interaction with offshore wind power park system," in *EWEA*, 2015.

[42] P. MONJEAN, “Optimisation de l’architecture et des flux énergétiques de centrales à énergies renouvelables offshore et onshore équipées de liaisons en continu,” PhD thesis, Arts et Métiers ParisTech, 2012.

[43] C. Meyer, *Key Components for Future Offshore DC Grids*. Shaker, 2007.

[44] S. Lundberg, *Wind Farm Configuration and Energy Efficiency Studies: Series DC Versus AC Layouts*. Chalmers University of Technology, 2006.

[45] J. Ehnberg and T. Nordlander, “Protection system design for MVDC collection grids for off-shore wind farms,” *Elforsk AB, Vindforsk-III, Tech. Rep*, 2012.

[46] L. Qi, J. Pan, Y. Chen, and G. Zhang, “Fault protection in converter-based dc distribution systems.” Google Patents, 2016.

[47] C. D. Barker, C. C. Davidson, D. R. Trainer, and R. S. Whithouse, “Requirements of DC-DC Converters to facilitate large DC Grids,” in *CIGRE B4-204*, 2012.

[48] P. Bauer, S. De Haan, C. Meyl, and J. Pierik, “Evaluation of electrical systems for offshore windfarms,” in *Industry Applications Conference, 2000. Conference Record of the 2000 IEEE*, 2000, vol. 3, pp. 1416–1423.

[49] J. Robinson, D. Jovcic, and G. Joós, “Analysis and design of an offshore wind farm using a MV DC grid,” *Power Delivery, IEEE Transactions on*, vol. 25, no. 4, pp. 2164–2173, 2010.

[50] L. Max and S. Lundberg, “System efficiency of a DC/DC converter-based wind farm,” *Wind Energy*, vol. 11, no. 1, pp. 109–120, 2008.

[51] T. Lagier and P. Ladoux, “A comparison of insulated DC-DC converters for HVDC off-shore wind farms,” in *Clean Electrical Power (ICCEP), 2015 International Conference on*, 2015, pp. 33–39.

[52] T. Luth, M. Merlin, T. C. Green, F. Hassan, and C. D. Barker, “High-frequency operation of a dc/ac/dc system for hvdc applications,” *Power Electronics, IEEE Transactions on*, vol. 29, no. 8, pp. 4107–4115, 2014.

[53] S. P. Engel, M. Stieneker, N. Soltau, S. Rabiee, H. Stagge, and R. W. De Doncker, “Comparison of the modular multilevel dc converter and the dual-active bridge converter for power conversion in HVDC and MVDC grids,” *Power Electronics, IEEE Transactions on*, vol. 30, no. 1, pp. 124–137, 2015.

[54] Y. Hu, R. Zeng, W. Cao, J. Zhang, and S. J. Finney, “Design of a modular, high step-up ratio DC–DC converter for HVDC applications integrating offshore wind power,” *IEEE Transactions on Industrial Electronics*, vol. 63, no. 4, pp. 2190–2202, 2016.

[55] J. Pan and P. Sandeberg, “DC Connection of Offshore Wind Power Plants without Platform,” *13th wind integration workshop: International Workshop on large-scale integration of wind power into power systems as well as on transmission networks for offshore wind power plants*, 2014.

[56] N. Ederer, “The right size matters: Investigating the offshore wind turbine market equilibrium,” *Energy*, vol. 68, pp. 910–921, 2014.

[57] J. Carr, D. Das, J. Li, J. Pan, S. Ebner, and O. Apeldoorn, “Modular multilevel converter for direct MVDC connection of offshore wind farms,” in *Energy Conversion Congress and Exposition (ECCE), 2015 IEEE*, 2015, pp. 976–982.

[58] M. R. Islam, Y. Guo, and J. Zhu, “A review of offshore wind turbine nacelle: technical challenges, and research and developmental trends,” *Renewable and Sustainable Energy Reviews*, vol. 33, pp. 161–176, 2014.

[59] S. Bala and D. Tremelling, “Turbine-Generator System with DC Output.” Google Patents, 2013.

[60] S. Hay, C. Cleary, G. McFadzean, J. McGray, and N. Kelly, “MVDC Technology Study – Market Opportunities and Economic Impact,” TNEI services Ltd, 2015.

[61] C. G. 13/14.08, “Switching devices other than circuit breakers for HVDC systems, Part 1: current commutation switches,” *Electra, 135, pp. 41-55*, 1989.

[62] H. J. Bahirat, B. A. Mork, and H. Hoidalen, “Comparison of wind farm topologies for offshore applications,” in *Power and Energy Society General Meeting, 2012 IEEE*, 2012, pp. 1–8.

[63] N. Holtsmark, H. J. Bahirat, M. Molinas, B. A. Mork, and H. K. Hoidalen, "An all-DC offshore wind farm with series-connected turbines: An alternative to the classical parallel AC model?," *Industrial Electronics, IEEE Transactions on*, vol. 60, no. 6, pp. 2420–2428, 2013.

[64] E. Veilleux and P. W. Lehn, "Interconnection of Direct-Drive Wind Turbines Using a Series-Connected DC Grid," 2010.

[65] T. Ackermann, N. B. Negra, J. Todorovic, and L. Lazaridis, "Evaluation of Electrical Transmission Concepts for Large Offshore Windfarms," in *Copenhagen Offshore Wind Conference and Exhibition, Copenhagen*, 2005.

[66] L. Lazaridis, "Economic Comparison of HVAC and HVDC Solutions for Large Offshore Wind Farms under Special Consideration of Reliability." 2005.

[67] J. Pierik, M. Damen, P. Bauer, and S. de Haan, "Steady state electrical design, power performance and economic modeling of offshore wind farms," in *EWEA Special Topic Conf. on Offshore Wind Energy, Brussel*, 2001.

[68] S. Rodrigues, C. Restrepo, G. Katsouris, R. Teixeira Pinto, M. Soleimanzadeh, P. Bosman, and P. Bauer, "A Multi-Objective Optimization Framework for Offshore Wind Farm Layouts and Electric Infrastructures," *Energies*, vol. 9, no. 3, p. 216, 2016.

[69] G. Stamatiou, K. Srivastava, M. Reza, and P. Zanchetta, "Economics of DC wind collection grid as affected by cost of key components," in *World Renewable Energy Congress*, 2011, vol. 159, p. 164.

[70] M. ʿAlī, "Probabilistic modeling techniques and a robust design methodology for offshore wind farms," University of Manchester, 2012.

[71] J. S. González, M. B. Payán, and J. R. Santos, "Optimum design of transmissions systems for offshore wind farms including decision making under risk," *Renewable energy*, vol. 59, pp. 115–127, 2013.

[72] K. Nieradzinska, C. MacIver, S. Gill, G. Agnew, O. Anaya-Lara, and K. Bell, "Optioneering analysis for connecting Dogger Bank offshore wind farms to the GB electricity network," *Renewable Energy*, vol. 91, pp. 120–129, 2016.

[73] D. Elliott, K. R. W. Bell, S. J. Finney, R. Adapa, C. Brozio, J. Yu, and K. Hussain, "A Comparison of AC and HVDC Options for the Connection of Offshore Wind Generation in Great Britain," *IEEE Transactions on Power Delivery*, vol. 31, no. 2, pp. 798–809, Apr. 2016.

[74] P. Lakshmanan, J. Liang, and N. Jenkins, "Assessment of collection systems for HVDC connected offshore wind farms," *Electric Power Systems Research*, vol. 129, pp. 75–82, 2015.

[75] S. Brisset, "Démarches et outils pour la conception optimale des machines électriques," Université des Sciences et Technologie de Lille-Lille I, 2007.

[76] K. Deb, S. Agrawal, A. Pratap, and T. Meyarivan, "A fast elitist non-dominated sorting genetic algorithm for multi-objective optimization: NSGA-II," in *International Conference on Parallel Problem Solving From Nature*, 2000, pp. 849–858.

[77] W. Short, D. J. Packey, and T. Holt, *A manual for the economic evaluation of energy efficiency and renewable energy technologies*. University Press of the Pacific Hawaii, 2005.

[78] "Python language. https://www.python.org/."

[79] A. Hagberg, D. Schult, P. Swart, D. Conway, L. Séguin-Charbonneau, C. Ellison, B. Edwards, and J. Torrents, "Networkx. High productivity software for complex networks," *Webová strá nka https://networkx. lanl. gov/wiki*, 2013.

[80] M. Almiray Jaramillo, I. Arana Aristi, P. Ejnar Sorensen, and I. Kozine, "Decision making tool: Optimum power rating for substation transformers in offshore power plants," *13th wind integration workshop*, 2014.

[81] D. Villanueva and A. Feijóo, "Wind power distributions: A review of their applications," *Renewable and Sustainable Energy Reviews*, vol. 14, no. 5, pp. 1490–1495, 2010.

[82] B. H. Bulder, E. T. G. Bot, E. Wiggelinkhuizen, and F. D. J. Nieuwenhout, "Quick scan wind farm efficiencies of the Borssele location," *Energy research Centre of the Netherlands*, 2014.

[83] S. Ott and M. Nielsen, "Developments of the offshore wind turbine wake model Fuga," DTU Wind Energy, 2014.

[84] J. Choi and M. Shan, "Advancement of Jensen (Park) wake model," in *EWEA Conference*, 2013.

[85] L. E. Jensen, C. Mørch, P. Sørensen, and K. Svendsen, "Wake measurements from the Horns Rev wind farm," in *European wind energy conference*, 2004, p. 9.

[86] F. González-Longatt, P. Wall, and V. Terzija, "Wake effect in wind farm performance: Steady-state and dynamic behavior," *Renewable Energy*, vol. 39, no. 1, pp. 329–338, 2012.

[87] J. F. Herbert-Acero, O. Probst, P.-E. Réthoré, G. C. Larsen, and K. K. Castillo-Villar, "A review of methodological approaches for the design and optimization of wind farms," *Energies*, vol. 7, no. 11, pp. 6930–7016, 2014.

[88] K. Schönleber, C. Collados, R. T. Pinto, S. Ratés-Palau, and O. Gomis-Bellmunt, "Optimization-based reactive power control in HVDC-connected wind power plants," *Renewable Energy*, vol. 109, pp. 500–509, 2017.

[89] K. Walker, N. Adams, B. Gribben, B. Gellatly, N. G. Nygaard, A. Henderson, M. Marchante Jiménez, S. R. Schmidt, J. Rodriguez Ruiz, D. Paredes, and others, "An evaluation of the predictive accuracy of wake effects models for offshore wind farms," *Wind Energy*, 2015.

[90] [online], "https://www.awstruepower.com/products/software/openwind/ OpenWind Enterprise Version."

[91] [online], "http://www.gl-garradhassan.com/en/software/GHWindFarmer.php WindFarmer Wind Farm Design Software."

[92] C. Montavon, I. Jones, and [online], "http://www.ansys. com/staticassets/ANSYS%20UK/ staticassets/WindFarmFlowModelingUsingCFD.pdf Wind farm flow modeling using CFD, ANSYS webinar, 2012."

[93] A. Feijoo and D. Villanueva, "Wind farm power distribution function considering wake effects," *IEEE Transactions on Power Systems*, 2016.

[94] G. Energy, "Modeling of GE Wind Turbine-Generators for grid studies." Version, 2010.

[95] E. Jones, T. Oliphant, and P. Peterson, "SciPy: Open Source Scientific Tools for Python (Enthought, 2016)." 2016.

[96] S. Lumbreras and A. Ramos, "Offshore wind farm electrical design: a review," *Wind Energy*, vol. 16, no. 3, pp. 459–473, 2013.

[97] P. Engel, "Berechnung der optimalen Auslegung von Offshore-Windkraftanlagen zur Erhöhung der Versorgungssicherheit," 2014.

[98] A. Madariaga, C. M. de Ilarduya, S. Ceballos, I. M. de Alegrıa, and J. Martın, "Electrical losses in multi-MW wind energy conversion systems," in *Proc. International Conference on Renewable Energies and Power Quality (ICREPQ'12), Santiago de Compostela, Spain*, 2012.

[99] J. Beerten, S. Cole, and R. Belmans, "Generalized steady-state VSC MTDC model for sequential AC/DC power flow algorithms," *IEEE Transactions on Power Systems*, vol. 27, no. 2, pp. 821–829, 2012.

[100] *60287-1: Electric cables – Calculation of the current rating - Current rating equations (100 % load factor) and calculation of losses*. IEC.

[101] *60287-2: Electric cables – Calculation of the current rating, Thermal resistance – Calculation of thermal resistance*. IEC.

[102] H. Brakelmann, "Loss determination for long three-phase high-voltage submarine cables," *European transactions on electrical power*, vol. 13, no. 3, pp. 193–197, 2003.

[103] *XLPE Submarine Cable Systems Attachment to XLPE Land Cable Systems User´s Guide*. ABB.

[104] *60228: Conductors of insulated cables*. IEC.

[105] *HVDC Light® Cables: Submarine and land power cables*. ABB.

[106] A. Papadopoulos, "Modeling of collection and transmission losses of offshore wind farms for optimization purposes," Master thesis, Delft University of Technology, 2015.

[107] F. of the Supergrid, "http://www.friendsofthesupergrid.eu/," *[online]*.

[108] N. Ahmed, A. Haider, D. Van Hertem, L. Zhang, and H.-P. Nee, "Prospects and Challenges of Future HVDC SuperGrids with Modular Multilevel Converters," *Power Electronics and Applications (EPE 2011), Proceedings of the 2011-14th European Conference*, 2011.

[109] P. Jarman, *Power transformers fundamentals*. Areva T&D, 2008.

[110] S. Rodrigues, A. Papadopoulos, E. Kontos, T. Todorcevic, and P. Bauer, "Steady-State Loss Model of Half-Bridge Modular Multilevel Converters."

[111] C. Oates and C. Davidson, "A comparison of two methods of estimating losses in the modular multi-level converter," in *Power Electronics and Applications (EPE 2011), Proceedings of the 2011-14th European Conference on*, 2011, pp. 1–10.

[112] A. Zama, D. Frey, S. Bacha, A. Benchaid, B. Luscan, and S. Silvan, "Impact of Ripple Based Balancing Control Algorithms on Half-Bridge MMC Losses for HVDC Application," in *IECON*, 2016.

[113] P. S. Jones and C. C. Davidson, "Calculation of power losses for MMC-based VSC HVDC stations," in *Power Electronics and Applications (EPE), 2013 15th European Conference on*, 2013, pp. 1–10.

[114] *Data sheet IGBT module FZ1500R33HL3*. Infineon.

[115] P. Monjean, J. Delanoe, D. Marin, J. Auguste, C. Saudemont, and B. Robyns, "Control strategies of DC-based offshore wind farm," in *Power Electronics and Applications (EPE 2011), Proceedings of the 2011-14th European Conference on*, 2011, pp. 1–9.

[116] R. Lincoln, "Pylon library, Copyright (C) 1996-2010 Power System Engineering Research Center (PSERC)."

[117] X. Yuan, H. Fleischer, G. Sande, and L. Solheim, "Integration of IEC 60287 in Power System Load Flow for Variable Frequency and Long Cable Applications," 2013.

[118] B. Gustavsen and O. Mo, "Variable Transmission Voltage for Loss Minimization in Long Offshore Wind Farm AC Export Cables," *IEEE Transactions on Power Delivery*, vol. 32, no. 3, pp. 1422–1431, Jun. 2017.

[119] L. Colla, F. M. Gatta, A. Geri, S. Lauria, and M. Maccioni, "Steady-state operation of very long EHV AC cable lines," *PowerTech, 2009 IEEE Bucharest*, 2009.

[120] R. D. Zimmerman and C. E. Murillo-Sánchez, "Matpower 4.1 User's manual," *Power Systems Engineering Research Center, Cornell University, Ithaca, NY*, 2011.

[121] G. Chang, S. Chu, and H. Wang, "An improved backward/forward sweep load flow algorithm for radial distribution systems," *Power Systems, IEEE Transactions on*, vol. 22, no. 2, pp. 882–884, 2007.

[122] S. Lundberg, *Wind Farm Configuration and Energy Efficiency Studies: Series DC Versus AC Layouts*. Chalmers University of Technology, 2006.

[123] H. Ergun, D. Van Hertem, and R. Belmans, "Transmission System Topology Optimization for Large-Scale Offshore Wind Integration," *Sustainable Energy, IEEE Transactions on*, vol. 3, no. 4, pp. 908–917, Oct. 2012.

[124] S. Lundberg, "Evaluation of wind farm layouts," *Epe journal*, vol. 16, no. 1, p. 14, 2006.

[125] D. G. Energy, "Tennet, NL Offshore Wind Farm Transmission Systems - 66 kV systems for offshore wind farms," prepared for TenneT, 2015.

[126] A. G. Gonzalez-Rodriguez, "Review of offshore wind farm cost components," *Energy for Sustainable Development*, vol. 37, pp. 10–19, 2017.

[127] R. Wirth and J. Hipp, "CRISP-DM: Towards a standard process model for data mining," in *Proceedings of the 4th international conference on the practical applications of knowledge discovery and data mining*, 2000, pp. 29–39.

[128] [online], "http://www.gridinnovation-on-line.eu/Technology-Database/. (consulted the 09/03/2017). Technology data based from E-Highway project."

[129] [online], "http://www.4coffshore.com. (consulted the 08/02/2016). 4C offshore data base."

[130] ENTSO-E, "Offshore Grid Development in the North Seas ENTSO-E views," 2013.

[131] T. N. (NORTH S. C. O. G. INITIATIVE), "Offshore Transmission Technology," ENSTSO-E, 2012.

[132] "On unit investment cost indicators and corresponding reference values for electricity and gas infrastructure," ACER, 2015.

[133] Nexans, *Submarine Power Cables*. .

[134] E. STERN, J. NASH, C. SCHOENIGER, and C. BARTZSCH, "THE NEPTUNE REGIONAL TRANSMISSION SYSTEM 500 kV HVDC PROJECT," in *CIGRE B4-118*, 2008.

[135] R. Allan and R. Billinton, "Power system reliability and its assessment. III. Distribution systems and economic considerations," *Power Engineering Journal*, vol. 7, no. 4, pp. 185–192, 1993.

[136] R. Billinton and R. N. Allan, *Reliability evaluation of power systems*, vol. 2. Plenum press New York, 1984.

[137] S. Zadkhast, M. Fotuhi-Firuzabad, F. Aminifar, R. Billinton, S. O. Faried, and A. Edris, "Reliability evaluation of an HVDC transmission system tapped by a VSC station," *Power Delivery, IEEE Transactions on*, vol. 25, no. 3, pp. 1962–1970, 2010.

[138] O. Dahmani, S. Bourguet, M. Machmoum, P. Guerin, and P. Rhein, "Reliability analysis of the collection system of an offshore wind farm," in *Ecological Vehicles and Renewable Energies (EVER), 2014 Ninth International Conference on*, 2014, pp. 1–6.

[139] M. de Prada Gil and others, "Design, operation and control of novel electrical concepts for offshore wind power plants," 2014.

[140] E. Zio, *The Monte Carlo simulation method for system reliability and risk analysis*. Springer, 2013.

[141] C. MacIver, "A Reliability Evaluation of Offshore HVDC Transmission Network Options," PhD thesis, University of Strathclyde, 2015.

[142] C. MacIver, K. R. W. Bell, and D. P. Nedić, "A Reliability Evaluation of Offshore HVDC Grid Configuration Options," *IEEE Transactions on Power Delivery*, vol. 31, no. 2, pp. 810–819, Apr. 2016.

[143] "National Electricity Transmission System Security and Quality of Supply Standard, Version 2.3.," National Grid.

[144] [online], "https://en.wikipedia.org/wiki/Inclusion%E2%80%93exclusion_principle, visited the 15/06/2017. Wikipedia page for 'Inclusion-exclusion principle'."

[145] O. Dahmani, S. Bourguet, M. Machmoum, P. Guerin, P. Rhein, and L. Josse, "Optimization and Reliability Evaluation of an Offshore Wind Farm Architecture," *IEEE Transactions on Sustainable Energy*, vol. 8, no. 2, pp. 542–550, Apr. 2017.

[146] GHD, "Calculating Availability Figures for HVDC Interconnector - Update, August 2017," OFGEM.

[147] SKM, "Calculating Target Availability Figures for HVDC Interconnector - December 2012," OFGEM.

[148] D. O. Koval, "Transmission equipment reliability data from Canadian Electrical Association," in *Industrial and Commercial Power Systems Technical Conference, 1995. Conference Record, Papers Presented at the 1995 Annual Meeting., 1995 IEEE*, 1995, p. 119–.

[149] "Update of service experience of HV underground and submarine cable systems," *CIGRE B1.10: technical brochure 379*, 2009.

[150] H. Dutrieux, "Methods for the multi-year planning of distribution networks. Application to the techno-economic analysis of the solutions for integrating intermittent renewable energy sources.," Ecole Centrale de Lille, 2015.

[151] [online], "https://en.wikipedia.org/wiki/Memoization, visited the 15/05/2017. Wikipedia page for 'Memoization'."

[152] M. Banzo and A. Ramos, "Stochastic optimization model for electric power system planning of offshore wind farms," *IEEE Transactions on Power Systems*, vol. 26, no. 3, pp. 1338–1348, 2011.

[153] S. Lumbreras and A. Ramos, "Optimal design of the electrical layout of an offshore wind farm applying decomposition strategies," *IEEE Transactions on Power Systems*, vol. 28, no. 2, pp. 1434–1441, 2013.

[154] A. Pillai, J. Chick, L. Johanning, M. Khorasanchi, and V. de Laleu, "Offshore wind farm electrical cable layout optimization," *Engineering Optimization*, vol. 47, no. 12, pp. 1689–1708, 2015.

[155] Y. Chen, Z. Y. Dong, K. Meng, F. Luo, Z. Xu, and K. P. Wong, "Collector System Layout Optimization Framework for Large-Scale Offshore Wind Farms," *IEEE Transactions on Sustainable Energy*, vol. PP, no. 99, pp. 1–1, 2016.

[156] M. Lee, C. Lu, and H. Huang, "Reliability and cost analyses of electricity collection systems of a marine current farm—A Taiwanese case study," *Renewable and Sustainable Energy Reviews*, vol. 13, no. 8, pp. 2012–2021, 2009.

[157] A. Madariaga, J. Martın, I. Zamora, I. Martınez de Alegrıa, and S. Ceballos, "Technological trends in electric topologies for offshore wind power plants," *Renewable and Sustainable Energy Reviews*, vol. 24, pp. 32–44, 2013.

[158] F. M. González-Longatt, P. Wall, P. Regulski, and V. Terzija, "Optimal electric network design for a large offshore wind farm based on a modified genetic algorithm approach," *IEEE Systems Journal*, vol. 6, no. 1, pp. 164–172, 2012.

[159] B. Ismail, "Contribution à la conception robuste de réseaux électriques de grande dimension au moyen des métaheuristiques d'optimisation," Université Paris-Est Créteil, 2014.

[160] D. D. Li, C. He, and H. Y. Shu, "Optimization of electric distribution system of large offshore wind farm with improved genetic algorithm," in *Power and Energy Society General Meeting-Conversion and Delivery of Electrical Energy in the 21st Century, 2008 IEEE*, 2008, pp. 1–6.

[161] M. Zhao, Z. Chen, and F. Blaabjerg, "Optimisation of electrical system for offshore wind farms via genetic algorithm," *IET Renewable Power Generation*, vol. 3, no. 2, pp. 205–216, 2009.

[162] J. Bauer and J. Lysgaard, "The offshore wind farm array cable layout problem: a planar open vehicle routing problem," *Journal of the Operational Research Society*, vol. 66, no. 3, pp. 360–368, 2015.

[163] G. Katsouris, "Infield cable topology optimization of offshore wind farms," Delft University of Technology, 2015.

[164] A. Klein, D. Haugland, J. Bauer, and M. Mommer, "An integer programming model for branching cable layouts in offshore wind farms," in *Modeling, Computation and Optimization in Information Systems and Management Sciences*, Springer, 2015, pp. 27–36.

[165] M. Fischetti, J. Leth, and A. B. Borchersen, "A Mixed-Integer Linear Programming approach to wind farm layout and inter-array cable routing," in *2015 American Control Conference (ACC)*, 2015, pp. 5907–5912.

[166] M. de Prada, C. Corchero, O. Gomis-Bellmunt, A. Sumper, and others, "Hybrid AC-DC Offshore Wind Power Plant Topology: Optimal Design," *IEEE Transactions on Power Systems*, vol. 30, no. 4, pp. 1868–1876, 2015.

[167] I. Gamvros, B. Golden, and S. Raghavan, "The multilevel capacitated minimum spanning tree problem," *INFORMS Journal on Computing*, vol. 18, no. 3, pp. 348–365, 2006.

[168] I. Gamvros, S. Raghavan, and B. Golden, "An evolutionary approach to the multi-level capacitated minimum spanning tree problem," in *Telecommunications Network Design and Management*, Springer, 2003, pp. 99–124.

[169] L. R. Esau and K. C. Williams, "On teleprocessing system design: part II a method for approximating the optimal network," *IBM Systems Journal*, vol. 5, no. 3, pp. 142–147, 1966.

[170] U. Wijk, J. Lindgren, J. Winther, and S. Nyberg, "DOLWIN1 – FURTHER ACHIEVEMENTS IN HVDC OFFSHORE CONNECTIONS," *EWEA Offshore*, 2013.

[171] M. Gaumond, P.-E. Réthoré, S. Ott, A. Peña, A. Bechmann, and K. S. Hansen, "Evaluation of the wind direction uncertainty and its impact on wake modeling at the Horns Rev offshore wind farm," *Wind Energy*, vol. 17, no. 8, pp. 1169–1178, 2014.

[172] J. S. Gonzalez, M. B. Payan, and J. M. Riquelme-Santos, "Optimization of wind farm turbine layout including decision making under risk," *IEEE Systems Journal*, vol. 6, no. 1, pp. 94–102, 2012.

[173] M. Lackner, A. Rogers, and J. Manwell, "Uncertainty analysis in wind resource assessment and wind energy production estimation," in *45th AIAA Aerospace Sciences Meeting and Exhibit*, 2007, p. 1222.

[174] G. T. Heydt, "A Probabilistic Cost/Benefit Analysis of Transmission and Distribution Asset Expansion Projects," *IEEE Transactions on Power Systems*, 2017.

[175] D. V. Hinkley, "On the ratio of two correlated normal random variables," *Biometrika*, vol. 56, no. 3, pp. 635–639, 1969.

[176] J. S. Jonhson, "Transformations and Expectations of random variables, California institute of Technology."

[177] C. H. Chien and R. W. Bucknall, "Analysis of harmonics in subsea power transmission cables used in VSC–HVDC transmission systems operating under steady-state conditions," *Power Delivery, IEEE Transactions on*, vol. 22, no. 4, pp. 2489–2497, 2007.

[178] D. LOUME, M. NGUYEN TUAN, A. BERTINATO, and B. RAISON, "DC cable modeling and High Voltage Direct Current grid grounding system," *JiCable: 9th International Conference on Insulated Power Cables9th International Conference on Insulated Power Cables*, 2015.

[179] M. M. Hatlo and J. J. Bremnes, "Current dependent armour loss in three-core cables: comparison of FEA results and measurements," *GIGRE*, 2014.

[180] J. Pilgrim, S. Catmull, R. Chippendale, and P. Lewin, "Offshore Wind Farm Export Cable Current Rating Optimisation," in *EWEA*, 2013.

APPENDIXES

APPENDIX A Cable model IEC 69287

A.1 Geometrical and physical parameters

The developed cable models are based on industrial design data (geometry, layers thickness and materials). As stated, the design of a cable is complex, involving many different layers. The materials and thickness of each layer is the result of holistic considerations that require an expertise that cable manufacturers have. Design for AC and DC cables used to build the cable models are presented in next sub-sections. Physical parameters of cable materials are gathered in Table A-1(for electrical modeling) and Table A-2 (for thermal modeling).

Table A-1: Classical geometrical values for AC cables

Material	Electrical resistivity at 20°C (Ω.m) [21]	temperature rise coefficient of electrical resistivity at 20 °C (K^{-1}) [21]	Relative permittivity	tanδ
copper	$1.72.10^{-8}$	$3.93.10^{-3}$	1.0	/
aluminum	$2.84.10^{-8}$	$4.03.10^{-3}$	1.0	/
lead	$2.14.10^{-7}$	$4.0.10^{-3}$	1.0	/
steel	$1.38.10^{-7}$	$4.5.10^{-3}$	1.0	/
XLPE	/	/	2.5	0.001 (HVAC) 0.004 (MVAC)

Table A-2: Physical parameters of non-conductive (electrically) materials used in cables

Material	Thermal resistivity (K.m/W) [101]
XLPE (and associated semiconductor)	3.5
PE (Polyethylene)	6.0
bitumen	6.0
PP (polypropylene)	5.5

A.1.1 AC cable design

A generic design for an AC cable is depicted in Figure A-1. The geometrical parameters are used for both thermic and electrical models. In this work, geometrical parameters are taken from public sources for HVAC cables [103] and MVAC cables [133] (summarized in Table A-3). Knowledge on material of each layer is also given in these sources (summed up in Table A-4). In specific cases, namely 66 kV MVAC submarine cables, these data were not existing in public sources and internal knowledge allowed to use generic values for some geometrical quantities. Geometrical locking used to determine some of the geometrical quantities is given in equation *(A-1)* (knowing that $s = \sqrt{3}c$).

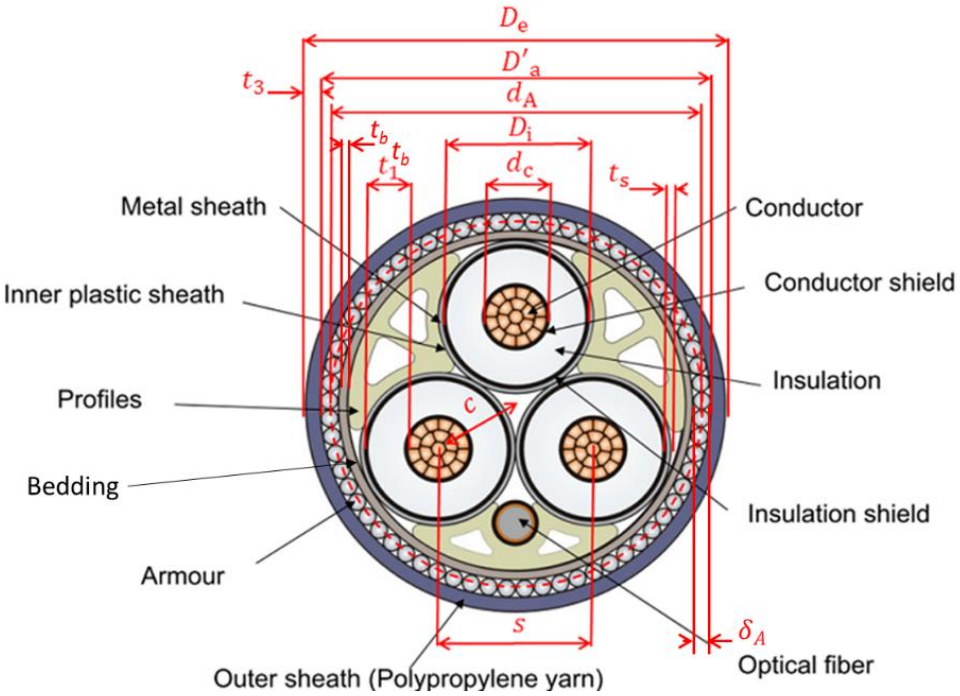

Figure A-1: Submarine AC cable layers and geometrical parameters definition

$$D_e = 2t_3 + 2\delta_A + 2t_b + \left(1 + \frac{2\sqrt{3}}{3}\right)[2t_{PE}^s + 2t_s + 2t_1 + d_c] \quad \text{(A-1)}$$

Table A-3: Classical geometrical values for AC cables

Layer	Thickness name	MVAC cable (33 kV)	MVAC cables (66 kV)	HVAC cables (150 kV)	HVAC cables (220 kV)
Conductor	d_c	Depends on section (see [133])	Same as MVAC 33 kV	Depends on section (see [103])	Depends on section (see [103])
Insulation	t_1	8.0 mm [133]	11 mm [125]	Depends on cross section (from 17 mm to 19 mm) [103]	Depends on cross section (from 23 mm to 24 mm) [103]
Metallic sheath	t_s	Depends on cross section (from 0.1 mm to 0.2 mm) [133]	Same as MVAC 33 kV assumed	Depends on cross section (from 2.4 mm to 2.8 mm) [103]	Depends on cross section (from 2.2 mm to 2.9 mm) [103]
Plastic sheath around metallic sheath	t_{PE}^s	From 2 mm to 2.7 mm [133] depending on the cross section	Same as MVAC 33 kV assumed	Recalculated in the model by geometrical locking (not given explicitly in [103])	Recalculated in the model by geometrical locking (not given explicitly in [103])
Bedding	t_b	2 mm (internal knowledge)	2 mm	0.5 mm	0.5 mm

Layer	Thickness name	MVAC cable (33 kV)	MVAC cables (66 kV)	HVAC cables (150 kV)	HVAC cables (220 kV)
Armor	δ_A	Depends on section (between 4.2 mm and 5.6 mm) [133]	Same as MVAC 33 kV assumed	Depends on section (between 5.0 mm and 5.6 mm) [103]	5.0 mm [103]
Outer sheath	t_3	4.2 mm [133]	Same as MVAC 33 kV assumed	5.0 mm [103]	5.0 mm [103]

Table A-4: material of different layers of AC cables

Layer	MVAC cable (33 kV)	MVAC cables (66 kV)	HVAC cables (150 kV and 220kV)
Conductor	copper or aluminum	copper or aluminum	copper or aluminum
Insulation	XLPE (doped for wet design)	XLPE (doped for wet design)	XLPE
Metallic sheath	copper	copper	lead
plastic sheath around metallic sheath	/	/	PE
Bedding	PE	PE	bitumen
Armor	steel	steel	steel
Outer sheath	bitumen	bitumen	PP and bitumen

A.1.2 DC cable design

DC cable design is not as complex as for AC cables (see Figure A-2). It follows basically the same structure starting from conductor as AC cables though. Different sources were put together so to determine the overall geometry of cables used as input for the models (summarized in Table A-5: Classical geometrical values for DC cables). The materials of the different layers are summarized in Table A-6.

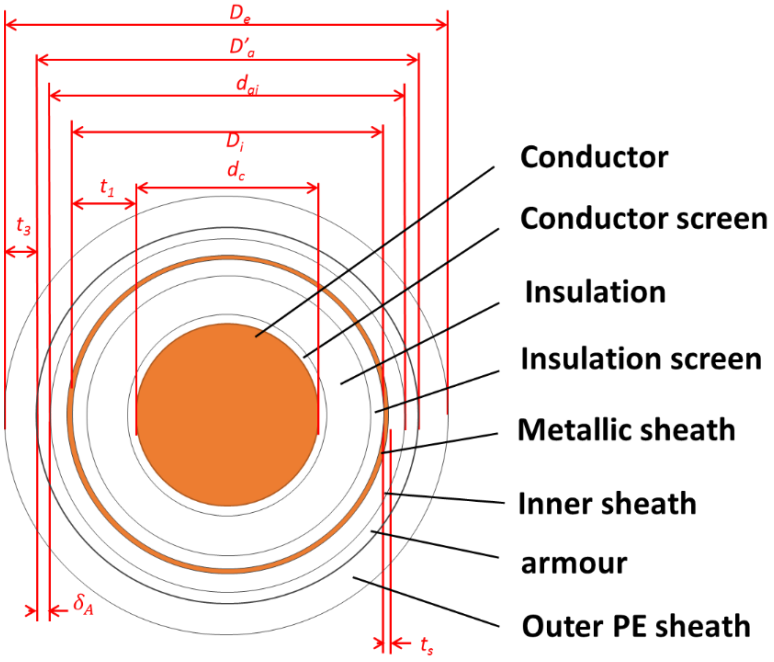

Figure A-2: Submarine DC cable layers and geometrical parameters definition

Table A-5: Classical geometrical values for DC cables

Layer	Thickness name	MVDC cable (± 25 kV)	MVDC cable (± 50 kV)	HVDC cable (± 220 kV)	HVDC cable (± 320 kV)
Conductor	d_c	Assumed same diameter as in for a given cross section [103]	Assumed same diameter as in for a given cross section [103]	Assumed same diameter as in for a given cross section [103]	Assumed same diameter as in for a given cross section [103]
Insulation (with conductor screen and insulation screen)	t_1	9.0 mm (assumed close as AC 33 kV [133]: 8.0 mm)	12 mm (assumed close as AC 66 kV [125]: 11 mm)	17 mm [177]	25 mm [178]
Metallic sheath	t_s	Assumed 0.2 mm as in [103] for MVAC cables	Assumed 0.2 mm as in [103] for MVAC cables	2.5 mm [178]	2.5 mm [178]
Inner sheath	t_{PE}^{s}	2 mm assumed as for MVAC cables [133]	2 mm assumed as for MVAC cables [133]	6 mm [178]	5 mm assumed
Armor	δ_A	5 mm assumed	5 mm assumed	5 mm assumed	5 mm assumed
Outer sheath	t_3	0.0 mm considered	0.0 mm considered	0.0 mm considered	0.0 mm considered

Table A-6: material of different layers of DC cables

Layer	MVDC cable (± 25 kV)	MVDC cable (± 50 kV)	HVDC cable (± 220 kV)	HVDC cable (± 320 kV)
Conductor	copper or aluminum	copper or aluminum	copper or aluminum	copper or aluminum
Insulation (with conductor screen and insulation screen)	XLPE + semi-conductive material	XLPE	XLPE	XLPE
Metallic sheath	copper	copper	copper	copper
Inner sheath	PE	PE	PE	PE
Armor	steel	steel	steel	steel
Outer sheath	PP	PP	PP	PP

A.2 Electrical models of cable based on standard IEC 60287

The equations of this section are based on the standard IEC 60287-1 [100]. For AC cables, they have been previously proposed in [25] and [106]. The model depends on geometrical and physical parameters for which typical values are given in the section A.1.

A.2.1 DC cables

An electric DC cable presents no skin and proximity effects. The model only consists in calculating the DC resistance R_{DC}^{θ} corresponding to the core conductor temperature θ expressed in equation (A-2).

$$R_{DC}^{\theta} = R_0.(1 + \alpha_{20}^{c}(\theta - 20)) \quad \text{(A-2)}$$

where:

R_{DC}^{θ} is the DC resistance of conductor at maximum operating temperature (Ω/m)

R_0 is the DC resistance of the conductor at 20°C; it is normalized depending on the section (see Table 2 of [104]) (Ω/m)

α_{20}^{c} is the conductor temperature rise coefficient of electrical resistivity at 20 °C, (K^{-1})

θ is the operating temperature of the conductor (°C)

In this equation, the DC resistance of the conductor at 20°C is normalized and depends on the cross section (see Table 2 of [104]).

A.2.2 AC cables

Unlike for DC cables, reactive power and induction losses must be considered for AC cables.

For the modeling of AC cable, per unit length inductances and capacitances are needed. They are usually extracted from datasheets [133], [103] or calculated directly by using equations (A-2) and (A-3).

$$C = \frac{\varepsilon_r}{18.\ln\left(\frac{D_i}{d_c}\right)}.10^{-9} \quad \text{(A-3)}$$

$$l = 2.10^{-7}.\left(\ln\left(\frac{2s}{d_c}\right) + 0.25\right) \quad \text{(A-4)}$$

where:

C is the core to ground equivalent capacitance (F/m)

ε_r is the relative permittivity of insulation

Di is the external diameter of insulation (m)

l is the inductance per core conductor (H/m)

s is the axial distance between core conductors (m)

d_c is the diameter of one core conductor (m)

AC conductor resistance

The model of the AC cable is based on the model of the DC cable. The first step is to compute the AC resistance which takes into account proximity and skin effects, expressed in the equations (A-5), (A-6) and (A-7).

$$R_{AC}^{\theta} = R_{DC}^{\theta}.\left(1 + y_s + y_p\right) \quad \text{(A-5)}$$

$$y_s = \frac{x_s^4}{192 + 0.8x_s^4} \quad \text{(A-6)}$$

$$y_p = \frac{x_p^4}{192 + 0.8x_p^4}\left(\frac{d_c}{s}\right)^2 . \left(0.312\left(\frac{d_c}{s}\right)^2 + \frac{1{,}18}{\frac{x_p^4}{192 + 0.8x_p^4} + 0.27} \right) \quad \text{(A-7)}$$

where:

R_{DC}^{θ} is the DC resistance of the conductor at maximum operating temperature (Ω/m)

R_{AC}^{θ} is the AC resistance of the conductor at maximum operating temperature (Ω/m)

s is the axial distance between core conductors (m)

d_c is the diameter of one core conductor (m)

x_s and x_p are arguments of a Bessel function used to calculate skin effect; it can be obtained with (A-8) and (A-9).

$$x_s^2 = \frac{8\pi f}{R_{DC}^{\theta}}.10^{-7}.k_s \quad \text{(A-8)}$$

$$x_p^2 = \frac{8\pi f}{R_{DC}^{\theta}}.10^{-7}.k_p \quad \text{(A-9)}$$

where:

f is the electrical frequency (Hz)

k_s and k_p are factors, which depend on the geometry of the conductor and are given in Table 2 of the standard IEC 60287-1. For example, for non-impregnated copper round stranded conductor, $k_s = 1$ and $k_p = 1$.

Power losses in metallic sheaths

The IEC 60287 standard specifies how to calculate the power losses in the metallic sheath by using the "sheath power losses factor" λ_{sheath}, which is the ratio between the losses in one metallic sheath and the power losses in the associated core conductor. It is calculated with (A-10).

$$\lambda_{sheath} = \lambda_{sheath}^{cir} + \lambda_{sheath}^{eddy} \quad \text{(A-10)}$$

where:

λ_{sheath}^{cir} is the part of λ_{sheath} caused by circulating current in the sheath, expressed in (A-11).

λ_{sheath}^{eddy} is the part of λ_{sheath} caused by circulating eddy currents in the sheath. For a three core cable such as the one considered here, with a metallic sheath per core conductor, there are no losses relative to eddy current, thus $\lambda_{sheath}^{eddy} = 0$.

$$\lambda_{sheath}^{cir} = \left(\frac{R_S^{\theta S}}{R_{AC}^{\theta}}\right).\frac{1.5}{1+\left(\frac{R_S^{\theta S}}{X}\right)^2} \quad \text{(A-11)}$$

where:

X is given in (A-12).

$R_S^{\theta S}$ is the resistance of the sheath, calculated in (A-13).

$$X = 4\pi.f.10^{-7}.\ln\left(\frac{2s}{D_i + t_s}\right) \quad \text{(A-12)}$$

$$R_S^{\theta S} = \frac{\rho_s}{\pi((D_i + t_s)^2 - D_i^2)}.\left(1 + \alpha_{20}^{s}(\theta_S - 20)\right) \quad \text{(A-13)}$$

where:

s is the axial distance between core conductors (m)

$(D_i + t_s)$ is the "mean diameter of the screen", as defined in the standard 60287-1, expressed in meters.

$\pi((D_i + t_s)^2 - D_i^2)$ is the cross section of the metallic sheath, expressed in square meters.

Power losses in the armor

The IEC 60287 standard specifies how to calculate the power losses in the armor sheath by using the "armor power losses factor" λ_{armor}. It is the ratio between the third of the power losses in the armor and the power losses in one core conductor. It is calculated with (A-14).

$$\lambda_{armor} = 1{,}23\frac{R_A^{\theta A}}{R_S^{\theta S}}\left(\frac{2c}{d_A}\right)^2.\frac{1-\frac{R}{R_S^{\theta S}}\lambda_1'}{\left(\frac{2.77R_A^{\theta A}10^6}{2\pi f}\right)^2 + 1} \quad \text{(A-14)}$$

where:

$R_A^{\theta A}$ is given in (A-15).

λ_1' is given in (A-16).

d_A is the internal diameter of the armor (m)

c is the distance between the axis of a conductor and the cable center (m)

$$R_A^{\theta_A} = \frac{4.\rho_A}{N_w.\pi.\delta_A^2}.\left(1 + \alpha_{20}^A(\theta_A - 20)\right) \quad \text{(A-15)}$$

$$\lambda_1' = \left(\frac{R_S^{\theta_S}}{R_{AC}^{\theta}}\right).\frac{1}{1 + \left(\frac{R_S^{\theta_S}}{X}\right)^2} \quad \text{(A-16)}$$

where:

ρ_A is the resistivity of the armor at 20°C (Ω.m)

N_w is the number of steel wires of the armor

δ_A is the diameter of one steel wire of the amour (m)

$N_w.\pi.\delta_A^2/4$ corresponds to the cross section of the armor (m^2)

α_{20}^A is the armor temperature coefficient of electrical resistivity at 20 °C, (K^{-1})

θ_A is the temperature of the armor (°C)

Cable manufacturers introduce an empirical formula to take into account skin effects in armors to calculate their per unit of length resistance. It is commonly acknowledged by the cable community that losses in three-core armored cables are overestimated when they are calculated according to IEC-60287 [179], [180].

Dielectric losses in the insulation

The dielectric power losses in the insulation w_d depends on the voltage. The dielectric loss per unit length in each phase is given in (A-17).

$$w_d = 2\pi f.C.U_0^2.tan\delta \quad \text{(A-17)}$$

where:

U_0 is the phase to ground (core to metallic sheath) rms voltage (V)

C is the capacitance per unit length calculated by using equation (A-3) (F/m)

$tan\delta$ is the loss angle of the insulating material

A.3 Thermal models of cable based on standard IEC 60287

The thermal model proposed in the IEC standard 60287-2 is based on the calculation of thermal resistances [101]. It is therefore assumed that the thermal steady state is reached, which can be a restrictive hypothesis. No thermal dynamics are modeled, thus, the resulting quantifications of power losses and ampacity are conservative. In the standard, four different thermal resistances are calculated, between the core conductor, the metallic sheath, the armor, the outer layer of the cable and the sea bed at the proximity of the cable, noted T_1 to T_4. T_1 and T_3 formally do not depend on whether the cable is for AC or DC currents. T_1 is proposed in (A-18) and T_3 in (A-19).

$$T_1 = \frac{\rho_t^i}{2\pi}.\ln\left(1 + \frac{2t_1}{d_c}\right) \quad \text{(A-18)}$$

where:

ρ_t^i is the thermal resistivity of the insulation (K.m/W)

d_c is the diameter of the core conductor (m)

t_1 is the thickness of the insulation including semi-conductive layers (m)

$$T_3 = \frac{\rho_t^{oc}}{2\pi}.\ln\left(1+\frac{2t_3}{D_a'}\right) \quad \text{(A-19)}$$

where:

ρ_t^{oc} is the thermal resistivity of the outer covering (K.m/W)

D_a' is the external diameter of the armor (m)

t_3 is the thickness of outer (m)

A.3.1 Specific thermal resistances for DC cables

For a DC cable, two specific thermal resistances are considered. The first one, T_2, is expressed by (A-20).

$$T_2 = \frac{\rho_t^b}{2\pi}.\ln\left(\frac{d_{ai}}{D_i+2t_s}\right) \quad \text{(A-20)}$$

where:

ρ_t^b is the thermal resistivity of the bedding of the cable (K.m/W)

d_{ai} is the internal diameter of the armour (m)

D_i is the diameter over insulation (m)

t_s is the metallic sheath thickness (m)

The second one, the thermal resistivity of surrounding soil, T_4, depends on the laying conditions. For existing DC power cables, there are normally two cables, with opposite polarities and with currents in opposite directions. They are buried in trenches, either in a common trench, or in two different ones. Depending on that, mutual heating will significantly influence ampacity and power losses. For a DC cable, T_4 is then defined by considering a mutual heating. In (A-21) the expression of T_4 is given for "two cables having equal losses, laid in a horizontal plane, spaced apart".

$$T_4 = \frac{1}{2\pi}\rho_T^s.\left(\ln\left(u+\sqrt{u^2-1}\right)+\frac{1}{2}\ln\left(1+\left(\frac{2L}{s_1}\right)^2\right)\right) \quad \text{(A-21)}$$

where:

ρ_T^s is the soil thermal resistivity (K.m/W)

L is the burying depth of cables (m)

s_1 is the distance between cable axes (m)

D_e is the external diameter of one cable (m)

u is given in (A-22).

$$u = \frac{2L}{D_e} \tag{A-22}$$

In practice, L and s_1 (parameters defining laying conditions) have a significant impact on T_4. L is usually standard (typically in the range of 1-2m to obtain a protection from all external damages such as anchors) but s_1 depends on installation choices. For example, if one trench is considered (because less costly), the worst case should be considered, where $s_1 = D_e$.

A.1.1 Specific thermal resistances for AC cables

For AC cables, T_2 is expressed in (A-23).

$$T_2 = \frac{1}{6\pi}\rho_t^b . G \tag{A-23}$$

where:

ρ_t^b is the equivalent resistivity of the bedding (K.m/W)

G is a factor obtained by using an empirical curve provided in the IEC 60297-2 standard. The value is obtained by calculating the rate r_G proposed in (A-24) and by using the bottom curve of [101] to get the corresponding factor. The curve can be implemented in the model of the cable as a look up table.

$$r_G = \frac{t_b + t_{PE}^s}{D_i + 2t_s} \tag{A-24}$$

For an AC cable, T_4 is given in (A-25), with u given in (A-22).

$$T_4 = \frac{1}{2\pi}\rho_T^s . \ln\left(u + \sqrt{u^2 - 1}\right) \tag{A-25}$$

where:

t_b is the thickness of the bedding itself (m)

t_{PE}^s is the thickness of the « inner plastic sheath » (in PE) (m)

D_i is the diameter over insulation (including semi conductive layer) (m)

t_s is the thickness of the metallic sheath (m)

A.4 Thermo-electric models coupling for more accurate losses and ampacity evaluation

A.4.1 Thermo-electric coupling for a DC cable

For a DC cable, the power balance between a conductor and its environment gives (A-26), where $\Delta\theta$ is the difference between the temperature of the core conductor and the external temperature of the sea bed.

$$\Delta\theta = R_{DC}^{\theta} . I^2[T_1 + T_2 + T_3 + T_4] \tag{A-26}$$

where I is the RMS current in one core conductor.

A.4.2 Thermo-electric coupling for an AC cable

The phenomenon is more complex for AC than for DC cables. For an AC cable, the power balance in steady state between the core conductor and the metallic sheath gives (A-27).

$$\theta_S = \theta - \left(R_{AC}^{\theta}.I^2 + 0.5.w_s\right).T_1 \quad \text{(A-27)}$$

The power balance in steady state between the core conductor and the armor gives (A-28), where n=3 for three core AC cables.

$$\theta_A = \theta - \left(\left(R_{AC}^{\theta}I^2 + 0.5.w_s\right).T_1 + \left(R_{AC}^{\theta}I^2(1+\lambda_{sheath}) + w_d\right).n.T_2\right) \quad \text{(A-28)}$$

For an AC cable, the power balance between the conductor and the sea bed gives the difference between the temperature of the core conductor and the external temperature of the sea bed in (A-29).

$$\Delta\theta = I^2.\left(R_{AC}^{\theta}T_1 + nR_{AC}^{\theta}(1+\lambda_{sheath})T_2 + n.R_{AC}^{\theta}(1+\lambda_{sheath}+\lambda_{armour}) * (T_3+T_4)\right) + W_d * \left(\frac{1}{2}.T_1 + n(T_2+T_3+T_4)\right) \quad \text{(A-29)}$$

A.4.3 Calculation of impedances and ampacity based on electrical, thermal and coupling models

The ampacity of a DC cable can be obtained by using the exposed models (which is the main objective of the standard IEC 60287). Beyond laying conditions (affecting T_4), an important parameter to take into account is the maximum temperature of the conductor θ_{max}, which is fixed to 70°C for XLPE DC cables. The Figure A-3presents the algorithm used to compute the ampacity of a DC cable.

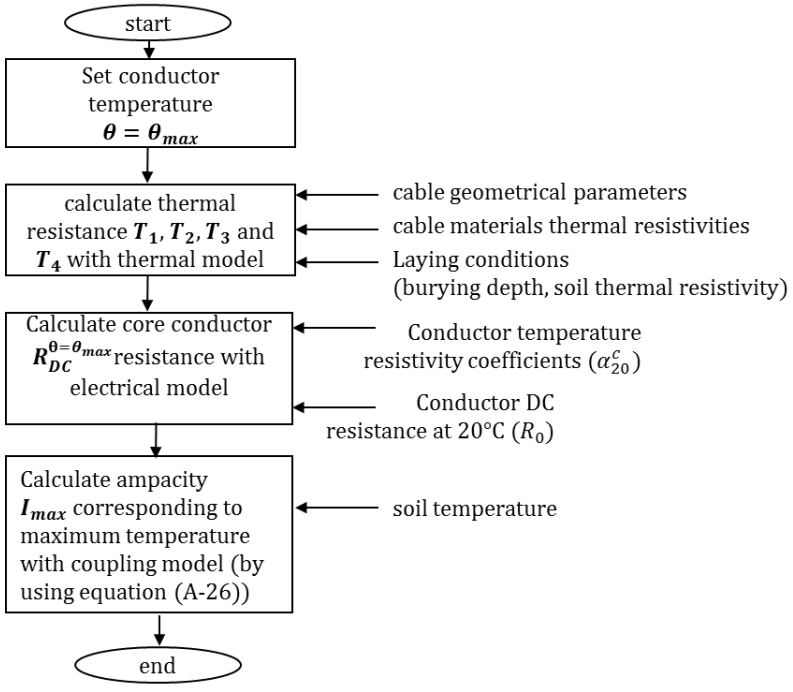

Figure A-3: Algorithm flow chart for calculation of ampacity of a DC cable

To perform a load flow involving DC cables with variable model parameters, it is necessary to quantify the resistance of the cable depending on its current I. The Figure A-4 shows how to calculate, based on the

current in the core conductor, the core conductor temperature θ and then the corresponding resistance of the core conductor R_{DC}^{θ}.

Similarly as for DC cable but in a slightly more complex way, ampacity of an AC cable can be calculated by using the algorithm depicted on the Figure A-5. For XLPE AC cable, the maximum operating temperature is 90°C.

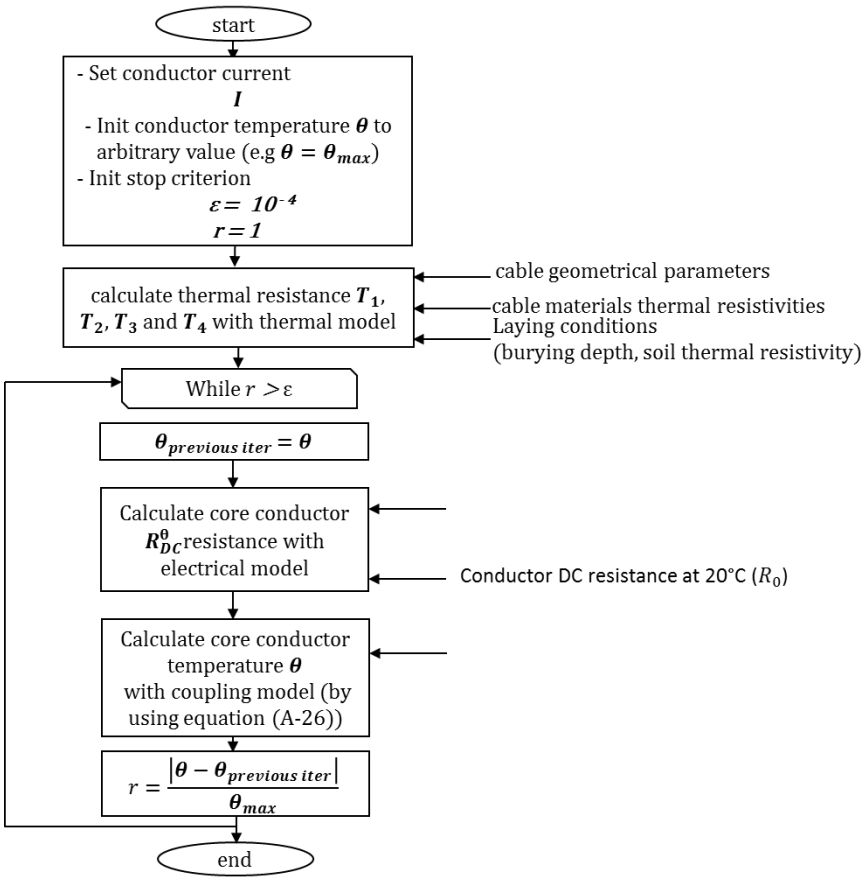

Figure A-4: Calculation of the resistance of a DC cable for a given current I

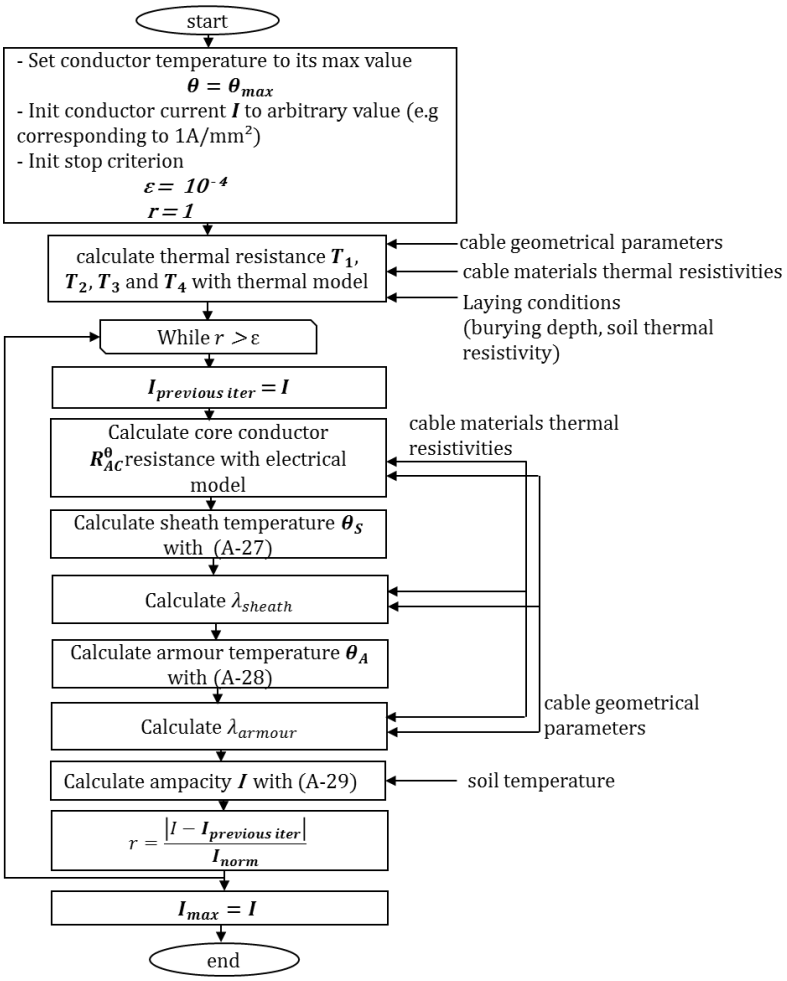

Figure A-5: Algorithm flow chart for calculation of ampacity of an AC cable

The temperature of an AC cable core conductor $\boldsymbol{\theta}$ corresponding to a current I and corresponding resistance R_{AC}^{θ} can be calculated by using the algorithm of Figure A-6. Loss factors for the metallic sheath λ_{sheath} and the armor λ_{armour} corresponding to this current I are also obtained in the process and the equivalent resistance allowing to take into account all current dependent losses in the cable, $R_{AC,eq}$, can be calculated (see section 2.3.1.5).

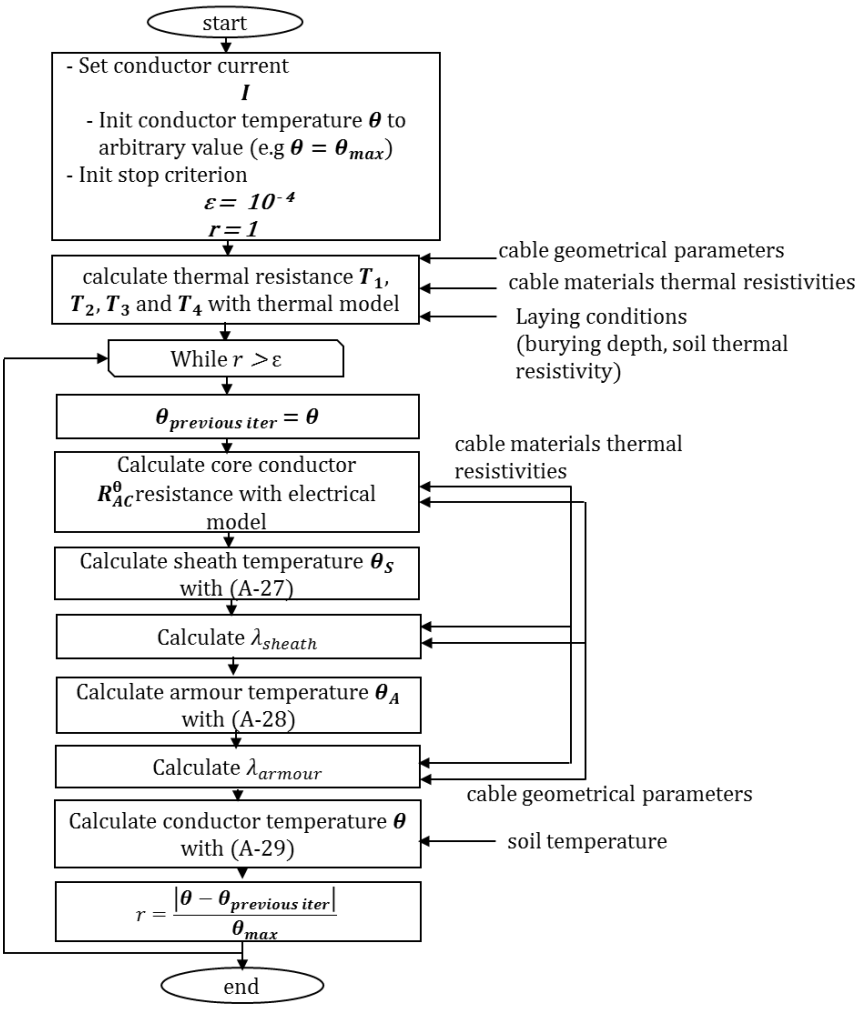

Figure A-6: Calculation of the resistance of an AC cable for a given current I

APPENDIX B Validation of the method for iterative calculation of cable resistances

The load flow methods (in both AC and DC, for collection and transmission) take into account cable resistance thermal dependence to temperature, depending itself on current. This is done by calculating variable resistances of cables depending on current. It is done iteratively as shown in the Figure B-1.

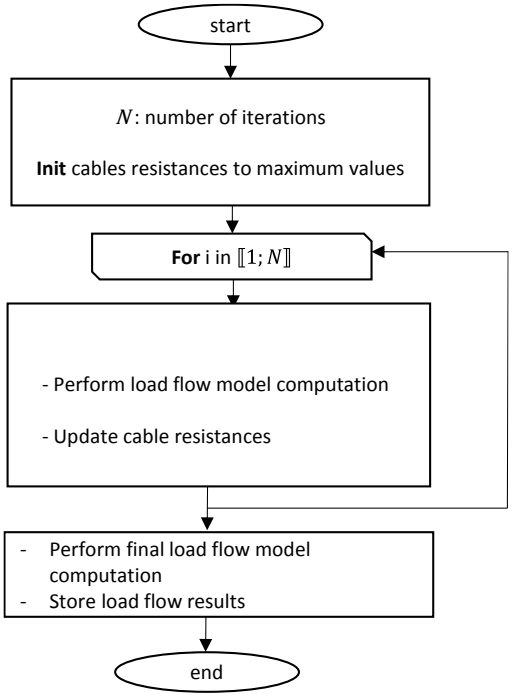

Figure B-1: Load flow method performing one load flow case calculation by taking into account temperature dependency of cables resistances

The objective of this section is to determine the number of iterations required to ensure that values of variable cable resistances and resulting losses converge. The validation is done on Borssele wind farm with 7 MW peak wind turbines and AC 66 kV inter-array cables and 150 kV AC export cables, whose sections are determined with the heuristic method using the results of sections 2.3.4.1and 2.3.4.2 and depicted in Figure B-2.

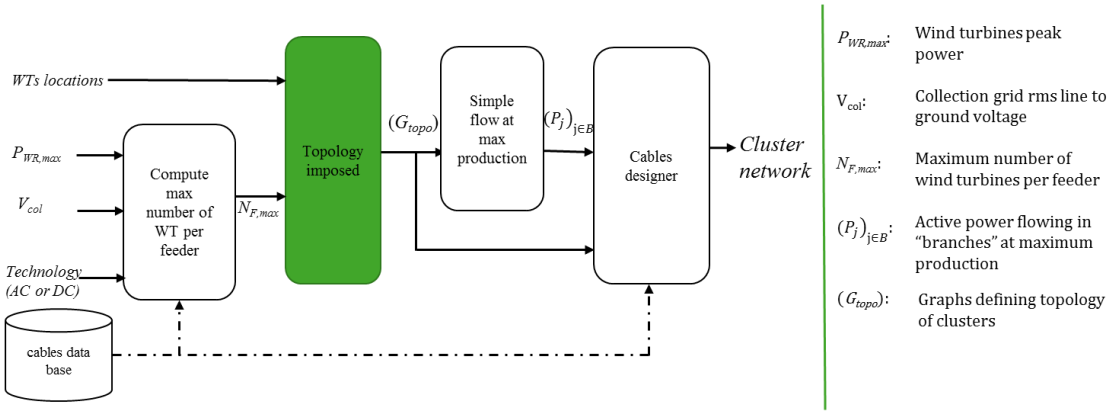

Figure B-2: Heuristic method used for the selection of the cables

The cable routing is the one given in [125] (see Figure B-3 (a)). Export cables are assumed to link AC substations to a MMC platform between the two AC substations as presented in Figure B-3 (b).

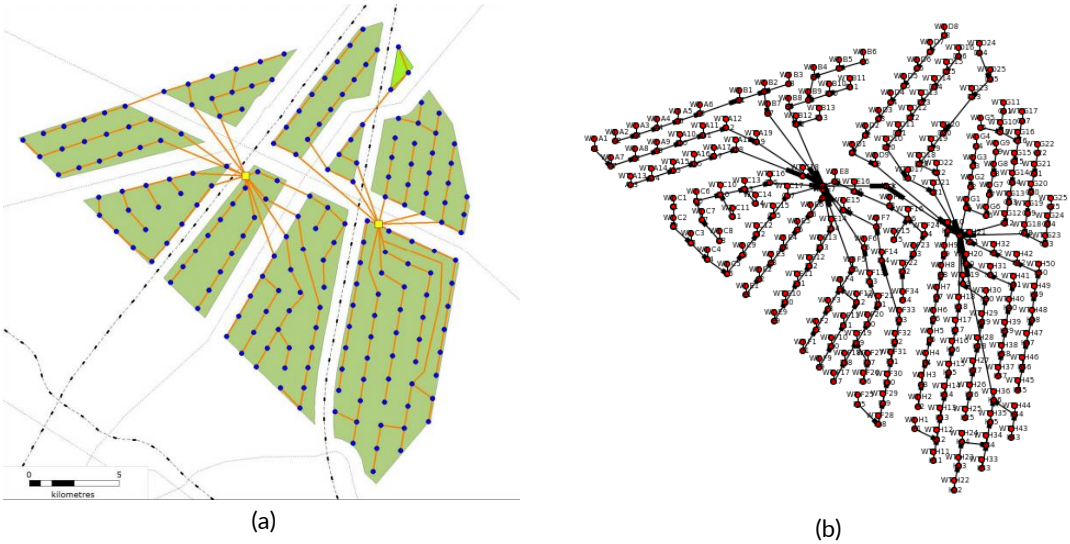

Figure B-3: Borssele wind farm layout proposed in [24] for 66 kV inter-array cables. (a) Original from source. (b) Implementation in tool with export cables

From a computational time point of view, it is very costly to consider a lot of iterations. Fortunately, as shown in Figure B-4 after one iteration, losses in the cluster network are nearly constant.

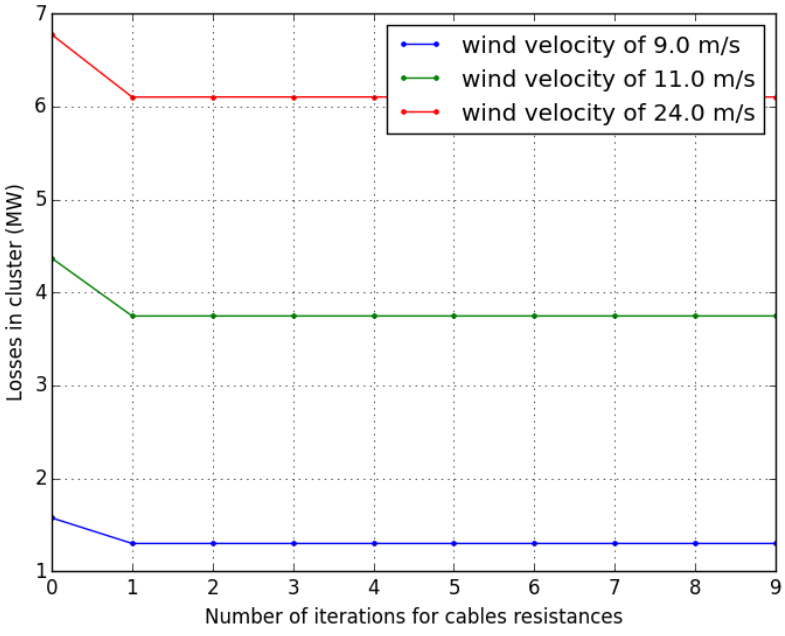

Figure B-4: Power losses in western AC network cluster (66 KV inter-array and 150 kV export) for different wind regimes depending on the number of iterations for the resistance temperature dependency

It is easily explained by the fact that with $N = 1$ (no iteration, refer to Figure B-1), for each cable, the used resistance is the maximal resistance corresponding to ampacity and maximal temperature of conductors, which means losses are over-estimated. Once a first load flow is performed, currents can be quantified with

values quite close to actual values: resistance values are therefore also close to actual values. However, a numerical oscillation occurs as shown in Figure B-5 but it is strongly "damped": this damping is above 100 p.u. per iteration.

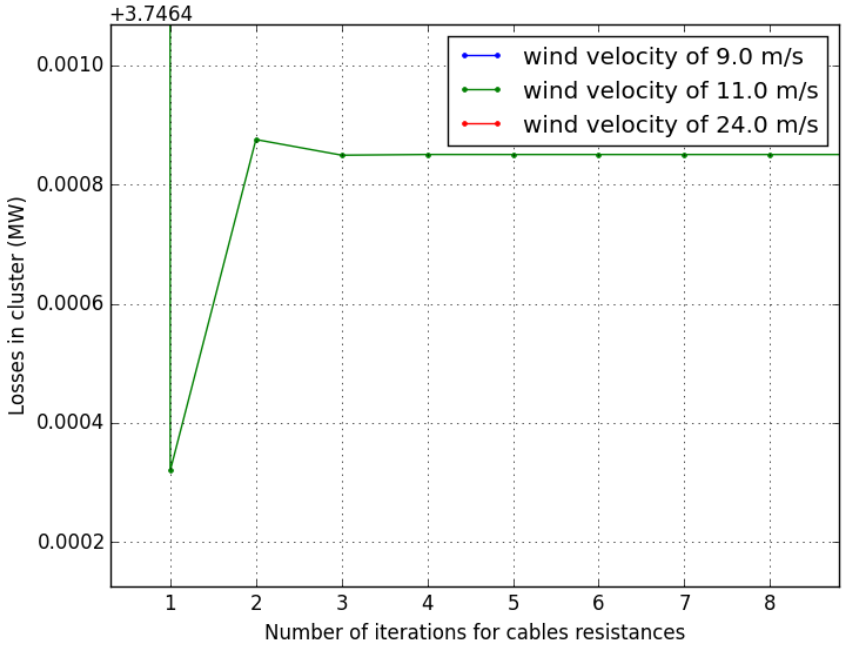

Figure B-5: Zoom on power losses in western AC network cluster (66 KV inter-array and 150 kV export) depending on number of iterations for the 11 m/s wind velocity.

Physically, for each iteration, if previous resistances are overestimated, cables currents will be underestimated (due to voltage rise in inter-array network) and new resistances will be underestimated. If previous resistances are underestimated, cable currents are overestimated and resistances are overestimated.

In future studies, one iteration is considered as sufficient to quantify resistances of cables for specific loading conditions (resulting from a wind power production, related to wind velocity). This is again justified when performing 100 iterations and comparing resistance values with those obtained with only one iteration: the maximal error committed is for export cables for which the relative error was below 0.1 %, which is below relative errors obtained with cable models (see section 2.3.1).

The same conclusion can be made for the DC case. The study was made with the same routing as for the AC case (see Figure B-3 (a)) with ±50 kV DC cables, whose sections are also determined with a heuristic method. The results are shown in Figure B-6 and Figure B-7.

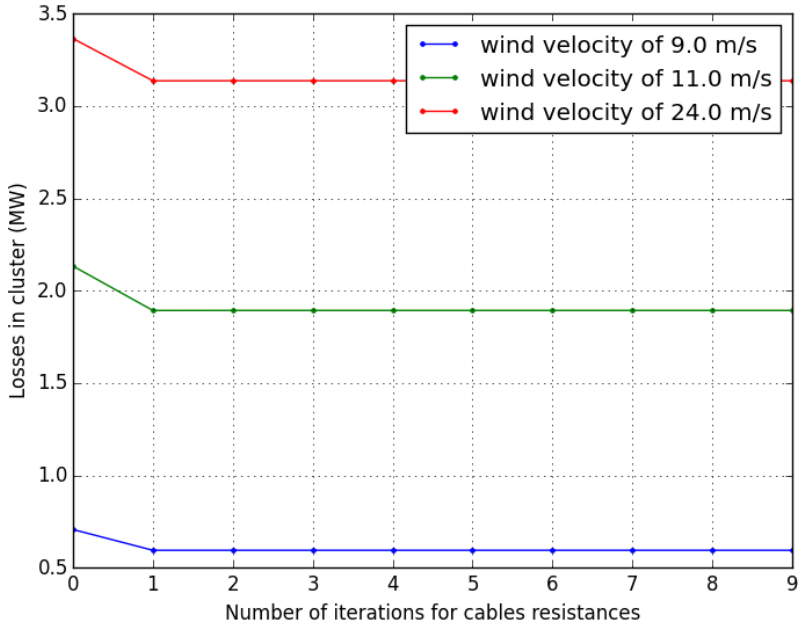

Figure B-6: Power losses in western DC network (±50 kV) cluster for different wind regimes depending on the number of iterations for resistance temperature dependency

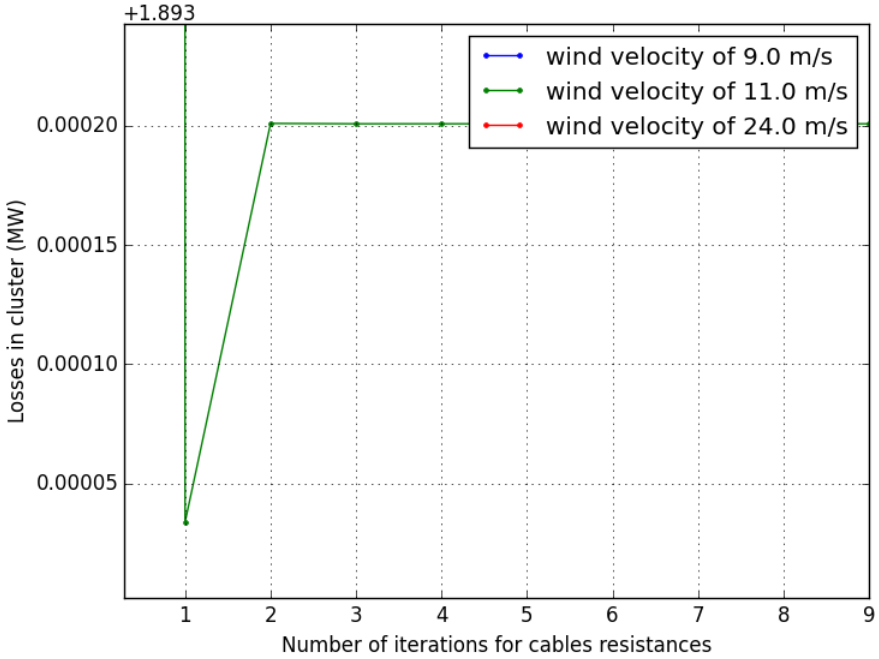

Figure B-7: Zoom on power losses in western DC network cluster (50 kV) depending on the number of iterations for the 11 m/s wind velocity.

RESUME ETENDU EN FRANÇAIS

Contexte et objectifs (chapitre 1)

Dans un contexte macro énergétique mondial, où la baisse des émissions de CO_2 s'avère indispensable, l'énergie éolienne en mer constitue une source d'électricité renouvelable prometteuse. Cette dernière connaît une forte croissance, et a en 2016 atteint une puissance installée de 12 GW en Europe. Néanmoins, sa compétitivité technico-économique (mesurable grâce au critère de coût de l'énergie, le LCOE, « Levelized Cost Of Energy ») dépend fortement de l'architecture considérée pour le raccordement électrique jusqu'au réseau terrestre.

L'infrastructure de raccordement électrique affecte en effet le rendement économique d'un projet de ferme éolienne en mer, d'autant plus que la distance du raccordement électrique est importante.

Un nombre important de principes d'architectures peut être considéré pour le raccordement électrique. Ainsi, au chapitre 1, une étude bibliographique en profondeur de telles architectures est effectuée. Cela avec un accent particulier mis sur les solutions technologiques utilisées pour remplir les différentes fonctions du raccordement (transformateur de tension, redresseur du courant ou onduleur de tension etc.). Une pré-sélection d'architectures candidates est ainsi établie. Elle correspond aux principes regroupés sous formes des schémas simplifiés de la Figure 1.

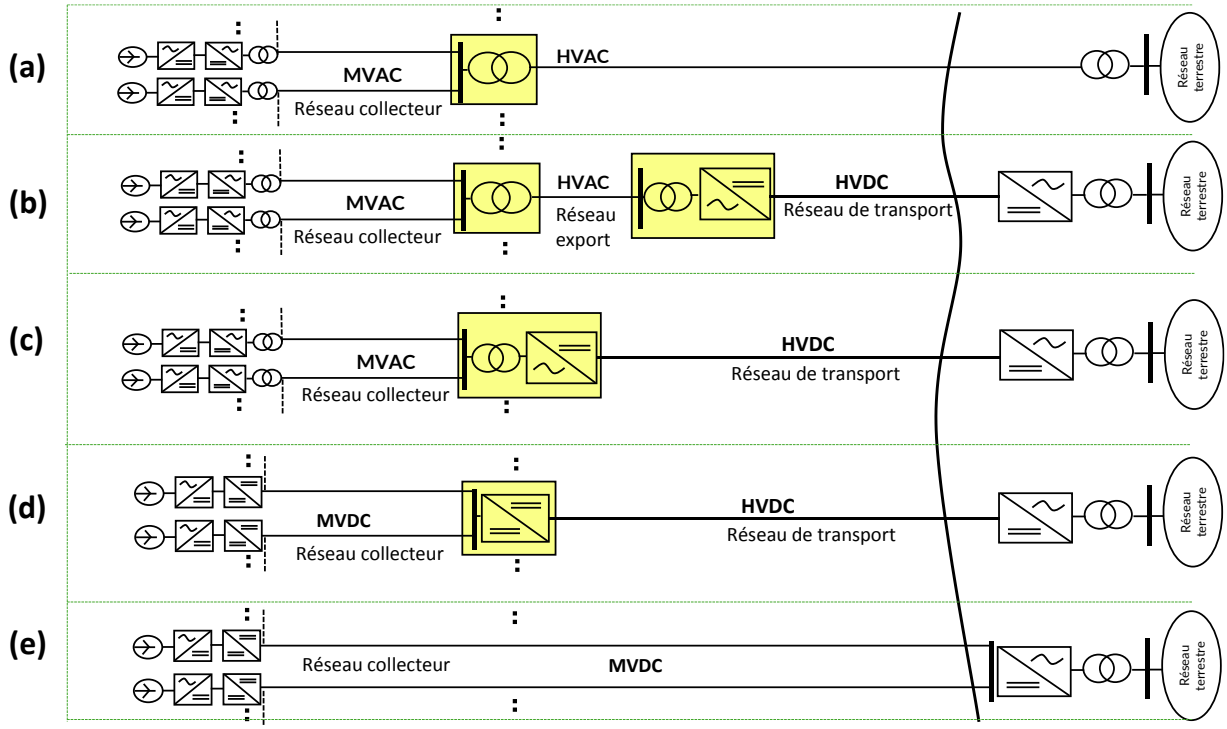

Figure 1: Principes d'architecture de raccordement sélectionnés dans la thèse

NB : MVAC correspond à « moyenne tension courant alternatif », MVDC à « moyenne tension courant continu », HVAC à « haute tension courant alternatif » et HVDC à « haute tension à courant continu ».

La problématique scientifique des présents travaux de recherche émerge alors : « quelle est la meilleure architecture » d'un point de vue technico-économique, pour une ferme éolienne donnée (caractérisée par la distance de raccordement, la puissance installée, le nombre et la densité spatiale des éoliennes). Répondre à cette question requiert la mise en place de divers modèles et méthodes. Afin d'y parvenir, une étude bibliographique des contributions scientifiques visant à évaluer et comparer des principes est effectuée. Cet état de l'art met notamment en évidence la nécessité de définir une conception presque optimale de chaque principe d'architecture considéré, afin de pouvoir l'évaluer, voire de le comparer à d'autres. La conception d'une architecture est désignée par la variable vecteur X.

La conception d'une architecture s'intègre alors dans un environnement qui reste à définir afin de permettre, a posteriori, la comparaison technico-économique des architectures. Un tel environnement doit pouvoir permettre de calculer les critères suivants (voir Figure 2) :

- Les pertes d'énergies dissipées ;
- Les coûts d'investissement (CAPEX) ;
- Les pertes énergétiques liées à l'effacement de production, en lien avec la fiabilité du réseau ;
- Les coûts de maintenance (OPEX).

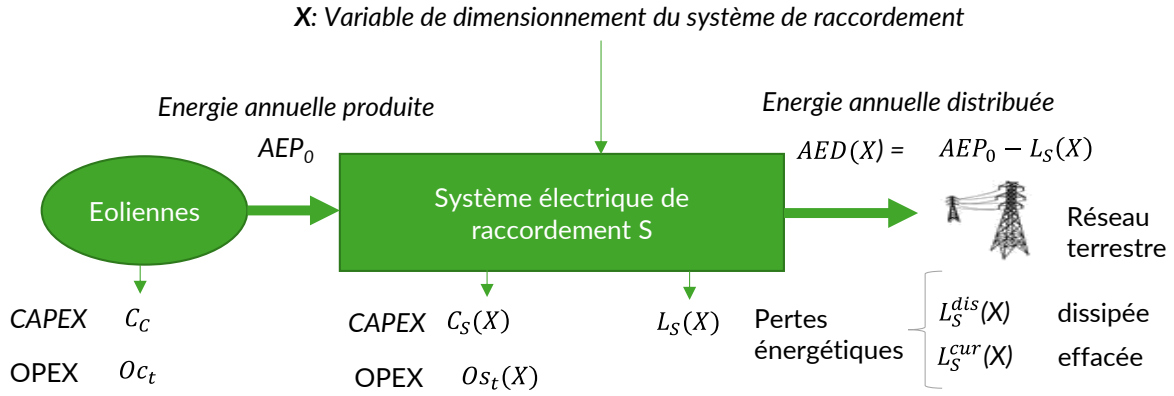

Figure 2: définition de critères de décision élémentaires en lien avec le système étudié

Dans le présent contexte d'aide à la décision, la question du choix entre une approche multi-objectif ou mono-objectif se pose. Dans la mesure où un critère largement utilisé dans la filière de l'éolien en mer existe, le LCOE, ce dernier est retenu. Le critère LCOE permet d'agréger les critères de décision élémentaires listés ci-dessus, tout en respectant la préférence des acteurs de l'industrie concernée. Il est calculé ainsi :

$$LCOE_{N,r}(\mathrm{X}) = \frac{C_S(X) + C_C + \sum_{t=1}^{N} \frac{Oc_t + Os_t(X)}{(1+r)^t}}{\sum_{t=1}^{N} \frac{AED(X)}{(1+r)^t}} \qquad (1)$$

où:

r est le taux d'intérêt ;

N est le nombre d'années d'exploitation ;

$C_S(X)$ est le CAPEX du réseau électrique S;

C_C est le CAPEX des éoliennes ;

$Os_t(\boldsymbol{X})$ est l' OPEX du réseau électrique S;

Oc_t est l' OPEX des éoliennes ;

AEP_0 est l'énergie annuellement produite par les éoliennes ;

$L_S(X)$ désigne l'énergie dissipée annuellement par S;

$AED(X)$ désigne l'énergie annuellement distribuée au réseau terrestre.

En complément du LCOE, un critère complémentaire, le NLCC, centré sur le coût du réseau de raccordement, est proposé au chapitre 1. Il est démontré que ce critère de décision est équivalent au LCOE du point de vue de l'optimalité. Il permet également de visualiser les coûts d'une manière plus adaptée au réseau électrique. Cela permet ainsi de faciliter la prise de décision concernant le choix de l'architecture de raccordement. Ce point est analysé en détails aux chapitres 5 et 6.

L'environnement d'aide à la décision proposé dans ces travaux de recherche est synthétisé à la Figure 3.

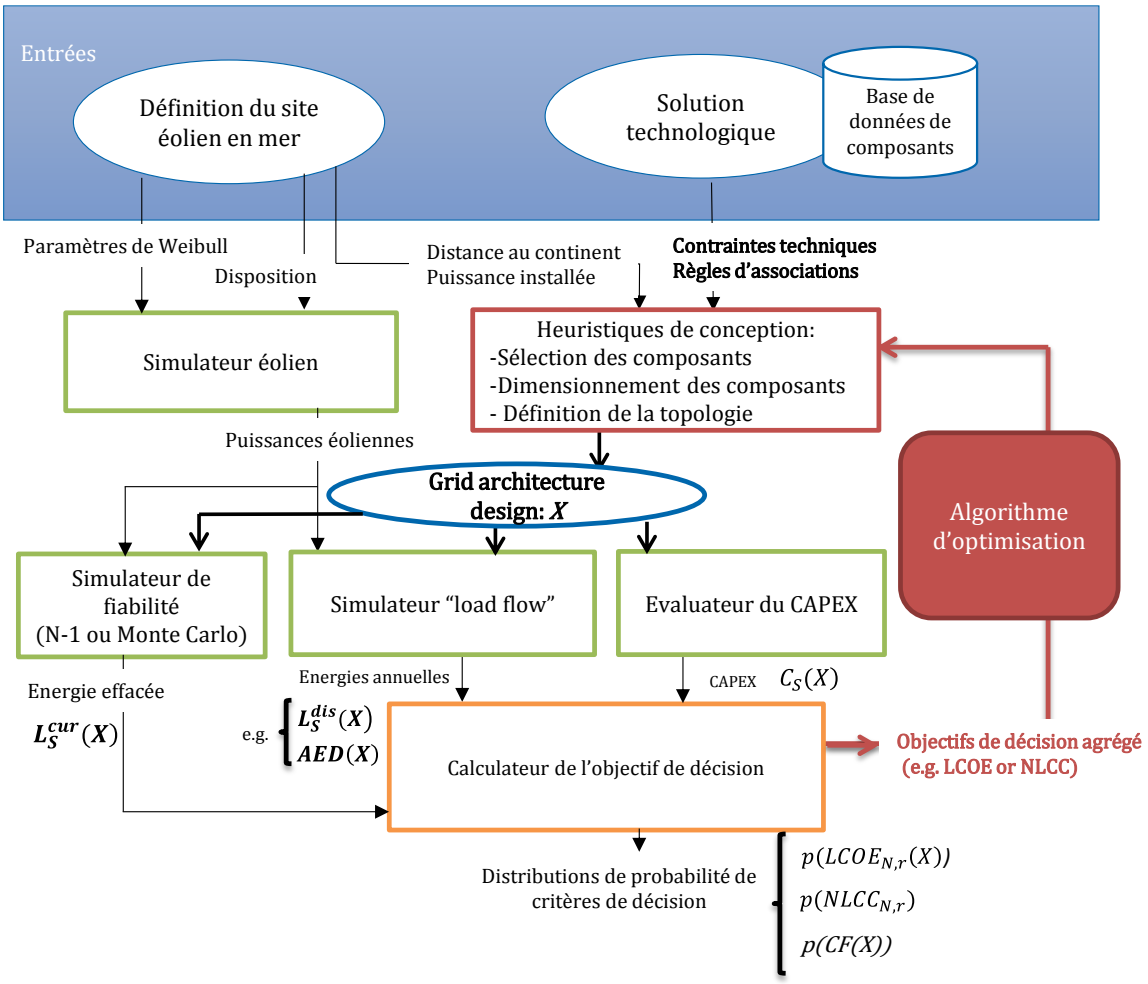

Figure 3: Synthèse de l'environnement d'aide à la décision pour le raccordement électrique d'une ferme éolienne en mer

Outre les entrées du problème que sont le principe d'architecture et un site éolien, la Figure 3 montre les modules nécessaires pour calculer les quantités nécessaires à la prise de décision. Ils sont à mettre en relation avec les objectifs scientifiques suivant :

- Le développement de modèles et méthodes permettant le calcul des grandeurs énergétiques qui sont présentés dans le chapitre 2. Ils correspondent aux « simulateur éolien » et « simulateur load flow ».
- La mise en œuvre d'une méthode de modélisation des coûts de composants du système étudié est proposée au chapitre 3. Les modèles économiques obtenus sont utilisés au sein du module « calculateur de CAPEX ».
- L'évaluation de la fiabilité du réseau de raccordement est un sujet à part entière, traité au chapitre 4, où plusieurs méthodes scientifiques sont établies. Elles permettent le calcul de l'énergie effacée au travers du « simulateur de fiabilité ».
- Une formulation pour le problème de conception d'architectures pour les différents principes considérés dans la thèse est proposée dans le chapitre 5. La méthode de résolution heuristique permet d'obtenir des solutions quasi-optimales, de manière rapide.
- La proposition de méthodes de prise en compte des incertitudes qui affectent la prise de décision est faite au chapitre 6. Elle est basée sur des résultats probabilistes et permet de prendre en compte les incertitudes liées à l'indisponibilité du réseau de raccordement ainsi que les incertitudes sur les paramètres de modèles de coûts et de fiabilité (proposés aux chapitres 3 et 4).

Méthodes de calcul des grandeurs énergétiques (chapitre 2)

Au chapitre 2, des modèles et méthodes sont proposés pour le calcul des grandeurs de décision énergétiques. Pour ce faire, les ressources éoliennes sont modélisées à l'aide d'une distribution de Weibull modélisant la vitesse du vent. Les turbines éoliennes sont modélisées par leurs caractéristiques de puissance (puissance électrique produite en fonction de la vitesse du vent). Les effets de sillage, qui impliquent des pertes énergétiques d'origine aérodynamique sont pris en compte par un facteur macroscopique dont la valeur (de l'ordre de 10% de pertes en énergie annuelle) provient de retours d'expériences industrielles.

Ensuite, des modèles électriques quasi-statiques avancés des composants de puissance du réseau électrique sont proposés, en vue de les intégrer dans des calculs d'écoulement de puissance. Les calculs d'écoulement de puissance s'appuient sur une méthode dite séquentielle qui permet la prise en compte de nombreux principes d'architectures, avec des portions en courant continu et d'autres en alternatif. Le calcul des grandeurs énergétiques requises repose alors sur un couplage des modèles éoliens et des calculs d'écoulement de puissance. Ce couplage vise à calculer les énergies par l'usage du théorème probabiliste dit du transfert.

Au sein du chapitre 2, des hypothèses de gestion des flux énergétiques dans le réseau de raccordement sont également posées et justifiées. L'analyse des flux énergétiques, résultats de ces hypothèses, justifie alors des règles de dimensionnement des câbles des réseaux collecteurs pour lesquels la puissance réactive et les chutes de tension peuvent être négligées. Cette simplification est utilisée au chapitre 5 dans lequel la méthode de conception de l'architecture est proposée. Les câbles alternatifs de haute tension (d'export)

impliquent d'importantes puissances réactives qui, elles, ne peuvent être négligées. Ces effets sont donc pris en compte lors du dimensionnement de ces câbles.

Modélisation économique des composants du système (chapitre 3)

Au chapitre 3, une méthode de modélisation des coûts d'investissement est proposée. Elle consiste principalement en l'identification des paramètres de formules analytiques expertes à partir de données de coûts. La méthode d'identification permet l'obtention de plusieurs jeux de paramètres par modèle de composant. Chacun des jeux de paramètres correspond à un scénario (parmi « optimiste », « pessimiste » et « moyen »). Ces jeux de paramètres capturent l'incertitude sur les données de coûts qui pourront être ainsi prise en compte au chapitre 6. Ces incertitudes sur les coûts sont liées aux conditions de marché ou encore aux cours des matières premières (comme le cuivre dans le cas des câbles de puissance).

Méthodes d'évaluation de la fiabilité du réseau (chapitre 4)

Le chapitre 4 porte sur l'évaluation de la fiabilité du réseau de raccordement. Un état de l'art des critères de fiabilité et des méthodes d'estimation de ces critères y est exposé. Le choix de l'énergie annuelle effacée, pour cause d'indisponibilité du réseau, est confirmé. Ensuite, une première méthode de calcul de l'espérance de la puissance effacée pour un état donné du réseau, basée sur le calcul de flot maximum contraint, est proposée. Cette méthode est la pierre angulaire de deux méthodes complémentaires pour le calcul de l'énergie effacée annuellement. La première méthode s'appuie sur un simple calcul algébrique et permet d'estimer rapidement l'espérance mathématique de l'énergie effacée. La seconde est basée sur des simulations de Monte Carlo, où les états de disponibilité des composants du réseau constituent les variables échantillonnées, par l'intermédiaire de la génération de processus stochastiques temporels. Cette seconde méthode permet la détermination d'une distribution de probabilité empirique de l'énergie effacée.

Les deux méthodes d'estimation de l'énergie effacée requièrent la connaissance de données de fiabilité des composants (les taux de défaillance et temps de réparation moyens), qui sont sujets à des incertitudes ; en particulier le taux de défaillance pour des composant technologiques nouveaux ou même prospectifs. Il est proposé de considérer trois jeux de données de fiabilité par type de composant, chacun correspondant à un des scenarios « optimiste », « pessimiste » et « moyen ».

Une validation croisée des méthodes proposées est effectuée sur un réseau d'étude comportant un petit nombre de nœuds.

Formulation et méthode de résolution du problème de conception de l'architecture du réseau (chapitre 5)

Au chapitre 5, un état de l'art des approches d'optimisation de la conception de réseaux électriques pour les fermes éoliennes est tout d'abord effectué. Cette étude bibliographique montre que le système de raccordement complet, comme celui étudié dans la présente thèse, est rarement optimisé en une fois. Le réseau de transport et les réseaux collecteurs sont généralement étudiés indépendamment. Le problème de

dimensionnement étudié est ainsi complexe et de grande taille, notamment pour un nombre important d'éoliennes (par exemple, 200).

Il est notable que la formulation et la méthode de résolution proposée est compatible avec l'ensemble des principes d'architecture considérés (voir Figure 1). La méthode de résolution du problème de conception du réseau qui est proposée, consiste en la séparation du problème complet en sous problèmes, résolus les uns après les autres, séquentiellement :

- (P1) Répartition des éoliennes par groupes spatiaux, positionnement des sous stations de groupes ;
- (P2) Conception du réseau collecteur de chacun des groupes d'éoliennes ;
- (P3) Dans le cas du principe d'architecture (a) de la Figure 1, positionnement des sous stations HVDC et associations aux sous stations AC ;
- (P4) Dimensionnement des composants de puissance, excluant les câbles collecteurs (traités au (P2) et de transport (traités au (P5));
- (P5) Quand le principe d'architecture en comporte un, conception du réseau de transport HVDC (topologie et choix des sections des câbles HVDC).

La méthode de résolution heuristique permet de trouver des solutions presque optimales du problème de dimensionnement. Une mise en œuvre sur plusieurs principes est proposée, avec réseau collecteur en courant alternatif ou en continu, avec ou sans réseau d'export HVAC, transport HVDC ou non (principes (a), (b), (d) de la Figure 1). Les cas d'études considérés comprennent un grand nombre d'éoliennes, entre 100 et 200, afin de démontrer la performance de la méthode (notamment en termes de temps de calculs).

Pour ces différents principes, une analyse des résultats sur les critères de décision (LCOE et NLCC) est proposée et montre que l'environnement d'aide à la décision développé permet en effet de réaliser des dimensionnement quasi-optimaux, de manière à permettre une évaluation technico économique non biaisée des principes d'architecture. Le temps de résolution du problème de dimensionnement est très réduit, malgré la prise en compte de contraintes géographiques correspondant à des obstacles que les câbles ne peuvent pas traverser. Il est notable que les sources d'incertitudes sur les modèles sont telles (notamment celles liées aux coûts d'investissement) qu'il est acceptable d'obtenir des dimensionnements légèrement sous-optimaux.

Prise en compte des incertitudes pouvant affecter la prise de décision (chapitre 6)

Au chapitre 6, il s'agit de prendre en compte certaines des incertitudes pouvant affecter l'évaluation technico-économique des architectures. En effet :

- d'une part les modèles de coûts et les données de fiabilité sont sujets à des incertitudes qui peuvent affecter le calcul des critères de décision.
- D'autre part, même en faisant l'hypothèse d'une connaissance parfaite des données de fiabilité, l'énergie effacée annuellement est une variable stochastique, qui dépend du processus de défaillances potentielles et de réparations des composants du réseau.

La source d'incertitude qui est propre au caractère stochastique de la fiabilité peut être analysée à l'aide de résultats de simulations de Monte Carlo avec la méthode proposée au chapitre 4. Dans le chapitre 6, de telles simulations de Monte Carlo sont mises en œuvres sur un réseau de grande taille (dimensionné au chapitre 5) et permettent l'obtention d'une distribution empirique de l'énergie effacée. A partir de cette dernière, la distribution empirique du LCOE correspondante est calculée. Ainsi, l'environnement proposé peut permettre à un investisseur d'évaluer le risque financier associé à l'indisponibilité du réseau électrique pouvant intervenir.

Dans la littérature, les incertitudes sur les modèles et leurs conséquences numériques sur un critère de décision sont parfois prises en compte par le biais de pseudo simulations de Monte Carlo consistant à établir un échantillonnage des paramètres des modèles afin de calculer les valeurs du critère de décision correspondant aux échantillons. Ce type d'étude permet d'obtenir plus d'informations qu'une simple analyse de sensibilité ; cette dernière ne permettant pas de déterminer la vraisemblance de telle ou telle valeur de sortie.

Dans cette thèse, une méthode probabiliste analytique, concurrente des méthodes basée sur des simulations dîtes de « pseudo Monte carlo », est proposée. La méthode analytique proposée permet la prise en compte des incertitudes sur les paramètres de modèles et d'analyser leurs propagations au critère de décision (LCOE ou NLCC). Cette méthode permet l'obtention de la fonction de distribution de probabilité analytique du critère de décision vu comme une variable aléatoire, conséquente de l'incertitude sur les paramètres (eux même modélisés comme des variables aléatoires, généralement gaussiennes). La méthode est mise en œuvre sur plusieurs architectures et met en évidence le fait que, pour les cas d'étude considérés, au regard du critère de décision (LCOE ou NLCC), les incertitudes sur les modèles de coûts sont plus impactantes que les incertitudes sur les données de fiabilité.

Conclusion

En conclusion, l'environnement d'aide à la décision proposé dans la thèse permet :

- Le dimensionnement quasi-optimal de l'architecture du réseau de raccordement d'un parc éolien en mer, pour un grand nombre de principes.
- L'évaluation technico-économique détaillée des architectures obtenues, prenant en compte les coûts d'investissement, de maintenance, les pertes électriques dissipées et celles effacées.

L'obtention de cet environnement d'aide à la décision repose sur des contributions scientifiques. Les contributions scientifiques majeures de ces travaux de recherche sont :

- La modélisation technico-économique avancée du système électrique de raccordement.
- La proposition d'une approche mono-objectif pour la prise de décision dans le contexte du raccordement de parcs éoliens en mer. Cela inclut la proposition d'un nouveau critère technico-économique (NLCC) qui facilite la prise de décision par rapport au critère industriel (LCOE), tout en lui restant fidèle du point de vue de l'optimalité.

- La proposition de quelques méthodes d'évaluation de la fiabilité du réseau de raccordement. Grâce à l'utilisation de résultats de la théorie des probabilités, ces méthodes sont peu coûteuses en temps de calcul pour l'estimation de l'énergie annuelle effacée. Elles permettent autant le calcul de l'espérance mathématique de cette grandeur que l'obtention des distributions empiriques associées.
- La proposition d'une formulation complète portant sur le problème de conception de l'architecture de raccordement. A cet égard, une particularité ce ces travaux est la généricité de la formulation et de la méthode de résolution vis-à-vis des principes d'architectures qui peuvent être considérés.

Un point particulier montrant les capacités de l'environnement proposé pour faciliter la prise de décision est l'usage du critère NLCC. Les cas d'étude proposés aux chapitres 5 et 6 montrent notamment comment le critère NLCC permet une analyse fine des résultats technico-économiques grâce à ses avantages :

- Possibilité d'analyser la responsabilité des sous-systèmes du réseau de raccordement sur le NLCC, c'est-à-dire sur les coûts totaux (comprenant CAPEX, OPEX, pertes électriques). Ce point s'avère notablement utile dans un contexte R&D où l'environnement proposé peut être utilisé pour orienter des innovations technologiques.
- Mitigation de l'impact des paramètres financiers lors de la comparaison des architectures. La connaissance précise des conditions financières retenues par un investisseur final n'est plus indispensable. Cela constitue également un avantage dans un contexte R&D.

Les perspectives de ces travaux de recherche sont les suivantes :

- Mise en œuvre de l'environnement d'aide à la décision proposé sur un grand nombre de cas d'étude et principes d'architectures, en vue d'orienter l'innovation technologique vers des architectures technico économiquement compétitives.
- Extension aux réseaux HVDC maillés, qui constituent le sujet de recherche majeur de SuperGrid Institute, entreprise au sein de laquelle, en plus de l'Ecole Centrale Lille et du L2EP, et du G2Elab, ces travaux de thèse ont été menés.
- Modification de la formulation et de la résolution du problème de dimensionnement des réseaux en vue d'obtenir des optimums globaux. Cela pourrait s'avérer utile dans un contexte où l'environnement proposé est utilisé pour la conception du réseau électrique de projets éoliens en mer réels ; auquel cas les incertitudes sur les coûts d'investissement sont normalement moindre par rapport à un contexte R&D. Pour atteindre cet objectif, une piste est donnée dans la thèse. Elle implique la modification mineure de certains des sous problèmes de dimensionnement et requiert peu d'efforts. Une autre piste consiste en l'usage d'une méthode d'optimisation dite de « target cascading », utilisée pour l'optimisation de système hiérarchisés complexes (« systèmes de système »), y compris, avec succès, dans le domaine du génie électrique.

Environnement d'aide à la décision pour les réseaux électriques de raccordement des fermes éoliennes en mer : conception et évaluation robuste sous incertitudes.

Résumé : L'énergie éolienne en mer connaît une croissance forte. Sa compétitivité économique, mesurée par le LCOE (coût d'énergie actualisé), n'a pas encore atteint celle de l'éolien terrestre. Le coût du raccordement électrique affecte cette compétitivité. Selon la distance et la puissance de la ferme, un panel important d'architectures et technologies du réseau de raccordement peut être considéré (AC ou DC etc.). L'objectif de cette thèse est de fournir un cadre méthodologique décisionnel pour l'évaluation et la planification de l'architecture du réseau de raccordement.

L'évaluation des architectures repose sur les calculs des énergies annuelles dissipées dans le réseau, des coûts d'investissement du réseau et de l'énergie non distribuée en lien avec la fiabilité du réseau. Pour calculer ces quantités, des modèles et méthodes de calculs sont proposés.

Il apparaît néanmoins nécessaire d'évaluer et de comparer des architectures ayant des dimensionnement optimaux. Ainsi, une formulation du problème de dimensionnement du réseau est proposée. La formulation est générique vis-à-vis des différentes architectures considérées. Une méthode de résolution heuristique rapide donnant des solutions quasi-optimales est mise en œuvre.

L'environnement d'aide à la décision qui permet le dimensionnement puis l'évaluation d'une architecture est mis en œuvre sur plusieurs cas d'application incluant des architectures très différentes. Finalement, une méthode probabiliste analytique est proposée afin de prendre en compte les incertitudes sur les modèles et leurs propagations aux critères de décision.

Mots clés : optimisation, analyse technico-économique, architectures de réseaux électriques, intermittence, fiabilité, formulation complexe, incertitudes, HVDC.

Decision support framework for offshore wind farm electrical networks: Robust design and assessment under uncertainties

Abstract: Offshore wind power is quickly developing. Its cost-effectiveness, measured with the LCOE (Levelized cost of Energy) has not reached the one of onshore wind power yet. The cost of electrical connection impacts this cost-effectiveness. Depending on the distance to the onshore grid, many possibilities of architectures and associated technologies can be considered for this connection network (AC, DC etc.). The goal of this research is to provide a decision support framework for the assessment and the planning of the architecture for the electrical connecting network.

The architecture assessment relies on the calculation of the annual energy dissipated through the network, of the investment costs and of the annual curtailed energy due to the network unavailability. To compute these quantities, models and methods are proposed.

It appears that to compare architectures, these must have near optimal designs. Thus, a formulation of the electrical network design optimization is proposed. The formulation is generic in regard to the various architectures which are considered. A quick heuristic solving approach, which gives near optimal solutions, is proposed and implemented.
The decision support framework makes it possible the design and the assessment of an architecture and is applied to three very different architectures concepts. Finally, a probabilistic analytical method is proposed to take into account the models uncertainties and to study their propagations to the decision criteria.

Key words: optimization, technical and economic analysis, electrical network architectures, intermittence, reliability, complex formulation, uncertainties, HVDC.